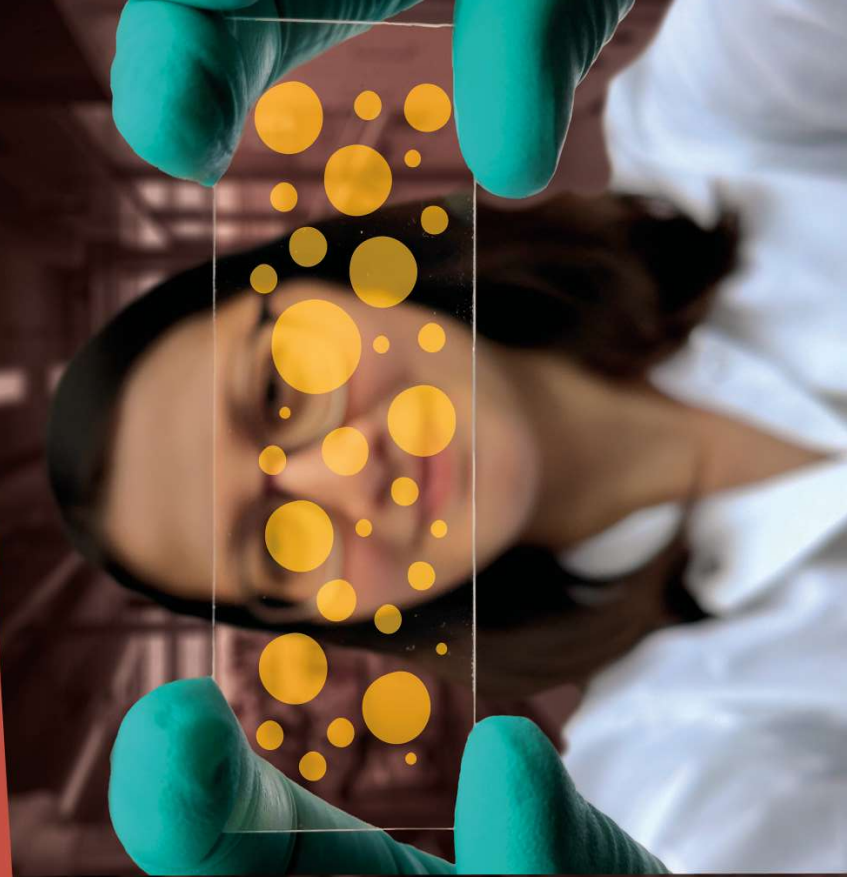# CHEMISTRY OF ACTIVE COACERVATE DROPLETS

Liquid droplets as a minimal model of life

Karina Nakashima

Karina Nakashima

CHEMISTRY OF ACTIVE COACERVATE DROPLETS

Chemistry of active coacervate droplets

Liquid droplets as a minimal model of life

Karina Kinuyo Nakashima

Chemistry of active coacervate droplets

Liquid droplets as a minimal model of life

Proefschrift ter verkrijging van de graad van doctor
aan de Radboud Universiteit Nijmegen
op gezag van de rector magnificus prof. dr. J.H.J.M. van Krieken,
volgens besluit van het college voor promoties
in het openbaar te verdedigen op

maandag 11 oktober 2021
om 14.30 uur precies

door

Karina Kinuyo Nakashima
geboren op 26 november 1991
te São Paulo, Brazilië

Chemistry of active coacervate droplets

Liquid droplets as a minimal model of life

Dissertation to obtain the degree of doctor
from Radboud University Nijmegen
on the authority of the Rector Magnificus prof. dr. J.H.J.M. van Krieken,
according to the decision of the Doctorate Board
to be defended in public on

Monday, October 11, 2021
at 2.30 pm

by

Karina Kinuyo Nakashima
born on November 26, 1991
in São Paulo, Brazil

Dedication

pro Jorge e pra Bebete

What an odd thing a diary is: the things you omit are more important than those you put in.

Simone de Beauvoir,
in *The Woman Destroyed*

Contents

List of Figures

List of Tables

Frequent acronyms and symbols

ADP   adenosine diphosphate
ATP   adenosine triphosphate
c   coacervate phase
FUCA   first universal common ancestor
HEPES   4-(2-hydroxyethyl)-1-piperazineethanesulfate buffer
HK   hexokinase, EC 2.7.1.1
HPLC   high performance liquid chromatography
IDP   intrinsincally disordered protein
IDR   intrinsincally disordered region
K, K$_P$ partitioning coefficient
k   reaction rate constant
K$_{72}$ protein
K$_M$ Michaelis constant
LLPS   liquid-liquid phase separation
LUCA   last universal common ancestor
MLO   membraneless organelle
OR   Ostwald ripening
PEP   phosphoenolpyruvate
PLL   poly-*L*-lysine, 15-30 kDa
PyK   pyruvate kinase, EC 2.7.1.40
RNA   ribonucleic acid
s   solution, dilute phase

Summary

THERE ARE so many things we do not understand about life. The most persistent one has got to be the origin of life, an open question common to all three natural sciences (Biology, Physics and the central science, Chemistry). Challenging as it is, developing and proving a consistent hypothesis for the appearance of the first living beings on Earth is beyond the scope of a PhD thesis; instead, this thesis chose one existing hypothesis and explored it further. The theory of our preference is the confluence of Oparin, Haldane and Bungenberg de Jong's independent work: that in the primitive ocean, organic molecules formed and slowly compounds with the tendency to accumulate together in microspheres (coacervates) appeared; the microspheres behaved like efficient micro-reactors, where more complex molecules could form, so that a cell encased by a lipid membrane, with nucleic acids and enzymes could emerge. But as many pointed out before us, coacervate droplets can loose their integrity due to fusion, ripening or dissolve altogether, and might not be the obvious protocell for the conditions on early Earth. We therefore put it to a test whether coacervate droplets can display behavior that we normally attribute to living cells — spatial organization and growth —, and took all the intermediate steps (and branches) needed to reach a positive conclusion:

Foundation

In Chapter 1, we introduced the concepts of organization and growth as compartmentalization and regeneration, respectively. This conceptual framework matters because the object of our investigation, life, does not have a unanimous definition. We selected a few life-defining features from the literature, and gave our perspective on them: compartmentalization and seclusion as the first developments to provide identity, organization and protection to protocells; followed by adaptability and regeneration to provide the tools for the protocell to persist under changing conditions; and energy to fuel metabolism, growth and select for dynamic structures, thus integrating all seven pillars of life. These concepts translate to chemistry as: *life needs compartments that self-assemble and chemical reactions that produce self-assembling molecules*, or in other words, protocells are active compartments.

We explored the self-assembly aspect of coacervate droplets in Chapter 2. There we

developed poly-lysine/ATP droplets that can form and dissolve reversibly and in a time-controlled manner, and also defined important protocols used throughout the thesis. We achieved this by selecting a pair of enzymes, compatible with each other, to produce and consume ATP *in situ*. The enzymatic network controls phase separation because the precursors (ADP and phosphoenol pyruvate) have a lower affinity for poly-lysine than the products (ATP and glucose), and therefore ATP production is accompanied by coacervation to the likes of spinodal decomposition. This system worked so well that we could adjust the ratio of all components (poly-lysine, phosphatase, kinase, ATP, ADP, phosphoenol pyruvate, glucose) to delay condensation for 50–400 seconds. Moreover, by supplying the substrates phosphoenol pyruvate and glucose externally, we could cycle between the two states up to six times, showing for the first time that the reaction control does not compromise the dynamic assembly of these compartments. More than that, we were surprised to find that we could explain the timing of condensation with a linear model for turbidity and Michaelis-Menten kinetics, even though the latter was never shown to apply to reactions in two phases.

Intermission

The realization that the enzymes were performing normally in poly-lysine/ATP coacervates was so intriguing that we decided to branch out and tackle the conundrum of chemical reactivity in coacervates. This is a matter of biological relevance as well: recently several droplet organelles were discovered in eukaryotic cells, and more and more proteins involved in gene expression were found to form liquid condensates, which all share many properties with coacervates. In Chapter 3 we expanded on our introduction on droplet organelles and concluded that, in order to understand their function, we need to understand how they affect reactivity. The best model for this investigation are peptide/nucleotide coacervates like the ones of Chapter 2. But for this goal, accurate measurements of concentration, partitioning coefficients and reaction rates are crucial, and we developed and tested an experimental approach to do so. We found that for the poly-lysine/ATP mixture, reaction rates in the presence and in the absence of coacervation are comparable, which we attribute to the low volume fraction of droplets in the emulsion limiting their contribution to the average signal measured.

In Chapter 4 we provided the theoretical framework to complement Chapter 3: a kinetic model to describe bimolecular reactions with and without enzymatic catalysis and inhibition, aiming to find conditions where distinctive kinetic properties can be obtained in coacervates. We investigated the role of volume fraction, partitioning coefficients, rate constant modification by the coacervate environment, in addition to new effects such as transient product accumulation and reversal of product inhibition. We proposed to put these predictions to a test with an experimental model of a chromogenic ester hydrolysis catalysed by lipases in different coacervate systems, for which we found promising preliminary results that highlight the conclusions of our model, but also experimental challenges

in this investigation.

Resumption

We went back to our original goal in Chapter 5. We were aware from the start that Ostwald ripening could compromise the stability of coacervate droplets and therefore our chance to observe and measure growth, and performed control experiments anticipating Chapter 6. We were then surprised to find that complex coacervates are remarkably stable towards ripening. We employed an accessible setup to observe droplets over time with microscopy, without the interference of wetting and fusing, and we could observe droplets for an hour (or a day in an extreme case) without detecting ripening. We were able to explain the absence of ripening with two hypothesis. The first, that Ostwald ripening is energetically disfavoured in complex coacervates due to the electrostatic penalty of removing individual macro-ions from one droplet, thus creating a charged surface, and transferring them to another droplet. While the concentration gradient between the interface of a small droplet and a large droplet makes the transfer favourable, the electric force opposes that tendency.

Our second hypothesis is that Ostwald ripening is effectively suppressed due to a large activation barrier to remove electroneutral complexes from the droplet. In this case, as opposed to the highly soluble individual macro-ions, the departing structure is a multi-ion complex with non-negligible surface energy. The intermediate state also causes a loss of entropy, as ions in the electroneutral complex are more restricted than in the coacervate droplet. Our results add a convincing argument in favor of coacervate-based protocells, as it disproves a widely criticized weakness.

Grounded in our results with reaction control from Chapter 2 and with stability from Chapter 5, in Chapter 6 we attempted and succeeded in developing a growing protocell. The replacement of poly-lysine for an elastin-like peptide, K_{72}, meant that we were able to observe nucleation and growth of coacervate droplets. Unlike previous studies in the literature that achieve growth via fusion, in our setup growth was unequivocally linked to the progress of the kinase-catalysed conversion of ADP into ATP. We applied our conclusions from Chapter 3 and fully mapped these active droplets, finding high partition coefficients for the protein K_{72} and the enzyme. ADP has a slight preference for ATP-K_{72} droplets over the dilute solution, from which we conclude, with our model from Chapter 4, that 40–60 % of it gets converted inside the droplets.

The distinctive feature of our work is that we measured individual droplet size and growth rate; the latter reflects the reaction rate, that determines how fast ATP super-saturation is reached, and the diffusion rate of K_{72}, recruited to nucleated droplets with excess ATP. The average growth rate of multiple droplets in a sample can be interpreted as a fitness parameter to distinguish two droplet populations, and we put this to the test. ATP-K_{72} droplets grow at different rates under different environmental conditions of fuel or enzyme availability; but under the same conditions, a population of droplets to which RNA was added grows more slowly than without RNA. This is likely due to ADP displace-

ment from the droplets by RNA, an effect mentioned in our discussion of partitioning in Chapter 3. Differential growth rates are an important result to the field, as we start to move towards a systems approach where different protocells are combined. The results in this chapter can provide a mechanism for protocell growth and proliferation before the appearance of specialized enzymes, and competition in a pre-Darwinian evolution scenario.

Finale

Finally, in Chapter 7, we integrated our results to provide an overview of intriguing questions and answers in the field of active coacervates. We looked at Chapters 2 and 6 together, pointing out the gain from control in both phase separation thermodynamics and kinetics. We grouped Chapters 3, 4 and 5 under the paradox of complex coacervate permeability (an open reactor, but stable towards ripening), and in Chapter 8 we suggested possible continuations of our work, such as exploring growth to achieve droplet division and coacervate droplet stability to perform competition experiments. We concluded with a brief reflection on the societal impact of this thesis.

Samenvatting

Vertaald uit het Engels door Alain André and Jan Harm Westerdiep

H ET ONTSTAAN van leven is een grote vraag binnen de natuurwetenschappen die zich niet beperkt tot de scheikunde. Zodoende ontbreekt een eenduidige en consistente hypothese hoe het eerste leven uit levenloze materie heeft kunnen ontstaan. In dit proefschrift zullen we ons beperken tot de hypotheses van Alexander Oparin, John Haldane, en Hendrik Bungenberg de Jong. Hoewel deze wetenschappers afzonderlijk van elkaar onderzoek deden, lijken hun theorieën op elkaar. Alle drie beginnen met het voorstellen hoe de oeraarde eruit zag; als een oceaan zonder levende materie. Hierin zouden de eerste moleculen zijn ontstaan die gaandeweg de eigenschap ontwikkelden om samen te kunnen assembleren in minuscule druppels, microsferen of met een moeilijker woord coacervaten genoemd. Deze microsferen fungeerden uiteindelijk als microreactoren waarin complexere moleculen gevormd konden worden. De oercel zou kunnen zijn ontstaan uit deze coacervaten waarin uiteindelijk membraanmoleculen, nucleïnezuren — die de basis vormen voor de informatieopslag — en proteïnes — zoals enzymen — worden gevormd.

Echter, deze theorie die ervan uitgaan dat oercellen zijn ontstaan uit coacervaten heeft ook veel kritiek moeten ondergaan die we niet kunnen negeren. Ten eerste zouden coacervaten verloren kunnen gaan na verloop van tijd door met elkaar te fuseren. Ten tweede kunnen kleinere coacervaten verloren gaan door Ostwaldrijping, een thermodynamisch proces waarin kleine druppels verloren gaan ten behoeve van grotere druppels. Tot slot zouden coacervaten verloren kunnen gaan door op te lossen in de waterige oplossing. In dit proefschrift observeren we eigenschappen van coacervaten die wel degelijk in de buurt komen van wat we als levend kunnen bestempelen. Daarmee weerleggen we de voornaamste kritiek dat coacervaten zeer labiel zouden zijn. De focus zal liggen op het organiseren van moleculen in de coacervaten, het compartimentaliseren, en of deze coacervaten kunnen groeien, beide eigenschappen van levende cellen. In de volgende hoofdstukken wordt uitgelicht hoe we tot onze positieve conclusie zijn gekomen.

Beginsel

In Hoofdstuk 1 introduceren we de concepten organisatie en groei als belangrijke eigenschappen van levende cellen. Vanwege het gebrek aan een eenduidige term zullen we in dit

hoofdstuk eerst deze definitie vastleggen, naast enkele andere definities voor eigenschappen die we aan het begrip leven toeschrijven. Zo is in de eerste plaats compartimentalisatie en het vormen van een fysische afscheiding een belangrijke stap richting de formatie van een cel. Het vormen van een gescheiden milieu geeft de cel een identiteit maar ook bescherming. In de tweede plaats moet een cel zich kunnen aanpassen aan zijn omgeving en energie kunnen omzetten. Dit is niet alleen belangrijk voor het behouden van een metabolisme in de cel, maar ook zodat de zichzelf kan regenereren. Als we deze concepten vertalen naar de scheikunde, komen we uit op de volgende definitie: het leven bestaat uit compartimenten die gedreven worden door zelfassemblage en die een chemische reactie moeten bevatten die de zelfassemblerende moleculen kunnen produceren. Kortom, de oercel zou een actief compartiment moeten zijn.

In Hoofdstuk 2 bestuderen we het zelfassemblage aspect van coacervaatdruppels. Hiervoor hebben we een reversibel systeem ontwikkeld waarbij de ATP concentratie de coacervatie van poly-lysine controleert. Door middel van een enzymatisch netwerk, bestaande uit twee enzymen, kan de concentratie van ATP worden gereguleerd. We beginnen met een homogene poly-lysine oplossing met de substraten ADP en fosfoenolpyruvaat, die door het toevoegen van het enzym pyruvaatkinase worden omgezet in ATP en glucose, waarna ATP en poly-lysine druppels vormen. Dit systeem werkte zo goed dat we de snelheid van condensatie konden manipuleren door het variëren van de ratio's tussen de componenten (poly-lysine, fosfatase, kinase, ATP, ADP, fosfoenolpyruvaat en glucose), waarin condensatie ontstond in een tijdsbestek van minder dan een minuut tot enkele minuten (50–400 secondes). De reversibiliteit van dit proces konden we bestuderen door het extern toevoegen van de verschillende substraten (glucose en fosfoenolpyruvaat). Op deze wijze hebben we kunnen demonstreren dat we zeker zes keer kunnen schakelen tussen de twee toestanden. Tegen onze verwachting in konden we de resultaten van het condenseren onderbouwen middels een lineair model op basis van turbiditeit (troebelheid) en Michaelis-Mentenkinetiek, iets wat nog niet eerder was aangetoond voor reacties in een tweefasenregime.

Tussenpoos

Na het realiseren van een enzymatische reactie in poly-lysine/ATP coacervaten wilden we meer inzicht in de manier waarop reacties zich kunnen gedragen in coacervaten. Dergelijke reacties zijn namelijk van groot belang voor recent onderzoek binnen de biologie waarbij verscheidene membraanloze organellen zijn ontdekt in eukaryote cellen. Wat steeds vaker wordt aangetoond is dat eiwitten die belangrijk zijn in genexpressie ook betrokken zijn in de formatie van vloeibare druppels in cellen, net als de coacervaten uit hoofdstuk 2. In Hoofdstuk 3 breiden we ons initieel onderzoek naar druppelorganellen uit en concluderen dat om hun functies beter te begrijpen we eerst moeten begrijpen hoe ze chemische reacties kunnen beïnvloeden. De beste modellen om dit te onderzoeken zijn peptidenucleotidecoacervaten, zoals beschreven in hoofdstuk 2. Ons doel is echter om nog accu-

rater de concentraties, verdelingscoëfficiënten, en reactiesnelheden te bepalen. Daarvoor hebben we een experimentele methode ontwikkeld en getest om kwantitatieve data te extraheren uit coacervaatemulsies. Hieruit bleek we dat de reactiesnelheden voor poly-lysine/ATP coacervaatmengsels vergelijkbaar waren met die van reacties in de afwezigheid van coacervaten., De geobserveerde geringe bijdrage aan de globale gemiddelde metingen zou mogelijk verklaard kunnen worden door de kleine volumefractie van de coacervaat-druppels in emulsies.

In Hoofdstuk 4 geven we de theoretische basis voor het implementeren van de re-sultaten uit hoofdstuk 3. Het resultaat hiervan is een kinetisch model dat beschrijft hoe bimoleculaire reacties met en zonder enzymatische katalysator en enzymremmers (in-hibitors) zich gedragen. Hierbij is het beoogde doel het vinden van de karakteristieke kinetische eigenschappen voor coacervaten. We bestudeerden de rol van volumefrac-ties, verdelingscoëfficiënten, en reactieconstanten in coacervaatmengsels. Verder werden de nieuwe effecten van productvorming en productinhibitie onderzocht. De theoretische waardes die we hieruit hebben verkregen, zijn vervolgens op de proef gesteld middels een modelreactie, een hydrolyse van een chromogene ester, onder enzymatische katalyse van lipase, voor verschillende modelsysteem coacervaten. De voorlopige resultaten van dit onderzoek gaven enkele conclusies maar laten ook de experimentele uitdagingen zien.

Hervatting

In Hoofdstuk 5 gaan we terug naar het originele doel. Het was ons bekend dat Ostwaldri-jping de stabiliteit van de coacervaatdruppels kan beïnvloeden en dat daarmee ook de waarschijnlijkheid om groei van deze druppels te observeren afneemt. Daarom voerden we in afwachting van hoofdstuk 6 enkele controle-experimenten uit. Tot onze verbazing bleek daarbij dat de coacervaatdruppels redelijk stabiel zijn tegen Ostwaldrijping. We gebruikten daarbij een opstelling waarin we druppels konden observeren met een fluores-centiemicroscoop, zonder beïnvloeding van bevochtiging (Engl. Wetting) of fusering van druppels. De coacervaatdruppels konden voor een uur (of zelfs een dag in uitzonderlij-ke gevallen) geobserveerd worden zonder dat Ostwaldrijping plaats vond. We verklaren de afwezigheid van deze rijping door middel van twee hypotheses. De eerste stelt dat Ostwaldrijping energetisch ongunstig is in het geval van complexe coacervaten door de elektrostatische barrière die bestaat voor het verwijderen en verplaatsen van individuele macroionen van de druppels. Hierbij moet een geladen oppervlak worden gemaakt dat zich vervolgens verplaatst naar een andere druppel. Hoewel de concentratiegradiënt tussen het grensvlak van een kleine druppel en een grote druppel het transport zouden faciliteren, geeft de elektrostatische kracht juist een tegenovergesteld – en groter - effect.

De tweede hypothese is dat Ostwaldrijping wordt onderdrukt door een grote acti-vatiebarrière voor het verwijderen van elektroneutrale complexen uit de druppel. In dit geval is de vertrekkende structuur, in tegenstelling tot de individuele macroionen met een hoge oplosbaarheid, een multi-ion complex met een niet te verwaarlozen oppervlakte-

energie. De intermediaire fase zal hierbij tevens een verlies van entropie geven, aangezien de bewegingsvrijheid van ionen in het elektroneutrale complex kleiner is dan in de coacervaatdruppel. Onze resultaten geven aan dat coacervaten helemaal niet zo labiel hoeven te zijn en kunnen bovendien dienen ter onderbouwing van een oerceltheorie op basis van coacervaten.

De resultaten rond gecontroleerde reacties in hoofdstuk 2 en de stabiliteit van coacervaten in hoofdstuk 5 vormen de grondslag voor Hoofdstuk 6, waarin we een nieuw groeiend oercelsysteem hebben ontworpen. De poly-lysine werd vervangen voor een elastine-achtige peptide, verder aangegeven als K_{72}, die het mogelijk maakte de nucleatie en groei van K_{72} coacervaatdruppels te bestuderen. In tegenstelling tot de actieve groei door middel van fusie, die in de literatuur is waargenomen, laten wij in dit hoofdstuk zien dat groei wordt behaald via de kinasegekatalyseerde conversie van ADP naar ATP. Als we deze resultaten combineren met de conclusies van hoofdstuk 3, volgden hieruit hoge partitiecoëfficiënten voor het eiwit K_{72} en het enzym binnen de druppels. ADP heeft maar een lichte voorkeur voor de ATP-K_{72}-coacervaatdruppels ten opzichte van de verdunde oplossing. Aan de hand van het model uit hoofdstuk 4, konden we hieruit concluderen dat 40–60 % van de conversie ADP naar ATP binnen de druppel plaatsvond.

Het unieke van dit onderzoek was dat we vanuit de data de druppelgrootte en -groeisnelheid hebben kunnen berekenen. Deze groeisnelheid is gekoppeld aan de enzymatische reactiesnelheid, die de snelheid waarmee de verzadiging van ATP behaald wordt bepaalt, en aan de diffusiesnelheid van K_{72} richting de genucleëerde druppels met een overvloed aan ATP. De gemiddelde groeisnelheid van meerdere druppels in een experiment kan worden geïnterpreteerd als "fitheidparameter" om onderscheid tussen twee druppelpopulaties te kunnen maken. Zodoende zagen we dat ATP-K_{72}-druppels met verschillende snelheden groeien onder verschillende omgevingscondities van substraat en aanwezig enzym. Daarnaast werd ook een systeem bestudeerd onder dezelfde condities, maar dan in de aanwezigheid van RNA. Hieruit bleek dat RNA-ATP-K_{72}-coacervaten veel langzamer groeiden dan in de afwezigheid van RNA. Dit effect wordt vermoedelijk veroorzaakt doordat RNA-moleculen ADP zouden kunnen vervangen binnen de druppel, een effect dat we in hoofdstuk 3 besproken hebben. Differentiële groeisnelheden zijn een belangrijk resultaat binnen ons vakgebied nu we ons beginnen te focussen op systemen waarbij we gaan werken met verschillende populaties protocellen. De resultaten in dit hoofdstuk kunnen een mechanisme geven voor protocelgroei en proliferatie voordat gespecialiseerde enzymen bestonden en een competitiecomponent in een pre-Darwin evolutionair scenario.

Finale

Tot slot zullen we in Hoofdstuk 7 onze resultaten integreren om een overzicht te geven van de interessante vragen en antwoorden binnen het vakgebied van actieve coacervaten. We bekeken hoofdstukken 2 en 6 samen, waarbij we de winst benadrukten die te halen

valt uit het controleren van zowel de thermodynamica en de kinetiek rond fasescheiding. We voegden de hoofdstukken 3, 4, en 5 samen onder het paradox van complexe coacervaatpermeabiliteit (een open reactor, maar stabiel tegen Ostwaldrijping). In Hoofdstuk 8 suggereren we enkele mogelijke voortzettingen van ons onderzoek, zoals onderzoek naar de vraag of de groei van druppels kan leiden tot deling en of we door coacervaatdruppels te stabiliseren competitie-experimenten kunnen uitvoeren tussen verschillende coacervaat-systemen. We sluiten het hoofdstuk af met een reflectie op de sociale impact van dit proefschrift.

Sumário

H Á TANTAS COISAS que nós não entendemos sobre a vida. A mais angustiante há de ser a *origem* da vida, uma pergunta em aberto compartilhada pelas três ciências naturais (Biologia, Física e a ciência central, Química). Desenvolver uma hipótese consistente para a aparição das primeiras formas de vida na Terra está aquém dos objetivos de qualquer tese de doutorado; por isso, esta tese (ou esta doutoranda) escolheu uma hipótese existente para explorar sob um novo ângulo. A teoria que escolhemos é a confluência, ao longo de décadas, dos trabalhos independentes de Oparin, Haldane e Bungenberg de Jong: a de que, no oceano primordial, mais e mais moléculas orgânicas se formaram até que aos poucos compostos com a propriedade de se associarem em micro-esferas (coacervados) surgiram; micro-esferas estas que serviam como eficientes frascos de reação, onde mais moléculas complexas puderam se formar, tal que a primeira célula, separada por uma membrana lipídica e contendo ácidos nucleicos e enzimas, pôde emergir. Mas como muitos já notaram antes de nós, coacervados tendem a perder sua integridade por conta de eventos de fusão (com outros coacervados) e *ripening*, ou se dissolverem por completo devido a mudanças de temperatura, pH e força iônica — isto é, não são óbvios candidatos a proto-células na Terra primitiva. Por isso, nós colocamos à prova a hipótese de que coacervados podem exibir propriedades típicas de células — organização espacial e expansão —, e percorremos as seguintes etapas antes de chegar a uma conclusão positiva:

Princípio

No Capítulo 1, nós introduzimos os conceitos de organização e crescimento na forma de compartimentalização e regeneração, em respectivo. Essa base conceitual é importante porque a qualidade de "estar vivo" não tem uma definição unânime na Química. Nós selecionamos na literatura alguns atributos que ajudam a definir vida no âmbito molecular, e explicamos a importância de cada um: compartimentalização e reclusão sendo os primeiros atributos que conferem identidade, organização e proteção às proto-células; em seguida, adaptabilidade e regeneração permitem que a proto-célula sobreviva e se prolifere em um meio-ambiente dinâmico; e por fim, energia, para alimentar o metabolismo e o crescimento das células primitivas e selecionar estruturas dinâmicas, integrando os sete

pilares da vida. Todos estes conceitos podem ser traduzidos em termos químicos como: *a vida precisa de compartimentos compostos por moléculas capazes de se auto-agregar, e de reações químicas que produzem tais moléculas*. Ou ainda, resumidamente, proto-células devem ser compartimentos *ativos*.

Nós exploramos a propriedade de auto-organização de coacervados no Capítulo 2. Lá nós desenvolvemos coacervados compostos de um polipeptídeo (PLL) e adenosina trifosfato (ATP) que podem ser formados e dissolvidos de forma reversível, e também definimos procedimentos experimentais que usamos em outros capítulos desta tese. Para controlar os coacervados, nós usamos um par de enzimas, compatíveis entre si, para produzir e consumir ATP *in situ*. O par de enzimas controla a separação de fase (em coacervados e solução) porque os reagentes têm menor afinidade pela macromolécula PLL do que os produtos, e assim a formação de ATP leva ao processo de *coacervação*. Esse sistema mostrou-se tão regrado que nós pudemos, pela proporção entre todos os componentes, atrasar ou adiantar o momento de separação de fase. Mais ainda, nós pudemos realizar repetir seis ciclos de coacervação/dissolução, mostrando que o controle reacional não compromete a propriedade de auto-organização. Surpreeendemente, o perfil temporal de formação e dissolução dos coacervados pode ser descrito por um modelo linear de turbidez e cinética enzimátican do tipo Michaelis-Menten, ainda que o último nunca tenha sido demonstrado para reações enzimáticas bifásicas.

Intervalo

A percepção de que enzimas estavam operando normalmente mesmo com a formação simultânea de coacervados nos intrigou a tal ponto que decidimos ramificar nossa pesquisa e investigar o enigma da reatividade em coacervados. Essa é uma questão de relevância biológica também: nas últimas décadas várias organelas não membranosas foram descobertas em células eucarióticas, e mais e mais proteínas envolvidas em expressão gênica foram descritas em estruturas similares às gotículas de coacervado. No Capítulo 3 nós aprofundamos nossa introdução às organelas não membranosas e concluímos que para entender sua função, é necessário que nós estudemos o efeito de estruturas similares para a reatividade química de biomoléculas. O melhor modelo para esse estudo são coacervados baseados em peptídeos e nucleotídeos como os do Capítulo 2. Mas para esse propósito, uma quantificação mais precisa de concentrações, constantes de partição e velocidades de reação é crucial, de modo que nós desenvolvemos e testamos um protocolo experimental para tal. Nós descobrimos que as atividades da kinase na presença e na ausência de coacervados de poli-lisina e ATP são comparáveis, a nosso ver devido ao pequeno volume de fase condensada (coacervados) na emulsão, o que mascara seu efeito sobre a reação como um todo.

No Capítulo 4, nós desenvolvemos um modelo teórico para complementar o Capítulo 3: as leis de reação com e sem catálise enzimática e inibição, com o objetivo de determinar condições em que a presença de coacervados pode levar a propriedades únicas. Nós

avaliamos o papel da quantidade de gotículas, da variação em constantes de partição, e da variação das constantes de velocidade em solução e dentro dos coacervados; ademais, encontramos efeitos novos para sistemas bifásicos, como acumulação transiente do produto de reação e supressão de inibição enzimática pela separação espacial dos reagentes. Como demonstração experimental do nosso modelo, nós propusemos acompanhar a hidrólise de ésteres cromogênicos, catalisada por uma lipase, em diferentes coacervados. Obtivemos resultados promissores que reforçam nosso modelo, mas também apontam os desafios experimentais nessa investigação.

Retomada

Retornamos ao objetivo central da tese no Capítulo 5. Nós já sabíamos que o fenômeno *Ostwald ripening* — em que, ao longo do tempo, gotículas grandes crescem às custas do encolhimento de gotículas menores — poderia afetar a estabilidade dos coacervados cujo tamanho pretendíamos monitorar. Ao testarmos a magnitude desse fenômeno como um experimento-controle para o capítulo 6, nos surpreendemos em observar que coacervados complexos são estáveis frente a *ripening*. Empregamos um arranjo experimental e de análise que nos permitiu observar as gotículas por horas (até um dia num caso extremo), sem a interferência de espalhamento ou fusão. Nós explicamos a ausência de *Ostwald ripening* com duas hipóteses: a primeira, de que o processo é energeticamente desfavorecido em coacervados complexos devido à separação de cargas necessária para remover um macro-íon de uma gotícula pequena e transferí-lo para uma gotícula maior. Embora o gradiente de concentração entre os arredores de um coacervado pequeno e um maior favoreça o deslocamento, a força elétrica segue o sentido oposto.

A segunda hipótese é que o fenômeno de *Ostwald ripening* é suprimido pela alta barreira cinética envolvida na remoção de um complexo neutro (de macro-íons de cargas opostas) da gotícula. O complexo neutro, ao contrário de um íon isolado, teria uma alta tensão superficial associada. Além disso, a saída do complexo implicaria em perda de entropia. Ainda não sabemos qual o mecanismo exato, mas nossos resultados dão um forte argumento em favor de coacervados como proto-células, pois a questão da estabilidade era tida como uma de suas maiores fraquezas.

Embasados pelos nossos resultados no Capítulo 2 com o controle via reação, e no Capítulo 5 com a estabilidade dos coacervados, no Capítulo 6 nós desenvolvemos uma proto-célula que cresce ao produzir ATP. A substituição de poli-lisina por uma proteína fluorescente inspirada em elastina, K_{72}, permitiu-nos visualizar a nucleação e crescimento das gotículas de coacervado. Ao contrário de estudos anteriores na literatura, que dependiam da fusão de vesículas ou gotículas para obter crescimento, no nosso sistema é a reação catalisada pela kinase que inequivocamente causa a expansão em volume das gotículas. Nós aplicamos as conclusões do Capítulo 3 e caracterizamos as gotículas, encontrando um alto coeficiente de partição para a proteína K_{72} e a enzima kinase. Como ADP também tem leve preferência pelos coacervados sobre a solução ao redor, nós con-

cluímos a partir do modelo do Capítulo 4 que 40–60 % do precursor é convertido dentro das gotículas.

O diferencial do nosso trabalho é que nós pudemos medir diâmetro e taxa de crescimento de cada gotícula separadamente; o último valor reflete a velocidade de reação, que determina quão rápido a mistura fica supersaturada em ATP, e a velocidade de difusão de K_{72}, recrutada para gotículas com excesso de ATP. A taxa média de crescimento em uma amostra pode ser vista como uma medida da aptidão daquela população de gotículas, e nós exemplificamos esse ideia. Gotículas de ATP-K_{72} crescem a taxas diferentes conforme as condições ambientais de concentração de enzima e substrato; nas mesmas condições, uma população de coacervados que também contém RNA cresce mais devagar do que sem RNA. Isso se deve ao deslocamento de ADP de dentro das gotículas pela presença de RNA, algo que mencionamos na discussão do Capítulo 3. A diferenciação nas taxas de crescimento é um resultado importante na área, que move gradualmente para uma abordagem de "sistemas" em que múltiplos tipos de protocélulas são combinados para obter um comportamento complexo. Os resultados desse capítulo proporcionam um mecanismo para o crescimento e proliferação de protocélulas sem requerer enzimas altamente especializadas, podendo produzir competição num cenário pré-darwiniano.

Final

Por fim, no Capítulo 7, nós integramos nossos resultados ao longo da tese buscando delinear as perguntas e respostas relevantes para o campo de sistemas ativos. Discutimos os Capítulos 2 e 6 juntos, enfatizando a vantagem do controle reacional tanto para a termodinâmica quanto para a cinética da separação de fases líquidas. Depois agrupamos os Capítulos 3, 4 e 5 sob o tema do paradoxo da permeabilidade de coacervados (frascos de reação abertos para os arredores, mas estáveis frente a *ripening*). No Capítulo 8, nós sugerimos direções para continuar este nosso trabalho, como aprimorar o controle do crescimento das gotículas para obter divisão espontânea, e aprimorar sua estabilidade para permitir experimentos com populações mistas. Concluímos a tese com uma breve reflexão sobre o impacto social do nosso tema de pesquisa.

Part I

Foundation

Chapter 1

General introduction
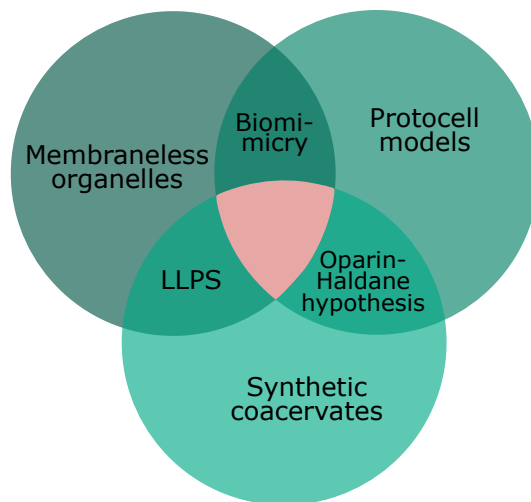
Ex omnibus aliquid, ex toto nihil
A little bit of everything, in nothing complete

1.1   Why, what and how

I will introduce this thesis the way I was, myself, introduced to it. It starts with the chemical quest for the origin of life, something that puzzled me since my undergraduate studies. You see, the origin of life is an open question in science, and one of the few that chemists can join in. That of course motivated me to pursue this research topic all the way from Brazil to the Netherlands, where origin of life and artificial cell research are boiling.

When trying to understand how an inanimate system on early Earth transitioned to something that can be called 'alive', many questions arise: what can be called 'alive'? Can we truly ever know what happened on early Earth? What if it was a one-time, random event? What if our sample size of life is just too small to conclude anything? Many times I was caught in such digressions, before realizing it is perfectly possible to carry on research without a definitive answer (though the reflection is very enriching, even for a hard sciences mind).

The strategy to tackle these open questions, taken by thousands of chemists like me, is to come up with a simplified version of life as we know it: a chemical model, simple enough to be plausible on early Earth and complex enough to resemble life. Again, choices had to be made: *plausibly simple* means that it cannot rely solely on highly specialized biomolecules present in modern cells, in the exact role they have now, because those likely took millions of years to evolve. And instead of using an inorganic or small molecules-framework, I am interested in classes of compounds that make sense as precursors of modern biomolecules. By *lively complex* I mean that it must display some dynamic behavior, such as growth, replication, division. There are many other features that are hallmarks of life (processing of information, dissipation of energy), but behavioural ones are just less controversial and easier to demonstrate. Growth, division, motility can be captured with a microscope, while the ability to process information may require the definition of 'processing' and 'information', both of which can yield pages of discussion.

The next step on my journey was to decide on a chemical model to use — I will call it protocell[i] from now on. With the previous conceptual choices in mind, I needed a well-defined protocell, that is, a compartment suitable for chemical reactions, accessible to be supplied with nutrients, and compatible with the requirements of growth and replication. One of the hypotheses for the origin of life, developed by Oparin and Haldane independently in the 1920s, describes such a compartment: the first cells were like garbage bags in a soup of prebiotic molecules. As short peptides, nucleosides and small sugars started to accumulate in the soup, the garbage bags became micro-reactors where reactions like condensation and replication could happen. Haldane borrowed a then-recent term from physical-chemistry and named the garbage bags *coacervates*. This hypotheses seemed

---

[i]The term may refer to a model for the historic precursor of modern cells, as well as a synthetic prototype for life.

like the perfect compromise between complexity and simplicity, the sweet spot for origin of life research.

As the name suggests, there are chemical systems quite close to such compartments, and the group I joined at Radboud University — the SpruijtLab — is specialized in them. Coacervates are a type of liquid, like oils. But *unlike* oils, they are still aqueous. Under certain conditions, soluble macromolecules interact more strongly with each other and separate as their own liquid phase (coacervate), dense and polymer rich. The process starts by nucleating droplets of coacervate, which are micrometre-sized compartments compatible with the requirements for a protocell. For chemical systems at equilibrium, phase separation is a well-known spontaneous process, described by classic thermodynamics. For systems where there is an ongoing reaction, or out of equilibrium, the kinetics and thermodynamics of phase separation are less well understood. That would have sufficed to carry on four years of research already. But at this point I also learned about membrane-less liquid organelles — about 10 years after the scientific world learned about them —, which confirmed I was in a good direction.

Membrane-less liquid organelles were discovered in 2009; before that, only membrane-bound organelles (Golgi complex, mitochondria), or specific cases of granular organelles (P-granules, proteasome) were known. Most of the latter have, by now, been shown to form through liquid-liquid phase separation. It is fascinating that a complex cell would rely on such a simple principle, and it reinforces coacervate droplets as candidates for primitive cells. In fact, many liquid organelles seem to have a vital composition of nucleic acids and proteins, a mixture that, *in vitro*, can form coacervates too. When you take on a project that considers that coacervation could have started cells on early Earth, it is at least reassuring to find the principles of coacervation in modern cells.

To come full circle, the father of coacervation studies was Dutch chemist Hendrik Bungenberg de Jong, under the supervision of Hugo Kruyt. A former biology student, de Jong already hinted at the prebiotic role of coacervate droplets in a paper from 1929. However, his idea and also the Oparin-Haldane hypothesis seem to have been forgotten for a while. The scientific community was focusing on other chemical models, like vesicles, and other prebiotic puzzles, such as the enzyme-free synthesis of biomolecules. But with the rise of liquid organelles, coacervates were back in the game. They bring additional advantages too: vesicles require phospholipids, molecules that are unlikely to have formed early on the timeline of life. Coacervates can have diverse compositions, including random polypeptides, that are slightly more prebiotically plausible. When the droplets form, other molecules in the surroundings with affinity for the scaffold will accumulate inside, and that can be a game-changing step for challenging prebiotic reactions. Most importantly, the content of coacervate droplets directly relates to their size, providing a strategy to achieve a growing protocell.

This is how I ended up interested the chemistry of active coacervate droplets. I will now go into more detail about each of the steps I described: first, an overview of origin

of life research. Secondly, I will describe the range of chemical models developed to study cells, and the limitations they pose to compartmentalization and growth. I will then describe coacervates and the connections with liquid organelles in the cell, to ultimately make a case for them as protocell models.
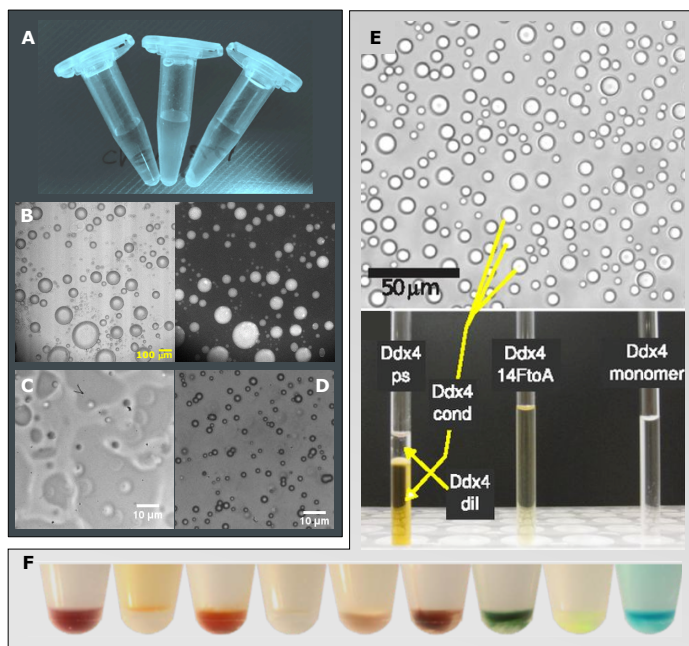
Figure 1.1: A glimpse at coacervates. (A) From left to right: flask containing a homogeneous, clear solution; dispersed coacervate droplets make a mixture turbid; given some time, coacervate droplets fuse and make up the small pellet at the bottom, with a dilute phase floating on top. (B) Coacervate droplets under the microscope - on the right, with a fluorescent dye that has affinity for the droplets. (C) Coacervates droplets can spread on glass surfaces, highlighting their liquid property. (D) Some coacervates have a more gel-like appearance and droplets fuse slowly, remaining rather small. (E) Coacervate droplets of protein Ddx4 under the microscope (top) and coalesced as a distinct liquid phase in the NMR tube (bottom). Images from ref. 1. (F) Lower section of coacervate mixtures containing dyes that were allowed to sit long enough to separate in two clear phases. The bottom phase is the coacervate phase, concentrated in dye as indicated by the strong color. Image from supporting information in ref. 2.

1.2 Some defining features of life

The origin of life is one of the biggest open questions in science today. Molecular biology has achieved an incredibly detailed understanding of the evolution of life on Earth, even providing insights into a presumed last universal common ancestor.[3] However, there is

still a large blind spot that biology alone cannot access: what sequence of events bridged non-living matter to the first life forms? Or, as formulated by Nobel laureate Jack Szostak, how did Chemistry make the transition to Biology? Although the relevance of a chemical perspective had already been noticed in the 1920s by Aleksandr Oparin and John Haldane, only recently chemists truly joined the quest. Bringing together organic, supramolecular and physical chemical tools has enriched and widened the debate: can we reproduce the emergence of a living system in the lab — the way it most likely happened 4, 4.5 billion years ago, or in any way at all?

The first instinct is to start answering these questions by defining life. However, as many philosophers and scientists — Aristotle, Oparin, Feynman — have put it, understanding the nature of life is conditional to understanding how life originates/originated. Therefore, before we know which set of conditions is sufficient for the emergence of living systems, we cannot define life. [4] Instead, we can debate around a list of life-like characteristics that appear to be shared by all living forms and can be expected to be present from the start: **compartmentalization, seclusion, improvisation, energy, adaptability, program and regeneration**. [5,6] I will summarize the seven pillars of life proposed by Koshland Jr. (Figure 1.2), as a starting point to discuss the strong points of different models used to investigate the principles of life.

The requirement of **compartmentalization** derives from the fact that all life known is cellular, but it is sometimes criticized for its narrow conception of what life can be. I would argue that, regardless of what the compartment looks like, the properties brought by compartmentalization are unmatched: even a so called living network of kinetically trapped molecules won't survive dilution and decomposition without the protection of a compartment. A compartment does not need a defined boundary, and there are hypotheses for how spatial or temporal organization can be achieved by thermal gradients or on solid surfaces. A similar requirement is that of **seclusion**, which is needed to separate living units from each other — e.g. two conflicting reaction pathways, protocell and parasitic populations, two different species that diverged. Seclusion can be a consequence of compartmentalization over millions of years of evolution, as molecules such as enzymes gained specificity. A different term for seclusion can be pattern formation, which is seen already in prokaryotes with bacterial division, and is an important mechanism to achieve functional configurations. [7]

Koshland Jr. also includes the requirements of a program and the abilities to improvise and adapt. The need for a **program** derives from our observations of extant life: all living organisms rely on genetic material (DNA or RNA) to assure their composition over time and over generations. Improvisation and adaptability are necessary because of the changing environmental conditions on Earth. **Adaptability** refers to being able to instantly respond to an environmental change and recover to an original state, which at the molecular level can be linked to feedback and feedforward mechanisms. **Improvisation** refers to the ability to change the program in such a way that it allows for better adaptive

The seven pillars of life
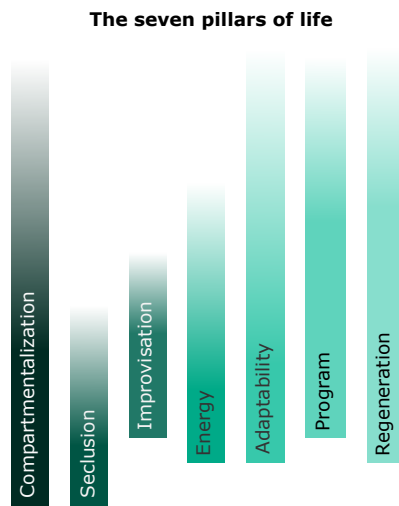
Figure 1.2: Features necessary and sufficient for life, figure based on the text of reference 5. I represent pillars that were important from emergence to extant life higher than pillars that gradually lost their critical role. For example, while seclusion may have been crucial at first, the specialization of enzymes over time allows different pathways to be mixed without loss of accuracy. Compartmentalization must be achieved prior to or at least simultaneously with all other living properties (and all life known is cell-based), or even a self-sustaining, regenerating chemical system with a program would have to rely/protect from diffusion across large volumes of diluted solutions.

responses, such as a genetic mutation.

Lastly, the pillars of regeneration and energy are the most relatable for chemists and physicists. **Regeneration** is, for Koshland, the replenishing or replacement of building blocks, as they get depleted or exhausted. Regeneration includes self-assembly, proof-reading and also the full refurnishing that takes place during replication. Like adaptability and improvisation, regeneration seems to conflict with the requirements of compartmentalization and a program. However, Jeremy England proposes that this precise balance between integrity and dynamicity is unique to living systems and is achieved by the way life absorbs and processes **energy**, the last pillar.[8] The building blocks of all living units are able to absorb energy without falling apart or without decaying to an equilibrium state, even though most building blocks are already quite high in energy.

1.3   A long standing question for chemistry

Not agreeing on a definition of life has not stopped biologists and chemists from making progress on models of life that satisfy at least one of the seven pillars, while being consistent with what we know of early Earth. The quest for the origin of life in western

science started in the 18th century, in the realm of Biology. Before that, we can cite the philosophical efforts in defining life by its causes and purposes (Aristotle) and whether it could be reduced to physical principles (Descartes). [4] With the advent of the microscope and Hooke's observation of cells, the overwhelmingly open question *How did life emerge?* was narrowed down to *How did cells emerge?* and *Is it happening right now under our eyes?* **Abiogenesis**, or the spontaneous generation of life from inanimate, organic matter, became a two-centuries long debate, famously disproved by Pasteur with a sterile, controlled experimental setup.

Naturally, the demonstration that life does not emerge spontaneously reinforced the question: so how did the first life forms emerge? Can it happen again, as long as a specific sequence of rare events can be reproduced? In the 1920s, Oparin and Haldane almost simultaneously suggested that the origin of life was actually the result of a continuous sequence of chemical events. Under a reducing atmosphere and with the sun as an energy source, the primitive ocean would have been a very diluted reaction mixture of small organic molecules. Eventually, larger polymeric molecules could have accumulated and assembled together into microspheres, which Oparin would later refer to as **coacervates**. These would have provided the proper environment for more complex molecules with replication functions to form and persist. [9,10]

The Oparin-Haldane theory was contemporary to Bungenberg de Jong's study on lyophilic colloids, in which he coined the term coacervation for the separation of an aqueous mixture in two phases: a dilute phase depleted of the colloid, and a dense phase organized as liquid droplets and highly concentrated in the colloid (coacervate phase). [11] Bungenberg de Jong also pointed out that coacervate droplets were very similar to the cytoplasm in appearance and their liquid-like nature, and as he observed the droplets had the tendency to take up material from the surroundings, he hypothesized they could have biological relevance as functional compartments or a type of protoplasm. Together with the Miller-Urey experiment's demonstration that aminoacids can be obtained from inorganic precursors, the **coacervate theory** reinforced the contributions of chemistry for the origin of life puzzle. However, it failed to explain the membrane barrier that all cells use to separate themselves from the environment and that eukaryotic cells further exploit to compartmentalize their interior. [12]

Several other theories appeared during the 20th century, as can be seen in Figure 1.3. A peptide-world scenario hypothesis, derived from the Oparin-Haldane theory, was developed as Fox and Harada obtained non-enzymatic synthesis of oligopeptides that could organize as microspheres. [13] Analogous theories appeared, [14] replacing the role of peptides as first functional biomolecules with lipids (Morowitz and Deamer, ref. 15, Luisi, ref. 16) or replicators (Orgel, ref. 17). Szostack's group performed non-enzymatic RNA replication, an argument in favour of RNA emergence prior to proteins, [18] and later successfully included it in a lipid vesicle, [19] an example of an increasing preference for integrative approaches in the field.
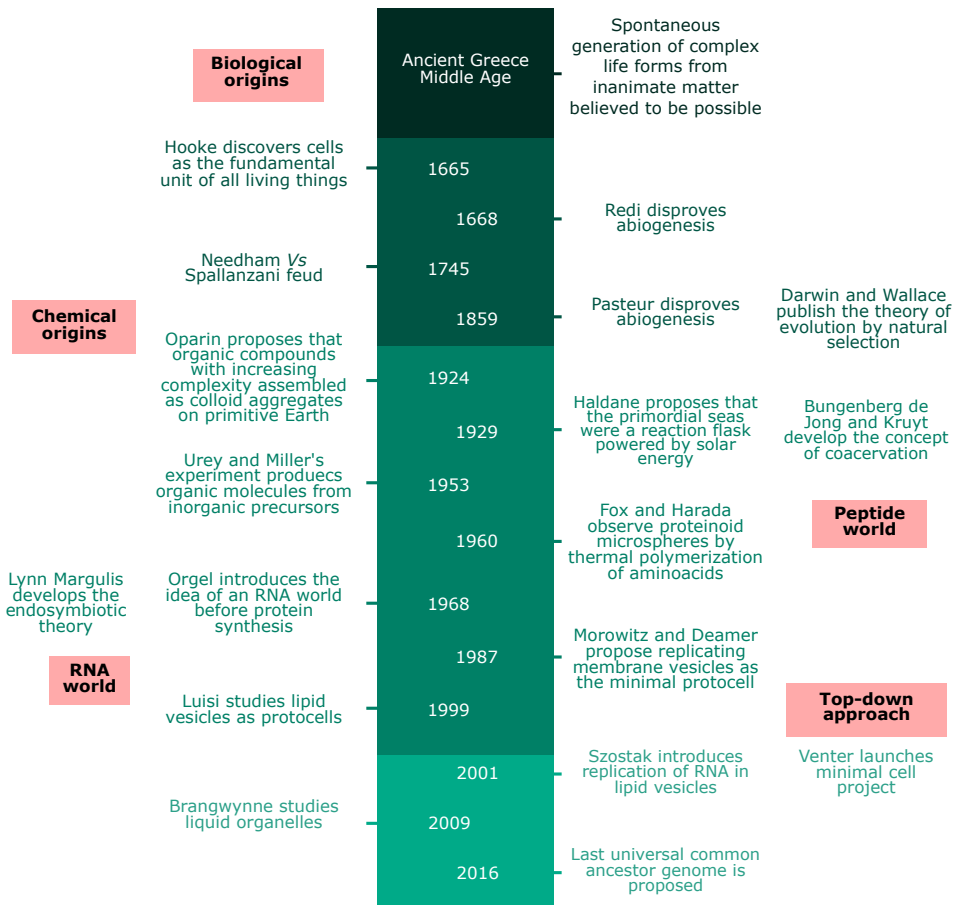
Figure 1.3: Timeline of origin of life research milestones relevant for this thesis.

The aforementioned hypotheses fit within a **bottom-up approach** in tackling the origin of life: deciding the minimal elements and putting them to proof in the test tube. A very distinct framework is the **top-down approach**, a consequence of an idea introduced in the late 1990s: all living organisms can be traced back to a single LUCA.[20] This ancestor would be the embodiment of the minimal requirements for life as we know it — which does not explain the emergence of life or the principles of a broader idea of life, but of course sheds light into the question, in a similar manner as endosymbiotic theory explained the origin of eukaryotes.[21] The existence of the LUCA motivated an effort to achieve a minimal cell by knocking out genes (Venter, ref. 22). However, as the LUCA might be millions of years away from the emergence of life (the *first universal common ancestor*),[23] this is not the preferred approach on this thesis.

Overall, enormous progress has been made: models for compartments that can be

obtained in the lab have been established, strategies to obtain dynamic behavior through chemical (dynamic covalent chemistry, self-assembly, the systems approach) or biochemical (cell-free gene expression) tools were developed along the way. Some of the life-defining pillars have been separately demonstrated with pure chemistry: oscillating enzymatic reaction networks that mimic metabolism and homeostasis;[24] dynamic combinatorial libraries of self-assembling peptides that self-replicate and diversify in composition over time;[25] and oil droplets with autonomous behavior.[26] In most cases where a strikingly life-like property is shown, there is a compromise of the plausibility of such a system on early Earth, although principles can still be derived. This compromise is reasonable, as any hypothesis about the first form of life, or cells, relies heavily on hypotheses about early Earth conditions that cannot be proved.

The research described in this thesis was designed in the context of the timeline in Figure 1.3. The most influential entries are the Oparin-Haldane hypothesis and the contemporary theory of coacervation. Out of the seven pillars used to discuss a definition of life, this thesis focus on the compartmentalization, seclusion and regeneration aspects; specifically, the final goal in this thesis is to obtain cell-like compartments that can absorb nutrients and grow in response. One of the reasons why I went back to the Haldane-Oparin hypothesis is related to an entry in the timeline that I did not mention yet: **droplet organelles**.
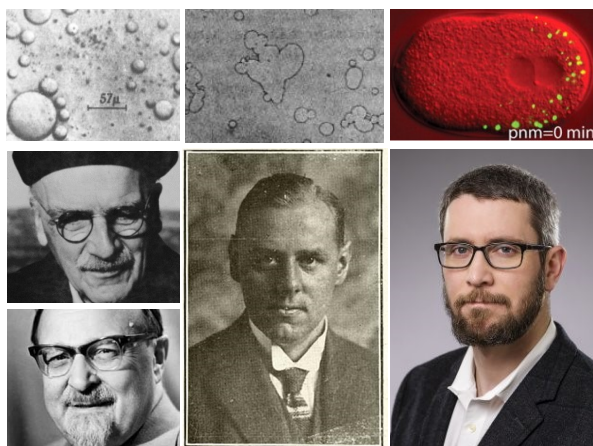
Figure 1.4: In order: J. B. S. Haldane and A. I. Oparin, with a depiction of the protocells they called coacervates; H. G. Bungenberg de Jong with a micrograph of albumin/gum arabic coacervates;[11] and C. P. Brangwynne next to P granules (in green) in C. elegans cells.[27]

1.4   Droplet organelles

Organization is a central theme in life across scales — from herds to individual organisms to cells —, and can be temporal or spatial.[28] Temporal organization is seen in the regulated changes living systems undergo over time: the circadian rhythm, the checkpoints in cell cycle that dictate division, and aging makers such as telomeres and methylated histones. Spatial organization *is* compartmentalization and seclusion, two pillars of life in our discussion. Most cellular processes cannot be fully understood without taking into account the **spatial distribution** of molecules in the cell. In eukaryotes, whose size makes visualization technically easier, subcompartments (organelles) encased by a lipid membrane are key organizing elements, even occupying a large fraction of the cellular volume.[29]

Nomenclature

Membraneless and liquid-like organelles are not synonyms, but are often used interchangeably in literature. We will also use membraneless-, membrane-free-, liquid- and droplet- organelles hereafter. Adding to the list of terms, we use condensates and biocondensates for structures that have not been unambiguously described as liquids.[30]

More and more organelles that lack a membrane have been identified in eukaryotic cells. The term membrane-free or **membraneless organelles (MLOs)** refers to a wide variety of subcellular bodies that lack a lipid boundary, with sizes in the order of 0.01–10 μm. Nuclear organelles often lack a membrane, such as the nucleolus,[31] Cajal bodies and paraspeckles.[32] Importantly, some nuclear membraneless structures are linked to the precious process of gene regulation, e.g. the unnamed transcriptional **condensates** that concentrate the transcription apparatus at super-enhancer regions,[33] and co-localize key elements such as RNA polymerase II and the mediator complex.[34] In the cytoplasm, processing bodies and stress granules,[35] and in the chloroplast of algae, the pyrenoid,[36] all lack any boundary. Some subcellular compartments lack a lipid boundary, but instead have a protein shell encasing (carboxysomes in prokaryotes),[37] or have properties closer to crystals (such as the proteasome)[38].

However, nucleoli, Cajal bodies, paraspeckles, stress granules, processing bodies additionally share other distinctive features: they are spherical, deform in flow and show wetting, dripping and fusion, and therefore can be described as **liquid-like**. This brings me back to the origin of life research timeline: the first organelle identified as a liquid droplet were *C. elegans* germline P granules, by Clifford Brangwynne and co-workers, in the group of Anthony Hyman in 2009.[27]

The liquid property is remarkable in itself: that protein- and RNA-rich droplets exist in the cell as a consequence of liquid-liquid phase separation. Unlike *conventional* organelles, not all membrane-free organelles are constitutively present, but rather assemble in response to the cell cycle state or to oxidative stress.[40–42] The **dynamicity** is an essential property of droplet organelles, and what makes them interesting for origin of life theories: if eukaryotic cells now contain droplets in their cytosol and nucleus that can
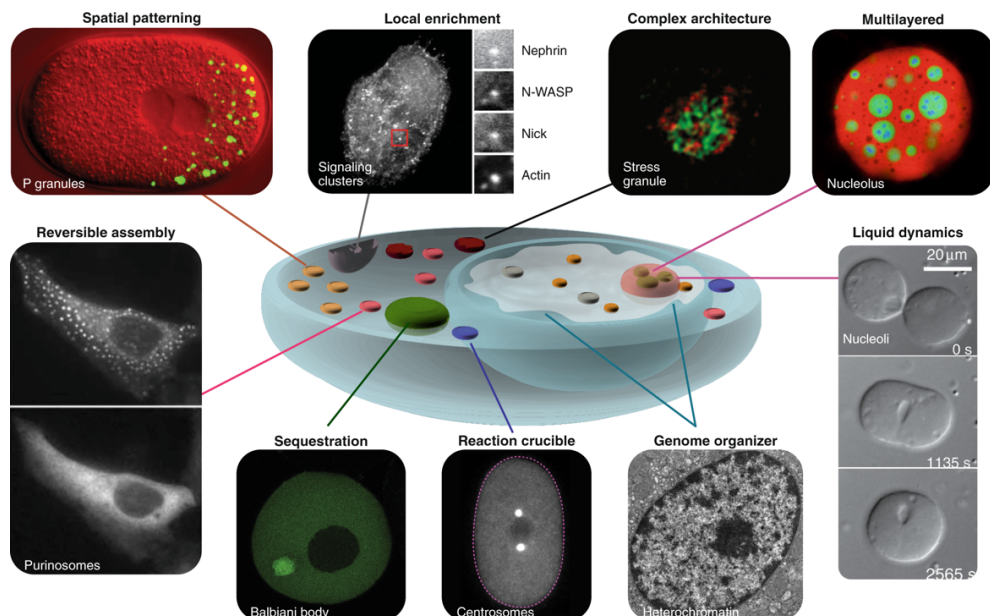
Figure 1.5: Collection of membraneless organelles with liquid properties and the proposed functions, image from reference 39.

assemble spontaneously, compartmentalize and seclude biomolecules, such droplets make excellent candidates for primitive cells. I do not mean that the first cell was a droplet of RNA and G3PB1 protein, but rather that it relied on similar principles to droplet organelles.

In physical chemical terms, droplet organelles can be called coacervates. The connection is not always made, and some papers about membraneless organelles assembly and regulation prefer to use the broader term of liquid-liquid phase separation (LLPS) — but even then there are exceptions that separate it from scaffolding and bridging.[43] However, this is more of a cautious approach; when a full characterization of droplet organelles is performed, viscosity, electric permittivity and density are often remarkably similar to that of coacervates, although is is true that time of coalescence and surface tension can differ widely.[44] In terms of composition, MLOs bear similarity with simple (single-component) and complex (two-components) coacervates.[ii] In general, each droplet organelle known is enriched in a particular set of proteins, many of which contain intrinsically disordered regions (IDRs) and charged patterns. Nucleic acids also frequently take part in MLO assembly, or are taken up in already formed organelles. Multiple weak interactions between blocks of charged or aromatic residues, or between specific binding domains drive the condensation,[12] all principles known to regulate coacervation.

[ii]This is a simplification, as described later in this chapter.

The link between membraneless organelles, coacervates, and Oparin-Haldane protocells enriches all three fields: we can take inspiration from extant cells to build dynamic protocells and we can use our knowledge of coacervation to investigate the implications of this new understanding of the cell, ripe with condensates. There are several indications that condensates may help filling a blind spot in our knowledge of cellular chemistry — how multimolecular, multiprotein processes such as transcription and translation achieve high rates of efficiency.[30] The central dogma of biology has been intensely studied over decades, more recently in the context of macromolecular crowding and confinement,[45] but still not taking into account these membraneless structures. Where we cannot accurately describe all MLOs as coacervates, we can at least defend their use as *in vitro* models to further understand cellular chemistry, and moreover, we can make a case for coacervates as as the ultimate biomimetic model: **protocells**.

1.5 Coacervates as protocells

Coacervates are dense liquid droplets composed of macromolecules that separate from the dilute phase through liquid-liquid phase separation either by segregation or association.[46] Simple coacervates are formed by maximizing favorable interactions between identical macromolecules (often polymers or proteins), thereby minimizing polymer-solvent interactions (*segregative*); complex coacervates are formed by maximizing favorable interactions between different types of macromolecules (*associative*), such as polyelectrolytes of opposite charge. In either case, de-mixing produces droplets enriched in macromolecules that resemble the compartmentalized and crowded environment proposed for protocells by Oparin and Haldane (Figure 1.4).

More than resonating with the Oparin-Haldane theory, coacervates have several chemical attributes consistent with the *pillars of life* we previously discussed. Coacervates assemble spontaneously and reversibly, and freely exchange material with the surroundings,[47] with the equilibrium position determined by **dynamic interactions** — some solutes accumulate inside the droplets, while others are overall excluded. The concentration of solutes supports the existence of crowded protocells before transport proteins or efficient enzymes came about, and can explain the preference for larger molecules. The dynamicity satisfies the pillars of adaptability and regeneration, as the droplets can **interact and respond** to their environment. Moreover, the absence of a boundary removes the limitations for the protocell to grow; in fact, molecules in coacervate droplets are bound to a partitioning equilibrium constant, and therefore any change in concentration comes with a change in size.

Dynamicity, permeability and prebiotic consistency may seem simple, but they are the main hurdles being addressed by the origin of life and protocell research community. Compartments proposed as alternatives have been colloidosomes,[48] proteinosomes,[49] and polyelectrolyte capsules.[50], but all the latter lack prebiotic consistency. Among works
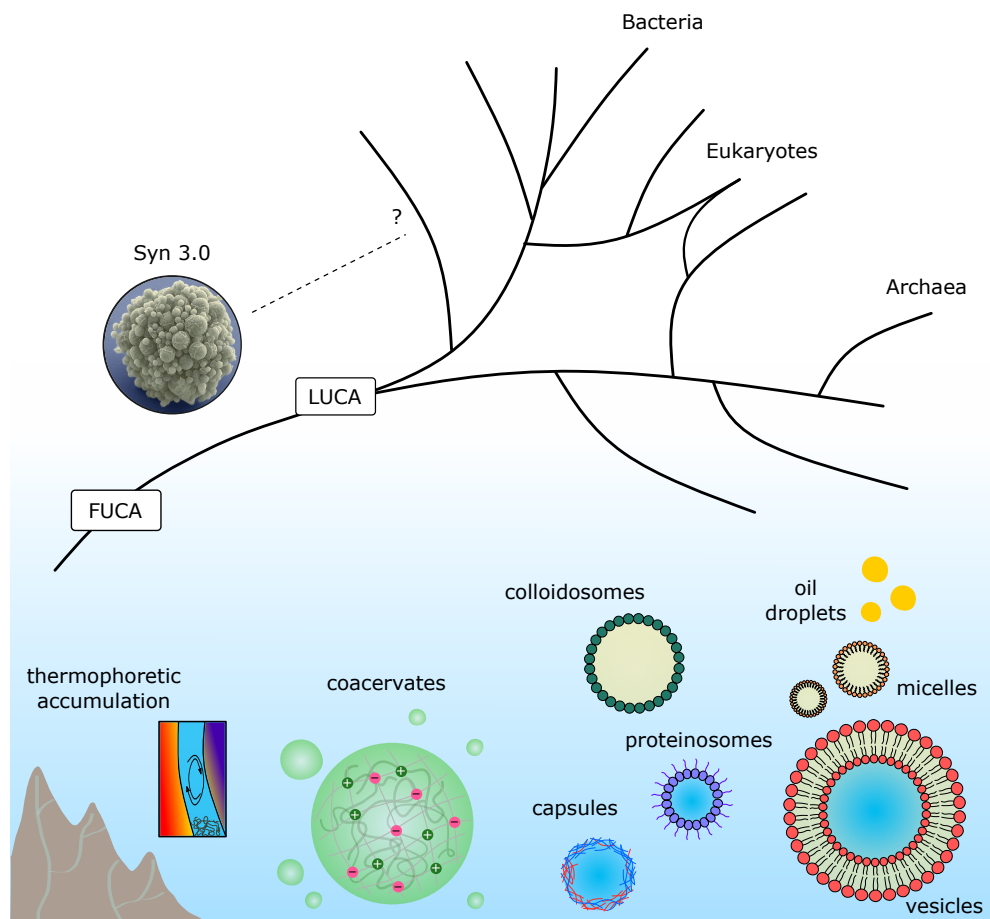
Figure 1.6: Top: a scheme of the tree of life; the search for the last universal common ancestor (LUCA) aims to find a minimal cell, which might differ from the first universal common ancestor (FUCA). The minimal cell Syn 3.0 inserts somewhere in between the tree. Bottom: models for the first cells to emerge. Temperature gradients in porous rocks produce thermal convection and can lead to accumulation of macromolecules, a form of pseudo-compartmentalization; coacervate droplets are membraneless, crowded and kept by dynamic interactions such as electrostatic attraction; proteinosomes, coloidosomes and capsules are based on polymers or proteins like coacervates, but have a defined interface; lipid-based protocells resemble cells and have a protective membrane. The gaps between protocells, the FUCA, the LUCA and the minimal cell are all unknown. *Illustrative depiction, not to scale.*

that use lipid-bound protocells, new promising approaches appeared: Bonfio *et al* used a more integrative approach (typical of systems chemistry), starting with prebiotically plausible fatty acids instead of phospholipids, and relying on prebiotic chemistry to incorporate functionality in the membrane.[51] A more extreme solution is the dismissal of

a compartment: temperature gradients (established in between walls of porous rocks for example) can drive convective currents that trap longer molecules at the bottom of the pore (Figure 1.6). [52,53]

But coacervates bring yet another undeniable advantage: the range of building blocks available. Coacervation may seem like a rare phenomenon at first, but it is actually **widespread** in chemistry. Examples are combinations of synthetic polyelectrolytes, [46,54] polysaccharides[55] and peptides, [56] or individual single-stranded nucleic acids[57,58] and partially disordered proteins that are purified from MLOs in cells. [59,60] Although coacervation relies on multivalent interactions, it is surprisingly observed with rather small molecules: Koga *et al* showed that oligo-lysine (of 5-24 monomer units) can phase separate with ADP, and Cakmak *et al* lowered this limit to monodisperse $(Lys)_{10}$ and ADP, that can barely be considered polymers. [2,61] Zhou *et al* recently developed single, low molecular weight surfactant-based condensates with a sponge-like structure[62] and Dr. Manzar Abbas' work in our group showed that bridged dipeptides are also suitable candidates. [63] Small molecule coacervates are the most attractive for prebiotic chemistry, although the window of conditions where coacervation happens may be narrower for them — which is probably why we don't see coacervate droplets even more often.

Because of the properties described, a system of interacting, (relatively) low molecular weight molecules, secluded at high concentration in a coacervate droplet could gradually **evolve** to produce more complex molecules (e.g. membrane molecules and cell division proteins); [10] and while doing so, display behaviors that define the transition from chemistry to biology: growth, division (regeneration), motility (adaptability), metabolism (energy). In this thesis, we take a particular focus on **growth**.

1.6 The need for active coacervates

For lipid-based protocells, growth has been achieved through an external supply of fatty acids, of fatty acids precursors that are converted in solution. [64,65] These can either be incorporated into the membranes leading to larger vesicles that fragment upon extrusion, or can form new vesicles that fuse to the pre-existing ones. Although fusion has been a common strategy, [66,67] it is actually opposite of the mechanism natural cells use to grow. The integration of lipid compartments to other pillars of life — such as implementing RNA replication inside vesicles — faces significant difficulties, mainly because both ribozyme and non-enzymatic RNA copying require Mg^{2+} concentrations high enough to disassemble vesicles. [68] Also, these protocells lack the transporting system to allow the uptake of nutrients and precursors and the supply of membrane material is not connected to RNA production — unlike natural cells, that grow mainly as a result of increase in internal protein synthesis.

A closer analogy to cellular growth was achieved via a self-reproducing system of oil droplets, sustained by an auto-catalytic imine formation reaction. [69] Although the study

employed unusual molecules for protocell applications — octylaniline and an aldehyde bearing an imidazolium moiety —, the principle behind it can serve as inspiration. In addition to catalyzing its own formation, the imine is amphiphilic, which helps recruiting more octyaniline into the droplets. The authors observe growth and division for three generations of droplets. Our main inspiration, however, comes from a theoretical prediction. The groups of Hyman and Julicher found that the growth and division of **active droplets** can serve as a model for protocells.[70,71]

Reaction-driven growing and dividing droplets are doing something other than reaching equilibrium, and for that they fall into the category of **active systems**. In the context of droplets, equilibrium behavior includes: nucleation, diffusion-limited growth, Brownian motion coalescence (fusion) and diffusion-limited coarsening (Ostwald ripening). Droplets that only undergo these processes are called **passive**, implying that the number of phase-separating particles is conserved.[72] The key structural aspect that distinguishes passive and active droplets is the presence of a chemical reaction producing droplet material.
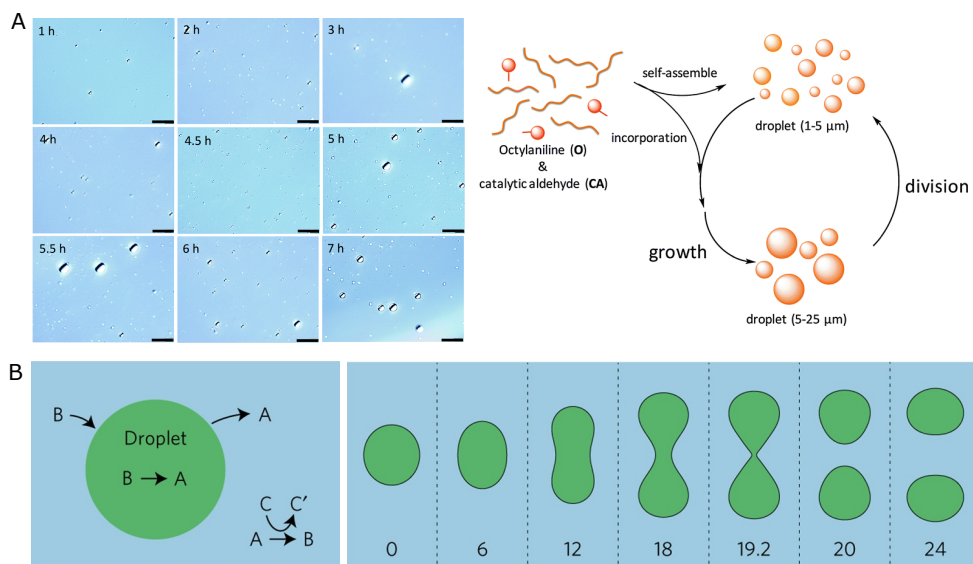
Figure 1.7: (A) Self-reproducing system of oil droplets sustained by an auto-catalytic imine formation reaction between octylaniline and an aldehyde. The oil droplets grow and transform into vesicles as the amphiphilic imine is formed. Figures from ref. 69. (B) Theoretical model of a growing and dividing liquid droplet, sustained by a chemical reaction. Schemes from ref. 71.

Consider a water-soluble precursor **A** and a molecule capable of self-assembly **B**. In the absence of a reaction, this is what we call a *passive* emulsion. Starting with multiple droplets, only droplets with a radius larger than a critical value will grow, by taking up material from the smaller ones (Ostwald ripening). Thus, in the long run, at most one large droplet is stable. But if **A** can be converted to **B** by a chemical reaction **A** → **B**,

the droplets are **active**. An external supply of a fuel assuring **A** → **B** does not reach equilibrium leads to a net flux of **B** towards the droplets. As a result, all nucleated droplets can grow until the net flux is zero, which will occur at different droplet sizes depending on reaction rates. At this critical size, multiple droplets are stable and Ostwald ripening can be suppressed. If supersaturation of the surrounding solution continues to increase, the droplet reaches a shape instability and undergoes elongation and fission in two daughter-droplets.

The theoretical and experimental examples given are extremely interesting because they suggest that a proto-metabolism (chemical reaction) combined with a compartment (droplet) inevitably leads to growth and division, thus integrating multiple pillars of life. Furthermore, suppression of Ostwald ripening under specific kinetic conditions may help to understand the fact that several liquid droplets can co-exist inside the cell (liquid organelles) without fusing. The function of centrosomes, for example, depends on both of them being equally sized and stable throughout mitosis. Now that my choice for coacervate-based protocells is clear and justified, it is time to properly define coacervation and the chemistry behind it, before moving to the main chapters of the thesis.

1.7 Fundamentals of coacervation

Portuguese-speakers will recognize the latin stem 'acervus' (*acervo*), which means collection. It is not clear if the term was used before Bungenberg de Jong, but coacervation therefore means to come together as a collection. In physico-chemical terms, a coacervate is the dense phase of a lyophilic[iii] colloid after LLPS. Coacervation can be described as a partial desolvation process[iv], as a result of either a change in solvent quality (**simple coacervation**) or the neutralisation of charged groups by oppositely charged species (**complex coacervation**).[73] When LLPS takes place in the binodal region (via nucleation-growth), the coacervate is an ensemble of dispersed microscopic droplets, which are sometimes referred to as microcoacervates. The coacervate phase is enriched in the solute — which is a macromolecule (polymers, proteins, polysaccharides) or a macromolecular structure (micelles, nanoparticles), but remains an aqueous phase. In fact, for some coacervates, the water content can range from 60 to 85%.[54]

Complex coacervates are composed of oppositely charged polyelectrolytes or macro-ions. The stability of most complex coacervates is a strong function of the charge density and overall charge of the oppositely charged components and the salt concentration of the medium.[76] Small ions have a destabilising effect on complex coacervates by competing for ion pair formation, and the concentration at which this competition leads to dissolution of droplets or macroscopic phases normally increases with increasing size and charge density

---

[iii]as opposed to lyophobic colloids, which are unstable and without agitation, collapse into solid aggregates and a liquid phase.

[iv]in contrast to full desolvation, the case of water and oil, for example.
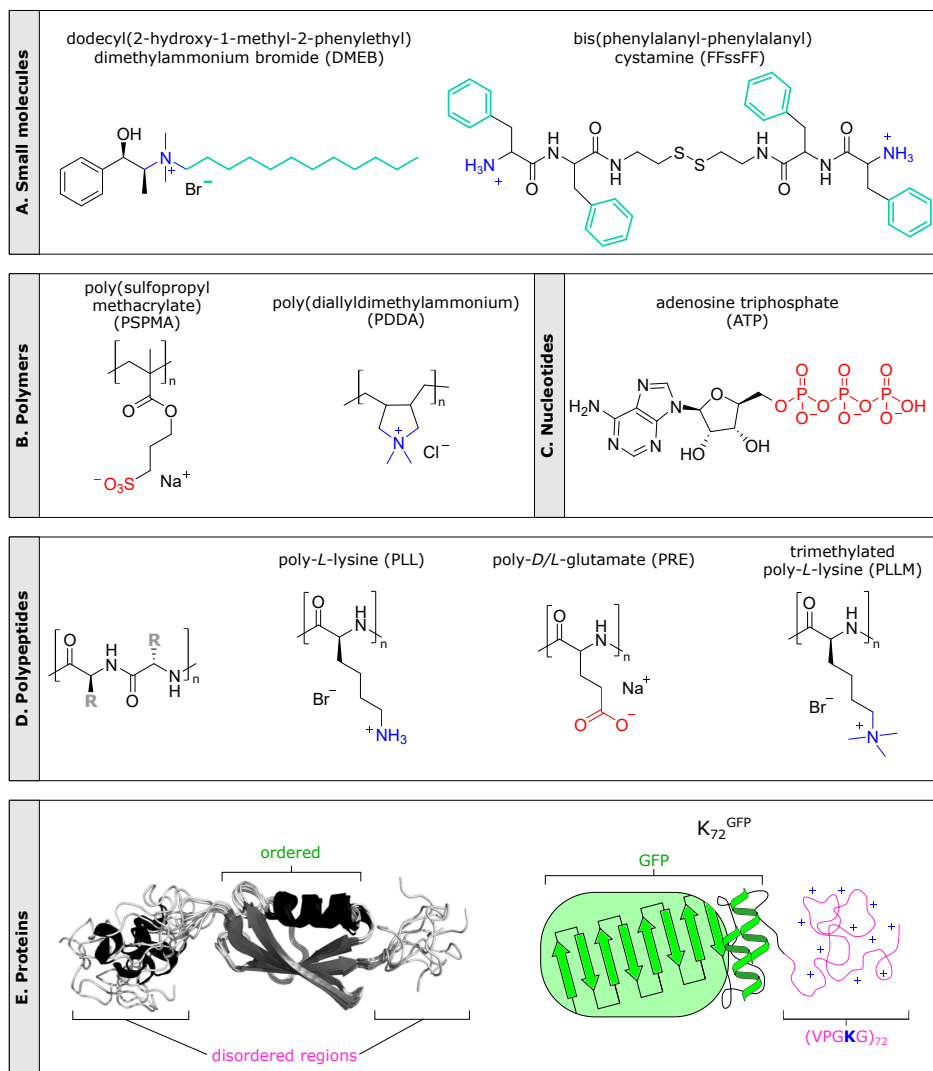
Figure 1.8: Molecular structures that can form coacervates, including compounds used in this thesis. (A) Small molecules that form simple (homotypic) coacervates normally contain flexible chains and hydrophobic groups (light blue). We show DMEB coacervates in Chapter 4. (B) Synthetic polymers with charged groups (cationic: blue, anionic: red). PSPMA-PDDA coacervates are present in Chapter 5. (C) A nucleoside triphosphate cannot be called a polyelectrolyte, but its multivalency allows it to form complex coacervates with oppositely charged polymers (e.g. with PLL, as in Chapter 2). (D) Polypeptides with charged residues (the pair PRE-PLLM was used in Chapter 4). (E) Proteins with disordered regions (in pink); the order/disorder scheme is from ref. 74 and schematic K_{72} is based on ref. 75. ATP-K_{72} droplets are the core of Chapter 6.

of the charged species.[76,77]

$$\Delta_{\text{mix}}G = \Delta_{\text{mix}}H - T\Delta_{\text{mix}}S$$

$$\Delta_{\text{mix}}G = \Delta_{\text{mix}}H + k_B T \left[\frac{\phi}{N} \ln \phi + (1 - \phi) \ln(1 - \phi) \right]$$

$$\frac{\Delta_{\text{mix}}H}{k_B T} = \chi \phi (1 - \phi)$$

(1.1)

The condensation process can be described by a mean-field **Flory-Huggins** solution theory (Equation 1.1). This model applies to solutions of chain-like macromolecules, such as linear polymers and random polypeptides, and determines the gain or loss in free-energy ($\Delta_{\text{mix}}G$) when the solute chains mix with the solvent. The enthalpic term ($\Delta_{\text{mix}}H$) is simplified by an interaction parameter χ, a measure of attraction or repulsion between solute molecules, solvent molecules, and solvent-solute. The entropic term $\Delta_{\text{mix}}S$ is of combinatorial nature, calculated based on the solute configurations occupying a lattice model of the solvent.[78,79]

In ideal polymer solutions, the free-energy of mixing is negative because the mixing entropy is negative and the interaction enthalpies are all taken as equivalent ($\Delta_{\text{mix}}H$ or χ = 0). In non-ideal solutions however, $\Delta_{\text{mix}}H$ can be different than zero, and the process can be endothermic enough to overcome the entropic term and favor the de-mixed state. Low molecular-weight solutes will hardly reach such non-ideality, whereas for polymeric solutes, with increasing interactions sites N and therefore decreasing entropic contribution, coacervation is much more likely. The equation describes the case of simple coacervation, but for complex coacervation of polymers with an identical length and charge density (σ), **Voorn and Overbeek**[80] employed a **Debye-Hückel** approximation for the electrostatic component of the mixing enthalpy, using an interaction constant α:

$$\frac{\Delta_{\text{mix}}H}{k_B T} = \chi \phi (1 - \phi) + \alpha (\sigma \phi)^{\frac{3}{2}}$$

(1.2)

For a pair of oppositely-charged polyelectrolytes (indexes + and -) in water (index w), the entropic and enthalpic (both electrostatic and non-ionic) terms must be summed over all species, yielding Equation 1.3:

$$\begin{aligned}
\frac{\Delta_{\text{mix}}G}{k_B T} =& \frac{\phi_+}{N_+} \ln \phi_+ + \frac{\phi_-}{N_-} \ln \phi_- + (1 - \phi_+ - \phi_-) \ln(1 - \phi_+ - \phi_-) \\
&+ \chi_{(+,-)} \phi_+ \phi_- + \chi_{(+,w)} \phi_+ \phi_w + \chi_{(-,w)} \phi_- \phi_w \\
&+ \alpha [(\sigma_+ \phi_+) + (\sigma_- \phi_-)]^{\frac{3}{2}}
\end{aligned}$$

(1.3)

From now on we focus on complex coacervates exclusively, which are the experimental systems used on this thesis. As a biphasic system, coacervates are described by a phase diagram like the ones in Figure 1.9. The width of the two-phase region is set by the relative interaction strength (χ or $\alpha \sigma^{\frac{3}{2}}$), which is in general a function of temperature, pH, salt concentration, and the chemical groups in the macromolecules.[46,79]
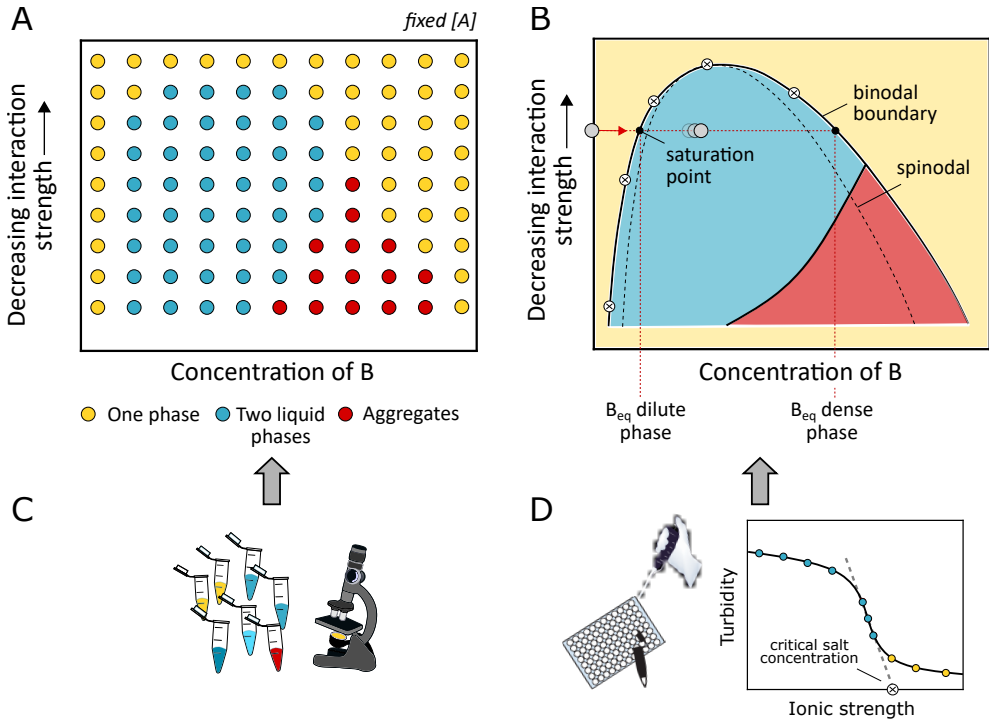
Figure 1.9: Schematic phase diagrams of complex coacervates of **A** and **B** in water. Coacervates are often characterized by a discrete (A) or continuous (B) type of phase diagram, obtained by method (C) and (D) respectively. The curve called the binodal connects the equilibrium concentration of B in the dilute and the dense phase. Under the binodal, the spinodal curve (dashed line) defines the unstable region where phase separation happens via spinodal decomposition. Method (C) involves preparing mixtures of **A** and **B** in different ratios, at different interaction strengths. Method (D) uses a titration (salt, pH, temperature) to measure the critical interaction strengths that define the binodal boundary.

The mean-field approach described above may be simplistic, and does not take into account many factors that can affect coacervation in the systems that are applied as protocells or model droplet organelles: sequence specificity, charge correlation and soluble complex formation. More complex theories of coacervation that account for most of these factors, as supported by numerical simulations, have recently been developed.[81] However, none of these provides a quantitative explanation for all types of liquid phase separating proteins and polymers found (and the list only grows)[82]. Moreover, even when coacervation involves proteins, as is the case of all droplet organelles, globular building blocks are less common than intrinsically disordered proteins (IDPs), which can be better approximated by chain polymers. The relative simplicity of the classical mean-field model, which can provide semi-quantitative agreement with experimental phase diagrams based

on a single effective interaction parameter (χ or α), is therefore still attractive.

Phase diagrams are a powerful tool to characterize coacervates, and we use it as first step to deciding for an experimental system in this thesis. In Chapters 2 and 6, we use the titration method (Figure 1.9D) to determine the "critical salt concentration" of different mixtures, that is, the salt concentration *from* which coacervate droplets dissolve. Instead of salt concentration, pH and temperature are other modifiers of the interaction strength (similar to the parameter χ) that can be used to build a phase diagram. The choice depends on which parameter will most likely vary in the experiments, or which one is most convenient to tune; for us, as we will perform reactions simultaneous to phase separation in buffered medium, ionic strength may vary due to formation of charged products and can be used as a way to prevent aggregation as well.

In order to use coacervates as protocells, we must aim at a system with a comfortably wide binodal, so that interaction strength can change without compromising the phase separation. Going back to the previous section, *The need for active coacervates*, when we refer to a coacervate droplet that produces its own material and becomes *lively*, what we mean is a system that continuously moves along the tie line in Figure 1.9B, and more coacervate phase (in volume) is produced as a result.

A feature that plays a prominent role in cells to control droplet organelles formation is the saturation concentration at which condensates start to form. Many intrinsically disordered proteins necessary for condensate formation are believed to exist close to their respective saturation concentration in the cell, and subtle changes in concentration, mixing ratio or mutual interaction through biochemical modifications or binding to regulatory proteins can shift or expand the area under the binodal, favoring coacervation. Among biochemical modifications, post-translational modifications such as phosphorylation, which affects the charge or charge distribution of amino acid residues, are a common mechanism to control a biomolecule's condensation propensity. [83,84] We will take inspiration from this strategy to move along phase diagrams in Chapter 2.

Experimentally, saturation concentration, equilibrium concentrations and partitioning coefficient can be extracted from the phase diagram, which can in turn be obtained via measurements of turbidity. There is no quantitative method to measure the extent of coacervation, but turbidity can help screening the two regions of the phase diagram: a turbid sample means that there are two phases, a clear sample means one phase (we elaborate on this method in Chapter 2). If the entire binodal — the dilute phase and the dense phase branches - can be characterized, the equilibrium concentrations of **B** can be taken from the phase diagram to determine a parameter known as partitioning coefficient (K_p): the ratio between the concentration of **B** in the dense phase and the dilute phase (see **Experimental notes**). If that is not the case, fluorescence microscopy or common analytical techniques can be used, something we discuss extensively in Chapter 3.

Experimental notes — phase diagrams from turbidity

The most often used observable to distinguish between a one- and two-phases mixture is turbidity. Turbidity (τ) is defined as the fraction of light scattered at a wavelength where the sample is transparent and expressed as:[85]

$$\tau = -\ln\left(\frac{I}{I_0}\right)$$

$$Abs = -\log\left(\frac{I}{I_0}\right) \qquad (1.4)$$

$$\tau = 2.3 \times Abs$$

Turbidity is also reported as a function of transmittance (100 - $T\%$), or the percentage of light that is transmitted. Either way, it can be calculated from the measured extinction (*Abs*), provided that no absorption of light occurs at the detection wavelength. It should therefore be measured at a wavelength far from absorption bands, which is why we commonly chose 520 or 600 nm. It is important to note this will also affect absorbance measurements performed in emulsions at any wavelength.

Although turbidity is not a direct and decisive measure of coacervation, it allows to determine the approximate dilute branch of the binodal in a fast and simple way. Still, for small timescales (minutes) it may correlate well to the progress of a reaction that results in the formation of droplet material. For longer observation periods, the gravitational settling of the droplets, coalescence or their adhesion to the walls of containers, start to interfere by decreasing turbidity even if the amount of droplet material remains the same.

First, we perform a titration with concentrated salt solution, added to different mixtures of **A** and **B** (**A** is fixed, and the concentration of **B** varies). Then we correct salt concentration for the dilution during titration and plot turbidity as a function of the *added* salt. Note that this concentration does not have to take into account the total ionic strength of the solution, which would include counterions from the polyelectrolytes, buffer components etc. At the critical concentration (circle with a cross in Figure 1.9D), the turbidity reaches zero (after baseline correction). If the turbidity does not reach zero, the critical salt concentration can also be found from a linear extrapolation of the points in the steepest part of the turbidity profile to the x-axis. We use this same approach in Chapter 6.

From titration plots to a phase diagram, the measured critical salt concentration is plotted as a function of polyelectrolyte **B** concentration. The ratio between **A** and **B**, which is constant during a titration, can be plotted instead. The disadvantage of the titration method is that the starting components get diluted, so it is important to maximize titrant concentration and minimize additions. To confirm that turbidity is caused by the nucleation of liquid droplets, it must be paired with microscopy, as aggregates in suspension will also result in increased turbidity — though over time, turbidity will have much more noise for suspensions than for emulsions.

1.8 Thesis goal and overview

This thesis is composed of the **introduction** you just read, five experimental chapters, and an **outlook**. In the introduction, I discussed the goals of origin of life research, and the features of living systems that help us look for chemical models to mimic life. I then presented droplet organelles as an argument in favor of a particular chemical model: liquids, and among liquids, coacervates. It did not stop there: in the category of coacervates, I made a distinction between passive and active, to highlight that an active coacervate model is needed to mimic a protocell. I concluded with an explanation of the thermodynamics of coacervation and connected it to experimental methods that permeate this thesis.

The main chapters tackle, together, the goal of this thesis: to investigate active coacervates in order to obtain a growing protocell. This goal can only be reached in Chapter 6, after answering a few questions:

How can we make coacervation dynamic, similarly to droplet organelles (and presumably protocells)? In Chapter 2, we combine the idea of compartmentalization and regeneration to develop coacervates controlled by a chemical reaction. We take inspiration from droplet organelles in our choice of composition, while still keeping the system minimal: poly-lysine (a polypeptide) and ATP. ATP is formed *in situ* from ADP and phosphoenolpyruvate, catalyzed by the enzyme pyruvate kinase, and coacervation happens as the reaction progresses. The same coacervates can then be dissolved by the phosphorylation of glucose by hexokinase, which converts ATP back to ADP. We determine the phase diagram of the two reaction states and explore the reversibility of the system to control the timing of compartmentalization.

What are the chemical implications when a reaction is coupled to phase separation? Can we obtain quantitative chemistry in active coacervates? After working on Chapter 2, a few questions arose and we make an intermission in Chapter 3 to discuss the blind spots in our knowledge of reactions in two phases in the coacervate context. We expand our introduction of droplet organelles to discuss their role in biochemical organization, and propose that more quantitative characterization is needed. We apply this advice to our system of poly-lysine and ATP coacervates, and provide a protocol to measure partitioning coefficient of large and small molecules, reaction rate and rate constants in a two phase system.

What aspects of coacervate droplets affect chemical reactions? Continuing on our intermission that started in Chapter 3, we were intrigued by the particularities of reactions in coacervate droplets, and its consequences to the function of droplet organelles but mostly to our goal of developing a growing protocell that produces its own material.

In Chapter 4 we focus on the effect of coacervates on reactivity: in terms of volume fraction, rate constant modification, partitioning coefficients and organization in droplets. We build a simple model to explore and demonstrate the role of each parameter, and predict whether such kinetic effects can be observed experimentally and possibly play a biological role.

Can active coacervates overcome passive processes in order to achieve growth?
Coming back to our main storyline and building towards our goal of achieving growing coacervate droplets, in Chapter 5 we investigate the stability of coacervate droplets to Ostwald ripening, following some surprising experimental observations. We show that complex coacervates in particular are remarkably stable towards ripening, due to its associative nature: the electrostatic attraction poses a barrier for the diffusion of the macro-ions between droplets, and the diffusion of soluble complexes is entropically hampered, altogether eliminating the drive for Ostwald ripening.

How do we build, characterize and prove a coacervate-based, protocell model?
Equipped with our built knowledge on dynamic poly-lysine/ATP coacervates, kinetics of the kinase reaction in the presence of coacervates, and stability of complex coacervates to Ostwald ripening, in Chapter 6 we develop a growing coacervate protocell. We employ the kinase reaction to nucleate and grow protein/ATP coacervates, and we show that growth is a good mimic of cellular growth — droplet radius increases, while droplet count does not decrease. We show that we can quantify growth rate and propose that it can be used as a fitness parameter to distinguish populations of droplets. Our findings can provide a mechanism for protocell growth and proliferation before the appearance of specialized enzymes.

Finally, in Chapter 7 we connect the dots in retrospect, and discuss how our findings contribute to the field's understanding of coacervates coupled to a chemical reaction. We highlight some additional questions that we came across during the work summarized in this thesis, and propose some short- and long-term investigations that can follow from our methods, results and conclusions in Chapter 8. We add a commentary on the societal impact of our research (and related research), targeted at non-chemist audiences that may end up reading this thesis.

References

[1] J. P. Brady, P. J. Farber, A. Sekhar, Y.-H. Lin, R. Huang, A. Bah, T. J. Nott, H. S. Chan, A. J. Baldwin, J. D. Forman-Kay, *et al.*, "Structural and hydrodynamic properties of an intrinsically disordered region of a germ cell-specific protein on phase separation," *Proceedings of the National Academy of Sciences*, vol. 114, no. 39, pp. E8194–E8203, 2017.

[2] S. Koga, D. S. Williams, A. W. Perriman, and S. Mann, "Peptide-nucleotide microdroplets as a step towards a membrane-free protocell model.," *Nature chemistry*, vol. 3, no. 9, pp. 720–4, 2011.

[3] M. C. Weiss, F. L. Sousa, N. Mrnjavac, S. Neukirchen, M. Roettger, S. Nelson-Sathi, and W. F. Martin, "The physiology and habitat of the last universal common ancestor," *Nature microbiology*, vol. 1, no. 9, pp. 1–8, 2016.

[4] M. A. Bedau and C. E. Cleland, *The Nature of Life*. Cambridge University Press, 2010.

[5] D. E. Koshland, "The seven pillars of life," *Science*, vol. 295, no. 5563, pp. 2215–2216, 2002.

[6] A. J. Dzieciol and S. Mann, "Designs for life: protocell models in the laboratory," *Chemical Society Reviews*, vol. 41, no. 1, pp. 79–85, 2012.

[7] R. M. Hazen, "The emergence of patterning in life's origin and evolution," *International Journal of Developmental Biology*, vol. 53, no. 5-6, pp. 683–692, 2009.

[8] J. England, *Every life is on fire. How thermodynamics explains the origins of living things*. New York: Basic Books, 2020.

[9] J. B. S. Haldane, "The origin of life," *Rationalist Annual*, vol. 148, pp. 3–10, 1929.

[10] A. Oparin, "Origin and evolution of metabolism," *Comparative biochemistry and physiology*, vol. 4, no. 2-4, pp. 371–377, 1962.

[11] H. Bungenberg de Jong and H. Kruyt, "Coacervation (partial miscibility in colloid systems)," in *Proc. K. Ned. Akad. Wet*, vol. 32, pp. 849–856, 1929.

[12] E. Gomes and J. Shorter, "The molecular language of membraneless organelles," *Journal of Biological Chemistry*, vol. 294, no. 18, pp. 7115–7127, 2019.

[13] K. Harada and S. W. Fox, "The thermal condensation of glutamic acid and glycine to linear peptides1," *Journal of the American Chemical Society*, vol. 80, no. 11, pp. 2694–2697, 1958.

[14] S. Rasmussen, L. Chen, M. Nilsson, and S. Abe, "Bridging nonliving and living matter," *Artificial life*, vol. 9, no. 3, pp. 269–316, 2003.

[15] H. J. Morowitz, B. Heinz, and D. W. Deamer, "The chemical logic of a minimum protocell," *Origins of Life and Evolution of the Biosphere*, vol. 18, no. 3, pp. 281–287, 1988.

[16] P. Walde, R. Wick, M. Fresta, A. Mangone, and P. L. Luisi, "Autopoietic self-reproduction of fatty acid vesicles," *Journal of the American Chemical Society*, vol. 116, no. 26, pp. 11649–11654, 1994.

[17] L. E. Orgel, "Evolution of the genetic apparatus," *Journal of molecular biology*, vol. 38, no. 3, pp. 381–393, 1968.

[18] D. Bartel, J. Doudna, N. Usman, and J. Szostak, "Template-directed primer extension catalyzed by the tetrahymena ribozyme.," *Molecular and cellular biology*, vol. 11, no. 6, pp. 3390–3394, 1991.

[19] K. Adamala and J. W. Szostak, "Nonenzymatic template-directed rna synthesis inside model protocells," *Science*, vol. 342, no. 6162, pp. 1098–1100, 2013.

[20] W. F. Doolittle, "Phylogenetic classification and the universal tree," *Science*, vol. 284, no. 5423, pp. 2124–2128, 1999.

[21] L. Sagan, "On the origin of mitosing cells," *Journal of theoretical biology*, vol. 14, no. 3, pp. 225–IN6, 1967.

[22] J. I. Glass, N. Assad-Garcia, N. Alperovich, S. Yooseph, M. R. Lewis, M. Maruf, C. A. Hutchison, H. O. Smith, and J. C. Venter, "Essential genes of a minimal bacterium," *Proceedings of the National Academy of Sciences*, vol. 103, no. 2, pp. 425–430, 2006.

[23] S. Tang, "Pre-darwinian evolution before luca," *Biological Theory*, vol. 15, no. 4, pp. 175–179, 2020.

[24] S. N. Semenov, A. S. Y. Wong, R. M. van der Made, S. G. J. Postma, J. Groen, H. W. H. van Roekel, T. F. A. de Greef, and W. T. S. Huck, "Rational design of functional and tunable oscillating enzymatic networks," *Nature Chemistry*, vol. 7, no. 2, pp. 160–165, 2015.

[25] J. W. Sadownik, E. Mattia, P. Nowak, and S. Otto, "Diversification of self-replicating molecules," *Nature chemistry*, vol. 8, no. 3, pp. 264–269, 2016.

[26] J. M. P. Gutierrez, T. Hinkley, J. W. Taylor, K. Yanev, and L. Cronin, "Evolution of oil droplets in a chemorobotic platform," *Nature communications*, vol. 5, no. 1, pp. 1–8, 2014.

[27] C. P. Brangwynne, C. R. Eckmann, D. S. Courson, A. Rybarska, C. Hoege, J. Gharakhani, F. Jülicher, and A. A. Hyman, "Germline P granules are liquid droplets that localize by controlled dissolution/-condensation," *Science*, 2009.

[28] T. Saha and M. Galic, "Self-organization across scales: from molecules to organisms," *Philosophical Transactions of the Royal Society B: Biological Sciences*, vol. 373, no. 1747, p. 20170113, 2018.

[29] R. Heald and O. Cohen-Fix, "Morphology and function of membrane-bound organelles," *Current opinion in cell biology*, vol. 26, pp. 79–86, 2014.

[30] B. R. Sabari, A. Dall'Agnese, and R. A. Young, "Biomolecular condensates in the nucleus," *Trends in biochemical sciences*, 2020.

[31] T. Mélèse and Z. Xue, "The nucleolus: an organelle formed by the act of building a ribosome," *Current opinion in cell biology*, vol. 7, no. 3, pp. 319–324, 1995.

[32] K. E. Handwerger, J. A. Cordero, and J. G. Gall, "Cajal bodies, nucleoli, and speckles in the xenopus oocyte nucleus have a low-density, sponge-like structure," *Molecular biology of the cell*, vol. 16, no. 1, pp. 202–211, 2005.

[33] B. R. Sabari, A. Dall'Agnese, A. Boija, I. A. Klein, E. L. Coffey, K. Shrinivas, B. J. Abraham, N. M. Hannett, A. V. Zamudio, J. C. Manteiga, *et al.*, "Coactivator condensation at super-enhancers links phase separation and gene control," *Science*, vol. 361, no. 6400, 2018.

[34] W.-K. Cho, J.-H. Spille, M. Hecht, C. Lee, C. Li, V. Grube, and I. I. Cisse, "Mediator and rna polymerase ii clusters associate in transcription-dependent condensates," *Science*, vol. 361, no. 6400, pp. 412–415, 2018.

[35] E. M. Courchaine, A. Lu, and K. M. Neugebauer, "Droplet organelles?," *The EMBO Journal*, vol. 35, no. 15, pp. 1603–1612, 2016.

[36] E. S. F. Rosenzweig, B. Xu, L. K. Cuellar, A. Martinez-Sanchez, M. Schaffer, M. Strauss, H. N. Cartwright, P. Ronceray, J. M. Plitzko, F. Förster, *et al.*, "The eukaryotic co2-concentrating organelle is liquid-like and exhibits dynamic reorganization," *Cell*, vol. 171, no. 1, pp. 148–162, 2017.

[37] C. A. Azaldegui, A. G. Vecchiarelli, and J. S. Biteen, "The emergence of phase separation as an organizing principle in bacteria," *Biophysical Journal*, vol. 120, no. 7, pp. 1123–1138, 2021.

[38] D. M. Rubin and D. Finley, "Proteolysis: The proteasome: a protein-degrading organelle?," *Current Biology*, vol. 5, no. 8, pp. 854–858, 1995.

[39] D. Bracha, M. T. Walls, and C. P. Brangwynne, "Probing and engineering liquid-phase organelles," *Nature biotechnology*, vol. 37, no. 12, pp. 1435–1445, 2019.

[40] S. Alberti, "The wisdom of crowds: regulating cell function through condensed states of living matter," *Journal of cell science*, vol. 130, no. 17, pp. 2789–2796, 2017.

[41] J. Smith, D. Calidas, H. Schmidt, T. Lu, D. Rasoloson, and G. Seydoux, "Spatial patterning of p granules by rna-induced phase separation of the intrinsically-disordered protein meg-3," *Elife*, vol. 5, p. e21337, 2016.

[42] P. Anderson and N. Kedersha, "Rna granules," *Journal of Cell Biology*, vol. 172, no. 6, pp. 803–808, 2006.

[43] S. C. Weber *et al.*, "Evidence for and against liquid-liquid phase separation in the nucleus," *Non-coding RNA*, vol. 5, no. 4, p. 50, 2019.

[44] N. A. Yewdall, A. A. M. André, T. Lu, and E. Spruijt, "Coacervates as models of membraneless organelles," *Current Opinion in Colloid & Interface Science*, p. 101416, 2020.

[45] R. Hancock, "The crowded nucleus," *International review of cell and molecular biology*, vol. 307, pp. 15–26, 2014.

[46] J. Van der Gucht, E. Spruijt, M. Lemmers, and M. A. C. Stuart, "Polyelectrolyte complexes: Bulk phases and colloidal systems," *Journal of colloid and interface science*, vol. 361, no. 2, pp. 407–422, 2011.

[47] W. M. Aumiller Jr and C. D. Keating, "Experimental models for dynamic compartmentalization of biomolecules in liquid organelles: Reversible formation and partitioning in aqueous biphasic systems," *Advances in colloid and interface science*, vol. 239, pp. 75–87, 2017.

[48] M. Li, R. L. Harbron, J. V. Weaver, B. P. Binks, and S. Mann, "Electrostatically gated membrane permeability in inorganic protocells," *Nature chemistry*, vol. 5, no. 6, p. 529, 2013.

[49] X. Huang, A. J. Patil, M. Li, and S. Mann, "Design and construction of higher-order structure and function in proteinosome-based protocells," *Journal of the American Chemical Society*, vol. 136, no. 25, pp. 9225–9234, 2014.

[50] C. S. Peyratout and L. Daehne, "Tailor-made polyelectrolyte microcapsules: from multilayers to smart containers," *Angewandte Chemie International Edition*, vol. 43, no. 29, pp. 3762–3783, 2004.

[51] C. Bonfio, D. A. Russell, N. J. Green, A. Mariani, and J. D. Sutherland, "Activation chemistry drives the emergence of functionalised protocells," *Chemical Science*, vol. 11, no. 39, pp. 10688–10697, 2020.

[52] A. Salditt, L. M. Keil, D. P. Horning, C. B. Mast, G. F. Joyce, and D. Braun, "Thermal habitat for rna amplification and accumulation," *Physical Review Letters*, vol. 125, no. 4, p. 048104, 2020.

[53] V. Erastova, M. T. Degiacomi, D. G. Fraser, and H. C. Greenwell, "Mineral surface chemistry control for origin of prebiotic peptides," *Nature communications*, vol. 8, no. 1, pp. 1–9, 2017.

[54] E. Spruijt, A. H. Westphal, J. W. Borst, M. A. Cohen Stuart, and J. van der Gucht, "Binodal compositions of polyelectrolyte complexes," *Macromolecules*, vol. 43, no. 15, pp. 6476–6484, 2010.

[55] C. G. De Kruif, F. Weinbreck, and R. de Vries, "Complex coacervation of proteins and anionic polysaccharides," *Current opinion in colloid & interface science*, vol. 9, no. 5, pp. 340–349, 2004.

[56] S. L. Perry, L. Leon, K. Q. Hoffmann, M. J. Kade, D. Priftis, K. A. Black, D. Wong, R. A. Klein, C. F. Pierce, K. O. Margossian, *et al.*, "Chirality-selected phase behaviour in ionic polypeptide complexes," *Nature communications*, vol. 6, no. 1, pp. 1–8, 2015.

[57] A. Jain and R. D. Vale, "Rna phase transitions in repeat expansion disorders," *Nature*, vol. 546, no. 7657, pp. 243–247, 2017.

[58] R. Merindol, S. Loescher, A. Samanta, and A. Walther, "Pathway-controlled formation of mesostructured all-dna colloids and superstructures," *Nature nanotechnology*, vol. 13, no. 8, pp. 730–738, 2018.

[59] T. J. Nott, T. D. Craggs, and A. J. Baldwin, "Membraneless organelles can melt nucleic acid duplexes and act as biomolecular filters," *Nature chemistry*, vol. 8, no. 6, pp. 569–575, 2016.

[60] S. Elbaum-Garfinkle, Y. Kim, K. Szczepaniak, C. C.-H. Chen, C. R. Eckmann, S. Myong, and C. P. Brangwynne, "The disordered p granule protein laf-1 drives phase separation into droplets with tunable viscosity and dynamics," *Proceedings of the National Academy of Sciences*, vol. 112, no. 23, pp. 7189–7194, 2015.

[61] F. P. Cakmak, S. Choi, M. C. Meyer, P. C. Bevilacqua, and C. D. Keating, "Prebiotically-relevant low polyion multivalency can improve functionality of membraneless compartments," *Nature Communications*, vol. 11, no. 5949, pp. 1–11, 2020.

[62] L. Zhou, Y. Fan, Z. Liu, L. Chen, E. Spruijt, and Y. Wang, "A Multiresponsive Transformation between Surfactant-Based Coacervates and Vesicles," *CCS Chemistry*, pp. 1–24, 2021.

[63] M. Abbas, W. P. Lipiński, K. K. Nakashima, W. T. S. Huck, and E. Spruijt, "A Short Peptide Synthon for Liquid-Liquid Phase Separation," *ChemRxiv*, 2020.

[64] P. Stano and P. L. Luisi, "Achievements and open questions in the self-reproduction of vesicles and synthetic minimal cells," *Chemical Communications*, vol. 46, no. 21, pp. 3639–3653, 2010.

[65] I. Budin, A. Debnath, and J. W. Szostak, "Concentration-driven growth of model protocell membranes," *Journal of the American Chemical Society*, vol. 134, no. 51, pp. 20812–20819, 2012.

[66] T.-Y. D. Tang, C. R. C. Hak, A. J. Thompson, M. K. Kuimova, D. Williams, A. W. Perriman, and S. Mann, "Fatty acid membrane assembly on coacervate microdroplets as a step towards a hybrid protocell model," *Nature chemistry*, vol. 6, no. 6, p. 527, 2014.

[67] T. F. Zhu and J. W. Szostak, "Coupled growth and division of model protocell membranes," *Journal of the American Chemical Society*, vol. 131, no. 15, pp. 5705–5713, 2009.

[68] K. Adamala and J. W. Szostak, "Competition between model protocells driven by an encapsulated catalyst," *Nature chemistry*, vol. 5, no. 6, p. 495, 2013.

[69] L. Sheng and K. Kurihara, "Transformation of oil droplets into giant vesicles," *Chemical Communications*, vol. 52, no. 50, pp. 7786–7789, 2016.

[70] D. Zwicker, A. A. Hyman, and F. Julicher, "Suppression of Ostwald ripening in active emulsions," *Physical Review E - Statistical, Nonlinear, and Soft Matter Physics*, vol. 92, no. 1, pp. 1–13, 2015.

[71] D. Zwicker, R. Seyboldt, C. A. Weber, A. A. Hyman, and F. Jülicher, "Growth and division of active droplets provides a model for protocells," *Nature Physics*, vol. 13, pp. 408–413, 2017.

[72] J. Berry, C. P. Brangwynne, and M. Haataja, "Physical principles of intracellular organization via active and passive phase transitions," *Reports on Progress in Physics*, vol. 81, no. 4, p. 046601, 2018.

[73] H. R. Kruyt, *Colloid Science Vol. 2: Reversible systems*. Elsevier, 1949.

[74] K. Majorek, L. Kozlowski, M. Jkakalski, and J. M. Bujnicki, "First steps of protein structure prediction," *Prediction of Protein Structures, Functions, and Interactions*, pp. 39–62, 2008.

[75] D. Pesce, Y. Wu, A. Kolbe, T. Weil, and A. Herrmann, "Enhancing cellular uptake of GFP via unfolded supercharged protein tags," *Biomaterials*, vol. 34, no. 17, pp. 4360–4367, 2013.

[76] E. Spruijt, A. H. Westphal, J. W. Borst, M. A. Cohen Stuart, and J. Van Der Gucht, "Binodal compositions of polyelectrolyte complexes," *Macromolecules*, vol. 43, no. 15, pp. 6476–6484, 2010.

[77] E. Spruijt, F. A. M. Leermakers, R. Fokkink, R. Schweins, A. A. Van Well, M. A. Cohen Stuart, and J. Van Der Gucht, "Structure and dynamics of polyelectrolyte complex coacervates studied by scattering of neutrons, X-rays, and light," *Macromolecules*, vol. 46, no. 11, pp. 4596–4605, 2013.

[78] A. Veis, "A review of the early development of the thermodynamics of the complex coacervation phase separation," *Advances in colloid and interface science*, vol. 167, no. 1-2, pp. 2–11, 2011.

[79] C. P. Brangwynne, P. Tompa, and R. V. Pappu, "Polymer physics of intracellular phase transitions," *Nature Physics*, vol. 11, no. 11, pp. 899–904, 2015.

[80] J. T. G. Overbeek and M. Voorn, "Phase separation in polyelectrolyte solutions. theory of complex coacervation," *Journal of Cellular and Comparative Physiology*, vol. 49, no. S1, pp. 7–26, 1957.

[81] K. T. Delaney and G. H. Fredrickson, "Theory of polyelectrolyte complexation—complex coacervates are self-coacervates," *The Journal of chemical physics*, vol. 146, no. 22, p. 224902, 2017.

[82] M. Hardenberg, A. Horvath, V. Ambrus, M. Fuxreiter, and M. Vendruscolo, "Widespread occurrence of the droplet state of proteins in the human proteome," *Proceedings of the National Academy of Sciences*, vol. 117, no. 52, pp. 33254–33262, 2020.

[83] A. K. Rai, J.-X. Chen, M. Selbach, and L. Pelkmans, "Kinase-controlled phase transition of membraneless organelles in mitosis," *Nature*, vol. 559, no. 7713, pp. 211–216, 2018.

[84] L. C. Reineke, W.-C. Tsai, A. Jain, J. T. Kaelber, S. Y. Jung, and R. E. Lloyd, "Casein kinase 2 is linked to stress granule dynamics through phosphorylation of the stress granule nucleating protein g3bp1," *Molecular and cellular biology*, vol. 37, no. 4, 2017.

[85] K. Kaibara, T. Okazaki, H. Bohidar, and P. Dubin, "ph-induced coacervation in complexes of bovine serum albumin and cationic polyelectrolytes," *Biomacromolecules*, vol. 1, no. 1, pp. 100–107, 2000.

Chapter 2

Control of coacervation with a chemical reaction
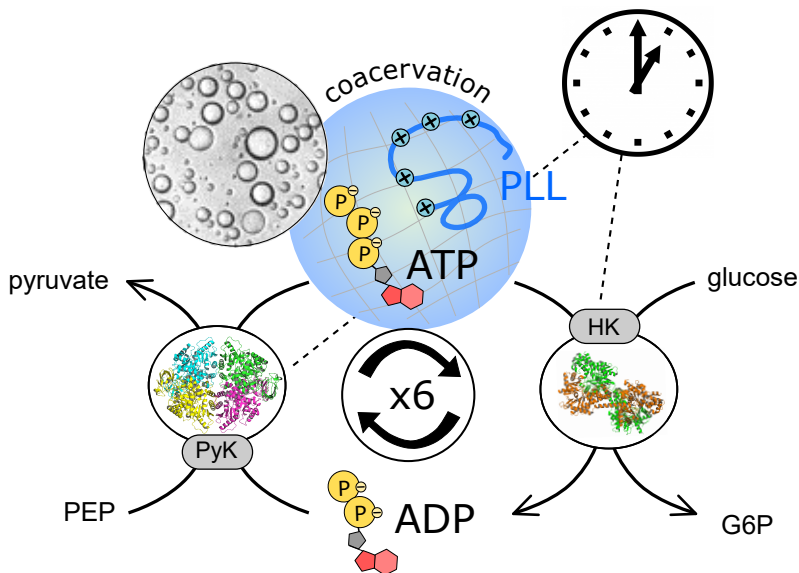
2.1 Active coacervates

Protocell models, membraneless organelles and coacervates share an intrinsic connection. When designing a protocell model, extant cells are a reference: these crowded compartments with internal organization are the minimal unit of life, channeling energy into functions such as replication, growth, division. An important aspect of cells recently emerged: they are ripe with condensates,[1,2] structures that lack a lipidic membrane, form by liquid-liquid phase separation (LLPS) and concentrate biomolecules through dynamic interactions. Principles as well studied as the central dogma of biology are now being re-interpreted in light of a heterogeneous nucleoplasm,[3] filling a blind spot in our knowledge of cellular chemistry, but also posing new questions. If cells now rely heavily on membraneless structures — examples include germ granules,[4,5] processing bodies,[6,7] stress granules[8,9] and nucleoli[10–12] —, would they have played a role in the emergence of cells altogether? In fact, this question had been posed decades before the discovery or membraneless organelles, formulated as the Oparin-Haldane hypothesis for the origin of life.[13,14] Coacervates come into play because increasing evidence indicates that most of these organelles can be classified as coacervates:[15,16] liquid droplets enriched in macromolecules and are formed by LLPS.[2,17,18] Interestingly, coacervates were also the protocellular structures in Oparin and Haldane's theory.
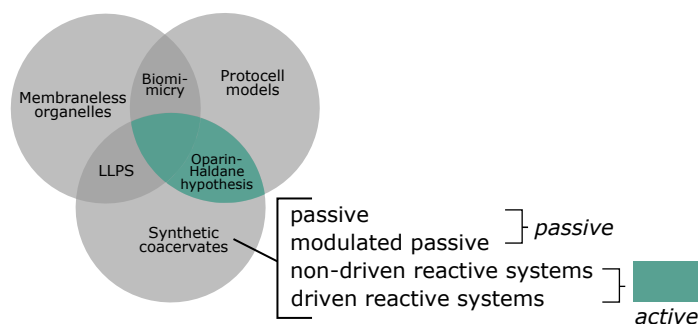
Figure 2.1: Concepts that make up the rationale of this thesis: in order to achieve growing protocell models, we take inspiration from membraneless organelles and use liquid-liquid phase separated systems, with focus on active coacervates.

In order to use coacervates as model organelles or protocells, we must demonstrate that coacervate droplets can achieve life-like behavior. Being compartments that selectively uptake some molecules and exclude others is one property typical of living systems (see Chapter 1), but there are some promising indications that coacervate droplets can go further, up to stability, growth and division.[19] To explain how, we need to introduce the concept of active droplets: droplets that are not simply nucleating, growing and coarsening towards equilibrium. The term *active systems* originally applies to assemblies

that can transduce free energy into movement, much like most biological systems. [20] In contrast, droplets that only undergo nucleation, diffusion-limited growth, Brownian motion-induced coalescence (fusion) and diffusion-limited coarsening (Ostwald ripening) are called **passive**.

Recently, motile, [21] growing and dividing [19] droplets have been described as active, and the common denominator is the presence of a chemical reaction, in addition to LLPS, leading to the formation of the droplet. Berry *et al* refined the definition of active in the context of LLPS, further distinguishing between "undriven chemically reactive" and "driven chemically reactive" droplets. In both cases a chemical reaction is present, but undriven systems have no internal or external supply of work and as a result, as the reaction reaches equilibrium or completion, an undriven mixture will relax to thermal equilibrium. [22] Importantly for our general goal of a reaction-driven growing droplet, the *kinetics* of phase separation can still be different from that of a passive system. In a driven chemically reactive mixture, there is an external source of energy to the system (e.g. light, radiation), or an internal fuel that can be recycled (e.g. ATP, molecular motors). Consequently, not only kinetics but thermodynamics can be affected — phase boundaries, saturation concentrations, the occurrence of phase separation at all —, which is beyond the scope of this work.

We can now formulate our goal in this chapter: developing coacervates that can be reliably controlled by a chemical reaction. A chemical reaction is our strategy in further chapters to obtain dynamic behavior from coacervate droplets that are otherwise in equilibrium. Moreover, the overwhelming amount of biomolecular condensates discovered in the past decade shows that the interplay between phase separation and chemical reactions has to be an integral part of cellular biochemistry. [23,24] Compositionally, we aimed at using biologically relevant molecules, and avoiding highly specific synthetic compounds and biomolecules. This makes our case to use coacervate droplets as artificial membraneless organelles or protocells to study chemical principles of life.

2.1.1   Reaction control over coacervation

The way to achieve active droplets is to control liquid-liquid phase separation by a chemical reaction. Huck and co-workers showed that disassembly of complex coacervates based on oppositely charged polypeptides can be triggered directly by an enzymatic reaction. [25] Keating and co-workers showed that an alternative composition allows enzymatic control over both formation and disassembly of coacervate microdroplets, by respective dephosphorylation and phosphorylation of the serine residues of the peptide. [26] The extreme sensitivity of their system was reflected by the fact that the difference between condensed and dissolved coacervates was as small as a single phosphate group. However, the reaction conditions required for the two enzymatic reactions were not mutually compatible and switching from condensation to dissolution always involved addition and removal of

cofactors.
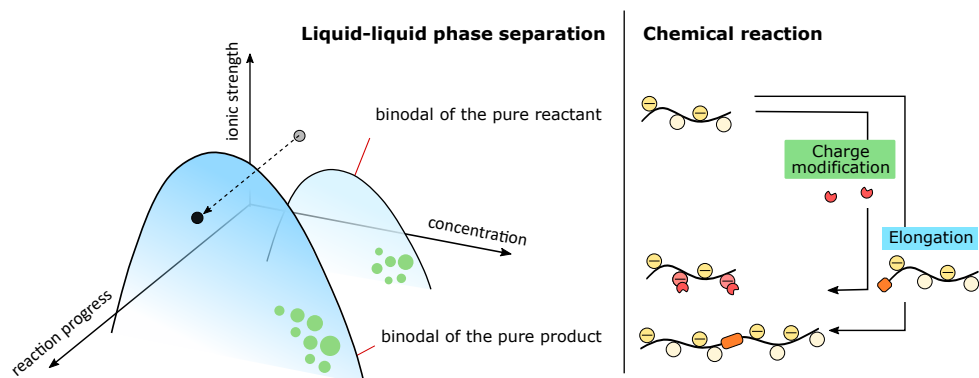
Figure 2.2: A mixture can navigate between two phase diagrams via a chemical reaction that converts a low molecular weight, low charge density reactant into a high multi-valency product. In this example, the phase diagram would refer to a mixture of the positively charged reactant or product, with a negatively charged polyelectrolyte, and we show ionic strength as an environmental parameter that remains constant during a reaction.

Fundamentally speaking, there are two large categories of strategies to couple a reaction to liquid-liquid phase separation (LLPS): elongation or charge-modifying reactions (Figure 2.2). The stability of complex coacervates is a strong function of the charge density and overall charge of the oppositely charged components.[27] Small ions have a destabilising effect on complex coacervates by competing for ion pair formation, and the concentration at which this competition leads to dissolution of droplets or macroscopic phases normally increases with increasing size and charge density of the charged species.[27,28] We can expect that the larger the molecule, and the more charged groups there are, the wider the coacervation window will be, for the same conditions and with the same oppositely charged partner. A reaction that elongates or increases charge density of a molecule will drive the system from the one-phase region of the phase diagram of the pure reactant to the two-phases region of the diagram of the pure product (Figure 2.2).

Elongation and charge-modification turn out to be abundant in cells, with strong evidence that they are the main regulators of biomolecular condensates: the phosphorylation of a single serine residue in G3PB1 protein dissolves stress granules *in vitro*,[29] methylation of arginine residues in DDx4 destabilizes nuage organelles[5] and polymerization of the nascent mRNA chain stimulates the formation of transcriptional condensates.[23,30] Reaction control over LLPS has been demonstrated for model membraneless organelles, including peptide-RNA complex coacervates formed via phosphorylation/dephosphorylation of serine residues. On the other side of the spectrum of biomimicry, imine formation has been used as an elongation strategy to form dynamic surfactant-polyacrylic acid coacervates.[31]

2.1.2   An ATP-based coacervate model system

We chose a combination of a small molecule and a polymer - the well known peptide-nucleotide coacervates inspired by membraneless organelles and Stephen Mann and Christine Keating groups' work — to design active poly-*L*-lysine and ATP coacervates. Poly-*L*-lysine brings the robustness, or stability, while ATP brings the "active" feature. We made this choice because there is a whole range of biochemical reactions involving ATP to choose from, very differently from the stable amide bond sustaining poly-lysine. Besides, the obvious ATP-precursor, ADP, has a lower charge density, meaning that it forms weaker coacervates than ATP with the same polycationic partner. The alternative, chemically modifying the amine residues would also be a valid strategy, but finding an efficient, prebiotically plausible charge-neutralizing reaction would be a project itself. For the purpose of achieving chemically-driven coacervates, we opted for enzymatic reactions to dynamically form and break ATP, and therefore condense and dissolve the droplets.
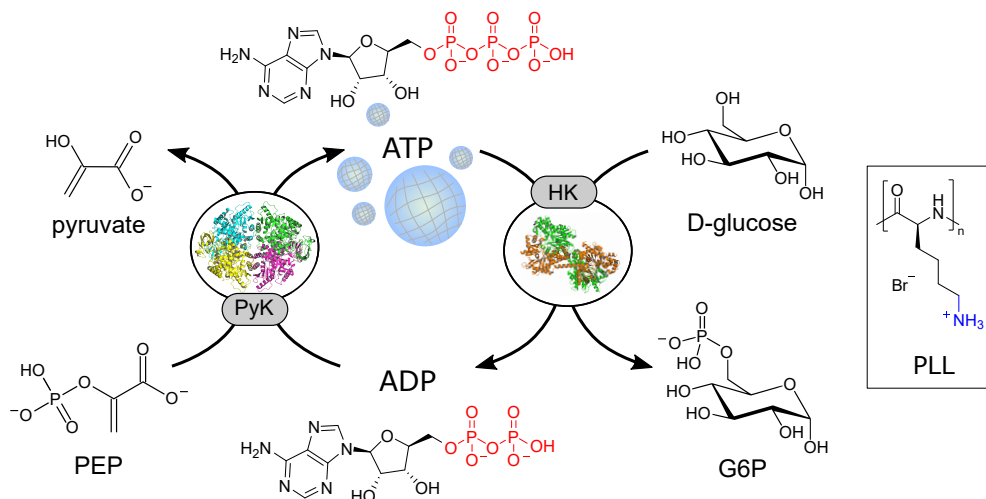
Figure 2.3: Schematic illustration of the enzymatic reaction network underlying dynamic and reversible formation and dissolution of ATP-PLL coacervate microdroplets.

Cells continuously convert ADP to ATP and back using a variety of different enzymes. Pyruvate kinase is a glycolytic enzyme that catalyzes the transfer of a phosphoryl group from phosphoenolpyruvate (PEP) to ADP, producing ATP and pyruvate (Figure 2.3). It requires monovalent and divalent cations to orient the random binding of ADP and PEP substrates to the active site. It can in principle phosphorylate all five NDPs and dNDPs to the corresponding triphosphates, but the isozyme we chose, rabbit muscle pyruvate kinase (PyK), is highly specific towards ADP/ATP. This enzyme is suitable for us because ADP has a much narrower coacervation window with polylysine, due to its lower multivalency. Moreover, pyruvate kinase is an ancient enzyme present before

the split between prokaryotes and eukaryotes, as suggested by the similarities between glycolysis in these two domains.[32]

For the reverse process — conversion of ATP back to ADP and dissolution of the coacervates — we chose another glycolytic enzyme, hexokinase. Hexokinase uses ATP to phosphorylate hexoses, yielding ADP and the hexose-6-phosphate (we chose glucose, see Figure 2.3). Our criterium was that yeast PI and PII isoenzymes work under the exact same conditions as rabbit muscle pyruvate kinase, enabling a fully reversible coacervation/dissolution cycle. In 2015, Aumiller Jr. and Keating introduced a phosphorylation-driven coacervation model, with the minor shortcoming that the kinase/phosphatase pair used required different conditions.[26] They were able to form peptide-RNA condensates using the de-phosphorylation of serines in a cationic peptide by protein kinase A; and the dissolution of the condensates via phosphorylation by lambda protein phosphatase. To produce a cycle, this system requires manganese ions to be added for phosphatase activity, and then chelated with EDTA for kinase activity. We hoped that the compatibility of pyruvate kinase and hexokinase, both magnesium-dependent, would allow us to achieve successive cycles of transient compartmentalization.

2.2   Characterization of ATP-PLL coacervates

To determine the conditions under which the reaction network in Figure 2.3 could give rise to reversible coacervate formation and dissolution, we first set out to determine phase diagrams of ADP/PLL and ATP-PLL coacervates, in the presence of magnesium, a critical cofactor for both enzymes. In our field, experimental phase diagrams are typically built as a chart of polyelectrolyte concentrations and ionic strengths, for which phase separation is observed or not. The ionic strength represents the inverse of the interaction parameter χ, and alternatively temperature or pH can be used. Phase separation can be judged visually (microscopically) and more quantitatively, via turbidity. While many studies screen the phase diagram by preparing samples at separate conditions of polyelectrolyte concentration and ionic strength, we performed salt titrations: we fixed the PLL concentration at 5 mM and varied ADP or ATP concentration between 1 and 30 mM; the samples then were titrated with a concentrated sodium chloride solution, thereby increasing the salt concentration while keeping the PLL/nucleotide ratio constant. The advantage of this method is that the binodal is determined rather than inferred in between experimental points; the disadvantage is that polyelectrolyte concentration varies during titration, but that can be minimized by using a concentrated titrant solution.

Figure 2.4 shows turbidity-based titration curves of PLL (5 mM monomer units), as a function of ADP or ATP concentration, and as a function of salt concentration. The results are in good agreement with previous reports on nucleotide/polyallylamine coacervates.[33] The onset of turbidity was found at lower nucleotide concentrations for ATP than for ADP, whereas the subsequent response to the addition of nucleotides was

steeper for ATP. Both effects can be explained by the higher charge density of ATP. Like the authors in reference 33, we found that samples remained turbid up to nucleotide concentrations of 25 mM at low salt. Interestingly, we found that addition of NaCl shifted the onset of turbidity to higher nucleotide concentrations and led to a decreased response steepness. The decrease of the turbidity with increasing salt concentration results from a combination of a lower coacervate volume (fewer droplets),[33] and a lower contrast between the coacervates and the surrounding solution.[27]
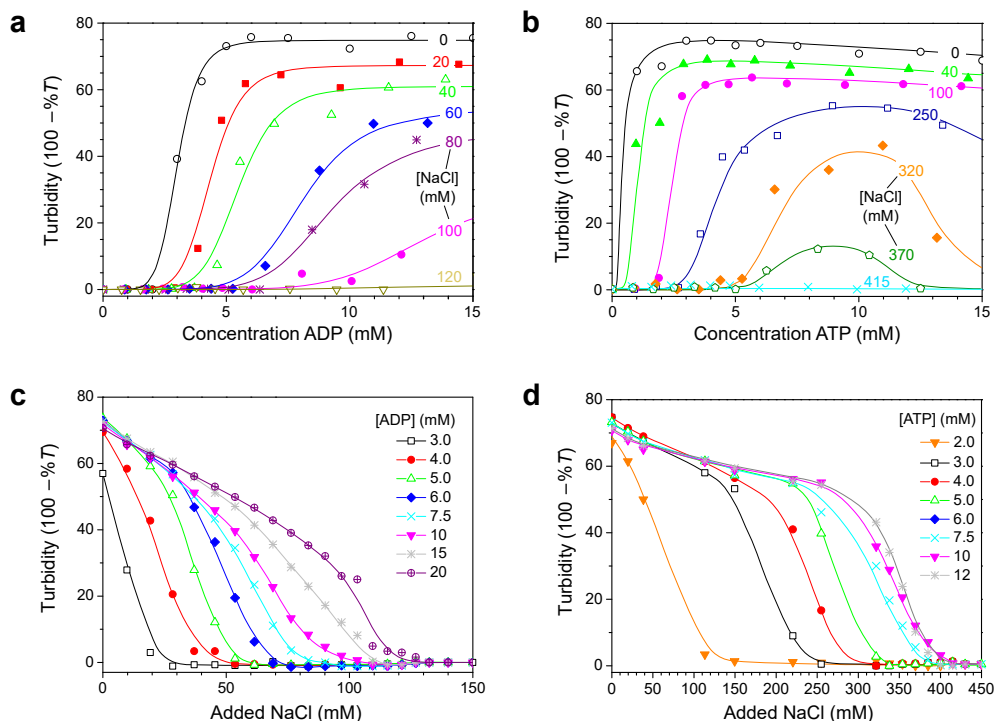
Figure 2.4: Turbidity of PLL/nucleotide mixtures as a function of nucleotide concentration (a,b) and concentration of added NaCl (c,d). The mixtures contained a fixed concentration of 50 mM HEPES, 5 mM MgCl$_2$ and 5 mM PLL (monomer units). The mixtures containing ADP was titrated with NaCl 0.5 M, while the mixture containing ATP was titrated with NaCl 2 M. The labels indicate the NaCl concentrations or nucleotide concentrations, and lines are drawn as guide to the eye.

The shift in the onset of turbidity is due to an increased nucleotide solubility in the solution that coexists with the droplets. In most coacervates consisting of two polymeric species, complexation remains centred around a 1:1 overall charge ratio, while turbidity decreases with increasing salt.[34] In the case of Mg-nucleotide/PLL coacervates without salt we found a maximal degree of coacervation near a 1:1 charge ratio, but with the addition of salt, the onset of coacervation was shifted beyond the point of charge com-

pensation. For example, the onset of coacervation of Mg-ADP/PLL in 50 mM HEPES pH 7.4 and 80 mM NaCl was observed around 8 mM ADP (Figure 2.4a), corresponding to an overall 5x excess of phosphate anions on ADP compared to amine cations on PLL (3X if Mg^{2+} is included in the complexation). It should be noted that this bears no direct implication for the charge ratio inside the coacervate droplets. Presumably, the unequal partitioning of nucleotides and PLL into the coacervate droplets still results in charge neutrality. [33,35,36] The observed shift of the onset of coacervation simply reflects the strong asymmetry between the interacting species: PLL is a long polyelectrolyte, whereas nucleotides bear resemblance to small ions. As a consequence, the concentration of ADP (and ATP) in the solution that coexists with the coacervate is significant, whereas the PLL concentration in solution is low. [35,37] The fact that the shift is more extreme for ADP than ATP already suggests that ATP partitions more strongly into PLL coacervates, something we discuss in Chapter 3 and measured for K_{72}-ATP coacervates in Chapter 6. For this chapter, we were more interested in a macrophase dynamic behavior, and do not focus on this quantification.

From plots of the turbidity as a function of added salt (Figure 2.4c,d) we determined the critical salt concentration, the point at which turbidity disappears. Figure 2.5a shows the resulting phase diagram of both ADP and ATP coacervates. As expected, ATP-based coacervates have a significantly higher salt stability. It is interesting to note that under physiological conditions (100–200 mM ionic strength, 1–10 mM ATP, 0.5–10 mM Mg^{2+}), ATP-PLL coacervates are expected to be stable, whereas ADP-PLL coacervates are not. Many enzymes could in principle be used under these conditions.

The operational window for the reversible coacervation in Figure 2.3 is highlighted in Figure 2.5a and was found to widen with increasing nucleotide concentration up to 5 mM, primarily because the ATP-based coacervates become more stable. Small amounts of charged enzymatic substrates, such as PEP-K, have no significant effect on the width of this window, as demonstrated in Figure 2.5b. We repeated the NaCl titrations of 5 mM PLL/ATP mixtures in the presence of 5-15 mM PEP. Because the substrate also significantly acidifies the medium, buffer concentration was increased from 50 to 100 mM. Even in a higher ionic strength and with the addition of PEP, there is still a wide operational window where ATP, but not ADP, coacervates with PLL. Based on these results, a composition of 5 mM ADP or ATP, 100 mM HEPES and addition of 1 equiv. of substrate (e.g., PEP) was considered to be safe in terms of differential coacervation of ADP and ATP.

To further illustrate the feasibility of the reaction network proposed in Figure 2.3, we prepared mixtures of both nucleotides with PLL under identical conditions within the highlighted region of Figure 2.5a. When observed under the microscope, the ATP-containing mixtures had clearly condensed into droplets, while the ADP-containing mixtures remained a homogeneous solution (Figure 2.5c).
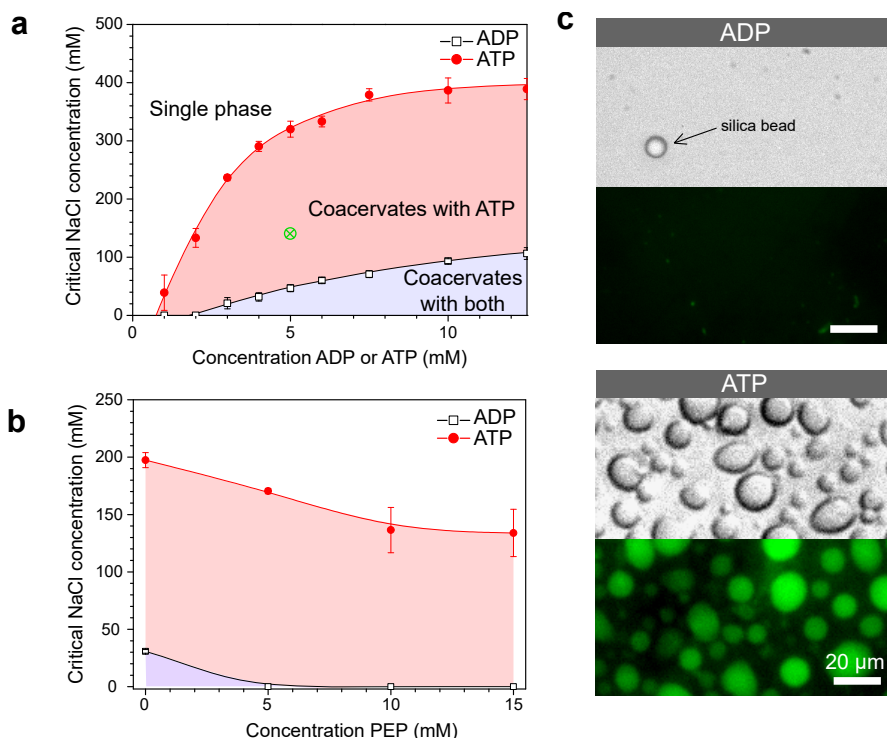
Figure 2.5: (a) Critical salt concentration for ADP and ATP coacervates with 5 mM PLL, determined from turbidity-based titrations. The red shaded region corresponds to conditions where ATP, but not ADP, forms coacervates with PLL, while in the lilac region the two nucleotides are not distinguishable. (b) Critical salt concentration for 5 mM ADP and ATP coacervates with 5 mM PLL in the presence of PEP. The red region is shifted towards lower added NaCl concentrations in comparison to mixtures without PEP and in a weaker buffer. (c) Representative microscope images (top: bright field, bottom: epifluorescence) of ADP and ATP-containing mixtures prepared at the point indicated by the green (x) in (a) and stained with SYBR Gold. Silica beads (diameter 8 μm) were added to the ADP mixture to assist in focussing.

2.3   Coupling of a kinase to phase separation

We established the conditions under which reversible switching of biomolecules from a condensed to a dissolved state is feasible. To realize this transition using enzymatic conversion, we prepared mixtures of nucleotides and PLL with the composition indicated in Figure 2.5a, with varying amounts of hexokinase and glucose to dissolve coacervates, or pyruvate kinase and PEP to generate coacervates. Figure 2.6a and b summarize our findings. Pyruvate kinase is able to use a stoichiometric amount of PEP to turn a homogeneous solution into a dispersion of microdroplet compartments of condensed ATP within one minute (Figure 2.6a), by converting ADP into ATP in the presence of PLL.
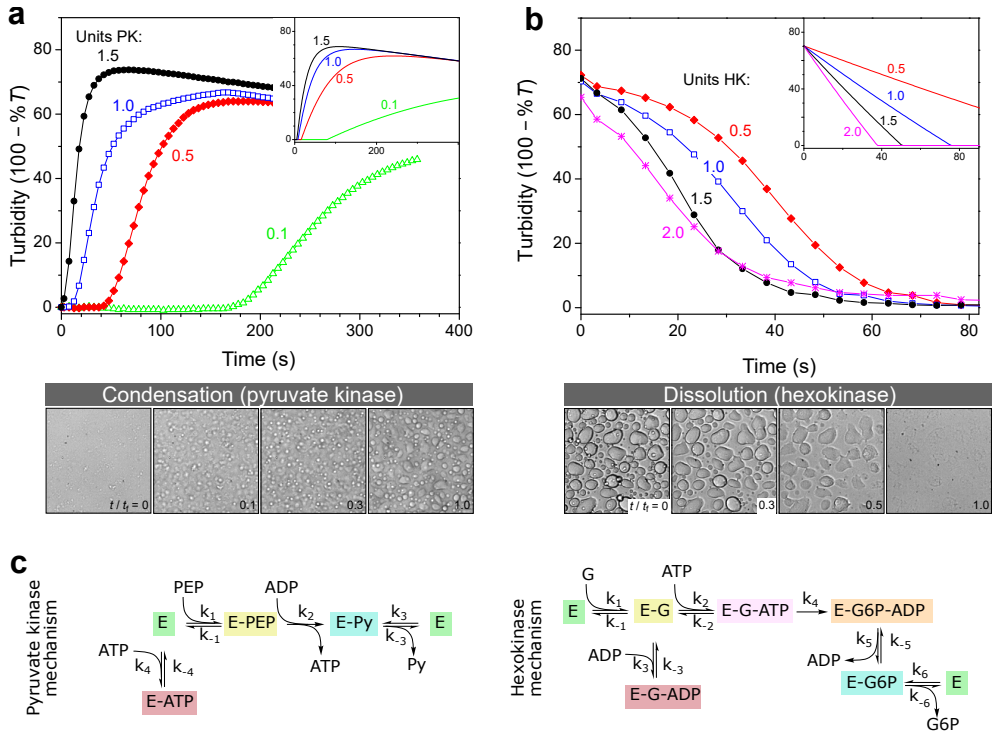
Figure 2.6: (a) Enzyme-catalyzed condensation of ATP-PLL coacervate microdroplets by pyruvate kinase (PyK) in the presence of 1 equivalent of PEP, and (b) dissolution catalyzed by hexokinase (HK) in the presence of 2 equivalents of D-glucose. The labels indicate the units of enzyme that were added to the mixtures, and the insets show the predicted changes in turbidity based on mass action kinetics in a single phase. Microscope images (200 μm × 200 μm) correspond to snapshots of a separate experiment that was carried out in parallel under the microscope. Time labels indicate relative times with t_f being the time to reach the final state of settled droplets or dissolved droplets. (c) Mechanism of pyruvate kinase and hexokinase-catalyzed reactions used to model the onset of coacervation or dissolution in the insets of a and b. In pyruvate kinase mechanism, E represents pyruvate kinase, PEP is phosphoenolpyruvate and Py is pyruvate. In hexokinase mechanism, E represents hexokinase, G is D-glucose and G6P is glucose-6-phosphate.

Inversely, hexokinase can completely dissolve a dispersion of ATP microdroplets using glucose to convert ATP back into ADP within ten seconds (Figure 2.6b). The rate of droplet formation and dissolution can be controlled by varying the amount of enzyme, highlighting the fact that this transition is a direct result of enzyme-catalyzed reactions.

To obtain better insight into the importance of the cooperating rates of binding, catalyzis and inhibition for the formation of microdroplets we built a mathematical model of the enzyme-catalyzed condensation and dissolution depicted in Figure 2.3. For the sake of simplicity, we restricted all reactions to a single phase and assumed rapid parti-

tioning of ATP into the droplets. As shown in the insets in Figure 2.6a and b, simple mass-action kinetics underlying our model is sufficient to qualitatively capture the observed condensation and dissolution rates and the timescales of beginning and end of both processes. The delay of condensation in Figure 2.6a for small amounts of pyruvate kinase results from a combination of product inhibition of the enzyme by ATP[36] and the nonzero threshold ATP concentration required for droplet formation (Figure 2.4b). By contrast, hexokinase is less strongly inhibited by ADP and the droplets started to dissolve directly after the addition of D-glucose. Although our model is able to qualitatively capture certain key aspects of the condensation and dissolution, it cannot predict droplet formation quantitatively for two main reasons. On the one hand, there is no clear way to convert ATP concentrations into turbidity, taking into account droplet sizes, nucleation, growth, coalescence and sedimentation. On the other hand, many enzymes have been found to partition into coacervate droplets, and retain their functionality to a certain degree.[35,38,39] For hexokinase, a partitioning coefficient of 20 was found for salt-free ATP-PLL coacervates,[35] but the partitioning coefficients and rate constants inside coacervates of almost all other components in Figure 2.3 are still unknown. This is an issue we further address in Chapter 3.

2.4   Timing of condensation and dissolution

A key advantage of our enzyme-catalyzed coacervate system is the fact that both enzymes are functional under the same conditions. It is therefore possible to switch between condensation and dissolution by simple addition of substrates (PEP and D-glucose). Figure 2.7a illustrates this reversibility: microdroplets could be generated and dissolved up to twelve times, and we were able to carry out identical transitions when starting from either ADP or ATP. After about twelve transitions, the system loses its ability to condense into droplets, which is mainly caused by the accumulation of waste products, *i.e.* pyruvate and glucose-6-phosphate (G6P). After twelve transitions, the present ATP has been converted six times into ADP and back, resulting in an estimated six-fold excess of pyruvate and G6P. Both small molecules exist as charged species under our reaction conditions and act to destabilize the coacervate droplets. Moreover, the traces in Figure 2.7a show that the pyruvate kinase activity decreases with increasing number of transitions, which is probably caused by both pyruvate inhibition and inactivation as a result of phosphorylation and aggregation.[36] Nevertheless, the level of enzymatic control over microdroplet generation shown in Figure 2.7a has not been achieved before, and holds great promise for the development of dynamic artificial organelles. Removal of waste products via dialysis or by downstream enzymatic conversion can further improve the system's durability.

In the reaction network underlying the observed condensation and dissolution of droplets, the two opposing pathways of ATP formation and consumption can operate simultaneously. Such a network can give rise to responses that are otherwise impossible
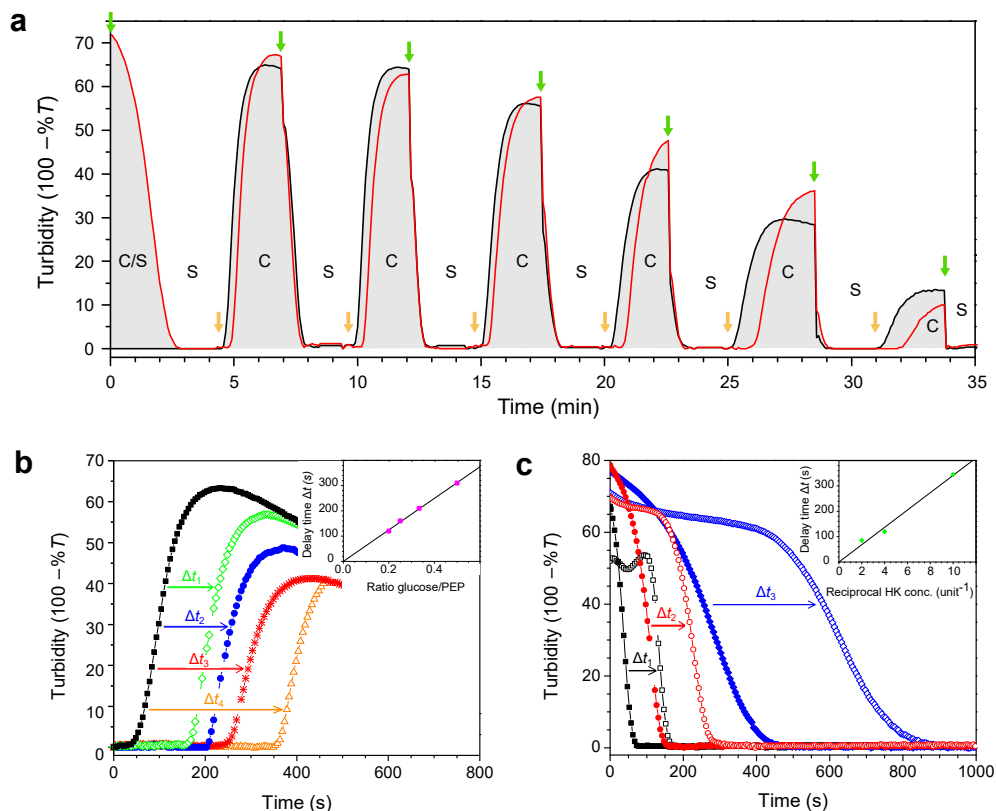
Figure 2.7: (a) Alternating additions of PEP and glucose show that condensation and dissolution are both reversible and that the system can be switched multiple times between a compartmentalized droplet state 'C' and a single-phase, homogeneous solution 'S'. The red line corresponds to a system that started in the compartmentalized droplet state (ATP), while the black line corresponds to a system that started as a homogeneous solution (ADP). At t = 0, 1 equiv. of glucose was added to the ATP-containing system. Further additions were made simultaneously to both mixtures: 1 equiv. of PEP (at orange arrows) and 0.9 equiv. of glucose (at green arrows). (b) Latent condensation of coacervate microdroplets in a system containing ADP, PyK, HK, and increasing amounts of glucose, to which PEP was added at t = 0. The inset shows the delay time as a function of the ratio glucose/PEP. (c) Delayed dissolution of coacervate microdroplets in a system containing ATP, either 0 or 5 mM PEP, PyK and varying amounts of HK, to which glucose was added at t = 0. The solid points refer to reference mixtures without PEP but with 5 mM glucose. The inset shows the delay time as a function of the reciprocal hexokinase concentration.

with simple linear reactions. For example, by introducing an excess of hexokinase, but limiting the amount of glucose relative to PEP, one can control the time at which the mixture starts to condense into droplets and thus trigger the storage of ATP and other

charged macromolecules. An excess of hexokinase results in faster ATP consumption than production by pyruvate kinase, preventing condensation. However, once all glucose has been consumed, ATP production by pyruvate kinase takes over and droplets are formed, as evidenced by an increase in turbidity. The amount of glucose, and indirectly the ratio of hexokinase and pyruvate kinase, set the time of droplet formation, as illustrated in Figure 2.7b. By also varying the absolute amount of enzyme, the onset of condensation can be further tuned. On the other hand, if an excess of pyruvate kinase is present but the amount of PEP is limited, droplet dissolution can be programmed with a delay time that depends on the amount of PEP and pyruvate kinase (Figure 2.7c).

We emphasize that the behavior shown in Figure 2.7b and c, in which a mixture displays a shift in time while maintaining the same responsiveness, can only be realised in a network of cooperating reactions. The possibility to program this behavior opens up a wide range of possibilities for use of this system as artificial organelles: it provides a natural way to control both spatial and temporal organization of biomolecules under physiological conditions.

2.5 Conclusion

In this chapter, we developed a reaction-driven coacervation model, as a first step in our path towards actively growing protocells. We demonstrated that an enzymatic reaction network can be used to both generate and dissolve coacervate droplets in a reversible way. The onset and rate of phase transitions can be controlled by enzyme kinetics. The performance of the system eventually decreases after twelve cycle repetitions (without enzyme or nucleotide added), as a result of the accumulation of reaction waste products. Using pyruvate kinase with PEP as substrate, ATP-PLL coacervates can be generated within a minute, whereas they can be dissolved again in tens of seconds using hexokinase with glucose as second substrate. Finally, another advantage of our enzyme pair is that, as both reactions take place simultaneously, we can combine all components and program the system to act as a chemical timer, condensing spontaneously into liquid droplets at a specified time after substrate addition.

In addition to demonstrating our level of control, the reversibility of coacervation may be relevant in a prebiotic context, providing a mechanism for coacervate droplets to overcome their inherently instability towards coarsening. Cycles of condensation/dissolution can also be seen as a form of transient compartmentalization, a process that has been proposed explain the emergence of functional replicators before dividing cells. [40]

The coacervate droplets formed in this way are natural storage compartments for nucleotides, charged biomolecules and organic compounds and the enzymatic network that governs their formation holds great promise in our attempt to build a synthetic cell: it allows control over both spatial and temporal organization of molecules, their interactions and reactions in complex systems. An important next step is to shift focus

from the thermodynamics of phase separation — under which conditions it can happen — to kinetics: can we control how coacervates are forming, in order to achieve growing droplets?

2.6 Experimental details

2.6.1 Materials and methods

All chemicals were purchased from Sigma Aldrich and used as received unless otherwise stated. poly-*L*-lysine hydrobromide (PLL, 15-30 kDa) was dissolved in Milli-Q water (18.2 M Ω cm) at a concentration of 50 mg mL^{-1} (0.28 M in monomer units). Adenosine triphosphate disodium salt (ATP) and adenosine diphosphate disodium salt (ADP) were freshly dissolved in water at a concentration of 100 mM and kept on ice throughout the experiments. Phosphoenolpyruvate monopotassium salt (PEP-K) solutions of 100 mM were prepared in 100 mM HEPES pH 7.4. A 0.5 M HEPES buffer was prepared from HEPES sodium salt, the pH was adjusted to 7.4 with 1 M HCl and the solution was filtered prior to use. D-glucose, sodium chloride and magnesium chloride solutions were prepared in Milli-Q water.

The pH of the all solutions was measured with a pH meter, whereas the pH of the coacervate dispersions was checked during dynamic measurements on a universal pH paper strip. Pyruvate kinase (PK) from rabbit muscle (EC 2.7.1.40, Sigma, type VII, 348 units mg^{-1}) was freshly diluted in Milli-Q water prior to use to avoid the introduction of additional ions into the coacervate-forming solutions. Hexokinase (HK) from Saccharomyces cerevisiae was purchased as a lyophilized powder (EC 2.7.1.1, Fluka, mixture of isoforms, 41 units mg-1) and was dissolved in 10 mM HEPES pH 7.4 containing 50% (v/v) glycerol to make a concentrated stock. Dilutions were made in water prior to use. SYBR gold nucleic acid stain (Thermo Fischer, 10,000x concentrate in DMSO) was used as a fluorescent dye for nucleotide-containing coacervates. The concentrated stock solution was diluted 100 times in buffer and added to the samples in a 1:10 ratio.

2.6.2 Coacervate formation

Samples for turbidity measurements were prepared directly into 96-well plates (Greiner Bio-one, clear flat-bottom wells), by adding, respectively, HEPES, MgCl$_2$, Milli-Q, hexokinase and/or pyruvate kinase (when applicable), PLL, ADP or ATP, and PEP and/or glucose (when applicable), to a total volume of 100 μL. Mixing was done by gentle pipetting (3X) before each measurement. Samples for the microscopy experiments were prepared in microcentrifuge tubes. After addition of the substrate, a 10 μL aliquot was immediately taken for imaging on a glass slide.

2.6.3 Turbidimetry

Turbidity measurements were performed in triplicate using a Berthold Tristar2 LB 942 microplate reader. Temperature was kept at 27$\pm$1 °C. The absorbance was measured at 520 nm, where none of the mixture components absorbed significantly, and turbidity is reported as $(100 - \%T)$ with $\%T$ being the fraction of transmitted light at this wavelength. The absorbance of a well filled with the same volume of water was used as a blank. Samples were shaken for 0.5 s before every readout.

2.6.4 Titrations

The critical salt concentration of ADP and ATP-coacervates with PLL was determined by mixing PLL (5 mM monomer concentration) and ADP or ATP in 50 mM HEPES pH 7.4 with 5 mM MgCl$_2$ and increasing concentrations of NaCl, and measuring turbidity as a function of the concentration of added NaCl (triplicate). To evaluate the influence of PEP-K, some titrations were conducted in the presence of the substrate (5-15 mM), but in absence of any enzyme. The critical point was determined by extrapolating the first order derivative at the inflection point to zero turbidity. The inflection point was usually located in the region just before the turbidity reached and stabilised at a minimum value (single-phase solution). Note that this critical salt concentration does not take into account ions from other sources than the added NaCl, and the actual critical ionic strength may therefore be higher.

2.6.5 Optical and fluorescence microscopy

Images were recorded on an Olympus UIS2 microscope, equipped with a motorized stage (Prior, Optiscan II). Fluorescent images were recorded with an EMCCD camera (Andor, iXon), using illumination from a mercury lamp, an excitation filter of 482/18 nm (Semrock BrightLine) and an emission filter of 525/45 nm (Semrock BrightLine). Images were analyzed and prepared for presentation in ImageJ.

2.6.6 Details of the kinetic model

We modelled the reaction network as a set of ordinary differential equations (ODE's), which are derived from the underlying reaction mechanisms, similar to the approach taken in the work of Semenov *et al.*[25] These ODE's were implemented in MATLAB and solved numerically.

For pyruvate kinase, we took into account that even in the presence of LLPS, the product ATP is a reversible inhibitor by binding to both the enzyme and the enzyme-pyruvate complex. ADP and ATP are thought to bind to the enzyme as a complex with Mg^{2+}, and we assume a random binding mechanism for ADP and PEP.[36] The enzyme concentration corresponding to 1 unit in 100 µL samples was set to 2.2 µM. Finally,

based on luciferase assays, we assumed that the ADP was contaminated with 10% ATP. In hexokinase mechanism, ADP is a reversible inhibitor by binding to both the enzyme-glucose and the enzyme-glucose-6-phosphate complex. ADP and ATP are thought to bind to the enzyme as a complex with Mg^{2+}.[41] The enzyme concentration corresponding to 1 unit in 100 μL was set to 3.5 μM.

In both cases, we assumed that reactions only take place in the solution phase, and that ATP is exchanged rapidly between the droplets and the solution. The solution is saturated with ATP at the binodal point,[27] $[ATP]_0 = 1.3$ mM. Excess ATP is condensed into droplets by nucleation and growth: $[ATP]_c = [ATP]_t - [ATP]_b$, where $[ATP]_t$ represents the ATP concentration that would be present if phase separation was suppressed, which is the total amount of ATP divided by the total volume. The turbidity was assumed to be directly proportional to $[ATP]_c$. To account for the observed slow coalescence and sedimentation, we included an empirical linear decrease of turbidity with time, starting from the point of the first droplet condensation.

The individual rates we used to produce the theoretical curves shown in Figure 2.6 are summarized in Table 2.1 below.

Table 2.1: Kinetic constants used for theoretical predictions of pyruvate kinase and hexokinase catalyzed droplet formation and dissolution in Figure 2.6a and b.

Pyruvate kinase		Hexokinase	
Rate constant	Value	Rate constant	Value
k_1	$1.0 \times 10^4 \, \text{mM}^{-1} \, \text{s}^{-1}$	k_1	$3.7 \times 10^3 \, \text{mM}^{-1} \, \text{s}^{-1}$
k_{-1}	$1.0 \times 10^2 \, \text{s}^{-1}$	k_{-1}	$1.5 \times 10^3 \, \text{s}^{-1}$
k_2	$25 \, \text{s}^{-1}$	k_2	$4.0 \times 10^3 \, \text{mM}^{-1} \, \text{s}^{-1}$
k_3	$1.0 \times 10^2 \, \text{mM}^{-1} \, \text{s}^{-1}$	k_{-2}	$6.5 \times 10^2 \, \text{s}^{-1}$
k_{-3}	$1.0 \times 10^2 \, \text{s}^{-1}$	k_3	$5.0 \times 10^3 \, \text{mM}^{-1} \, \text{s}^{-1}$
k_4	$2.0 \times 10^3 \, \text{mM}^{-1} \, \text{s}^{-1}$	k_{-3}	$2.0 \times 10^4 \, \text{s}^{-1}$
k_{-4}	$4.0 \times 10^1 \, \text{s}^{-1}$	k_4	$15 \, \text{s}^{-1}$
		k_5	$2.0 \times 10^3 \, \text{mM}^{-1} \, \text{s}^{-1}$
		k_{-5}	$2.0 \times 10^3 \, \text{s}^{-1}$
		k_6	$1.2 \times 10^2 \, \text{mM}^{-1} \, \text{s}^{-1}$
		k_{-6}	$1.5 \times 10^3 \, \text{s}^{-1}$

2.6.7 Alternative source of PLL

We initially had the goal of using homemade poly-*L*-lysine (PLL), produced by solution polymerization, because it aligned with our goals of creating a more prebiotically relevant model. The results presented in this chapter were achieved with commercial PLL, but we include the synthetic procedure here, with the goal to make this system even more available.

Poly-lysine hydrobromide was synthesized from N_ϵ-carbobenzyloxy-*L*-lysine (H-Lys(Z)-OH) following the procedure described in reference 42 and represented in the reaction

scheme below. First, the aminoacid was activated by converting it into a N-carboxy anhydride (Lys-NCA) form. H-Lys(Z)-OH (5.00 g, 17.8 mmol, 1 equiv.) was suspended in tetrahydrofuran (THF, 80 mL) and α-pinene (7.36 g, 54 mmol, 4 equiv.) in a two-neck round-bottom flask kept under argon. Triphosgene (2.65 g, 8.95 mmol, 0.5 equiv.) was dissolved in THF (15 mL) and added via an addition funnel during 15 minutes (*see safety sheet before handling*). The reaction was left to stir for 2 hours, at which point the suspension had become clear. The mixture was concentrated in a rotary evaporator to 30 % its original volume, and n-heptane was added. Lys-NCA (2.04 g) was recrystallized thrice from this mixture and dried under vacuum overnight. Lys-NCA was stored under -20 °C.
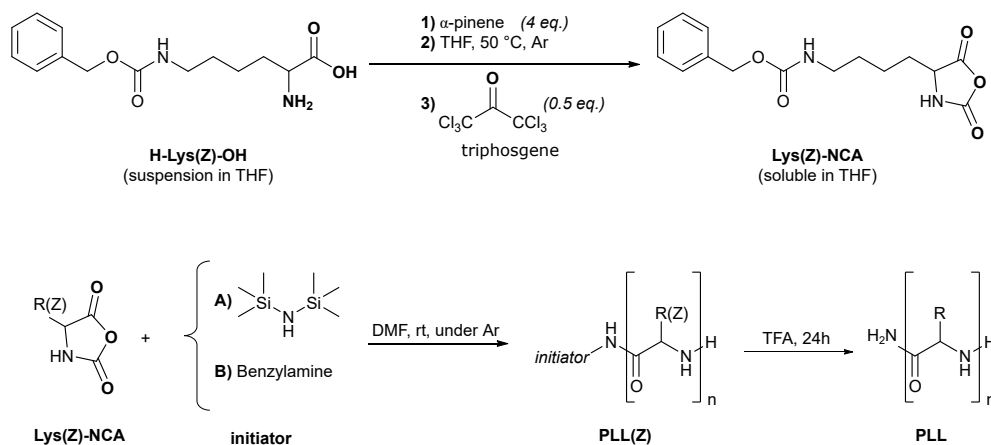
Then, ring-opening polymerization was performed in dry dimethylformamide (DMF). The solvent was freeze-thawed thrice to remove oxygen, and 10 mL were used to dissolve the Lys(Z)-NCA (1.01 g, 3.31 mmol, 1 equiv.). Hexamethyldisiloxane (HMDS, 5.54 mg, 34.3 µmol, 1/100 equiv) was added last via a syringe as an initiator (the ratio determines the theoretical polymerization degree). After 24 hours, the polymeric chains of PLL(Z) were precipitated by adding diethyl ether (50 mL). A solid was isolated via successive centrifugation/decantation cycles with diethyl ether (20 mL).

Finally, PLL(Z) was deprotected in TFA (5.8 mL) and hydrobromic acid (HBr, 3.5mL of a 33 % solution in acetic acid, 21.5 mmol). After 24 hours diethyl ether was added and the centrifugation/decantation repeated to isolate a solid (248.8 mg). After drying under vacuum overnight, the solid was subjected to Maldi-TOF and H-NMR analysis to confirm the polymerization to PLL. Once confirmed, it was dissolved in water and dialyzed against HBr (10 mM) to remove DMF and short chains (MWCO 10 kDa).

Lys(Z)-NCA: ^{1}H-NMR (400 MHz, CDCl$_3$, δ) 7.35 (m, 5H), 6.81 (bs, 1H), 5.10 (t, 2H), 4.91 (bs, 1H), 4.27 (t, 1H), 3.2 (m, 2H), 2-1.8 (m, 2H), .6-1.4 (m, 4H).

A 1H-NMR

H-Lys(Z)-OH

Lys(Z)-NCA

PLL

8.0   7.0   6.0   5.0   4.0   3.0   2.0   1.0   0.0

δ (ppm)

B Maldi-TOF

PLL
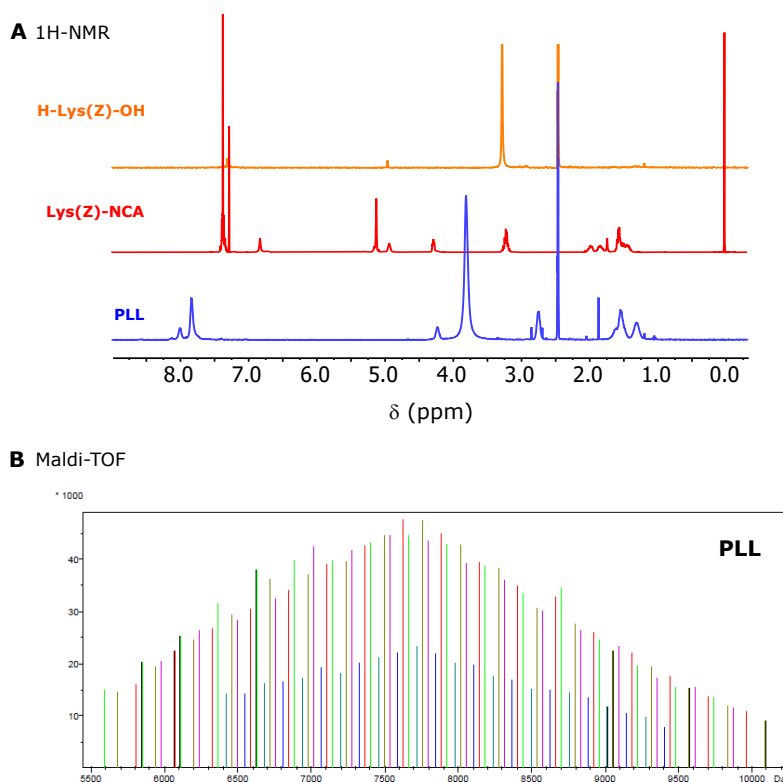
Figure 2.8: (A) 1H-NMR of the synthesized PLL, the synthesized monomer Lys(Z)-NCA and its precursor H-Lys(Z)-OH. (B) Maldi-TOF spectrum of the synthesized PLL, confirming polymerization.

Acknowledgements

References

[1] J. Shively, "Inclusion bodies of prokaryotes," *Annual Reviews in Microbiology*, vol. 28, no. 1, pp. 167–188, 1974.

[2] E. M. Courchaine, A. Lu, and K. M. Neugebauer, "Droplet organelles?," *The EMBO Journal*, vol. 35, no. 15, pp. 1603–1612, 2016.

[3] B. R. Sabari, A. Dall'Agnese, and R. A. Young, "Biomolecular condensates in the nucleus," *Trends in biochemical sciences*, 2020.

[4] C. P. Brangwynne, C. R. Eckmann, D. S. Courson, A. Rybarska, C. Hoege, J. Gharakhani, F. Jülicher,

and A. A. Hyman, "Germline P granules are liquid droplets that localize by controlled dissolution/-condensation," *Science*, 2009.

[5] T. J. Nott, E. Petsalaki, P. Farber, D. Jervis, E. Fussner, A. Plochowietz, T. D. Craggs, D. P. Bazett-Jones, T. Pawson, J. D. Forman-Kay, *et al.*, "Phase transition of a disordered nuage protein generates environmentally responsive membraneless organelles," *Molecular cell*, vol. 57, no. 5, pp. 936–947, 2015.

[6] U. Sheth and R. Parker, "Decapping and decay of messenger RNA occur in cytoplasmic processing bodies," *Science*, vol. 300, no. 5620, pp. 805–808, 2003.

[7] C. J. Decker, D. Teixeira, and R. Parker, "Edc3p and a glutamine/asparagine-rich domain of Lsm4p function in processing body assembly in Saccharomyces cerevisiae," *Journal of Cell Biology*, vol. 179, no. 3, pp. 437–449, 2007.

[8] J. R. Buchan and R. Parker, "Eukaryotic Stress Granules : The Ins and Out of Translation," *Molecular cell*, vol. 36, no. 6, p. 932, 2009.

[9] J. R. Wheeler, T. Matheny, S. Jain, R. Abrisch, and R. Parker, "Distinct stages in stress granule assembly and disassembly," *eLife*, 2016.

[10] C. P. Brangwynne, T. J. Mitchison, and A. A. Hyman, "Active liquid-like behavior of nucleoli determines their size and shape in Xenopus laevis oocytes," *Proceedings of the National Academy of Sciences of the United States of America*, vol. 108, no. 11, pp. 4334–4339, 2011.

[11] M. Feric, N. Vaidya, T. S. Harmon, D. M. Mitrea, L. Zhu, T. M. Richardson, R. W. Kriwacki, R. V. Pappu, and C. P. Brangwynne, "Coexisting Liquid Phases Underlie Nucleolar Subcompartments," *Cell*, vol. 165, no. 7, pp. 1686–1697, 2016.

[12] H. Falahati and E. Wieschaus, "Independent active and thermodynamic processes govern the nucleolus assembly in vivo," *Proc Natl Acad Sci U S A*, vol. 114, no. 6, pp. 1335–1340, 2017.

[13] A. Oparin, "Origin and evolution of metabolism," *Comparative biochemistry and physiology*, vol. 4, no. 2-4, pp. 371–377, 1962.

[14] J. B. S. Haldane, "The origin of life," *Rationalist Annual*, vol. 148, pp. 3–10, 1929.

[15] W. M. Aumiller and C. D. Keating, "Experimental models for dynamic compartmentalization of biomolecules in liquid organelles: Reversible formation and partitioning in aqueous biphasic systems," *Advances in Colloid and Interface Science*, vol. 239, pp. 75–87, 2017.

[16] Y. S. Jho, H. Y. Yoo, Y. Lin, S. Han, and D. S. Hwang, "Molecular and structural basis of low interfacial energy of complex coacervates in water," *Advances in Colloid and Interface Science*, vol. 239, pp. 61–73, 2016.

[17] H. Bungenberg de Jong and H. Kruyt, "Coacervation (partial miscibility in colloid systems)," in *Proc. K. Ned. Akad. Wet*, vol. 32, pp. 849–856, 1929.

[18] J. T. G. Overbeek and M. Voorn, "Phase separation in polyelectrolyte solutions. theory of complex coacervation," *Journal of Cellular and Comparative Physiology*, vol. 49, no. S1, pp. 7–26, 1957.

[19] D. Zwicker, R. Seyboldt, C. A. Weber, A. A. Hyman, and F. Jülicher, "Growth and division of active droplets provides a model for protocells," *Nature Physics*, vol. 13, pp. 408–413, 2017.

[20] S. Ramaswamy, "The mechanics and statistics of active matter," *Annu. Rev. Condens. Matter Phys.*, vol. 1, no. 1, pp. 323–345, 2010.

[21] E. Tjhung, D. Marenduzzo, and M. E. Cates, "Spontaneous symmetry breaking in active droplets provides a generic route to motility," *Proceedings of the National Academy of Sciences*, vol. 109, no. 31, pp. 12381–12386, 2012.

[22] J. Berry, C. P. Brangwynne, and M. Haataja, "Physical principles of intracellular organization via active and passive phase transitions," *Reports on Progress in Physics*, vol. 81, no. 4, p. 046601, 2018.

[23] D. Hnisz, K. Shrinivas, R. A. Young, A. K. Chakraborty, and P. A. Sharp, "A phase separation model for transcriptional control," *Cell*, vol. 169, no. 1, pp. 13–23, 2017.

[24] G. Laflamme and K. Mekhail, "Biomolecular condensates as arbiters of biochemical reactions inside the nucleus," *Communications Biology*, vol. 3, no. 1, pp. 1–8, 2020.

[25] S. N. Semenov, A. S. Y. Wong, R. M. van der Made, S. G. J. Postma, J. Groen, H. W. H. van Roekel, T. F. A. de Greef, and W. T. S. Huck, "Rational design of functional and tunable oscillating enzymatic networks," *Nature Chemistry*, vol. 7, no. 2, pp. 160–165, 2015.

[26] W. M. Aumiller Jr and C. D. Keating, "Phosphorylation-mediated RNA/peptide complex coacervation as a model for intracellular liquid organelles," *Nature Chemistry*, vol. 8, no. 2, pp. 129–137, 2015.

[27] E. Spruijt, A. H. Westphal, J. W. Borst, M. A. Cohen Stuart, and J. Van Der Gucht, "Binodal compositions of polyelectrolyte complexes," *Macromolecules*, vol. 43, no. 15, pp. 6476–6484, 2010.

[28] E. Spruijt, F. A. M. Leermakers, R. Fokkink, R. Schweins, A. A. Van Well, M. A. Cohen Stuart, and J. Van Der Gucht, "Structure and dynamics of polyelectrolyte complex coacervates studied by scattering of neutrons, X-rays, and light," *Macromolecules*, vol. 46, no. 11, pp. 4596–4605, 2013.

[29] L. C. Reineke, W.-C. Tsai, A. Jain, J. T. Kaelber, S. Y. Jung, and R. E. Lloyd, "Casein kinase 2 is linked to stress granule dynamics through phosphorylation of the stress granule nucleating protein g3bp1," *Molecular and cellular biology*, vol. 37, no. 4, 2017.

[30] J. E. Henninger, O. Oksuz, K. Shrinivas, I. Sagi, G. LeRoy, M. M. Zheng, J. O. Andrews, A. V. Zamudio, C. Lazaris, N. M. Hannett, *et al.*, "Rna-mediated feedback control of transcriptional condensates," *Cell*, vol. 184, no. 1, pp. 207–225, 2021.

[31] W. Zhao, H. Wang, and Y. Wang, "Coacervation of dynamic covalent surfactants with polyacrylamides: properties and applications," *Soft matter*, vol. 14, no. 20, pp. 4178–4184, 2018.

[32] N. A. Liapounova, V. Hampl, P. M. Gordon, C. W. Sensen, L. Gedamu, and J. B. Dacks, "Reconstructing the mosaic glycolytic pathway of the anaerobic eukaryote monocercomonoides," *Eukaryotic cell*, vol. 5, no. 12, pp. 2138–2146, 2006.

[33] E. A. Frankel, P. C. Bevilacqua, and C. D. Keating, "Polyamine/Nucleotide Coacervates Provide Strong Compartmentalization of Mg2+, Nucleotides, and RNA," *Langmuir*, vol. 32, no. 8, pp. 2041–2049, 2016.

[34] S. Lindhoud, R. de Vries, W. Norde, and M. A. Stuart, "Structure and stability of complex coacervate core micelles with lysozyme," *Biomacromolecules*, vol. 8, no. 7, pp. 2219–2227, 2007.

[35] S. Koga, D. S. Williams, A. W. Perriman, and S. Mann, "Peptide-nucleotide microdroplets as a step towards a membrane-free protocell model.," *Nature chemistry*, vol. 3, no. 9, pp. 720–4, 2011.

[36] C. Wang, L. R. Chiarelli, P. Bianchi, D. J. Abraham, A. Galizzi, A. M. A. Zanella, and G. Valentini, "Human erythrocyte pyruvate kinase: Characterization of the recombinant enzyme and a mutant form (R510Q) causing nonspherocytic hemolytic anemia," *Blood*, 2001.

[37] J. Wang, M. A. Cohen Stuart, and J. Van Der Gucht, "Phase diagram of coacervate complexes containing reversible coordination structures," *Macromolecules*, vol. 45, no. 21, pp. 8903–8909, 2012.

[38] S. Lindhoud and M. M. Claessens, "Accumulation of small protein molecules in a macroscopic complex coacervate," *Soft Matter*, vol. 12, no. 2, pp. 408–413, 2015.

[39] E. Sokolova, E. Spruijt, M. M. K. Hansen, E. Dubuc, J. Groen, V. Chokkalingam, A. Piruska, H. A. Heus, and W. T. S. Huck, "Enhanced transcription rates in membrane-free protocells formed by coacervation of cell lysate," *Proceedings of the National Academy of Sciences*, vol. 110, no. 29, pp. 11692–11697, 2013.

[40] S. Matsumura, Á. Kun, M. Ryckelynck, F. Coldren, A. Szilágyi, F. Jossinet, C. Rick, P. Nghe, E. Szathmáry, and A. D. Griffiths, "Transient compartmentalization of rna replicators prevents extinction due to parasites," *Science*, vol. 354, no. 6317, pp. 1293–1296, 2016.

[41] G. Noat, J. Ricard, M. Borel, and C. Got, "Kinetic study of yeast hexokinase: 1. steady-state kinetics," *European journal of biochemistry*, vol. 5, no. 1, pp. 55–70, 1968.

[42] V. Dmitrovic, G. J. Habraken, M. M. Hendrix, W. J. Habraken, A. Heise, N. A. Sommerdijk, *et al.*, "Random poly (amino acid) s synthesized by ring opening polymerization as additives in the biomimetic mineralization of caco3," *Polymers*, vol. 4, no. 2, pp. 1195–1210, 2012.

Part II

Intermission

Chapter 3

Towards a kinetic understanding of chemistry in coacervates
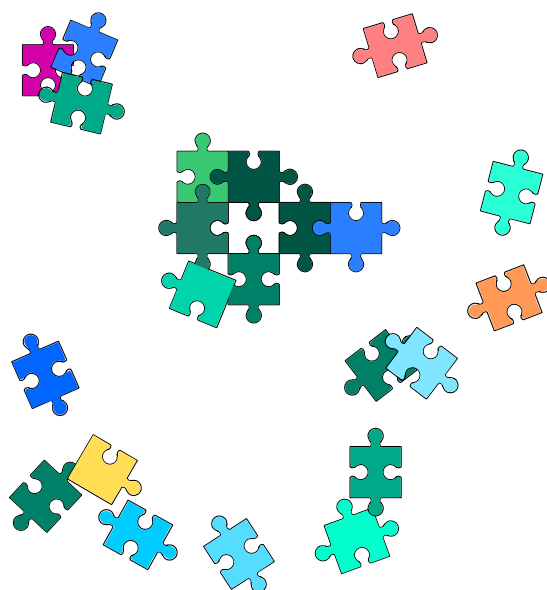
This chapter is based on:

KK Nakashima*, MA Vibhute* & E Spruijt. Biomolecular chemistry in liquid phase separated compartments. *Front. Mol. Biosci.* **2019**.

KK Nakashima*, AAM André* & E Spruijt. Enzymatic control over coacervation. *Methods in Enzymology vol. 646* **2021**. *equal contributions*

3.1   Nothing in Biology makes sense except in the light of Chemistry

Droplet organelles were an exciting discovery by Clifford Brangwynne and co-workers in 2009, when they were still thought to be exceptions among the traditional, membrane-bound organelles (e.g. mitochondrion, Golgi body, nucleus).[1] Since then, there has been an overwhelming amount of reports of new organelles with liquid-like properties and proteins with phase-separating properties. More than adding to the list of known cellular organelles, widespread occurrence of membraneless organeless (MLOs, sometimes also called condensates) can be paradigm-shaking: an alternative to the idea of a homogeneous cytosol or nucleus, where dozens of biomolecules meet by chance to participate in high fidelity, high efficiency enzymatic processes. American geneticist Richard Young says about condensates:

> *"In retrospect it's amazing that we allowed ourselves to think that processes that happen in the cell that involve many different components that need to get together, that that would occur by random chance, and that we'd have enough molecules of each type, that they would randomly come and associate with one another. One question I get fairly frequently is — to what extent is the formation of condensates a property of just a few things in the cell, and most of the rest of the cell just operates the way we've always thought. So far, the record of studying a new protein and finding that it's in a condensate is 100%. So we're beginning to wonder if in fact all of what the cell does is controlled in this context of membraneless organelles that operate by these properties".*

Although the 100% score is clearly an exaggeration, the ability to form reversible condensates, or in other words, exist in a liquid state, has been predicted for most proteins in the human proteome.[2] This finding becomes even more relevant if we take into account research proposing that reversible condensates act as intermediates in the formation of pathological, irreversible amyloid aggregates.[3] The widespread ocurrence of the liquid state and of condensates not only in human cells, but in both eukaryotic and prokaryotic cells suggests though that they play key roles beyond in disease.

The natural hypothesis after the discovery of MLOs is that they have a vital, beneficial function in the cell, such as (1) they sequester and protect key molecules from undesired reactions in the cytosol or (2) they catalyze reactions that are inefficient in the cytosol. A less exciting possibility is that (3) they have no function *per se*, but are instead merely a consequence of the cytosolic composition.[4] Experimental evidence for both enhanced reactivity (1), and reaction quenching (2) has been found in specific cases,[5,6] but a

general picture of how reactivity can be different inside condensates and coacervate models is still lacking.

In this chapter, we will make a short intermission in our development of active coacervates to take a closer look into hypotheses (1) and (2), and explore how we can experimentally fulfill the blind spot in our understanding of cellular chemistry. For this goal, we will discuss condensates in the context of biphasic reactions, and we will use the system developed in Chapter 2 to present a protocol for quantitative measurements of kinetics in coacervates.

3.2 Concentration effect

Reaction rates inside droplets could differ from those in bulk solutions for two main reasons: the local concentration of reactants inside coacervate droplets may be different from outside, or the rate constant k may be affected by their unique environment (Equation 3.3), or a combination of both effects. Although solutes are not bound to the MLOs by a membrane, and can freely move in and out, it is likely that partitioning affects their availability to biochemical reactions outside condensates, while favoring reactions with species inside — what we call a **concentration effect** (Figure 3.2A). [7,8]

Besides the phase-separating biomolecules that make up the mesh of condensates (which we call *hosts*), there is a wide range of additional molecules (*clients*) that are spontaneously taken up into nucleated organelles by partitioning or sequestration, like in P-granules. The distinction between hosts and clients is not always sharp, and clients that reach high concentrations inside MLOs have been found to significantly affect the phase diagram of the original hosts. [9,10] We focus on the case where client concentrations remain sufficiently low, and explain client distribution from a partitioning point of view. To start the discussion of concentration, we consider a bimolecular reaction between a substrate **S** and an enzyme **E** taking place in two phases: the dilute, solution phase (*1*); and the coacervate, dense phase (for which we use the index *2*).

Experiments suggest that many enzymatic reactions involving small molecule substrates are primarily affected by enhanced substrate and cofactor concentration. [11–13] Hexokinase partitions inside polylysine-ATP droplets with $K_p \simeq 20$, and its activity is enhanced twofold, because of high local ATP and Mg^{2+} concentrations. [11] Lipase activity is increased about twofold in coacervate micelles, because of a combination of substrate concentration and stabilization of the enzyme's active form. [14]

The distribution of biomolecules, or any solute, between two coexisting liquids, like the cytosol and the membraneless organelles in the cell, or the dilute phase and the coacervate droplets in a cytomimetic model, is governed by the relative standard free energy of the solute in the different phases (Figure 3.1A). In Equation 3.1, c_c and c_s are the concentration of a solute **S** in the coacervate and the dilute phase, respectively, K_p is the partitioning coefficient and λ is a correction factor that accounts for differences

in activity between both phases. The standard molar Gibbs free energy difference of the solute between the two phases (ΔG^0) sets the degree of partitioning Equation 3.1, and is generally composed of multiple contributions (Equation 3.2, Figure 3.1B).

$$\mathbf{S}_{(1)} \rightleftharpoons \mathbf{S}_{(2)}$$
$$\frac{S_2}{S_1} = K_P^S \simeq \lambda e^{-\frac{\Delta G^0}{RT}} \tag{3.1}$$

$$\Delta G^0 = \Delta G^0_{\text{hphob}} + \Delta G^0_{\text{charge}} + \Delta G^0_{\text{Hbond}} + \Delta G^0_{\text{mesh}} + \ldots \tag{3.2}$$

Generally speaking, a solute partitions in coacervates or MLOs if it has a preference for the building blocks over the solvent (water). Models for the salt tolerance of coacervates provide estimates of the relative permittivity of coacervates between 45 and 60, caused by the presence of hydrophobic elements (e.g., amino acids residues, polymer backbone) and strongly bound hydration water.[15–17] For hydrophobic solutes, such as Nile red and bromothymol blue ($K_p \simeq 10^2$),[18] the free energy of solvation in the condensate environment (ΔG^0_{hphob}) is the principal driving force for partitioning. Although ΔG^0_{hphob} can predict that unfolded proteins, which have their hydrophobic cores exposed, partition in PDDA-PAA coacervates with K_p 1, it fails to explain why native proteins have a similar if not higher K_p,[19] and we must look at additional contributions to the free energy.
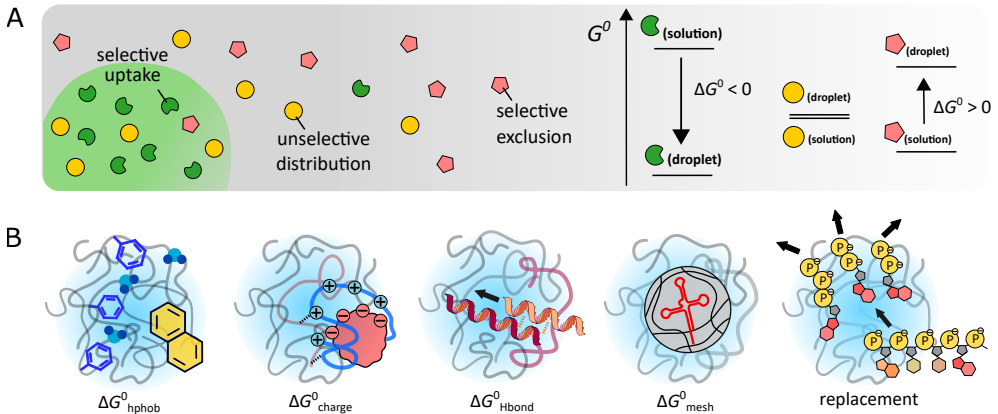
Figure 3.1: (A) Schematic illustration of three scenarios for partitioning, depending on the relative free energy levels of the client molecule in both phases. (B) Contributions to the free energy that governs partitioning in coacervates.

Many IDPs and coacervate-forming polymers contain extensive charged regions. The interaction with these charged regions (ΔG^0_{charge}) is likely to be the main driving force for partitioning of the majority of biomolecules. The entropically favored release of bound counter-ions upon complexation accounts for a significant part of ΔG^0_{charge}. In Ddx4 droplets, both positively and negatively charged proteins are selectively taken up, while

neutral proteins are excluded. Small, highly charged proteins, such as lysozyme, are also readily incorporated into complex coacervates of polymers PDMAEMA and PAA, reaching concentrations up to 150–200 g/L. [20]

Besides charge complexation, solutes can also interact with the coacervate matrix through hydrogen bonding (ΔG^0_{Hbond}). Nucleic acids in particular may form base pairs with complementary sequences in model MLOs. Poly-U-spermine coacervates, a simple model for nucleotide-protein droplets, are able to selectively concentrate oligonucleotides and oligopeptides. For such coacervates, poly-A has a partitioning coefficient two orders of magnitude higher than poly-N or poly-U, because of base-pairing interactions. [21] However, a similar system, based on poly-U and the peptide RRASLRRASL, does not distinguish between poly-A and poly-N: both are highly concentrated inside coacervates, most likely because charge complexation dominates this partitioning. [22]

To accommodate large and rigid biomolecules, including base-paired nucleic acid duplexes, the mesh of IDP or polymer chains must be deformed significantly, which disfavors partitioning (ΔG^0_{mesh}) and destabilizes coacervates. [23] Ddx4 droplets were found to concentrate single-stranded RNA and DNA ($\Delta G^0_{hphob} + \Delta G^0_{charge}$), while excluding double-stranded DNA of the same length and inducing strand dissociation of shorter DNA duplexes. [24] In some cases, client molecules are taken up by replacing other species in the coacervates. Although this displacement no longer qualifies as simple partitioning, it can have a very similar strong concentrating effect. In PAH-ATP droplets, RNA is concentrated by a factor 10^5. [21] As a single RNA chain can replace multiple nucleotides, this exchange is driven by a significant increase in entropy. The same mechanism accounts for the uptake of many polymers and colloids in polylysine-ATP droplets. [11]

In cells, partitioning of biomolecules in MLOs is often more selective than *in vitro*. Specific interactions between binding domains in IDPs and client molecules, such as tubulin, may partly explain this. [25] In addition, all interactions discussed above coincide in MLOs, and their balance is different for every client. Finally, it is important to also look beyond partitioning, and take into account the actual number of molecules available inside or outside MLOs: for low-copy-number biomolecules, stochastic effects come into play, [26] and even weak partitioning can drastically alter the cellular fate.

3.3   Reaction modulation

The second hypothesis for the cellular function of condensates is the acceleration of reactions too slow otherwise. The effect of coacervates on the **rate constant** k is even harder to predict than partitioning, as reactions may be either diffusion-limited (k_0) or transition-state-limited (ΔG^*) (Figure 3.2B). Moreover, in heterogeneous and crowded environments, such as coacervates, k generally becomes a time-dependent quantity and the distribution of reactants and the tortuosity of the reaction path must be taken into account. [27–29]
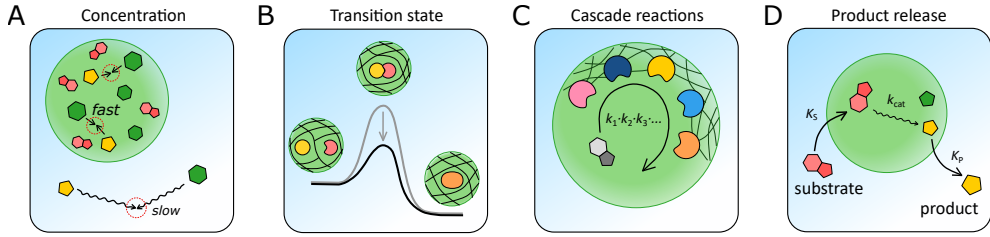
Figure 3.2: Possible effects of coacervate-based compartments on reaction kinetics.

$$k_i = k_{0,i}(t, T)e^{-\frac{\Delta G_i^*}{RT}} \tag{3.3}$$

While in the hexokinase and lipase examples of the previous section high partitioning equated enhanced reaction rates, when moving to larger substrates, the examples become more conflicting: substrate cleavage by hammerhead ribozyme in dextran droplets is about 70 times faster than in solution, which was attributed to an increased ribozyme ($K_p \simeq 3{,}000$) and substrate ($K_p \simeq 40$) concentration.[30] However, despite enhanced concentration, a 60-fold *decrease* of reaction rate was measured for the same ribozyme in polylysine-CMDex coacervates, suggesting that the physico-chemical details of the coacervate environment also impact reactivity.[31]

A similar paradox is seen for the cell-free gene expression and folding of fluorescent reporter proteins: inside PEG-based coacervates, transcription was found to take place with a two orders of magnitude higher polymerase association constant and a six-fold higher transcription rate constant.[32] However, in polylysine-CMDex coacervates, gene expression appeared to be slower overall, and the yield was reduced significantly by protein aggregation in the coacervates.[33] This paradox is likely a consequence of the fact that both diffusion and the energy landscape can be affected by confinement in MLOs, and in either direction. Macromolecular crowding and strong interactions inside the droplets (Figure 3.2B) can lead to anomalous, often reduced diffusion,[34–36] thus contributing to slower kinetics. However, those same effects can also favor a more active enzyme conformation or lower the energy barrier, resulting in a higher rate constant, or they could trap an enzyme in an inactive form, resulting in a vanishing reactivity.

For more complex processes, including multi-step reactions and reaction networks, coacervates could further affect the kinetics. The coacervate matrix can act as scaffold to spatially organize enzymatic cascades, and enhance overall processivity (Figure 3.2B).[37–39] Such a functional role has been proposed for example for nucleoli and processing bodies. Finally, differential partitioning of substrates and products of a reaction could result in an effective rate acceleration (Figure 3.2), akin to what happens in phase transfer catalysis. The uptake of a fusion protein with one or more LAF-1-derived RGG domains and subsequent release of a cargo domain after cleavage from the fusion

protein inside coacervates provides a promising example, although rates have not been determined in this case.[40]

Specifics of enzymatic kinetics also come into play. The components of the enzymatic reaction, including the enzyme, substrate and possible cofactors, distribute over the two phases (neglecting interfacial partitioning), and although there is free exchange between droplets and solution, the droplets represent a new chemical micro-environment to which enzyme activity is likely to be sensitive. Recent studies combining enzymes and LLPS rarely mention K_M and k_{cat} determination (exceptions are 38, 41), which could provide insight in how condensates affect biochemical reactions. Several additional variables need to be assessed: additional rate constant in the droplet ($k_{cat,in}$), new reactant and enzyme concentrations inside and outside of the droplets, and partitioning coefficient of all components.

Beyond the goal of understanding MLO's function, a more complete characterization would contribute to the purpose of controlled phase separation, a goal for example in the protocell field. The biphasic enzymatic reaction may result in a situation in which Michaelis-Menten conditions no longer apply, making it difficult to modulate the kinetics to achieve a behavior like droplet growth, highly dependent on reaction rates.[42] Given how sensitive enzyme activity can be to the precise buffer conditions and other environmental factors, it may seem surprising that these reactions still proceed at all beyond the phase saturation point, especially if the enzymes are taken up inside the droplets. For example, in Chapter 2 we took for granted that pyruvate kinase (PyK) converts ADP to ATP in presence of poly-lysine to form coacervates, but it is not obvious how PyK overcomes the expected inhibition by ATP, which is now present at high concentrations inside the droplets.

3.4   How can these hypotheses be proved?

With the increasing amount of research on condensates and MLOs, why is it that we are still speculating about their cellular function? *In vitro* research has focused on whether potential host molecules can phase separate and the required conditions. Even if phase separation is found to be regulated by a chemical reaction such as protein phosphorylation, few papers compare the progress of the reaction in presence of phase separation with that in a homogeneous solution, or monitor reaction progress and concentration of individual components in each phase separately. Only by carefully measuring the concentrations and rates in the different phases, can the hypotheses about the function of condensates in cells be proved.

It is easy to forget that the complexity of reactions in the presence of liquid compartments is not new to Chemistry (Figure 3.3). Reactivity in heterogeneous media is a central part of studies on nano- and microemulsions, micellar catalysis and phase transfer catalysis, to name a few.[43] Emulsion reactions are used as a strategy to work around the

incompatibility of solubility between reactants and catalysts. A known example, emulsion polymerization, works by isolating monomers in hydrophobic droplets and initiator in the aqueous phase to prevent early radical termination; initially polymerization effectively takes place within micelles rich in monomer, also speeding up the reaction. [44,45]
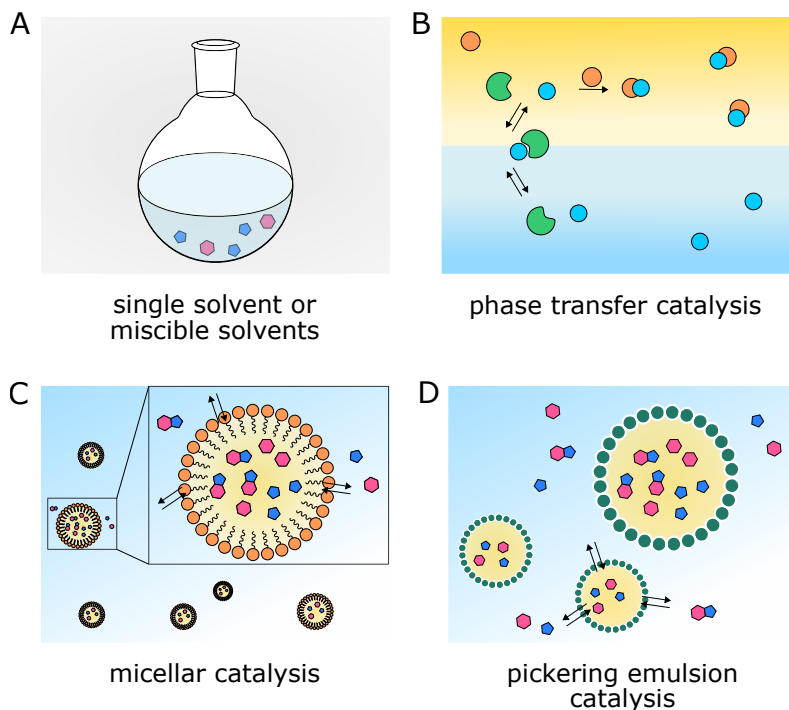
Figure 3.3: Multiphase reaction systems are not rare in chemistry: alternatives to (A) conventional, single solvent systems that introduce physical catalysis are: (B) biphasic mixtures, such as normal and reverse phase transfer catalysis, (C) nano- and micro-emulsions, such as micellar catalysis and (D) pickering emulsion catalysis.

Micellar catalysis has been studied for decades in the context of reactions between organic and ionic compounds. [46] It works by increasing the solubility and local concentration of hydrophobic reactants (without the need of a solvent) and it takes place in discrete compartments, which in comparison to continuous phases, increases the interfacial area and facilitates transfer between polar (aqueous) and apolar (micelle) phases. Often surfactants are functionalized with catalytic moieties and the reaction effectively takes place at the interface. There is now a solid understanding of the capabilities of micellar catalysis and the factors determinant for reactivity: the charge balance of the reaction, the surfactant structure, substrate partitioning and interfacial water. [47–50] Phase transfer catalysis can be compared to emulsion reactions, as it takes place in an aqueous/organic mixture. However, here the reaction does not take place at the interface, but a phase transfer

agent — an organic salt — carries reactants from the aqueous to the organic phase in the form of ion pairs.[51] In view of the similarities between classical emulsion reactions and condensate reactions, it is important to study reactions taking place in the presence of condensates in an equivalent systematic and detailed manner in order to understand MLO's functioning and design functional protocells.

All studies on the formation of condensates or MLOs and their *in vitro* models deal with a heterogeneous reaction medium, more specifically, a heterogeneous emulsion as droplets tend to be polydisperse in size. Even in dynamic studies where condensates form, initially the amount of dense phase may be negligible, but if concentrations or partitioning coefficients are high enough, the contribution of the dense phase can become comparable to that of the dilute phase. All simultaneous processes must be looked at as heterogeneous, biphasic chemical reactions — including the cytosol. This is still often a simplification, because it ignores the interface of the droplets. Like in emulsion reactions and micellar catalysis, condensate catalysis may work by segregating biomolecules from degradation agents or by providing an interface where incompatible solutes can react; or like in phase transfer catalysis, condensates may create a flux of client molecules that partition inside them and meet substrates or catalysts to react with.

We can take inspiration from physical organic chemistry to for the conceptualization and for the experimental design of studies with reactions and LLPS systems. Firstly, quantifying the composition of coacervates provides valuable information. In organic chemistry, partitioning coefficients are measured using separatory funnels, in a mililiter scale, posing a challenge for condensates. Secondly, when diffusion between phases is orders of magnitude faster than reaction rates, it can be assumed only one spectroscopic (NMR) signal and one rate constant are observed for the emulsion (k_{obs}, a weighted average of the phases). Unless relaxation and extremely fast spectroscopical techniques are used, equilibrium can be assumed.[52] Again, for microemulsions it might be a challenge to obtain sharp NMR signals. Finally, to determine separate rate constants per phase, and more complex parameters such as interfacial partitioning coefficient, heterogeneous catalysis studies make use of a model to fit to k_{obs}.

We propose that the biocondensates field and its related fields (coacervate-based protocells, biomimetic phase separation) can benefit from this biphasic system approach. This poses many analytical challenges as not all techniques are suitable for inhomogeneous mixtures or for the scale common to MLO studies. That is why we end this chapter by applying the suggestions so far to our own model system.

3.5 Experimental workflow for studying coacervates

The goal of the experimental part of this chapter was to provide a general protocol that can be applied to other coacervate systems. After discussing our methods and results, we include a detailed description of our protocols so as to encourage reproduction.

3.5.1 Equilibrium concentrations

Even active coacervates like in Chapter 2 — where one of the host molecules is formed *in situ* by a chemical reaction — are, in fact, a biphasic reaction system. Once the enzyme has catalyzed formation of enough of the phase separating form of a (macro)molecule (this is sometimes referred to as "droplet material"), the system enters a two-phase regime. With this in mind, we will use the example of the system from Chapter 2 to show how the quantification of partitioning coefficients and the measurement of kinetic constants can improve our understanding of our findings. In Figure 3.4, this means moving further to the determination of partitioning coefficients and quantification of small molecules, also over time. The development of a kinetic model to fit the experimental data collected will be the center of Chapter 4.
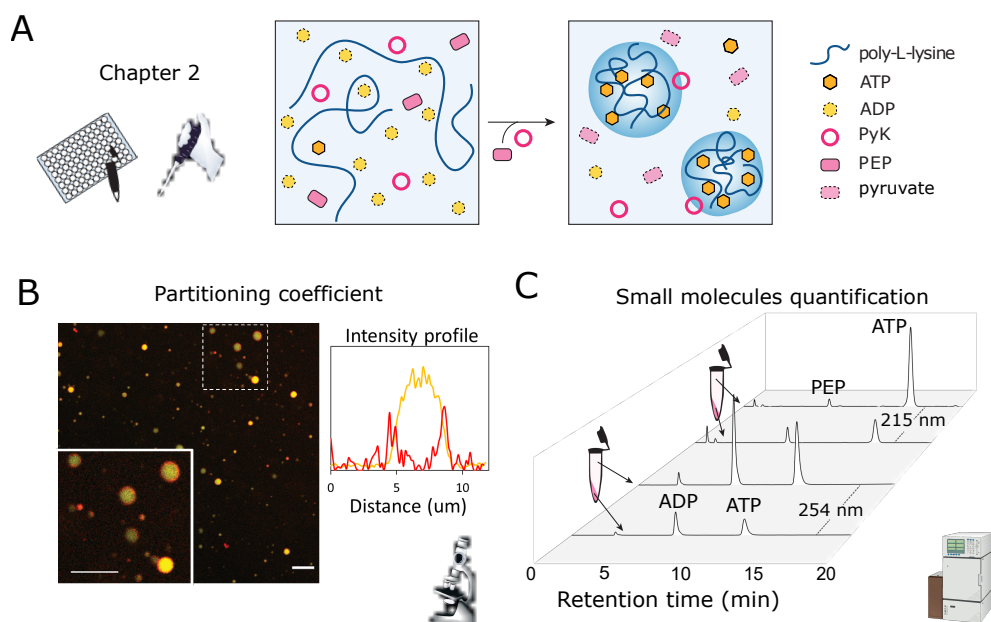
Figure 3.4: More detailed characterization of the ATP-PLL coacervates from Chapter 2. (A) Scheme recapitulating the composition of this model system: ADP does not form droplets with PLL, but when converted to ATP by pyruvate kinase and a co-substrate phosphoenolpyruvate, phase separation takes place. (B) Microscopic evidence of liquid condensates of ATP-PLL and data for partitioning coefficient measurement. PLL labelled with TAMRA is shown in yellow; PyK labelled with Alexa-647 is shown in red. The plot profile of a droplet in the insert highlights the partitioning difference. (C) Chromatograms of ATP-PLL mixtures after centrifugation, used to determine ADP, ATP and PEP concentrations in both phases.

For the partitioning coefficient of the macromolecule components (poly-lysine and pyruvate kinase), fluorescent labeling is the most convenient method. We performed

fluorescence microscopy on passivated glass surfaces to produce a detailed picture of the two-phase system. The ATP-PLL coacervates from Chapter 2 nucleate immediately upon mixing, or 5 minutes after reaction is triggered, and move in and out of the focal plane. Light intensity profiles of both excitation wavelengths were plotted using ImageJ software for the ATP-PLL coacervates. A clear difference in partitioning can be observed between PLL and PyK (Figure 3.4C). While TAMRA-labelled PLL completely co-localizes with the observed coacervates from transmission images, PyK labelled with Alexa-647 accumulates at the coacervate. We include some experimental notes in the next page, as this is a technique we use in other chapters.

In turn, for the partitioning coefficient of the small molecules, we tested different conventional analytical techniques: the luciferase assay for ATP quantification, 31P-NMR, UV/Vis absorption and HPLC/UV. All methods involved separation of the phases by centrifugation and treatment of the coacervate phase with a saline solution to homogenize the mixture prior to the measurement. Chromatography with UV detection produced the most consistent results, which we can confirm by comparing the concentrations found to the total added concentration. In this particular case of ADP and ATP coacervates, separation is crucial as ADP and ATP share absorption maxima, extinction coefficients and two out of three peaks in 31P-NMR (Figure 3.6A), affecting accuracy in their simultaneous quantification. With a weak anion exchange column, ADP and ATP can be clearly separated and UV absorption used for quantification, and also PEP and PLL can be detected at 215 nm (Figure 3.6B). Figure 3.4C shows the chromatograms of the treated dense and dilute phases of ATP-PLL coacervates. After applying the dilution factors, we obtained the partitioning coefficients in table Table 3.1.

Table 3.1: Partitioning coefficients obtained using different methodologies.

Component	K_p	Determination method
PLL	98 ± 16	FL-microscopy
PyK	interfacial	-
ATP	52 ± 18	HPLC-UV 254 nm
ADP	18 ± 4	HPLC-UV 254 nm
PEP	0.8 ± 0.5	HPLC-UV 215 nm

3.5.2 Kinetic measurements

The accuracy of HPLC can be exploited to produce a reliable kinetic profile of ATP formation, that can be used to obtain the enzymatic parameters K_M and k_{cat}. Because analysis requires quenching and dissolution prior to analysis, it is difficult to perform a continuous measurement or obtain several time points in the linear range of the kinetic curve, so we fitted the exponential curve to derive the initial velocities as first derivatives

calculated at time t = 0. The details of the fit in Figure 3.5 can be found in table Table 3.2.

We use the following kinetic equations (typical Michaelis-Menten) for the totality of the emulsion, where **E** stands for enzyme, **S** for substrate, and **P** for product, and the italicized letters represent their respective concentrations.

$$\begin{aligned}
\text{E} + \text{S} &\rightleftharpoons \text{ES} \qquad (k_1, k_{-1}) \\
\text{ES} + \text{C} &\rightarrow \text{E} + \text{P} \qquad (k_2) \\
\frac{\mathrm{d}P}{\mathrm{d}t} &= \frac{k_2 E_0 S}{\frac{k_{-1}+k_2}{k_1}+S}
\end{aligned} \tag{3.4}$$
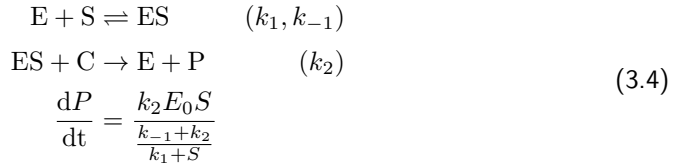
With a first order approximation:

$$\begin{aligned}
S &= S_0(1 - e^{-k_{\text{obs}}t}) \\
k_{obs} &= \frac{k_2 E_0}{\frac{k_{-1}+k_2}{k_1}+S} = \frac{v_{\max}}{K_M}
\end{aligned} \tag{3.5}$$

The range of concentrations is limited by two decisions: we stay within the coacervation window of ADP/ATP; because pyruvate kinase uses two substrates (ADP and PEP), we use ADP concentrations for which we can keep an excess of PEP and assume a pseudo-first order condition. Nonetheless, from initial velocities we build a Michaelis-Menten plot to extract enzymatic constants. Figure 3.5 reveals that coacervation hardly affects the overall reaction rate, which can be due to the small number of coacervates.

The K_M and k_{cat} values (and considering an enzyme concentration of 80 nM) obtained, although not remarkably different, demonstrate that it is possible to perform a typical enzyme-kinetics study with coacervates droplets using this method. Microscopy can be misleading in terms of the ratio between coacervates and solution, but our volume measurements confirm that ATP-PLL coacervates take up no more than 1% of the total mixture volume (10–13 μL for 1000 μL). These results also match the micrographs showing that after 10 minutes, the nucleation of new coacervates seems to stall and only coalescence events are observed. Additional information could be obtained by carrying out the kinetic analysis in the two phases separately, which would be less challenging for coacervates of higher volume fraction, or for fluorogenic enzymatic reactions.

3.6 Conclusion

The present chapter represents an intermission to address several questions that we think are overlooked in the literature, and that we did not address in Chapter 2. We started by justifying the relevance of studying membraneless organelles, condensates and their chemical models: they are a crucial part of chemistry in the cell, necessary to understand the efficiency of reactions such as transcription and translation. We explored two hypotheses
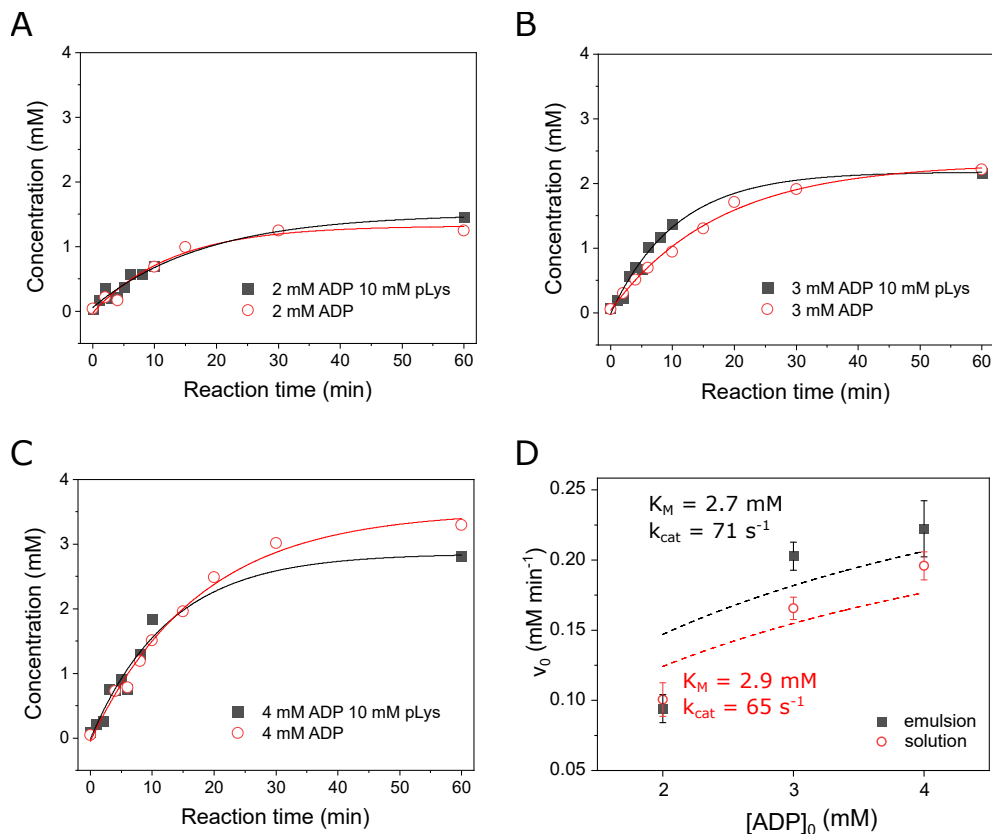
Figure 3.5: Kinetic analysis of the PyK reaction mixture over time. (A-C) Concentration profile of ATP for different initial concentrations of ADP (2-4 mM), under the same enzyme concentration of 80 nM, and on the presence and on the absence of poly-lysine. (D) After extracting the initial velocities of the PyK reaction (first derivative at t = 0), a Michaelis-Menten fit shows K_M and v_{max} for emulsion and solution conditions.

for the functions performed by condensates: selective partitioning and changed reactivity. Our discussion on reactivity highlighted the value in approaching condensates and related structures as biphasic reactions, but also evidenced the lack of quantitative measurements of partitioning coefficients and reaction rates in the literature.

These reflections allowed us to go deeper in the work presented in Chapter 2. Since coacervates can serve as model systems to investigate MLOs and condensates *in vitro*, we decided to apply our suggestions to our ATP-PLL coacervates, and extract partitioning coefficients and rate constants. The physical organic chemistry approach faces many challenges in the scale of condensates, and we developed a characterization protocol that can be applied to other systems. We successfully determined the localization and concentration of the components of the ATP-PLL coacervates, in equilibrium and over time.

Table 3.2: Parameters used in the Michaelis-Menten analysis of ATP concentration progress. k_{obs}, $[ADP]_0$ and t_c are parameters from the exponential fit to the concentration plots.

Experimental conditions			Fit parameters $[\text{ATP}]_t = A_0 e^{-k_{obs}(t-t_c)}$			
[PyK] (nM)	[ADP] (mM)	[PLL] (mM)	k_{obs} (min^{-1})	A_0 (mM)	t_c (min)	$[\text{ATP}]'_t\|_0$ (mM min^{-1})
	2	-	0.056	1.5	-0.67	0.10
	3	-	0.094	2.2	+0.08	0.17
80	4	-	0.079	2.9	+0.07	0.20
	2	5	0.078	1.3	+0.26	0.094
	3	5	0.057	2.3	-0.30	0.20
	4	5	0.057	3.5	+0.26	0.22

Pyruvate kinase activity in the emulsion is, surprisingly, very similar to a homogeneous solution, suggesting that (i) other factors must be taken into account to explain lack of product inhibition; or (ii) the coacervate volume in these emulsions does not allow us to capture the distinct kinetics of the reaction within. For this, we need a model to predict what rate differences to expect, which will be our focus on the next chapter. Ultimately, the work in this chapter shows the potentially rich chemistry of reactions in condensates.

3.7 Experimental details

The goal of the experimental part of this chapter was to provide a general protocol that can be applied to other coacervate systems. Therefore we include a more detailed description of our protocols, so as to encourage reproduction.

3.7.1 Fluorescent labelling of macromolecules

Pyruvate kinase was labelled using a Thermo Fisher Alexa-647-NHS-ester labelling kit and the accompanying instructions.

> **Labelling solutions**
> 10 mg mL^{-1} Alexa-647 NHS ester in DMF (ca. 10 mM)
> 1.0 M NaHCO$_3$ pH 8.3
> 2 mg mL^{-1} PyK (50% aqueous glycerol solution, approx. 40 μM)

a. to 500 μL of enzyme solution (around 2 mg mL^{-1} in a 50% glycerol solution), 50 μL of 1.0 M NaHCO$_3$ (pH 8.3) was added and mixed gently. Subsequently, 14 μL of the dye stock was added and incubated in a thermoshaker for 2 hours at room temperature (20 °C).

b. Excess dye (unbound) was removed with a disposable centrifugal membrane filter unit (e.g. VivaSpin concentrator). A molecular weight cut-off of 10 kDa was used (less than half the molecular weight of the enzyme). The membrane filter unit was first blocked with a Tween-20 solution (0.1 wt%), to minimize irreversible adsorption of the enzyme or protein to the membrane, and rinsed 5 times with MilliQ water, and then with 10 mM phosphate buffer (pH 7).

c. After washing, the labelled protein was added to the centrifugal filtration tube and centrifuged at low speed (500 rpm) until it was concentrated to 250 μL. An equal volume of glycerol was added before storing at 4 °C. *The recommended storage conditions may vary depending on the type and stability of the enzyme.*

PLL was labelled in a similar protocol, using TAMRA as a labelling agent, together with EDC and NHS as activators.

Labelling solutions
100 mM carboxytetramethylrhodamine (TAMRA) in DMF
100 mM 1-ethyl-3-(3-dimethylaminopropyl)carbodiimide (EDC) in DMF
100 mM N-hydroxysuccinimide (NHS) in DMF
200 mM PLL in MilliQ

---

a. 50 μL of each stock described previously (TAMRA, EDC, NHS) were mixed and added to 430 μL of 0.20 M PLL solution in water. The reaction was left overnight in a thermoshaker at room temperature.

b. Excess dye was removed by concentrating the reaction mixture in a Centricon filter unit with a molecular weight cut-off of 5 kDa. Washing steps were repeated as for pyruvate kinase, replacing the phosphate buffer with 10 mM HBr and eliminating the addition of glycerol.

3.7.2   Passivation of glass surfaces

We observe that different coacervate compositions require different coatings for droplet stabilization. For our purposes, we use a PEGylation protocol.

Materials
Glass bottom petri dish (Cell-vis)
Borosilicate cover glass (24 × 50 mm, thickness No. 1.5 from VWR)
Ethanol 70%
O_2-plasma or ozone cleaner
30 mg mL-1 mPEG-silane (mPEG-silane, M_n 5000 Da, from JenKem Technology) in toluene
1 hour at 65 °C

---

a. The cover glass was cleaned with distilled water, 70% ethanol and MilliQ water, and then dried using pressurized air or nitrogen.

b. The glass surface was cleaned/activated using a plasma or ozone cleaner, according to the manufacturer's instructions for cleaning glassware. Plasma treatment will result in removal of any leftover contaminants on the glass surface, and expose surface hydroxyl groups that are required for modification.

c. The cover glass was incubated with mPEG-silane, covering the surface with excess solution, for 1 hour in the 65 °C oven.

d. Subsequently, the glass surface was washed with copious amounts of MilliQ water and dried with compressed air or nitrogen. If the solution has dried during the reaction, the wash may require sonication. The glass surfaces were kept at 65 °C inside the oven until 1 hour before use, or in a covered Petri dish, and used in the course of two weeks.

3.7.3 Determination of partitioning coefficients with fluorescence microscopy

Stock solutions	ATP-PLL coacervates composition
100 mM ATP	100 mM HEPES pH 7.4
100 mM PLL (15-30 kDa)	5.0 mM PLL
0.50 M HEPES pH 7.4	5.0 mM $MgCl_2$
100 mM $MgCl_2$	5.0 mM ATP
1.0 M NaCl	130 mM NaCl
	1% v/v of Alexa-labelled PyK
	1% v/v of TAMRA-labelled PLL

a. ATP-PLL coacervates were prepared in volumes ranging from 0.10 to 1.0 mL. Two variations of the passive coacervates were prepared: one with lower ATP concentration (e.g. 3.0 mM) and one with higher PLL concentration (e.g. 20 mM). This is to verify that K_p is independent of the concentration.

b. The samples were injected into the microscopy chambers as described above. The well was covered with a circular coverslip to minimize evaporation.

c. An image was recorded of a well filled with coacervate mixture but without fluorophore with the same laser settings to use as a blank. A blank was recorded for every filter cube or emission wavelength used.

d. The partitioning coefficient (K_p) is determined from the ratio of emission intensity between the inner coacervate region and its surroundings, taken for 5-10 droplets in the center of the frame using ImageJ software. We use the integrated intensity (I) in a fixed squared area, and correct it for the emission of a blank (same excitation settings, no fluorophore).

3.7.4 Separation of the coacervate and dilute phase and volume estimation

We determine the concentrations of unlabelled components in the mixture using HPLC with UV/Vis detection.

Stock solutions	ATP-PLL coacervates
100 mM ADP	100 mM HEPES pH 7.4
100 mM PEP	5.0 mM PLL
100 mM ATP	5.0 mM $MgCl_2$
100 mM PLL (15-30 kDa)	5.0 mM ATP
100 mM $MgCl_2$	130 mM NaCl
0.50 M HEPES pH 7.4	5.0 mM PEP or ADP
1.0 M NaCl	

a. 0.10–1.0 mL of ATP-PLL coacervates were prepared. In order to measure the partitioning of PEP and ADP, those components were included, separately, in the ATP-PLL coacervate mixture the same concentration as in the reaction mixture (5.0 mM). Mixing was by vortexing.

b. The sample was centrifuged at a low speed for an extended period. We used 3000 rpm and 30 min after observing that for shorter spinning times, the system had not reached a constant concentration (the determined concentration in the dilute phase were still slowly decreasing after 15 min due to very small coacervate droplets that had not settled yet). The low speed prevents the accumulation of a dense phase film (pellet) at the side wall of the eppendorf tube.

c. The dilute phase (supernatant) was collected carefully with a pipette by stopping just above the interface between the dense coacervate phase (bottom phase) and the dilute phase (top phase), to avoid contamination of the dilute phase with the coacervate phase. The collected dilute phase was transferred to a separate eppendorf tube. The amount was measured by setting the volume of the automatic pipette to an estimated value and attempting to aspirate all fluid with the pipette; the set volume was adjusted until no liquid was left, and no air was aspirated. This was set as the volume of the dilute phase, V_{out}. For the ATP-PLL system, V_{out} was very close to the total volume of the mixture.

d. The remaining dilute phase from the centrifuged tube was slowly collected using a thin pipette tip (0.20–10 µL). The volume of the pellet left behind (V_{in}) was measured by first dissolving it by adding a known volume of 1.0 M NaCl (V_{salt}). This decreased the viscosity of the coacervate phase and facilitated easy handling by pipetting. The pipetting step was repeated for the dissolved coacervate solution, obtaining V_{new}. From this, we obtain $V_{in} = V_{new} - V_{salt}$. V_{in} is typically 1-10% of the total volume.

e. The typical concentrations determined in the ATP-PLL mixtures (5.0 mM in each component) are in the 0–10 mM range for the dilute phase, and 30–50 mM range for

the dense phase. For that, we recommend for a first attempt, respectively, 100X and 500X dilution prior to HPLC injection.

3.7.5   Classic analysis of the separate phases

Column settings	Eluents
Shim-pack WAX-1, 3 μm particles,	20 mM phosphate buffer pH 7.0 (A)
4.0 x 50 mm (anion exchange)	480 mM phosphate buffer pH 7.0 (B)
45 °C, 1 mL/min	
	Gradient program
Stock solutions	0–100% B in 20 min
1.0 M KH$_2$PO$_4$ (500 mL)	100% B for 5 min
1.0 M K$_2$HPO$_4$ (500 mL)	100–0% B in 5 min
	0% B for 5 min
31P-NMR materials	
D$_2$O	
100 mM acetyl phosphate	

a. Each of the phases were diluted around 100x before injection in the HPLC or insertion in the magnet to reach concentrations around 100 μM (this may require several optimizations as concentrations are unknown a priori).

b. For chromatographic analysis, detection at 215 and 254 nm (for PLL and PEP, and ADP and ATP, respectively) were used. The separation of the nucleotides required normal-phase HPLC with a weak anion exchange column in a gradient elution, as described in the chart above.

c. Using a calibration curve (peak area versus concentration), we determined the concentrations of the desired components considering dilutions (from V_{out} to the vial; from V_{in} to V_{new} and then to the vial). If the final dilution was the same for both phases, the partitioning coefficient (K_p) of A was calculated as:

$$K_p = \frac{[A]_{\mathrm{in,measured}} \times V_{\mathrm{out}}}{[A]_{\mathrm{out,measured}} \times V_{\mathrm{in}}}$$

d. For quantitative 31P-NMR analysis, we used 1 mM of acetyl phosphate as an internal standard, and 10:90 D$_2$O/H$_2$O as solvent. We chose a delay time between pulses of D1 = 20s, based on the measured relaxation time of all $_{31}$P nucleii in an inversion recovery experiment.
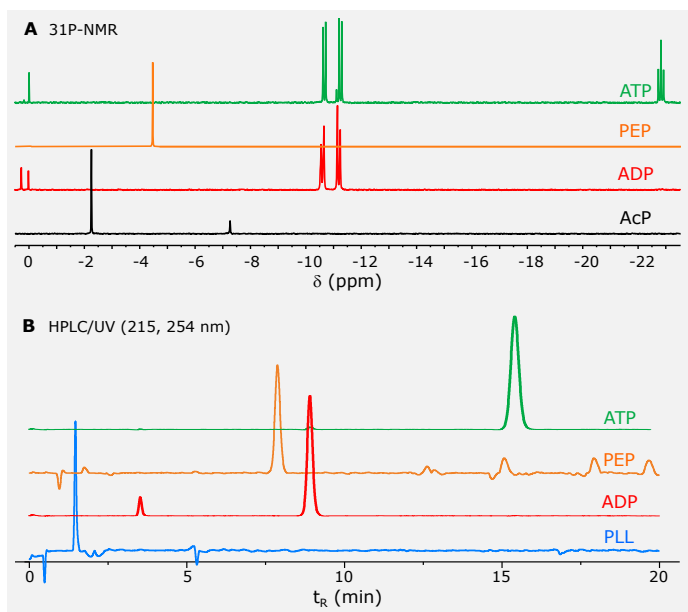
Figure 3.6: (A) Quantitative 31P-NMR spectra in 10:90 D_2O/H_2O of pure samples of ADP, phosphoenolpyruvate (PEP) and ATP; acetyl phosphate (AcP) was used as an internal standard. (B) Chromatogram of pure samples of poly-lysine (PLL), PEP, ADP and ATP (all 100 µM). The residual peak at 3 min in the chromatogram of ADP originates from hydrolysis to AMP. Chromatographic conditions: anion exchange column (Shim-pack WAX-1, 3 µm particles, 4.0 x 50 mm), 45 °C at flow rate 1 mL/min; eluents 20 mM (A) and 480 mM (B) phosphate buffer pH 7.0; gradient program 0–100% B in 20 min.

3.7.6   HPLC analysis of the reaction mixture over time

Stock solutions	PyK reaction mixture	PyK reaction mixture without PLL
100 mM ADP	100 mM HEPES pH 7.4	100 mM HEPES pH 7.4
100 mM PLL (15-30 kDa)	5.0 mM PLL	5.0 mM ADP
0.50 M HEPES pH 7.4	5.0 mM ADP	130 mM NaCl
100 mM MgCl$_2$	130 mM NaCl	10 units mL^{-1} PyK
100 mM PEP	10 units mL^{-1} PyK	(approx. 80 nM)
1.0 M NaCl	(approx. 80 nM)	5.0 mM PEP
10% v/v acetic acid	5.0 mM PEP	5.0 mM MgCl$_2$
	5.0 mM MgCl$_2$	(added at t = 0)
	(added at t = 0)	0.2% acetic acid
	0.2% acetic acid	(when quenching only)
	(when quenching only)	

a. A 1.0 mL PyK reaction mixture was prepared as described in Materials, including the PEP but leaving out the MgCl$_2$ (to make sure that the enzyme remains inactive until

the start of the reaction). Adding the PEP before aliquoting minimized the effect of small variations among the samples on the final reaction rate.

b. The reaction mixture was split in 10 samples of 95 µL each and added to separate eppendorf tubes. 5 µL of the 100 mM $MgCl_2$ stock was added to each of the sample tubes, which were placed in a thermoshaker at 25 ˚C.

c. One tube at a time was quenched by adding 2 µL of 10% (v/v) acetic acid (the final pH should be around 3 and the turbid mixture should turn clear). Initial time points are more important for for K_M and k_{cat} determination.

d. The samples were diluted around 100x and HPLC analysis was performed as described above to obtain the kinetic profile of ATP concentration.

e. The same procedure was used with a sample without PLL, as a "solution phase control".

f. Substrate concentrations were varied to obtain a typical Michaelis-Menten plot for coacervates and solution phase. For the PyK reaction, ADP could be varied from 2-5 mM whilst still working in the coacervation window.

Acknowledgements

Experimental notes — equilibrium concentrations from fluorescence microscopy

To produce a detailed picture of the reaction mixture, including equilibrium concentrations, fluorescence microscopy and labelling of at least one of the polyelectrolytes is often used. The drawback is that the choice of covalent fluorescent labels is crucial as to not drastically affect the structure (charge density or length)[53] and reactivity in the case of active coacervates. In the case of small molecules, such as ATP, attachment of a fluorescent label can strongly affect partitioning.[54] Also for enzymes, the degree of labelling, and the hydrophobicity of the label can completely change properties. One way to find out if labelling affects partitioning is to repeat the labelling with a different fluorophore, for example with a different charge and/or hydrophobicity,[55] and compare the partitioning coefficients for both labels. We perform a similar assay in Chapter 6.

An additional requirement of microscopy is that, in order to monitor coacervates as single droplets, with a stable position over time, the observation surface must be treated to minimize wetting. With regular and non-interacting surfaces (e.g. PVA, PEG), the midplane of the droplets directly on the glass can be analysed for extended periods, as a way to prove the condensation process and to estimate the volume of coacervate phase. Light intensity profiles of the excitation channel can be plotted using ImageJ software. The partitioning coefficient (K_p) is determined from the ratio of emission intensity between the inner coacervate region and its surroundings. We use the integrated intensity (I) in a fixed squared area, and correct it for the emission of a blank (same excitation settings, no fluorophore). K_p must be measured under equilibrium conditions, and it is therefore crucial to perform the measurement with different droplet incubation times to check for variation.

$$K_p = \frac{I_{\mathrm{in}} - I_{\mathrm{blank}}}{I_{\mathrm{out}} - I_{\mathrm{blank}}} \tag{3.6}$$

Note that the blank emission can drastically affect K_p. For example, for a droplet with integrated Alexa-647 fluorescence intensity of 100, and an intensity in the surrounding solution of 10, a blank intensity of either 1 or 9 will result in a K_p of 10 or 91. The difference in midplanes also requires that coacervates of different sizes and frame positions, are used for a reliable determination of K_p.

Equilibrium concentrations of unlabelled components can be determined by usual analytical techniques, such as chromatography, mass spectrometry, NMR. It is essential to separate the coacervate phase and the dilute phase by centrifugation. For small-scale experiments, for example with a limited amount of protein, it will generate a supernatant and a tiny coacervate pellet of volume V_{in}, which must be diluted or dissolved again before analysis. We measure the pellet's volume by pipetting it, and try to improve accuracy by adding concentrated salt solution (V_{salt}) to dissolve it and decrease its viscosity. V_{in} is then given by Equation 3.7. In our experience, the potential error arising from this technique is smaller than the typical uncertainties introduced in any of the alternative methods to determine ultra-small volumes of liquids with unknown densities.[56]

$$V_{\mathrm{in}} = V_{\mathrm{new}} - V_{\mathrm{salt}}$$
$$\mathrm{Dilution\,factor} = \frac{V_{\mathrm{new}}}{V_{\mathrm{in}}} \tag{3.7}$$

References

[1] C. P. Brangwynne, C. R. Eckmann, D. S. Courson, A. Rybarska, C. Hoege, J. Gharakhani, F. Jülicher, and A. A. Hyman, "Germline P granules are liquid droplets that localize by controlled dissolution/condensation," *Science*, 2009.

[2] M. Hardenberg, A. Horvath, V. Ambrus, M. Fuxreiter, and M. Vendruscolo, "Widespread occurrence of the droplet state of proteins in the human proteome," *Proceedings of the National Academy of Sciences*, vol. 117, no. 52, pp. 33254–33262, 2020.

[3] W. M. Babinchak and W. K. Surewicz, "Liquid–liquid phase separation and its mechanistic role in

pathological protein aggregation," *Journal of molecular biology*, vol. 432, no. 7, pp. 1910–1925, 2020.

[4] S. F. Banani, H. O. Lee, A. A. Hyman, and M. K. Rosen, "Biomolecular condensates: Organizers of cellular biochemistry," *Nature Reviews Molecular Cell Biology*, vol. 18, no. 5, pp. 285–298, 2017.

[5] S. Alberti, "The wisdom of crowds: regulating cell function through condensed states of living matter," *Journal of cell science*, vol. 130, no. 17, pp. 2789–2796, 2017.

[6] A. Aguilera-Gomez and C. Rabouille, "Membrane-bound organelles versus membrane-less compartments and their control of anabolic pathways in drosophila," *Developmental biology*, vol. 428, no. 2, pp. 310–317, 2017.

[7] D. M. Mitrea and R. W. Kriwacki, "Phase separation in biology; functional organization of a higher order," *Cell Communication and Signaling*, vol. 14, no. 1, pp. 1–20, 2016.

[8] S. Elbaum-Garfinkle, Y. Kim, K. Szczepaniak, C. C.-H. Chen, C. R. Eckmann, S. Myong, and C. P. Brangwynne, "The disordered p granule protein laf-1 drives phase separation into droplets with tunable viscosity and dynamics," *Proceedings of the National Academy of Sciences*, vol. 112, no. 23, pp. 7189–7194, 2015.

[9] V. Nguemaha and H.-X. Zhou, "Liquid-liquid phase separation of patchy particles illuminates diverse effects of regulatory components on protein droplet formation," *Scientific reports*, vol. 8, no. 1, pp. 1–11, 2018.

[10] J. A. Ditlev, L. B. Case, and M. K. Rosen, "Who's in and who's out—compositional control of biomolecular condensates," *Journal of molecular biology*, vol. 430, no. 23, pp. 4666–4684, 2018.

[11] S. Koga, D. S. Williams, A. W. Perriman, and S. Mann, "Peptide-nucleotide microdroplets as a step towards a membrane-free protocell model.," *Nature chemistry*, vol. 3, no. 9, pp. 720–4, 2011.

[12] T. Kojima and S. Takayama, "Membraneless compartmentalization facilitates enzymatic cascade reactions and reduces substrate inhibition," *ACS applied materials & interfaces*, vol. 10, no. 38, pp. 32782–32791, 2018.

[13] W. Stroberg and S. Schnell, "Do cellular condensates accelerate biochemical reactions? lessons from microdroplet chemistry," *Biophysical journal*, vol. 115, no. 1, pp. 3–8, 2018.

[14] S. Lindhoud, W. Norde, and M. A. Cohen Stuart, "Effects of polyelectrolyte complex micelles and their components on the enzymatic activity of lipase," *Langmuir*, vol. 26, no. 12, pp. 9802–9808, 2010.

[15] T. J. Nott, E. Petsalaki, P. Farber, D. Jervis, E. Fussner, A. Plochowietz, T. D. Craggs, D. P. Bazett-Jones, T. Pawson, J. D. Forman-Kay, *et al.*, "Phase transition of a disordered nuage protein generates environmentally responsive membraneless organelles," *Molecular cell*, vol. 57, no. 5, pp. 936–947, 2015.

[16] E. Spruijt, S. A. van den Berg, M. A. Cohen Stuart, and J. van der Gucht, "Direct measurement of the strength of single ionic bonds between hydrated charges," *Acs Nano*, vol. 6, no. 6, pp. 5297–5303, 2012.

[17] D. S. Williams, S. Koga, C. R. C. Hak, A. Majrekar, A. J. Patil, A. W. Perriman, and S. Mann, "Polymer/nucleotide droplets as bio-inspired functional micro-compartments," *Soft Matter*, vol. 8, no. 22, pp. 6004–6014, 2012.

[18] M. Zhao, S. A. Eghtesadi, M. B. Dawadi, C. Wang, S. Huang, A. E. Seymore, B. D. Vogt, D. A. Modarelli, T. Liu, and N. S. Zacharia, "Partitioning of small molecules in hydrogen-bonding complex coacervates of poly (acrylic acid) and poly (ethylene glycol) or pluronic block copolymer," *Macromolecules*, vol. 50, no. 10, pp. 3818–3830, 2017.

[19] N. Martin, M. Li, and S. Mann, "Selective uptake and refolding of globular proteins in coacervate microdroplets," *Langmuir*, vol. 32, no. 23, pp. 5881–5889, 2016.

[20] S. Lindhoud and M. M. Claessens, "Accumulation of small protein molecules in a macroscopic complex coacervate," *Soft Matter*, vol. 12, no. 2, pp. 408–413, 2016.

[21] E. A. Frankel, P. C. Bevilacqua, and C. D. Keating, "Polyamine/Nucleotide Coacervates Provide Strong Compartmentalization of Mg2+, Nucleotides, and RNA," *Langmuir*, vol. 32, no. 8, pp. 2041–

2049, 2016.

[22] W. M. Aumiller Jr and C. D. Keating, "Phosphorylation-mediated RNA/peptide complex coacervation as a model for intracellular liquid organelles," *Nature Chemistry*, vol. 8, no. 2, pp. 129–137, 2015.

[23] A. A. André and E. Spruijt, "Rigidity rules in dna droplets: nucleic acid flexibility affects model membraneless organelles," *Biophysical journal*, vol. 115, no. 10, p. 1837, 2018.

[24] T. J. Nott, T. D. Craggs, and A. J. Baldwin, "Membraneless organelles can melt nucleic acid duplexes and act as biomolecular filters," *Nature chemistry*, vol. 8, no. 6, pp. 569–575, 2016.

[25] H. Jiang, S. Wang, Y. Huang, X. He, H. Cui, X. Zhu, and Y. Zheng, "Phase transition of spindle-associated protein regulate spindle apparatus assembly," *Cell*, vol. 163, no. 1, pp. 108–122, 2015.

[26] M. M. Hansen, L. H. Meijer, E. Spruijt, R. J. Maas, M. V. Rosquelles, J. Groen, H. A. Heus, and W. T. Huck, "Macromolecular crowding creates heterogeneous environments of gene expression in picolitre droplets," *Nature nanotechnology*, vol. 11, no. 2, pp. 191–197, 2016.

[27] A. P. Minton, "Macromolecular crowding," *Current Biology*, vol. 16, no. 8, pp. R269–R271, 2006.

[28] O. Bénichou, C. Chevalier, J. Klafter, B. Meyer, and R. Voituriez, "Geometry-controlled kinetics," *Nature chemistry*, vol. 2, no. 6, pp. 472–477, 2010.

[29] M. Tabaka, T. Kalwarczyk, J. Szymanski, S. Hou, and R. Holyst, "The effect of macromolecular crowding on mobility of biomolecules, association kinetics, and gene expression in living cells," *Frontiers in Physics*, vol. 2, p. 54, 2014.

[30] C. A. Strulson, R. C. Molden, C. D. Keating, and P. C. Bevilacqua, "Rna catalysis through compartmentalization," *Nature chemistry*, vol. 4, no. 11, pp. 941–946, 2012.

[31] B. Drobot, J. M. Iglesias-Artola, K. Le Vay, V. Mayr, M. Kar, M. Kreysing, H. Mutschler, and T. Y. Tang, "Compartmentalised RNA catalysis in membrane-free coacervate protocells," *Nature Communications*, vol. 9, no. 3643, 2018.

[32] E. Sokolova, E. Spruijt, M. M. K. Hansen, E. Dubuc, J. Groen, V. Chokkalingam, A. Piruska, H. A. Heus, and W. T. S. Huck, "Enhanced transcription rates in membrane-free protocells formed by coacervation of cell lysate," *Proceedings of the National Academy of Sciences*, vol. 110, no. 29, pp. 11692–11697, 2013.

[33] T.-Y. D. Tang, D. van Swaay, A. DeMello, J. R. Anderson, and S. Mann, "In vitro gene expression within membrane-free coacervate protocells," *Chemical Communications*, vol. 51, no. 57, pp. 11429–11432, 2015.

[34] A. R. Menjoge, A. B. Kayitmazer, P. L. Dubin, W. Jaeger, and S. Vasenkov, "Heterogeneity of polyelectrolyte diffusion in polyelectrolyte- protein coacervates: A 1h pulsed field gradient nmr study," *The Journal of Physical Chemistry B*, vol. 112, no. 16, pp. 4961–4966, 2008.

[35] R. Kausik, A. Srivastava, P. A. Korevaar, G. Stucky, J. H. Waite, and S. Han, "Local water dynamics in coacervated polyelectrolytes monitored through dynamic nuclear polarization-enhanced 1h nmr," *Macromolecules*, vol. 42, no. 19, pp. 7404–7412, 2009.

[36] A. Shakya and J. T. King, "Non-fickian molecular transport in protein–dna droplets," *ACS Macro Letters*, vol. 7, no. 10, pp. 1220–1225, 2018.

[37] P. L. Kastritis and A.-C. Gavin, "Enzymatic complexes across scales," *Essays in biochemistry*, vol. 62, no. 4, pp. 501–514, 2018.

[38] B. W. Davis, W. M. Aumiller Jr, N. Hashemian, S. An, A. Armaou, and C. D. Keating, "Colocalization and sequential enzyme activity in aqueous biphasic systems: experiments and modeling," *Biophysical journal*, vol. 109, no. 10, pp. 2182–2194, 2015.

[39] M. Klingauf, D. Stanek, and K. M. Neugebauer, "Enhancement of u4/u6 small nuclear ribonucleoprotein particle association in cajal bodies predicted by mathematical modeling," *Molecular Biology of the Cell*, vol. 17, no. 12, pp. 4972–4981, 2006.

[40] B. S. Schuster, E. H. Reed, R. Parthasarathy, C. N. Jahnke, R. M. Caldwell, J. G. Bermudez, H. Ramage, M. C. Good, and D. A. Hammer, "Controllable protein phase separation and modular recruitment to form responsive membraneless organelles," *Nature communications*, vol. 9, no. 1,

pp. 1–12, 2018.

[41] N. A. Yewdall, B. C. Buddingh, W. J. Altenburg, S. B. Timmermans, D. F. Vervoort, L. K. Abdel-mohsen, A. F. Mason, and J. C. van Hest, "Physicochemical characterization of polymer-stabilized coacervate protocells," *ChemBioChem*, vol. 20, no. 20, p. 2643, 2019.

[42] D. Zwicker, R. Seyboldt, C. A. Weber, A. A. Hyman, and F. Jülicher, "Growth and division of active droplets provides a model for protocells," *Nature Physics*, vol. 13, pp. 408–413, 2017.

[43] M. Pera-Titus, L. Leclercq, J.-M. Clacens, F. De Campo, and V. Nardello-Rataj, "Pickering interfacial catalysis for biphasic systems: from emulsion design to green reactions," *Angewandte Chemie International Edition*, vol. 54, no. 7, pp. 2006–2021, 2015.

[44] J. Bonham, M. Faers, and J. Van Duijneveldt, "Non-aqueous microgel particles: synthesis, properties and applications," *Soft matter*, vol. 10, no. 47, pp. 9384–9398, 2014.

[45] C. Chern, "Emulsion polymerization mechanisms and kinetics," *Progress in polymer science*, vol. 31, no. 5, pp. 443–486, 2006.

[46] F. M. Menger and C. E. Portnoy, "Chemistry of reactions proceeding inside molecular aggregates," *Journal of the American Chemical Society*, vol. 89, no. 18, pp. 4698–4703, 1967.

[47] E. H. Cordes and R. B. Dunlap, "Kinetics of organic reactions in micellar systems," *Accounts of Chemical Research*, vol. 2, no. 11, pp. 329–337, 1969.

[48] F. H. Quina and H. Chaimovich, "Ion exchange in micellar solutions. 1. conceptual framework for ion exchange in micellar solutions," *Journal of Physical Chemistry*, vol. 83, no. 14, pp. 1844–1850, 1979.

[49] L. Romsted, "Micellar effects on reaction rates and equilibria," *Chemischer Informationsdienst*, vol. 16, no. 1, pp. no–no, 1985.

[50] G. Savelli, R. Germani, and L. Brinchi, "Reactivity control by aqueous amphiphilic self-assembling systems," *SURFACTANT SCIENCE SERIES*, pp. 175–246, 2001.

[51] M. Häger and K. Holmberg, "Phase-transfer agents as catalysts for a nucleophilic substitution reaction in microemulsions," *Chemistry–A European Journal*, vol. 10, no. 21, pp. 5460–5466, 2004.

[52] C. Bravo-Díaz, L. S. Romsted, C. Liu, S. Losada-Barreiro, M. J. Pastoriza-Gallego, X. Gao, Q. Gu, G. Krishnan, V. Sánchez-Paz, Y. Zhang, *et al.*, "To model chemical reactivity in heterogeneous emulsions, think homogeneous microemulsions," *Langmuir*, vol. 31, no. 33, pp. 8961–8979, 2015.

[53] M. Quinn, N. Gnan, S. James, A. Ninarello, F. Sciortino, E. Zaccarelli, and J. McManus, "How fluorescent labelling alters the solution behaviour of proteins," *Physical Chemistry Chemical Physics*, vol. 17, no. 46, pp. 31177–31187, 2015.

[54] S. Deshpande, F. Brandenburg, A. Lau, M. G. Last, W. K. Spoelstra, L. Reese, S. Wunnava, M. Dogterom, and C. Dekker, "Spatiotemporal control of coacervate formation within liposomes," *Nature Communications*, vol. 10, no. 1800, pp. 1–11, 2019.

[55] L. D. Hughes, R. J. Rawle, and S. G. Boxer, "Choose your label wisely: water-soluble fluorophores often interact with lipid bilayers," *PloS one*, vol. 9, no. 2, p. e87649, 2014.

[56] W. M. Aumiller and C. D. Keating, "Experimental models for dynamic compartmentalization of biomolecules in liquid organelles: Reversible formation and partitioning in aqueous biphasic systems," *Advances in Colloid and Interface Science*, vol. 239, pp. 75–87, 2017.

Chapter 4

Fundamentals of chemical kinetics inside coacervates
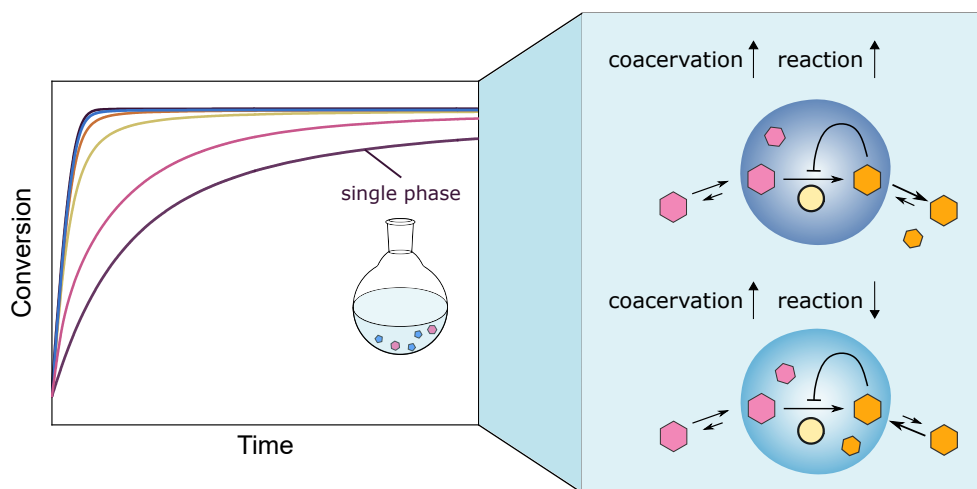
Festina lente
Make haste slowly

4.1   Kinetic model of reactions in coacervates

In Chapter 3, while discussing possible functions of condensates in the cell, we proposed — like many in the literature — that reaction kinetics is likely to be at least different in the presence of these droplets, not to say accelerated or inhibited. At that point, we focused on hypothesizing *why* reactions could be favored or inhibited in membraneless organelles: the polarity of the droplets, the crowded interior, enzyme conformations and substrate concentrations. We found some conflicting examples, indicating that the balance between favoring and inhibitory factors is delicate. Now, we take a closer look at this balance, with the goal of understanding which experimental design can provide more evidence on the role of condensates to chemical kinetics in biomimetic models and within the cell.

There are two types of experiments that measure kinetics in condensates, or their chemical versions, coacervates; bulk experiments that work with the emulsion as a whole, and measure the average signal of the two phases; and experiments that analyze the phases separately. Bulk measurements typically use a spectrometer or a plate reader, and provide kinetic constants that are the weighted average of coacervate and solution phase. Phase volumes and partitioning coefficients determine how close the average is to the reaction rate in a single phase. To perform measurements per phase, the emulsion is forcefully separated in two macrophases, that can then be analyzed individually, which makes measurements over small time intervals challenging. Alternatively, fluorescence microscopy can be used to spatially resolve measurements, but as we discussed in the previous chapter, fluorescent labeling is not always a harmless strategy.

We set out to develop a kinetic model of reactions in two phases that takes into account typical coacervate properties: free exchange of molecules between dense and dilute phase, low volume fractions and partitioning/exclusion of molecules. Such a model is crucial to define in which reaction and coacervate systems we can expect an effect in reactivity.

4.2   Minimal model

So far in this thesis, we have been looking at reactions that start homogeneous but gradually become an emulsion (coacervate). In this chapter, for the sake of simplicity, we will separate the reaction components from the coacervate building blocks, and therefore fix the volume fraction: we assume the host coacervates are unreactive, and that reactants and products behave as inert client molecules, such that droplets do not grow or dissolve during the reaction.

In order to develop a model of reactions in coacervate emulsions, we combine reaction kinetics with a pseudophase model, where each phase is regarded as a distinct and continuous reaction medium.[1] We start with a minimal system of a bimolecular reaction described by mass action kinetics, giving rise to reactive and transport fluxes

(Equation 4.1). We assume that all reaction components distribute over the dilute and the coacervate phases, neglecting the interface.
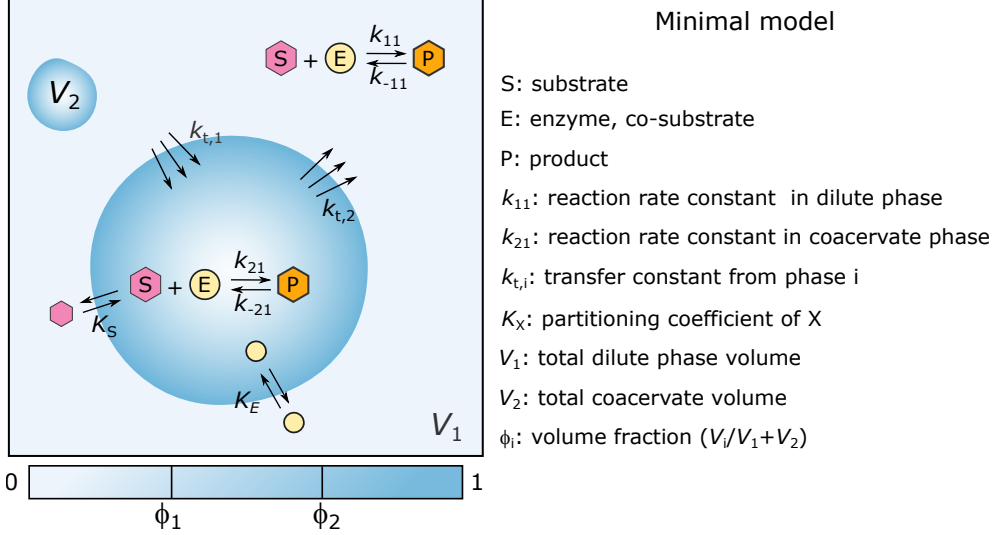
Figure 4.1: Pseudophase model of reactions in coacervates, with all parameters represented.

$$
\begin{aligned}
\mathbf{S}_{(1)} + \mathbf{E}_{(1)} &\rightleftharpoons \mathbf{P}_{(1)} \quad (k_{11}; k_{-11}) \\
\mathbf{S}_{(2)} + \mathbf{E}_{(2)} &\rightleftharpoons \mathbf{P}_{(2)} \quad (k_{21}; k_{-21}) \\
\mathbf{S}_{(1)} &\rightleftharpoons \mathbf{S}_{(2)} \quad (k_{t,1}^{\mathrm{S}}; k_{t,2}^{\mathrm{S}}) \\
\mathbf{E}_{(1)} &\rightleftharpoons \mathbf{E}_{(2)} \quad (k_{t,1}^{\mathrm{E}}; k_{t,2}^{\mathrm{E}})
\end{aligned}
\tag{4.1}
$$
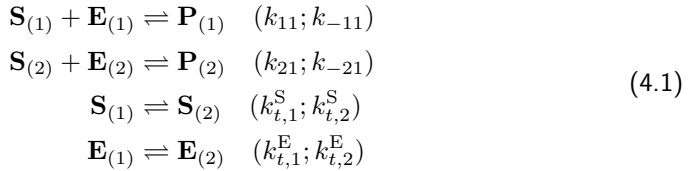
The reaction rate constants are k_{11} (forward) and k_{-11} (reverse) in the dilute phase, and k_{21} and k_{-21} in the coacervate phase. The rate of formation of product **P** is given per phase ($i = 1, 2$), by Equation 4.2: a term of reaction flux ($J_{r,i}$) and the phase flux that connects the two pseudophases ($J_{t,i}$). We represent hereafter chemical species symbols in upright bold letters, and their respective concentration in italicized letters.

$$
\frac{\mathrm{d}P, i}{\mathrm{d}t} = J_{r,i}^{\mathrm{P}} + J_{t,i}^{\mathrm{P}}
\tag{4.2}
$$

$$
\frac{\mathrm{d}P_i}{\mathrm{d}t} = k_{i,1} S_i E_i - k_{-i,1} P_i + J_{t,i}^{\mathrm{P}}
\tag{4.3}
$$

The reaction term is regular mass action kinetics and likely has a much longer timescale than diffusion;[2] therefore, at all reaction times, the concentration of all components (**S**, **E** and **P**) in each compartment satisfies the partitioning coefficient K ($K_{\mathrm{X}} = \frac{k_{t,2}^{\mathrm{X}}}{k_{t,1}^{\mathrm{X}}}$). Chemical reaction and phase equilibrium are coupled, as expressed by $J_{t,i}$ in Equation

4.4. We define $J_{t,i}$ as the flux of molecules **P** per volume in phase i in order to maintain phase equilibrium upon perturbations caused by the chemical reaction. Molecules of **P** that cross the interface from $s \rightarrow c$ have a large contribution on concentration of **P** in the coacervate, as normally $V_2 << V_1$, and the phases volume must be taken into account to correct for the dilution or concentration.

$$J_{t,1}^{\mathrm{P}} = -k_{t,1}^{\mathrm{P}} P_1 + k_{t,2}^{\mathrm{P}} P_2 \frac{V_2}{V_1}$$
$$J_{t,2}^{\mathrm{P}} = -k_{t,2}^{\mathrm{P}} P_2 + k_{t,1}^{\mathrm{P}} P_1 \frac{V_1}{V_2}$$

(4.4)

Equation 4.4 can be re-written, considering that at equilibrium the rate of molecules (per volume) that go from $1 \rightarrow 2$ is equal to the rate of molecules that go from $2 \rightarrow 1$. With the kinetic formulation of the partitioning coefficient in Equation 4.5, we can define the phase transfer flux by Equation 4.6.

$$k_{t,2}^{\mathrm{P}} P_2^{\mathrm{eq}} = k_{t,1}^{\mathrm{P}} P_1^{\mathrm{eq}}$$
$$k_{t,2}^{\mathrm{P}} K_{\mathrm{P}} = k_{t,1}^{\mathrm{P}}$$

(4.5)

$$J_{t,1}^{\mathrm{P}} = +k_{t,2}^{\mathrm{P}} \frac{V_2}{V_1}(P_2 - K_{\mathrm{P}} P_1)$$
$$J_{t,2}^{\mathrm{P}} = -k_{t,2}^{\mathrm{P}}(P_2 - K_{\mathrm{P}} P_1)$$

(4.6)

The transfer rate constant $k_{t,2}^{\mathrm{P}}$, that we define as the amount of molecules of **P** crossing the interface from phase (2) to (1) per second, is dependent on the interface size, which is dictated by the coacervate volume (V_2). We can therefore include V_2 ($k_t^{\mathrm{P}} = k_{t,2}^{\mathrm{P}} V_2$), making it explicit that $J_{t,2} = -J_{t,1}$ and the total number of molecules **P** is conserved (Equation 4.7). The constant k_t^{P} can be limited by diffusion, and determined by the diffusion coefficient of the species, but for the sake of simplicity we will use a single constant for all species (k_t).

$$J_{t,1}^{\mathrm{P}} = +k_t \frac{(P_2 - K_{\mathrm{P}} P_1)}{V_1}$$
$$J_{t,2}^{\mathrm{P}} = -k_t \frac{(P_2 - K_{\mathrm{P}} P_1)}{V_2}$$
$$J_{t,i}^{\mathrm{P}} = \pm k_t \frac{(P_2 - K_{\mathrm{P}} P_1)}{V_i}$$

(4.7)

We can now explicitly write the differential equations for concentration of **P** in each phase (Equation 4.8), which are in accordance to the expression obtained by Weber and Michaels in ref. 2 for the coupling between aggregation and partitioning. Our reasoning in this chapter is in fact largely based on this work, but applied to bimolecular reactions instead of aggregation.

$$\frac{dP_1}{dt} = k_{11}S_1E_1 - k_{-11}P_1 + k_t\frac{(P_2 - K_P P_1)}{V_1}$$
$$\frac{dP_2}{dt} = k_{21}S_2E_2 - k_{-21}P_2 - k_t\frac{(P_2 - K_P P_1)}{V_2}$$

$$(4.8)$$

For the other reaction components, the same logic follows: mass action kinetics and a phase transfer term, completing the set of differential equations 4.9 and 4.10. For most of our analysis of how the presence of coacervate droplets can affect a reaction, it is useful to define the overall product formation, which is a weighted average of the **P** concentration profiles in each phase and can be expressed in terms of the volume fraction ($\phi = \frac{V_2}{V_1+V_2}$). Adding together the rates in each phase cancels the phase fluxes J_t and yields Equation 4.11, if we also assume $k_{-11} = k_{-21} \simeq 0$.

$$\frac{dS_1}{dt} = -k_{11}S_1E_1 + k_{-11}P_1 + k_t\frac{(S_2 - K_S S_1)}{V_1}$$
$$\frac{dS_2}{dt} = -k_{21}S_2E_2 + k_{-21}P_2 - k_t\frac{(S_2 - K_S S_1)}{V_2}$$

$$(4.9)$$

$$\frac{dE_1}{dt} = -k_{11}S_1E_1 + k_{-11}P_1 + k_t\frac{(E_2 - K_E E_1)}{V_1}$$
$$\frac{dE_2}{dt} = -k_{21}S_2E_2 + k_{-21}P_2 + k_t\frac{(E_2 - K_E E_1)}{V_2}$$

$$(4.10)$$

$$\frac{dP}{dt} = \frac{k_{11}S_1E_1C_1 + k_{21}S_2E_2V_2}{V_1 + V_2}$$
$$= k_{11}S_1E_1(1 - \phi) + k_{21}S_2E_2\phi$$

$$(4.11)$$

We can solve Equation 4.11 analytically with a few assumptions: (i) **E** remains approximately constant, as would be the case for a catalyst; (ii) at equilibrium, concentrations follow the partitioning coefficients leading to the relations in Equation 4.12 and (iii) reactants and product do not affect the degree of phase separation, so that ϕ is constant. Condition (ii) holds for equilibrium, but while the chemical reaction can cause small perturbations, the phase transfer fluxes constantly act to re-establish equilibrium. Although not instantaneous, for high phase transfer constants, out-of-equilibrium situations are merely transient.

$$\frac{X_2}{X_1} = K_X$$

$$(4.12)$$

$$X_2\phi V + X_1(1 - \phi)V = XV$$

$$(4.13)$$

$$X_1 = \frac{X}{1 - \phi + K_X\phi}$$

$$(4.14)$$

$$X_2 = \frac{K_X X}{1 - \phi + K_X\phi}$$

$$(4.15)$$

Substituting E_2 and S_2 in Equation 4.11:

$$\begin{aligned}
\frac{\mathrm{d}P}{\mathrm{d}t} &= k_{11}S_1E_1(1-\phi) + k_{21}K_SS_1K_EE_1\phi \\
&= k_{11}S_1E_1(1-\phi) + k_{21}K_SS_1K_EE_1\phi
\end{aligned} \tag{4.16}$$

Continuing to substitute E_1 and S_1, we obtain a typical pseudo-first order kinetic law, with an observed rate constant dependent on volume fraction and partitioning coefficient of substrate and catalyst. Effectively, the reaction in two phases proceeds as two parallel reactions in one phase.

$$\frac{\mathrm{d}P}{\mathrm{d}t} = k_{obs}(S_0 - P) \tag{4.17}$$

$$k_{obs} = \frac{Ek_{11}(1-\phi) + k_{21}K_SK_E\phi}{(1-\phi+K_S\phi)(1-\phi+K_E\phi)} \tag{4.18}$$

$$P = S_0(1 - e^{-k_{obs}t}) \tag{4.19}$$

In the following sections, we numerically solve the set of differential equations for different conditions of volume fraction, partitioning coefficients, and coacervate micro-environment, to demonstrate their effect on the observed reaction kinetics.

4.3 Effect of partitioning, volume fraction and transition state

Although Equation 4.17 is just what you would expect from a pseudo-first order reaction, it shows a few important experimental points. First, that if the volume fraction is close to zero, $k_{obs} \simeq k_{11}E$, which means that experiments that measure an averaged signal will not capture any difference between a homogeneous reaction and a two-phase one, regardless of partitioning coefficients and rate constants. Secondly, that for a low volume fraction ($\simeq 1\%$), co-localization of reactants **S** and **E** is crucial: although both reactants contribute equally to k_{obs}, if both K_S and K_E are high, even for a low volume fraction and equal reactivity in the coacervate and dilute phases, the observed rate constant can be higher than in a single phase. However if $K_S < 1$, a K_E orders of magnitude higher is needed to even reach the same overall rate as single phase.

To illustrate our argument, we numerically integrated (see Python codes at the end of the chapter) the set of differential equations 4.8, 4.9 and 4.10 for conditions similar to what we use in Chapters 2, 3 and 6, and we looked at two aspects: product formation in the coacervate phase, and overall product formation. In this section, as we consider an irreversible process and no product inhibition, the partitioning coefficient of the product should not affect our discussion, so we infer product formation by looking at substrate

depletion (in other words, we can omit the transfer flux for the overall concentration of **P** in Equation 4.8).

We start with the case where $K_S = 1$, $K_E = 10^2$ and $k_{21} = k_{11}$. That would make a coacervate environment not much different than the dilute phase, but to justify why a two-phase model is still worth discussing, we evaluated how much of the reaction takes place in the coacervate phase. Even at a low volume fraction of $\phi = 10^{-2}$, 20% of the product, in copy number, is formed within the coacervate (Figure 4.2).
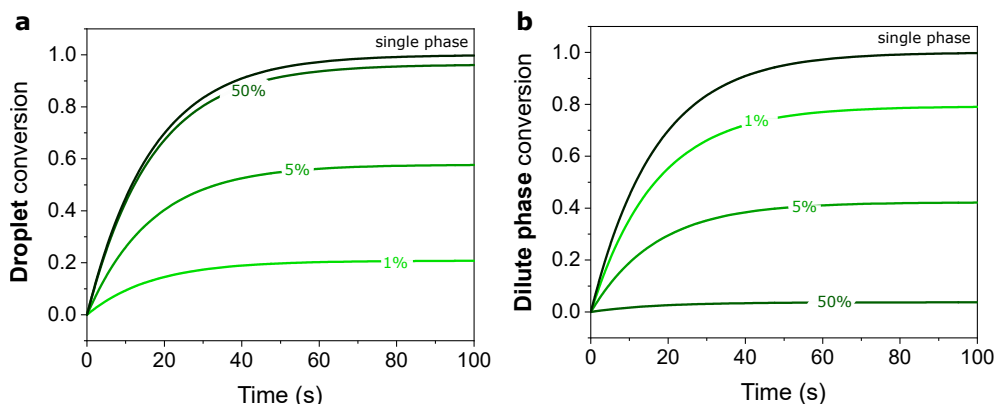
Figure 4.2: Reaction progress in the coacervate macrophase (a) and the dilute phase (b), depending on the volume fraction. The black curve represents the progress in the condition of a single-phase, meaning that at $\phi = 50\%$, almost the entire reaction takes place in the coacervate. Parameters used: $K_E = 10^2$, $k_{11} = 2\,\mathrm{mM}^{-1}\,\mathrm{s}^{-1}$ and $k_t = 10^3\,\mathrm{\mu L\,s}^{-1}$.

In practice, the expressive fraction of reaction in the coacervate phase does not cause a difference in reactivity if the coacervate micro-environment is similar to a solution. Even a $K_E = 10^2$ is not high enough to impact the overall product formation in comparison to a single phase system, as the higher concentration of **E** in the droplet is balanced by its lower concentration in the dilute phase (Figure 4.3a). Only if we increase K_S by a factor of 10, we start seeing a difference for low volume fractions (Figure 4.3b). A partitioning coefficient of 10 is not unreasonable, as in Chapter 3 we measured values in that order of magnitude or higher for ADP and ATP. This simple simulation shows that there are optimal reactant structures and volume fractions for experiments that aim to detect the effect of phase separation on reaction rates.

High partitioning at low volume fraction can explain some enzymatic reactions shown to be accelerated in the presence of biomimetic coacervates.[3–5] In the study where *Koga et al* linked hexokinase enhanced activity in the presence of poly-lysine-ATP droplets to the enzyme's partitioning ($K_E \simeq 20$), the volume fraction was around 1%.[3] Although in that case there was an interplay between phase separation and reaction (unlike our model), the balance between K_E and ϕ is in agreement to our predictions of an overall

acceleration. This is a rare example of an experimental study that includes all partitioning and kinetic constants measurable, something we pointed out in Chapter 3 as crucial for the field of biomimetic coacervates.

The interesting case of lowered hammerhead ribozyme activity in polylysine-CMDex coacervates described by Drobot *et al* is harder to explain.[6] In that case volume fraction is ca. 2%, but it is not clear whether the activity measured is restricted to the droplets, or to the entire emulsion. An important difference are the reported partitioning coefficients for substrates, in the order of 10^3–10^4, which could mean the droplets act as a sink of reactants thus suppressing the reaction in the dilute phase. But factors other than concentration might be playing a role in this case.

The effect of concentration by strong partitioning is already interesting and it can be tuned by the range of interactions that determine K_X, it is not the only way by which coacervates could affect chemical reactions. In Chapter 3 we discussed how the environment of condensates can affect reactivity otherwise (Figure 3.2): by changing transition state, organizing cascade reactions, or by preventing product inhibition.

The change in the transition state would result in $k_{21} \neq k_{11}$ in our model. It is worth pointing out again that we are interested in conditions where a change of reactivity can be measured in experiments that look at both phases together. And indeed, when we increase or decrease k_{21} by a factor of 10, even when $K_S = 1$, we start to see differences in the overall rate of product formation (Figure 4.3C and D). This result shows that at the fairly reasonable condition of 5% volume fraction, a significant decrease in reaction rate can be attributed to a lowered rate constant, which can be the case in the system described by Drobot *et al* also mentioned in the previous section.[6] Importantly, the effect of higher k_{21} is similar to that of increasing reactant partitioning K_S to 10 (Figure 4.3b), which highlights the significance of measuring partitioning coefficients as we did in the previous chapter.

4.4 Enzymatic model: effect of product partitioning and binding

Following the predictions with a minimal model, we went on to include product partitioning in the system, as that might play a role in reversible reactions and cascades. Aiming at creating a model that applies to enzymatic systems, we introduce substrate binding, product release and product inhibition equilibria. This can be seen as a generic reaction scheme based on the mechanism of pyruvate kinase we already used in Chapter 2. The full description of an enzymatic reaction in two phases results in the scheme below, with partitioning coefficients for each reaction component, from which we build the set of differential equations according to Equation 4.8, 4.9 and 4.10. For simplicity, we used the same coefficient for enzyme and enzyme-complexes in our simulations, and equal phase
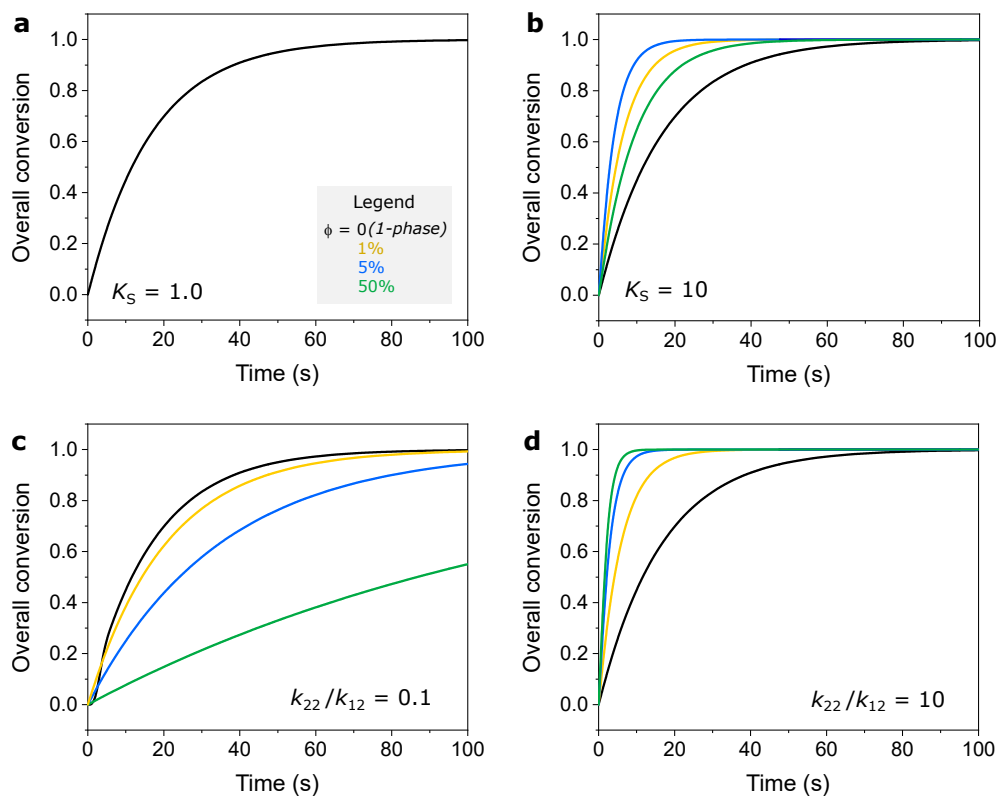
Figure 4.3: Reaction progress in two phases. The overall conversion of reaction $S \to P$ is given by the sum of conversion in each phase, normalized by the total amount of reactant S. Top: effect of volume fraction for $K_S = 1$ (a) or 10 (b); rate constants in each phase are equal, and there is no observed effect. Bottom: effect of volume fraction for a coacervate environment that hampers (c) or favors (d) the reaction; in this case, $K_S = 1$. In all plots, $K_E = 10^2$, $k_{11} = 2\,\mathrm{mM}^{-1}\,\mathrm{s}^{-1}$ and $k_t = 10^3\,\mathrm{\mu L\,s}^{-1}$.

transfer rates for all compounds.

Reactions in the dilute phase

$$
\begin{aligned}
\mathbf{E}_{(1)} + \mathbf{S}_{(1)} &\rightleftharpoons \mathbf{ES}_{(1)} & (k_{11}; k_{-11}) \\
\mathbf{ES}_{(1)} + \mathbf{C}_{(1)} &\to \mathbf{ER}_{(1)} + \mathbf{P}_{(1)} & (k_{12}) \\
\mathbf{ER}_{(1)} &\rightleftharpoons \mathbf{E}_{(1)} + \mathbf{R}_{(1)} & (k_{13}; k_{-13}) \\
\mathbf{E}_{(1)} + \mathbf{P}_{(1)} &\rightleftharpoons \mathbf{EP}_{(1)} & (k_{14}; k_{-14})
\end{aligned}
\tag{4.20}
$$
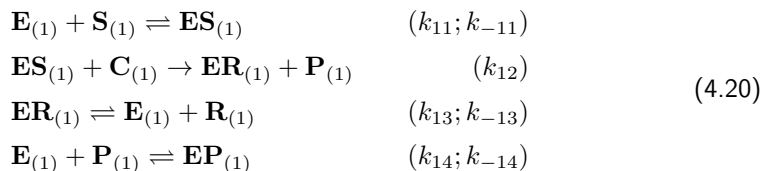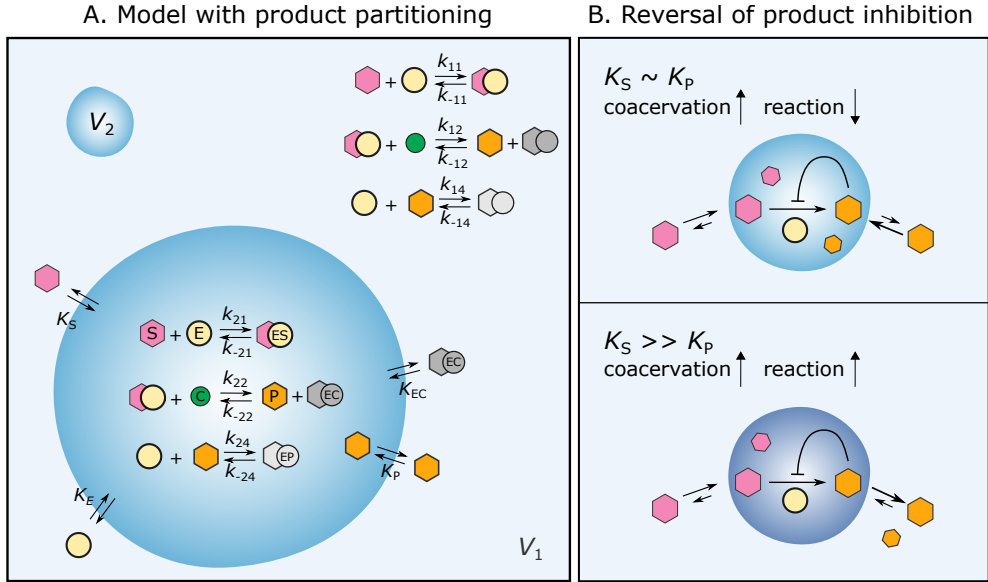
Figure 4.4: Extended model of reactions in coacervates: (A) with product partitioning, binding equilibrium and product inhibition taken into account. (B) The extent of product inhibition depends on partitioning coefficients. A few parameters are omitted for clarity.

Reactions in the coacervate phase

$$
\begin{aligned}
\mathbf{E}_{(2)} + \mathbf{S}_{(2)} &\rightleftharpoons \mathbf{ES}_{(2)} && (k_{21}; k_{-21}) \\
\mathbf{ES}_{(2)} + \mathbf{C}_{(2)} &\rightarrow \mathbf{ER}_{(2)} + \mathbf{P}_{(2)} && (k_{22}) \\
\mathbf{ER}_{(2)} &\rightleftharpoons \mathbf{E}_{(2)} + \mathrm{R}_{(2)} && (k_{23}; k_{-23}) \\
\mathbf{E}_{(2)} + \mathbf{P}_{(2)} &\rightleftharpoons \mathbf{EP}_{(2)} && (k_{24}; k_{-24})
\end{aligned}
\tag{4.21}
$$

Phase transfer fluxes

$$
\begin{aligned}
\mathbf{S}_{(1)} &\rightleftharpoons \mathbf{S}_{(2)} && (k_{t,1};\ k_{t,2};\ K_{\mathrm{S}}) \\
\mathbf{E}_{(1)} &\rightleftharpoons \mathbf{E}_{(2)} && (k_{t,1};\ k_{t,2};\ K_{\mathrm{E}}) \\
\mathbf{P}_{(1)} &\rightleftharpoons \mathbf{P}_{(2)} && (k_{t,1};\ k_{t,2};\ K_{\mathrm{P}}) \\
\mathbf{C}_{(1)} &\rightleftharpoons \mathbf{C}_{(2)} && (k_{t,1};\ k_{t,2};\ K_{\mathrm{C}}) \\
\mathbf{ES}_{(1)} &\rightleftharpoons \mathbf{ES}_{(2)} && (k_{t,1};\ k_{t,2};\ K_{\mathrm{ES}}) \\
\mathbf{ER}_{(1)} &\rightleftharpoons \mathbf{ER}_{(2)} && (k_{t,1};\ k_{t,2};\ K_{\mathrm{ER}}) \\
\mathbf{EP}_{(1)} &\rightleftharpoons \mathbf{EP}_{(2)} && (k_{t,1};\ k_{t,2};\ K_{\mathrm{EP}})
\end{aligned}
\tag{4.22}
$$
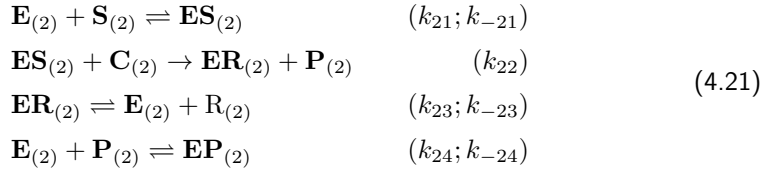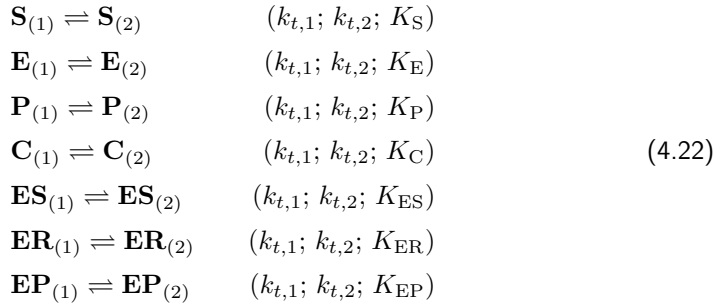
Similar to the minimal model without product partitioning, we looked at conditions that affect the measured reaction progress in the emulsion as a whole, what we call *overall conversion*, and compared it to a one phase reaction. At a volume fraction of

$\phi = 5\%$, strong substrate partitioning can, as in the minimal model, lead to a faster overall reaction, even though we assume reaction and binding rate constants are equal in both phases (Figure 4.5a). For a given K_S, however, product partitioning does not affect further the measured rate, as no product inhibition is present ($k_{14} = k_{24} = 0$). This result places the focus on substrate(s), rather than product, when designing a system to demonstrate change in reactivity by partitioning. Volume fraction is also crucial, as with strong partitioning, the coacervate compartment can act as an *endless* sink to reactant molecules and suppress the reaction in the dilute phase; in such a case, concentration and suppression effects cancel each other and the global effect to k_{obs} is lessened (Figure 4.5B, $\phi = 50\%$). In practice however, at a threshold concentration the coacervate phase cannot accomodate more solute molecules without disrupting phase separation.
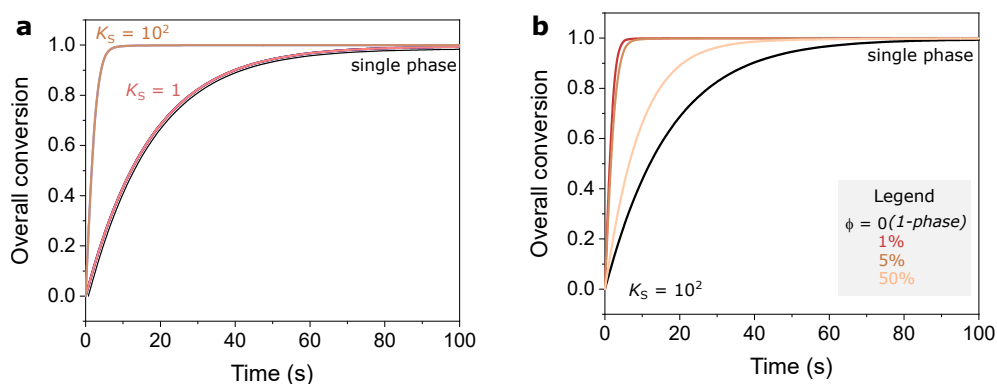
Figure 4.5: (a) Different kinetic profiles when reactant partitioning is changed; including product partitioning does not affect the curves. (b) Effect of volume fraction to the total product formation when product partitioning is accounted for. Parameters used: $K_E = K_S$, $k_{11} = k_{21} = 10^4 \, \text{mM}^{-1} \, \text{s}^{-1}$, $k_{-11} = k_{-21} = 10^2 \, \text{s}^{-1}$, $k_{12} = k_{22} = 2 \, \text{mM}^{-1} \, \text{s}^{-1}$, $k_{13} = k_{23} = 10^2 \, \text{s}^{-1}$, $k_{-13} = k_{-23} = 10^2 \, \text{mM}^{-1} \, \text{s}^{-1}$, $k_{14} = k_{24} = k_{-14} = k_{-24} = 0$ and $k_t = 10^3 \, \mu\text{L} \, \text{s}^{-1}$. In (a), $\phi = 5\%$; in (b), $K_P = 10^{-1}$.

Next, we evaluated the effect of reaction rate constant and binding constants, which we speculated can favor or hamper reactions in the crowded milieu of coacervates. Macromolecular crowding inside droplets can lead to reduced diffusion, which can either slow down reactions or trap reactants, such as an enzyme, in a more active conformation.[7–9] Reaction rate differences can indeed affect overall reaction rate at a volume fraction as low as 5% (Figure 4.6a). Enhanced or decreased binding constants in coacervates also have a pronounced effect on the measured reaction rate, although that requires a substrate-enzyme pair with a low binding constant in one phase already (Figure 4.6b).

Finally, with the inclusion of product partitioning and product inhibition, we could predict two interesting effects: transient product accumulation and reversal of product inhibition. The first is predicted for a transfer rate constant k_t lower than the reaction
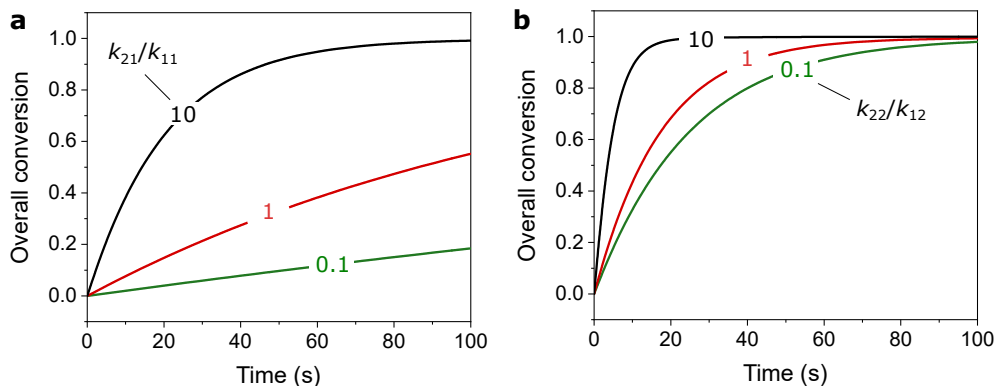
Figure 4.6: (a) Effect of different binding constants in the coacervate phase (k_{21}). (b) Effect of different reaction rate constant in the coacervate phase (k_{22}). Parameters used: $K_E = K_S = K_P = 10$, $k_{12} = 2\,\text{mM}^{-1}\,\text{s}^{-1}$, $k_{13} = k_{23} = 10^2\,\text{s}^{-1}$, $k_{-13} = k_{-23} = 10^2\,\text{mM}^{-1}\,\text{s}^{-1}$, $k_{14} = k_{24} = k_{-14} = k_{-24} = 0$, $k_t = 10^3\,\mu\text{L}\,\text{s}^{-1}$ and $\phi = 5\%$. In (a), $k_{11} = 10^{-1}\,\text{mM}^{-1}\,\text{s}^{-1}$ and $k_{-11} = k_{-21} = 10^{-3}\,\text{s}^{-1}$; in (b) $k_{11} = k_{21} = 10^4\,\text{mM}^{-1}\,\text{s}^{-1}$ and $k_{-11} = k_{-21} = 10^2\,\text{s}^{-1}$.

rate constant $(k_{12},\ k_{22})$, that is, a situation where our initial assumption about the phase equilibrium does not apply. When reactants partition strongly in the coacervate phase, but product does not, the reaction necessarily creates excess product, which can appear as a transient peak of high concentration if the relaxation to phase equilibrium is slow (Figure 4.7a). A constant influx of substrate (external or internally driven by fuel conversion) could sustain the concentration of **P** out of its phase equilibrium values or reach the saturation concentration for a subcompartment of **P**, in agreement to a dynamic approach to partitioning in multi-component systems. [10]

Slow diffusion in the dense phase is not impossible to achieve experimentally: a diffusion coefficient two orders of magnitude lower was found for globular proteins in liquid condensates. [11] Our *transfer rate constant* k_t is dependent on the diffusion coefficient and on the compartment (coacervate) radius ($k_t = 4\pi R D_m$, derived in ref. 2), and the distribution of the coacervate phase into multiple droplets with a high interface/volume ratio might play a role in increasing it.

The second effect resulting from the spatial segregation of reactants and products is the reversal of product inhibition (Figure 4.7b). Consider that competitive inhibition by the product is possible in both phases, that is, that now $k_{14} = k_{24} \neq 0$ and the product can reversibly bind to the enzyme, preventing binding of the substrate. Using low inhibition constants ($k_{14}/k_{-14} = 0.5$), we obtain that the ratio between K_S and K_P is crucial. The higher the difference between K_S and K_P, the closer the reaction curve gets to a reaction without inhibition, as we showed previously in Figure 4.5a). This means that seclusion of substrate and enzyme in the coacervate phase, while the product has

preference for the dilute phase (and vice-versa), can be a strategy to overcome product inhibition. This is of particular interest to us, as we have seen that pyruvate kinase retains its activity in the presence of poly-lysine, when coacervates form and concentrate ATP 18 times in comparison to the solution phase (Chapter 3). It is worth noticing that continuous product extraction, but in a macroscopic column instead of dilute phase, is a strategy to overcome product inhibition in enzymatic reactions of industrial interest such as lipase-catalyzed hydrolysis.[12]
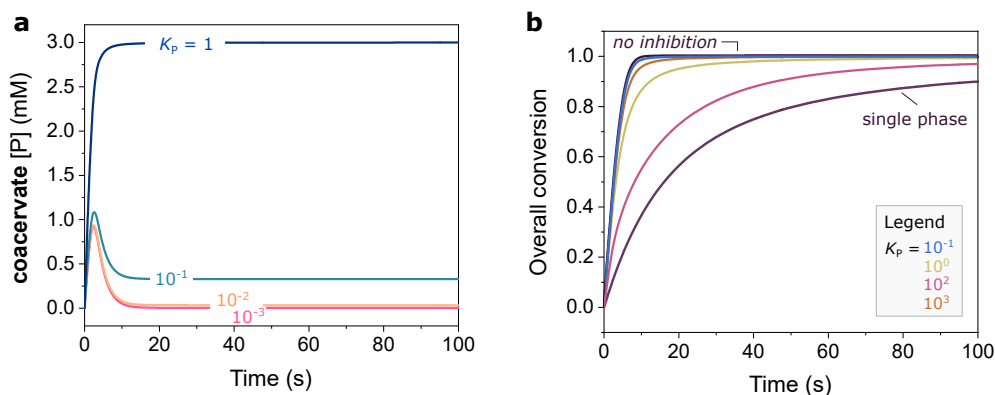
Figure 4.7: Effect of slow partitioning and product inhibition. (a) A slow phase equilibrium leads to accumulation of product in the coacervate phase as partitioning coefficient of the product is lowered. (b) Product and enzyme segregation reduces product inhibition in the total emulsion. Parameters used: $K_E = K_S = 100$, $k_{11} = k_{21} = 10^4 \, \text{mM}^{-1} \, \text{s}^{-1}$, $k_{-11} = k_{-21} = 10^2 \, \text{s}^{-1}$, $k_{12} = k_{22} = 2 \, \text{mM}^{-1} \, \text{s}^{-1}$, $k_{13} = k_{23} = 10^2 \, \text{s}^{-1}$, $k_{-13} = k_{-23} = 10^2 \, \text{mM}^{-1} \, \text{s}^{-1}$, $k_{14} = k_{24} = 2 \times 10^1 \, \text{mM}^{-1} \, \text{s}^{-1}$, $k_{-14} = k_{-24} = 4 \times 10^1 \, \text{s}^{-1}$. In (a), $\phi = 10\%$ and $k_d = 10^1 \, \mu\text{L} \, \text{s}^{-1}$; in (b), $k_t = 10^3 \, \mu\text{L} \, \text{s}^{-1}$ and $S = 10$ mM.

4.5 Towards an experimental proof of concept

We developed a kinetic model for bimolecular reactions in two phases, compatible with the partitioning of all components, separate rate constants per phase and Michaelis-Menten mechanism. We paid particular attention to our formulation, so that this model can be used and improved further by colleagues in the field of protocells and condensates. We were able to: demonstrate the effect of partitioning in enhancing the reaction rate inside droplets, or condensates, while simultaneously suppressing the reaction in the dilute phase; explain the role of reactants and product co-localization; and predict some interesting new properties such as transient product accumulation and surmounting of inhibition. Finally, we projected a realistic set of parameters for which an accessible, bulk reaction measurement could demonstrate the principles that are speculated to underlie the role of condensates for reactivity.

Our results point to three clear requirements for a good experimental model: (i) the reaction components must not interfere with phase separation, and therefore work under low concentrations; (ii) the coacervate components must allow to screen different volume fractions, which can be indicated by wide coacervation window; and (iii) the more the reaction is susceptible to differences in the chemical micro-environment, the more expressive the effect will be. In our kinetic analysis, we separately varied each parameter to highlight its role, but in practice all effects described are likely to be present and could counter-act or amplify each other; therefore in a first moment, a biomimetic system where we can attain full control should be preferred to *in vivo* measurements.

We envisage that lipase-catalyzed ester hydrolysis reactions could be a versatile model to demonstrate the effects in this chapter. Lipase activity is widely studied in multiphase mixtures, including coacervates, [13] in particular because lipases are water soluble enzymes that catalyze the hydrolysis of lipophilic substrates. The catalytic site of porcine pancreatic lipase (PPL) is protected by a *lid*, which opens up at interfaces to form the enzyme's active state. [14] As a result, PPL show enhanced activity in emulsions, at interfaces and in fat globules, [15] suggesting it is highly sensitive to factors such as polarity, crowding and water content, all of which can be altered in coacervates too. Chromogenic substrates of diverse polarities are available for lipases, such as 4–nitrophenylacetate (NPA) and 4–nitrophenylbutyrate (NPB), allowing the continuous monitoring of both phases together (see reaction scheme). Polarity is a determinant of partitioning coefficients, which enables to perform a study of different K_S for a fixed K_E for example.
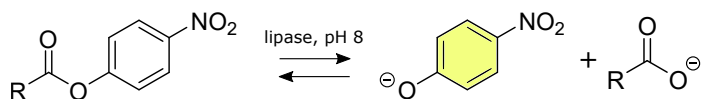
Perhaps the most difficult choice in the experimental design is the selection of the coacervate *host* molecules, as they must be inert towards enzyme activity. Biological coacervates are commonly composed of proteins and although macrophases can be obtained, [16] volume fractions are normally limited to low ranges. For a proof-of-concept study, we recommend the use of biomimetic coacervates built of small molecules or synthetic polymers. In our preliminary studies with porcine pancreas lipase, we tested the reaction compatibility with coacervates of varying hydrophobicity, including: the typical complex coacervates ATP/poly-lysine (chapters 2 and 3) and poly-glutamate/trimethylated poly-lysine (PRE-PLLM); and the single component coacervates of FFssFF (a disulfide bridged peptide) [17] and of DMEB (a surfactant) (see structures in Figure 1.8). [18] Poly-lysine has reactive primary amine residues that interfere with ester hydrolysis and ATP can interfere with enzymes, which is why we also suggest the inert, trimethylated poly-lysine-poly-glutamate version. We applied our protocol from Chapter 3 to a first selection of coacervates and substrates, and we present the preliminary — and promising — results below.

In short, we prepared DMEB and PRE-PLLM coacervates and assured they were stable

to the addition of the reaction components. We labelled the enzyme PPL to determine its partitioning coefficient by fluorescence microscopy, and in this case to prevent the interference of changes in enzyme activity due to the labelling, we worked with 100% labelled enzyme in all experiments. We then monitored the kinetics of hydrolysis in the total emulsion by measuring nitrophenolate absorbance in a plate reader. We applied an initial velocities method to determine k_{obs}, which we normalized by the value obtained with a negative control, with enzyme but without coacervates (k_0). The ratio k_{obs}/k_0 directly relates to the parameter k_{obs} defined in our model for the overall product conversion.
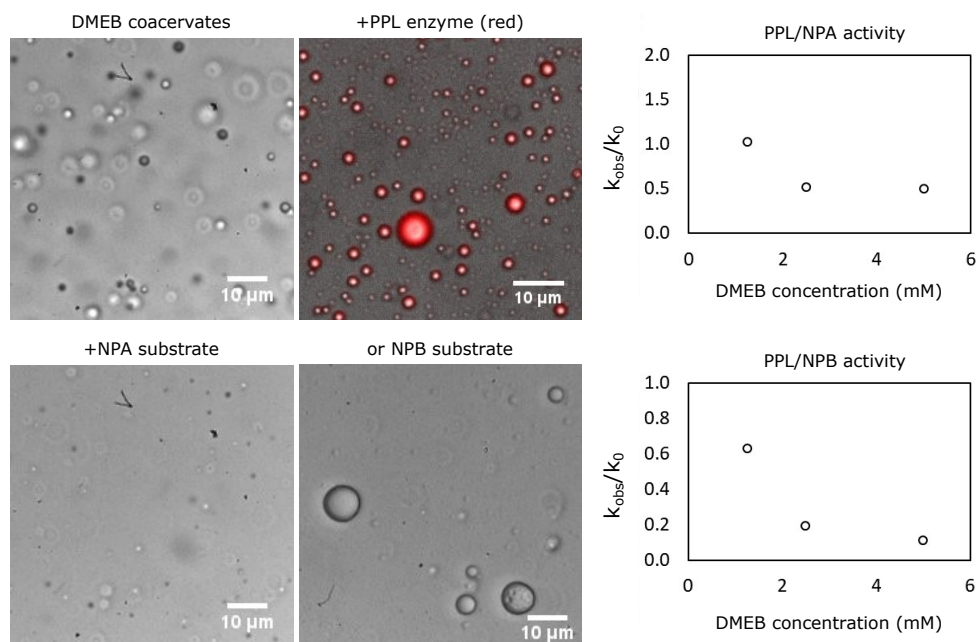
Figure 4.8: Lipase-catalyzed hydrolysis in DMEB (dodecyl(2-hydroxy-1-methyl-2-phenylethyl)dimethylammonium bromide) coacervates. Porcine pancreas lipase (PPL) was labeled with Alexa-647, yielding $K_E \simeq 836$. NPA denotes 4-nitrophenylacetate ($K_S \simeq 7$) and NPB, 4-nitrophenylbutyrate ($K_S \simeq 86$).

Our preliminary findings reflect our rationale in choosing the reaction and coacervates: DMEB and PRE-PLLM coacervates have distinct environments, with the surfactant droplets offering a more hydrophobic alternative to charge-based coacervates. As a result, the partitioning of the enzyme differs by ca. two orders of magnitude, and substrate partitioning differs by a factor of 2 — where the wide range of lipase substrates also proves useful. In our experience, two key limiting factors in this investigation are: ensuring that the emulsion remains well mixed throughout the measurement, and measuring volume fraction accurately. DMEB and PRE-PLLM offer a wide range of concentrations,
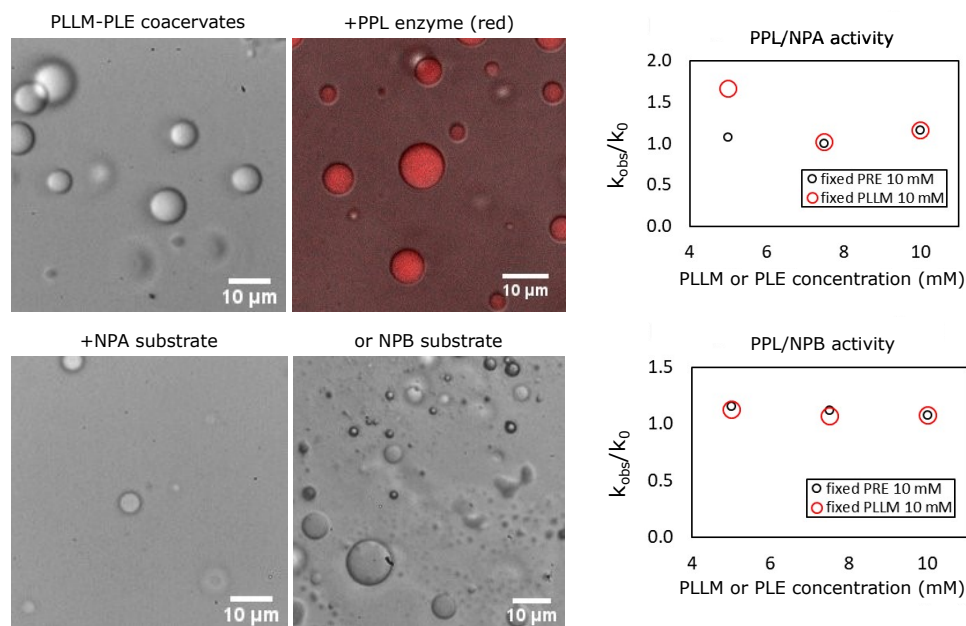
Figure 4.9: Lipase-catalyzed hydrolysis in PRE-PLLM coacervates (trimethylated poly-lysine and poly-glutamate). Porcine pancreas lipase (PPL) was labeled with Alexa-647, yielding $K_{\mathrm{E}} \simeq 6$. NPA denotes 4-nitrophenylacetate ($K_{\mathrm{S}} \simeq 11$) and NPB, 4-nitrophenylbutyrate ($K_{\mathrm{S}} \simeq 34$). The range of polymer concentrations led to 1–10% volume fraction.

but even then it can be hard to obtain significantly different volume fractions.

We believe future work in this direction, combining experiment and modeling, can provide a definite demonstration of the principles proposed in this chapter; moreover, the inclusion of more complex networks, such as that of auto-catalytic or replicating systems, might bring up new properties of coacervates even more relevant to protocells and membraneless organelles. We now move on to the main goal of this thesis: reaction-driven, growing coacervate droplets. Although the coupling of reaction and phase separation is the opposite of the premise of our model, we can as an approximation apply our conclusions here to propose a molecular mechanism to growth in Chapter 6.

Acknowledgements

References

[1] C. A. Bunton, "Reactivity in aqueous association colloids. descriptive utility of the pseudophase model," *Journal of molecular liquids*, vol. 72, no. 1-3, pp. 231–249, 1997.

[2] C. Weber, T. Michaels, and L. Mahadevan, "Spatial control of irreversible protein aggregation," *Elife*, vol. 8, p. e42315, 2019.

[3] S. Koga, D. S. Williams, A. W. Perriman, and S. Mann, "Peptide-nucleotide microdroplets as a step towards a membrane-free protocell model.," *Nature chemistry*, vol. 3, no. 9, pp. 720–4, 2011.

[4] T. Kojima and S. Takayama, "Membraneless compartmentalization facilitates enzymatic cascade reactions and reduces substrate inhibition," *ACS applied materials & interfaces*, vol. 10, no. 38, pp. 32782–32791, 2018.

[5] W. Stroberg and S. Schnell, "Do cellular condensates accelerate biochemical reactions? lessons from microdroplet chemistry," *Biophysical journal*, vol. 115, no. 1, pp. 3–8, 2018.

[6] B. Drobot, J. M. Iglesias-Artola, K. Le Vay, V. Mayr, M. Kar, M. Kreysing, H. Mutschler, and T. Y. Tang, "Compartmentalised RNA catalysis in membrane-free coacervate protocells," *Nature Communications*, vol. 9, no. 3643, 2018.

[7] A. R. Menjoge, A. B. Kayitmazer, P. L. Dubin, W. Jaeger, and S. Vasenkov, "Heterogeneity of polyelectrolyte diffusion in polyelectrolyte- protein coacervates: A 1h pulsed field gradient nmr study," *The Journal of Physical Chemistry B*, vol. 112, no. 16, pp. 4961–4966, 2008.

[8] R. Kausik, A. Srivastava, P. A. Korevaar, G. Stucky, J. H. Waite, and S. Han, "Local water dynamics in coacervated polyelectrolytes monitored through dynamic nuclear polarization-enhanced 1h nmr," *Macromolecules*, vol. 42, no. 19, pp. 7404–7412, 2009.

[9] A. Shakya and J. T. King, "Non-fickian molecular transport in protein–dna droplets," *ACS Macro Letters*, vol. 7, no. 10, pp. 1220–1225, 2018.

[10] J. A. Riback, L. Zhu, M. C. Ferrolino, M. Tolbert, D. M. Mitrea, D. W. Sanders, M.-T. Wei, R. W. Kriwacki, and C. P. Brangwynne, "Composition-dependent thermodynamics of intracellular phase separation," *Nature*, vol. 581, no. 7807, pp. 209–214, 2020.

[11] T. J. Nott, E. Petsalaki, P. Farber, D. Jervis, E. Fussner, A. Plochowietz, T. D. Craggs, D. P. Bazett-Jones, T. Pawson, J. D. Forman-Kay, *et al.*, "Phase transition of a disordered nuage protein generates environmentally responsive membraneless organelles," *Molecular cell*, vol. 57, no. 5, pp. 936–947, 2015.

[12] S. Jeong, B.-Y. Hwang, J. Kim, and B.-G. Kim, "Lipase-catalyzed reaction in the packed-bed reactor with continuous extraction column to overcome a product inhibition," *Journal of Molecular Catalysis B: Enzymatic*, vol. 10, no. 6, pp. 597–604, 2000.

[13] S. Lindhoud, W. Norde, and M. A. Cohen Stuart, "Effects of polyelectrolyte complex micelles and their components on the enzymatic activity of lipase," *Langmuir*, vol. 26, no. 12, pp. 9802–9808, 2010.

[14] H. van Tilbeurgh, M.-P. Egloff, C. Martinez, N. Rugani, R. Verger, and C. Cambillau, "Interfacial activation of the lipase–procolipase complex by mixed micelles revealed by x-ray crystallography," *Nature*, vol. 362, no. 6423, pp. 814–820, 1993.

[15] F. Su, G. Li, Y. Fan, and Y. Yan, "Enhanced performance of lipase via microcapsulation and its application in biodiesel preparation," *Scientific reports*, vol. 6, no. 1, pp. 1–12, 2016.

[16] J. P. Brady, P. J. Farber, A. Sekhar, Y.-H. Lin, R. Huang, A. Bah, T. J. Nott, H. S. Chan, A. J. Baldwin, J. D. Forman-Kay, *et al.*, "Structural and hydrodynamic properties of an intrinsically

disordered region of a germ cell-specific protein on phase separation," *Proceedings of the National Academy of Sciences*, vol. 114, no. 39, pp. E8194–E8203, 2017.

[17] M. Abbas, W. P. Lipiński, K. K. Nakashima, W. T. S. Huck, and E. Spruijt, "A Short Peptide Synthon for Liquid-Liquid Phase Separation," *ChemRxiv*, 2020.

[18] L. Zhou, Y. Fan, Z. Liu, L. Chen, E. Spruijt, and Y. Wang, "A Multiresponsive Transformation between Surfactant-Based Coacervates and Vesicles," *CCS Chemistry*, pp. 1–24, 2021.

Python code I: minimal reaction system

```python
1   # Import Python libraries with pre-defined functions:
2
3   # Import the whole NumPy module with the short name "np"
4   import numpy as np
5
6   # Import a module to plot in a MatLab fashion, with the short name "plt"
7   import matplotlib.pyplot as plt
8
9   # Import selected functions to solve differential equations
10  from scipy.integrate import odeint
11
12  # Import module to export to excel
13  import xlsxwriter
14
15  # A function to calculate phase equilibrium concentrations, given a partitioning
        coefficient Kp, a volume fraction f and a total concentration
16  def partitioningIn(concentrationTotal, partitioningCoefficient, volumeFraction):
17      concentrationIn = ( concentrationTotal/(1 - volumeFraction +
            partitioningCoefficient*volumeFraction) )*partitioningCoefficient
18      return concentrationIn
19
20  def partitioningOut(concentrationTotal, partitioningCoefficient, volumeFraction):
21      concentrationOut = concentrationTotal / (1 - volumeFraction +
            partitioningCoefficient*volumeFraction)
22      return concentrationOut
23
24  # Input partitioning coefficient (pcSpeciesName)
25  pcADP          = 10
26  pcPK           = 26
27  pcATP          = 3
28  vPartitioning = [pcADP, pcPK, pcATP]
29
30  # Input volume fraction, which is constant over time and common for all species (
        uL)
31  volumeTotal    = 2e1
32  volumeFraction = 5e-1
33  volumeDroplets = volumeFraction*volumeTotal
34  volumeDilute   = (1 - volumeFraction)*volumeTotal
35  shrinkage      = volumeDroplets/volumeDilute
36
37  # Input initial total concentrations and combine in a vector (mM)
38  concADP_0      = 3
39  concPK_0       = 3e-2
40  concATP_0      = 0
41  vSpeciesTot_0 = [concADP_0, concPK_0, concATP_0]
42
43  # Organize inner concentrations in one array, and outer in a separate one
44  vSpeciesOut_0 = []
45  vSpeciesIn_0  = []
46  for i in range(3):
47      vSpeciesOut_0.append(partitioningOut(vSpeciesTot_0[i], vPartitioning[i],
            volumeFraction))
48      vSpeciesIn_0.append(partitioningIn(vSpeciesTot_0[i], vPartitioning[i],
            volumeFraction))
49
```

```
50  # Put everything together in an initial state vector, to which concentration(t)
        will be added during the solution
51  vSpecies_0 = np.concatenate((vSpeciesOut_0, vSpeciesIn_0))
52
53  # Create the reaction function: bimolecular catalyst + substrate
54  # Reactions in the dilute phase (1)
55      # conversion              k12, k−12    E + ADP  <−> E + ATP
56
57  # Reactions in the droplets (2)
58      # conversion              k22, k−22    E + ADP  <−> E + ATP
59
60  # Input all rate constants
61  # Reactions in the dilute phase (1) (mM/s or /s)
62  k12  = 2
63  k_12 = 0
64
65  # Reactions in the droplets (2)
66  k22  = 2
67  k_22 = 0
68
69  # Phase equilibrium
70  kTransfer = 1e3
71
72  # Define functions per chemical process, or flux
73
74  # Bimolecular reaction
75  def rxn(concSubstrate, concCatalyst, rateConstant):
76      return rateConstant*concSubstrate*concCatalyst
77
78  # eLife phase exchange until equilibrium is reached
79  def phaseFlux(concentrationIn, concentrationOut, partitionCoeff, volumePhase,
        kTransfer):
80      return (−kTransfer*concentrationIn + kTransfer*partitionCoeff*concentrationOut
            )/volumePhase
81  # for a species inside:  use +phaseFlux, volumePhase = volumeDroplets
82  # for a species outside: use −phaseFlux, volumePhase = volumeDilute
83
84  # Initialize species concentrations per phase
85  concADPout    = vSpecies_0[0]
86  concPKout     = vSpecies_0[1]
87  concATPout    = vSpecies_0[2]
88  #
89  concADPin     = vSpecies_0[3]
90  concPKin      = vSpecies_0[4]
91  concATPin     = vSpecies_0[5]
92
93  # Define a function for the set of differential equations
94  # dydt lists the dy/dt of each species
95  def twoPhasesODE(y, t, k12, k_12, k22, k_22, pcADP, pcPK, kTransfer):
96      [concADPout, concPKout, concATPout, concADPin, concPKin, concATPin] = y
97
98      dydt = [−rxn(concADPout, concPKout, k12) +rxn(concATPout, concPKout, k_12) −
            phaseFlux(concADPin, concADPout, pcADP, volumeDilute, kTransfer),
99          0,
100         +rxn(concADPout, concPKout, k12) −rxn(concATPout, concPKout, k_12),
101         −rxn(concADPin, concPKin, k22) +rxn(concATPin, concPKin, k_22) +phaseFlux(
                concADPin, concADPout, pcADP, volumeDroplets, kTransfer),
102         0,
103         +rxn(concADPin, concPKin, k22) −rxn(concPKin, concATPin, k_22)
104         ]
```

```
105
106         return dydt
107
108  # Define the timespan for solving the ODEs: from [1] to [2] with [3] samples. Time
          is in seconds
109  timespan = np.linspace(0, 100, 50)
110
111  # Solve the differential equations for the initial state defined by vSpecies_0
112  aSpecies = odeint(twoPhasesODE, vSpecies_0, timespan, args=(k12,k_12,k22,k_22,
          pcADP,pcPK,kTransfer))
113
114  # Assign a species concentration to each row in the array aSpecies. Column = time
115  concADPout  = aSpecies[:,0]
116  concPKout   = aSpecies[:,1]
117  concATPout  = aSpecies[:,2]
118  #
119  concADPin   = aSpecies[:,3]
120  concPKin    = aSpecies[:,4]
121  concATPin   = aSpecies[:,5]
122  #
123  molATPin  = concATPin*volumeDroplets
124  molATPout = concATPout*volumeDilute
125
126  # Complete aSpecies with time
127  aSpecies = np.column_\mathrm{S}tack((aSpecies, timespan))
128
129  # Plot
130  plt.figure()
131  plt.plot(timespan, molATPin, 'g—', label = 'produced inside')
132  plt.plot(timespan, molATPout, 'b—', label = 'produced outside')
133  plt.legend()
134  plt.xlabel('Time (s)')
135  plt.ylabel('ATP (nmol)')
136
137  # Input desired figure name
138  plt.savefig('filename.png',dpi=300)
139  plt.show()
140
141  # Export to excel
142  # Input filename that we want to create
143  workbook   = xlsxwriter.Workbook('filename.xlsx')
144  worksheet1 = workbook.add_worksheet("Model")
145
146  # Write the headers
147  worksheet1.write('A1', 'concADPout')
148  worksheet1.write('B1', 'concPKout')
149  worksheet1.write('C1', 'concATPout')
150  worksheet1.write('D1', 'concADPin')
151  worksheet1.write('E1', 'concPKin')
152  worksheet1.write('F1', 'concATPin')
153  worksheet1.write('G1', 'timespan')
154
155  # Index rows and columns to 0 before starting to iterate through the concentration
          list
156  row     = 1
157  column  = 0
158
159  # Iterate through concentration list
160  for concADPout,concPKout,concATPout,concADPin,concPKin,concATPin,time in (aSpecies
          ):
```

111

```
161        worksheet1.write(row, column,    concADPout)
162        worksheet1.write(row, column+1, concPKout)
163        worksheet1.write(row, column+2, concATPout)
164        worksheet1.write(row, column+3, concADPin)
165        worksheet1.write(row, column+4, concPKin)
166        worksheet1.write(row, column+5, concATPin)
167        worksheet1.write(row, column+6, time)
168        row += 1
169
170  # Add simulation conditions to the file
171  worksheet2     = workbook.add_worksheet("Conditions")
172  lstConditions = (k12, k_12, k22, k_22, kTransfer, volumeTotal, volumeDroplets,
         pcADP, pcPK, pcATP)
173  row     = 0
174  column = 0
175
176  for value in (lstConditions):
177      worksheet2.write(row, column, value)
178      row += 1
179
180  # Close file
181  workbook.close()
```

Python code II: enzymatic reaction system

```python
1   # Import Python libraries with pre-defined functions:
2
3   # Import the whole NumPy module with the short name "np"
4   import numpy as np
5
6   # Import a module to plot in a MatLab fashion, with the short name "plt"
7   import matplotlib.pyplot as plt
8
9   # Import selected functions to solve differential equations
10  from scipy.integrate import odeint
11
12  # Import module to export to excel
13  import xlsxwriter
14
15  # A function to calculate phase equilibrium concentrations, given a partitioning
16        coefficient Kp, a volume fraction f and a total concentration
16  def partitioningIn(concentrationTotal, partitioningCoefficient, volumeFraction):
17      concentrationIn = ( concentrationTotal/(1 - volumeFraction +
18          partitioningCoefficient*volumeFraction) )*partitioningCoefficient
18      return concentrationIn
19
20  def partitioningOut(concentrationTotal, partitioningCoefficient, volumeFraction):
21      concentrationOut = concentrationTotal / (1 - volumeFraction +
22          partitioningCoefficient*volumeFraction)
22      return concentrationOut
23
24  # Input partitioning coefficient (pcSpeciesName)
25  pcADP          = 1e2
26  pcPEP          = 1
27  pcPK           = 1e2
28  pcATP          = 1e-1
29  pcPYR          = 1
30  pcPKPEP        = pcPK
31  pcPKATP        = pcPK
32  pcPKPYR        = pcPK
33  vPartitioning = [pcADP, pcPEP, pcPK, pcATP, pcPYR, pcPKPEP, pcPKATP, pcPKPYR]
34
35  # Input volume fraction, which is constant over time and common for all species (
36        unit uL)
36  # missing: add conditions for a one-phase system
37  volumeTotal    = 2e1
38  volumeFraction = 5e-2
39  volumeDroplets = volumeFraction*volumeTotal
40  volumeDilute   = (1 - volumeFraction)*volumeTotal
41  shrinkage      = volumeDroplets/volumeDilute
42
43  # Input initial total concentrations and combine in a vector (mM)
44  concADP_0      = 3
45  concPEP_0      = 3
46  concPK_0       = 3e-2
47  concATP_0      = 0
48  concPYR_0      = 0
49  concPKPEP_0    = 0
50  concPKATP_0    = 0
51  concPKPYR_0    = 0
52  vSpeciesTot_0 = [concADP_0, concPEP_0, concPK_0, concATP_0, concPYR_0, concPKPEP_0
```

```
          , concPKATP_0 , concPKPYR_0]
53
54   # Organize inner concentrations in one array, and outer in a separate one
55   vSpeciesOut_0 = []
56   vSpeciesIn_0  = []
57   for i in range(8):
58       vSpeciesOut_0.append( partitioningOut( vSpeciesTot_0[i], vPartitioning[i],
             volumeFraction) )
59       vSpeciesIn_0.append( partitioningIn( vSpeciesTot_0[i], vPartitioning[i],
             volumeFraction) )
60
61   # Put everything together in an initial state vector, to which concentration(t)
        will be added during the solution
62   vSpecies_0 = np.concatenate(( vSpeciesOut_0 , vSpeciesIn_0 ))
63
64   # Create the reaction function: bimolecular catalyst + substrate
65   #Reactions in the dilute phase (1)
66       # substrate binding   k11, k−11    E + PEP       <−>  E−PEP
67       # conversion          k12, k−12    E−PEP + ADP  −>  E−PY + ATP
68       # product release     k13, k−13    E + PY        <−>  E−PY
69       # product inhibition  k14, k−14    E + ATP       <−>  E−ATP
70
71       #Reactions in the droplets (2)
72       # substrate binding   k21, k−21    E + PEP       <−>  E−PEP
73       # conversion          k22, k−22    E−PEP + ADP  −>  E−PY + ATP
74       # product release     k23, k−23    E + PY        <−>  E−PY
75       # product inhibition  k24, k−24    E + ATP       <−>  E−ATP
76
77   # Input all rate constants
78   # Reactions in the dilute phase (1) (mM/s or /s)
79   k11  = 1e4
80   k_11 = 1e2
81   k12  = 2
82   k_12 = 0
83   k13  = 1e2
84   k_13 = 1e2
85   k14  = 2e3
86   k_14 = 4e1
87   vReactionRateOut = [k11,k_11,k12,k_12,k13,k_13,k14,k_14]
88
89   #Reactions in the droplets (2)
90   k21  = 1e4
91   k_21 = 1e2
92   k22  = 2
93   k_22 = 0
94   k23  = 1e2
95   k_23 = 1e2
96   k24  = 2e3
97   k_24 = 4e1
98   vReactionRateIn = [k21,k_21,k22,k_22,k23,k_23,k24,k_24]
99
100  # Phase equilibrium
101  kTransfer = 1e3
102
103  # Define functions per chemical process, or flux
104  def bind(concSubstrate,concEnzyme,rateConstant):
105      return rateConstant*concSubstrate*concEnzyme
106
107  def dissoc(concComplex,rateConstant):
108      return rateConstant*concComplex
```

```
109
110  def rxn(concFirstSubstrate, concSecondSubstrate, rateConstant):
111      return rateConstant*concFirstSubstrate*concSecondSubstrate
112
113  # eLife phase exchange until equilibrium is reached
114
115  def phaseFlux(concentrationIn, concentrationOut, partitionCoeff, volumePhase,
         kTransfer):
116      return (-kTransfer*concentrationIn + kTransfer*partitionCoeff*concentrationOut
             )/volumePhase
117  # for a species inside:  use +phaseFlux, volumePhase = volumeDroplets
118  # for a species outside: use -phaseFlux, volumePhase = volumeDilute
119
120  # Initialize species concentrations per phase
121  concADPout    = vSpecies_0[0]
122  concPEPout    = vSpecies_0[1]
123  concPKout     = vSpecies_0[2]
124  concATPout    = vSpecies_0[3]
125  concPYRout    = vSpecies_0[4]
126  concPKPEPout  = vSpecies_0[5]
127  concPKATPout  = vSpecies_0[6]
128  concPKPYRout  = vSpecies_0[7]
129  #
130  concADPin     = vSpecies_0[8]
131  concPEPin     = vSpecies_0[9]
132  concPKin      = vSpecies_0[10]
133  concATPin     = vSpecies_0[11]
134  concPYRin     = vSpecies_0[12]
135  concPKPEPin   = vSpecies_0[13]
136  concPKATPin   = vSpecies_0[14]
137  concPKPYRin   = vSpecies_0[15]
138
139  # Define a function for the set of differential equations
140  # dydt lists the dy/dt of each species
141  def twoPhasesODE(y, t, k11, k_11, k12, k_12, k13, k_13, k14, k_14, k21, k_21, k22, k_22, k23,
         k_23, k24, k_24, pcADP, pcPEP, pcPK, pcATP,
142                   pcPYR, pcPKPEP, pcPKATP, pcPKPYR, kTransfer):
143      [concADPout, concPEPout, concPKout, concATPout, concPYRout, concPKPEPout,
             concPKATPout, concPKPYRout,
144      concADPin, concPEPin, concPKin, concATPin, concPYRin, concPKPEPin, concPKATPin
             , concPKPYRin] = y
145
146      dydt = [-rxn(concADPout, concPKPEPout, k12) +rxn(concPKPYRout, concATPout, k_12) -
             phaseFlux(concADPin, concADPout, pcADP, volumeDilute, kTransfer),
147              -bind(concPKout, concPEPout, k11) +dissoc(concPKPEPout, k_11) -phaseFlux(
                     concPEPin, concPEPout, pcPEP, volumeDilute, kTransfer),
148              -bind(concPKout, concPEPout, k11) +dissoc(concPKPEPout, k_11) -bind(
                     concPKout, concPYRout, k13) +dissoc(concPKPYRout, k_13) -bind(
                     concPKout, concATPout, k14)
149                +dissoc(concPKATPout, k_14) -phaseFlux(concPKin, concPKout, pcPK,
                     volumeDilute, kTransfer),
150              +rxn(concADPout, concPKPEPout, k12) -rxn(concPKPYRout, concATPout, k_12) -
                     bind(concPKout, concATPout, k14) +dissoc(concPKATPout, k_14) -
                     phaseFlux(concATPin, concATPout, pcATP, volumeDilute, kTransfer),
151              +dissoc(concPKPYRout, k_13) -bind(concPKout, concPYRout, k13) -phaseFlux(
                     concPYRin, concPYRout, pcPYR, volumeDilute, kTransfer),
152              +bind(concPEPout, concPKout, k11) -dissoc(concPKPEPout, k_11) -rxn(
                     concPKPEPout, concADPout, k12) +rxn(concPKPYRout, concATPout, k_12) -
                     phaseFlux(concPKPEPin, concPKPEPout, pcPKPEP, volumeDilute, kTransfer)
                     ,
```

```
153                     +bind ( concPKout , concATPout , k14 ) −dissoc ( concPKATPout , k_14 ) −phaseFlux (
                           concPKATPin , concPKATPout , pcPKATP , volumeDilute , kTransfer ) ,
154                     +rxn ( concADPout , concPKPEPout , k12 ) −rxn ( concPKPYRout , concATPout , k_12 ) +
                           bind ( concPKout , concPYRout , k13 ) −dissoc ( concPKPYRout , k_13 ) −
                           phaseFlux ( concPKPYRin , concPKPYRout , pcPKPYR , volumeDilute , kTransfer )
                           ,
155
156                     −rxn ( concADPin , concPKPEPin , k22 ) +rxn ( concPKPYRin , concATPin , k_22 ) +
                           phaseFlux ( concADPin , concADPout , pcADP , volumeDroplets , kTransfer ) ,
157                     −bind ( concPKin , concPEPin , k21 ) +dissoc ( concPKPEPin , k_21 ) +phaseFlux (
                           concPEPin , concPEPout , pcPEP , volumeDroplets , kTransfer ) ,
158                     −bind ( concPKin , concPEPin , k21 ) +dissoc ( concPKPEPin , k_21 ) −bind ( concPKin
                           , concPYRin , k23 ) +dissoc ( concPKPYRin , k_23 ) −bind ( concPKin , concATPin
                           , k24 )
159                        +dissoc ( concPKATPin , k_24 ) +phaseFlux ( concPKin , concPKout , pcPK ,
                              volumeDroplets , kTransfer ) ,
160                     +rxn ( concPKPEPin , concADPin , k22 ) −rxn ( concPKPYRin , concATPin , k_22 ) −bind
                           ( concPKin , concATPin , k24 ) +dissoc ( concPKATPin , k_24 ) +phaseFlux (
                           concATPin , concATPout , pcATP , volumeDroplets , kTransfer ) ,
161                     +dissoc ( concPKPYRin , k_23 ) −bind ( concPKin , concPYRin , k23 ) +phaseFlux (
                           concPYRin , concPYRout , pcPYR , volumeDroplets , kTransfer ) ,
162                     +bind ( concPEPin , concPKin , k21 ) −dissoc ( concPKPEPin , k_21 ) −rxn (
                           concPKPEPin , concADPin , k22 ) +rxn ( concPKPYRin , concATPin , k_22 ) +
                           phaseFlux ( concPKPEPin , concPKPEPout , pcPKPEP , volumeDroplets ,
                           kTransfer ) ,
163                     +bind ( concPKin , concATPin , k24 ) −dissoc ( concPKATPin , k_24 ) +phaseFlux (
                           concPKATPin , concPKATPout , pcPKATP , volumeDroplets , kTransfer ) ,
164                     +rxn ( concPKPEPin , concADPin , k22 ) −rxn ( concPKPYRin , concATPin , k_22 ) +bind
                           ( concPKin , concPYRin , k23 ) −dissoc ( concPKPYRin , k_23 ) +phaseFlux (
                           concPKPYRin , concPKPYRout , pcPKPYR , volumeDroplets , kTransfer )
165                     ]
166         return dydt
167
168  # Define the timespan for solving the ODEs : from [1] to [2] with [3] samples . Time
         is in seconds
169  timespan = []
170  timespan = np . linspace ( 0 , 100 , 50 )
171
172  # Solve the differential equations for the initial state defined by vSpecies_0
173  aSpecies = odeint ( twoPhasesODE , vSpecies_0 , timespan , args=(k11 , k_11 , k12 , k_12 , k13 ,
         k_13 , k14 , k_14 , k21 , k_21 , k22 , k_22 , k23 , k_23 , k24 , k_24 , pcADP , pcPEP , pcPK , pcATP ,
174                     pcPYR , pcPKPEP , pcPKATP , pcPKPYR , kTransfer ) )
175
176  # Assign a species concentration to each row in the array aSpecies . Column = time
177  concADPout     = aSpecies [ : , 0 ]
178  concPEPout     = aSpecies [ : , 1 ]
179  concPKout      = aSpecies [ : , 2 ]
180  concATPout     = aSpecies [ : , 3 ]
181  concPYRout     = aSpecies [ : , 4 ]
182  concPKPEPout   = aSpecies [ : , 5 ]
183  concPKATPout   = aSpecies [ : , 6 ]
184  concPKPYRout   = aSpecies [ : , 7 ]
185  #
186  concADPin    = aSpecies [ : , 8 ]
187  concPEPin    = aSpecies [ : , 9 ]
188  concPKin     = aSpecies [ : , 10 ]
189  concATPin    = aSpecies [ : , 11 ]
190  concPYRin    = aSpecies [ : , 12 ]
191  concPKPEPin  = aSpecies [ : , 13 ]
192  concPKATPin  = aSpecies [ : , 14 ]
```

```
193   concPKPYRin = aSpecies [: ,15]
194
195   # Correct concentrations to include complexed forms
196   concTotATPout = np.add((concATPout),(concPKATPout))
197   concTotPEPout = np.add((concPEPout),(concPKPEPout))
198   concTotPYRout = np.add((concPYRout),(concPKPYRout))
199   concTotPKout  = np.add((concPKout),(concPKPEPout))
200   concTotPKout  = np.add((concTotPKout),(concPKATPout))
201   concTotPKout  = np.add((concTotPKout),(concPKPYRout))
202   concTotADPout = concADPout
203   #
204   concTotATPin = np.add((concATPin),(concPKATPin))
205   concTotPEPin = np.add((concPEPin),(concPKPEPin))
206   concTotPYRin = np.add((concPYRin),(concPKPYRin))
207   concTotPKin  = np.add((concPKin),(concPKPEPin))
208   concTotPKin  = np.add((concTotPKin),(concPKATPin))
209   concTotPKin  = np.add((concTotPKin),(concPKPYRin))
210   concTotADPin = concADPin
211   #
212   molATPin  = concTotATPin*volumeDroplets
213   molATPout = concTotATPout*volumeDilute
214
215   # Make a new aSpecies with relevant data
216   aSpeciesNew = []
217
218   # Plot
219   plt.figure()
220   plt.plot(timespan, molATPin, 'g-', label = 'inside')
221   plt.plot(timespan, molATPout, 'b-', label = 'outside')
222   plt.legend()
223   plt.xlabel('Time (s)')
224   plt.ylabel('ATP (nmol)')
225
226   # Input desired figure name
227   #plt.savefig('filename.png',dpi=300)
228   plt.show()
229
230   # Input excel file name
231   workbook = xlsxwriter.Workbook('filename.xlsx')
232   worksheet1 = workbook.add_worksheet("Model")
233
234   # Write the headers
235   worksheet1.write('A1', 'concADPout')
236   worksheet1.write('B1', 'concPEPout')
237   worksheet1.write('C1', 'concPKout')
238   worksheet1.write('D1', 'concATPout')
239   worksheet1.write('E1', 'concPYRout')
240   worksheet1.write('F1', 'concPKPEPout')
241   worksheet1.write('G1', 'concPKATPout')
242   worksheet1.write('H1', 'concPKPYRout')
243   worksheet1.write('I1', 'concADPin')
244   worksheet1.write('J1', 'concPEPin')
245   worksheet1.write('K1', 'concPKin')
246   worksheet1.write('L1', 'concATPin')
247   worksheet1.write('M1', 'concPYRin')
248   worksheet1.write('N1', 'concPKPEPin')
249   worksheet1.write('O1', 'concPKATPin')
250   worksheet1.write('P1', 'concPKPYRin')
251
252   # Index rows and columns to 0 before starting to iterate through the concentration
```

```
              list
253    row      = 1
254    column = 0
255
256    # Iterate through concentration list
257    for concADPout , concPEPout , concPKout , concATPout , concPYRout , concPKPEPout ,
            concPKATPout , concPKPYRout , concADPin , concPEPin , concPKin , concATPin , concPYRin ,
            concPKPEPin , concPKATPin , concPKPYRin  in  ( aSpecies ) :
258        worksheet1 . write ( row , column ,      concADPout )
259        worksheet1 . write ( row , column+1, concPEPout )
260        worksheet1 . write ( row , column+2, concPKout )
261        worksheet1 . write ( row , column+3, concATPout )
262        worksheet1 . write ( row , column+4, concPYRout )
263        worksheet1 . write ( row , column+5, concPKPEPout )
264        worksheet1 . write ( row , column+6, concPKATPout )
265        worksheet1 . write ( row , column+7, concPKPYRout )
266        worksheet1 . write ( row , column+8, concADPin )
267        worksheet1 . write ( row , column+9, concPEPin )
268        worksheet1 . write ( row , column+10,concPKin )
269        worksheet1 . write ( row , column+11,concATPin )
270        worksheet1 . write ( row , column+12,concPYRin )
271        worksheet1 . write ( row , column+13,concPKPEPin )
272        worksheet1 . write ( row , column+14,concPKATPin )
273        worksheet1 . write ( row , column+15,concPKPYRin )
274        row += 1
275
276    # Add simulation conditions to the file
277    worksheet2     = workbook . add_worksheet ( " Conditions " )
278    lstConditions = ( k11 , k_11 , k12 , k_12 , k13 , k_13 , k14 , k_14 , k21 , k_21 , k22 , k_22 , k23 , k_23 ,
            k24 , k_24 , kTransfer , pcADP , pcPEP , pcPK , pcATP , pcPYR , pcPKPEP , pcPKATP , pcPKPYR ,
            volumeTotal , volumeDroplets )
279    row      = 0
280    column = 0
281
282    for value in ( lstConditions ) :
283        worksheet2 . write ( row , column , value )
284        row += 1
285
286    # Close file
287    workbook . close ( )
```

Part III

Resumption

Chapter 5

Stability of coacervate droplets as protocells

Typical Ostwald ripening
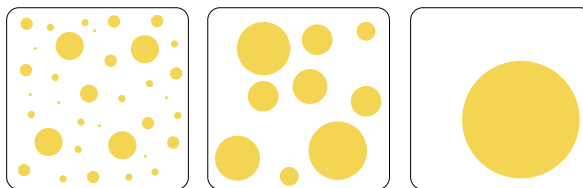
Complex coacervate droplets
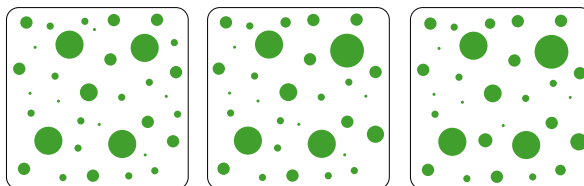
5.1   Can coacervate protocells survive?

"Before replicators and reproducers, there must be survivors"
(Szathmary, 1997)[1]

So far when talking about life-like behaviors, we highlighted processes that classify as actions: growth, division, motility and even metabolism are very clear to observe or measure. A less active process, but extremely important if we want to understand how droplets could have become cells, is persistence. Persistence is often overlooked as a component of fitness, but arguably the most important feature in a pre-Darwinian scenario.[2] In the context of this thesis, persistence or survival is defined by the droplets physical stability.

Several works have pointed out the lack of a membrane as a disadvantage of coacervates as protocellular models.[3,4] Membrane-less droplets have no barrier to prevent fusion and spreading on the observation surface. Experimental attempts to stabilize droplets include: a protective block co-polymer self-assembled layer around droplets,[3] a proteinaceous pseudo-membrane[5], microfluidic encapsulation[6] and lipid bilayers.[7,8] Although successful, these strategies bring their own shortcomings: they limit the permeability of coacervate droplets, a crucial advantage over lipid-based protocells, or the amount of droplets that can be studied together; and by relying on specific interactions on sophisticated production, they are not as strong in terms of prebiotic plausibility.
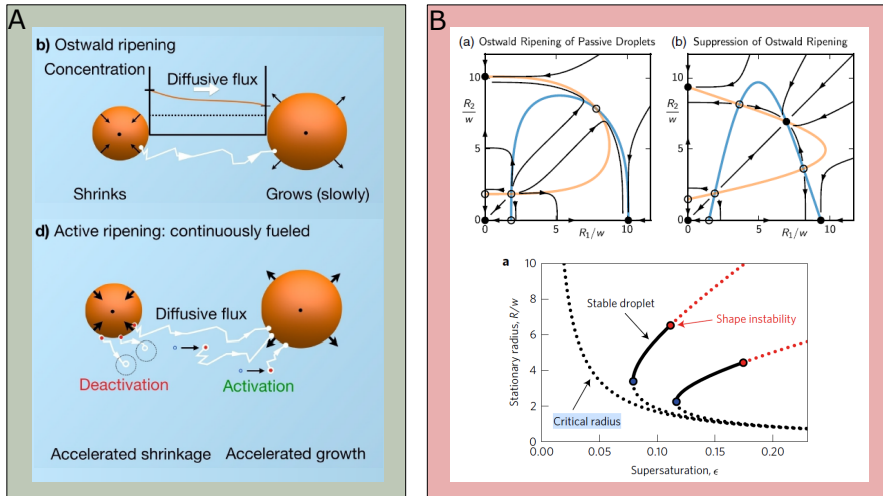
Figure 5.1: (A) Tena-Solsona et al found that a reaction cycle accelerates ripening by introducing processes of activation and deactivation that follow the same diffusive flux as Ostwald ripening.[9] (B). Zwicker et al and Weber et al developed a model that explains how an active process can introduce a stable stationary state (black disk) where two droplets of the same size co-exist.[10,11]

However, no systematic experimental study on the rate of Ostwald ripening specifically in coacervates exists. There is the indication from membraneless organelles, considered to be biological coacervates, that ripening is in fact suppressed. Cellular condensates can coexist, such as centrosomes that occur in pairs, while Ostwald ripening dictates that ultimately only one droplet can persist.[12] The hypothesis for the coexistence and stability of multiple droplet condensates is that an active process creates a situation where a critical radius exists. If the influx of droplet material generated by a chemical reaction is fast enough, small droplets can grow until a critical radius — *i.e.* a new stable stationary state exists with multiple droplets (or two droplets as concluded in the study in Figure 5.1B). Experimentally, this prediction was only tested for oil (anhydride) droplets coupled with a reaction cycle, and in this case the opposite was observed: anhydride hydrolysis accelerates ripening, by creating local undersaturations that establish a similar gradient as typical ripening, thus adding a second driving force for the shrinkage of small droplets (Figure 5.1A).[9] In general, studies of Ostwald ripening are performed with bulk measurements of average droplet size in water/oil emulsions, but observing individual droplets would be crucial to propose a more detailed mechanism of the process.

While developing an experimental setup to observe the growth of active coacervate droplets, we established that passivation of microscope glass slides with PEG was sufficient to prevent wetting and enabled monitoring of droplets for extended times. Once we started to monitor complex coacervate droplets over time, it became clear that they were remarkably stable. We used ATP-based coacervates just as in Chapter 2, but we replaced poly-L-lysine by K_{72} protein as a the positively charged component. This protein contains 72 repeats of the pentapeptide VPGKG (an elastin-like sequence)[13,14] and has already been used to form droplets with RNA.[15] K_{72} can form condensates at low concentrations with ATP and the GFP label means we can easily monitored droplets by fluorescence microscopy.

Over the course of an hour, ATP-K_{72} droplets on passivated glass retain the spherical shape and their liquid state can be confirmed by a few fusion events; they retain their position on the glass slide; and most remarkably, we do not observe a gradual increase in average radius, a typical sign of Ostwald ripening (Figure 5.3A and B). Importantly, these are passive droplets, that is, formed by mixing two poly-electrolytes with no chemical reaction involved. Findings by another PhD in our group, Tiemei Lu (Figure 5.3C) — who observed no measurable size changes in complex coacervates of PDDA-PSPMA for more than 18 hours — gave further indication
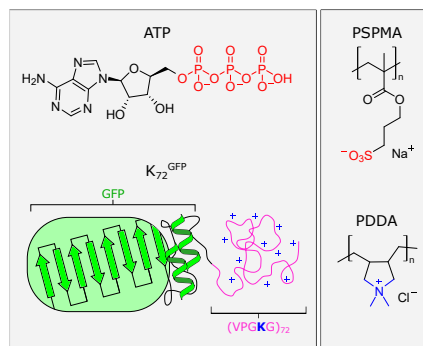
Figure 5.2: Building blocks of the complex coacervates in this chapter.

this could be an intrinsic property of coacervate droplets, or more specifically, complex coacervates. A similar observation was made by Dine *et al* for droplets of an intrinsically disordered protein, *in vivo* and *in silico*: multiple large droplets persist over long periods of time, and in simulations after some initial coarsening, five droplets remain stable for 1000 time units. The authors suggest that either the final fusion events are extremely slow, or Ostwald ripening is opposed by an active process such as regulated disassembly of large droplets, but the reason remains elusive. [16]

5.2 Prediction of Ostwald ripening in ATP droplets

In this chapter, we propose two mechanisms of Ostwald ripening in complex coacervates that takes into account their unique structure, and evaluate if they can explain the slowing down or suppression of ripening experimentally. We consider the balance of thermodynamic forces underlying Ostwald ripening. We focused this study on ATP-K_{72} coacervates, which we looked into detail for Chapter 6 of this thesis.

$$\frac{\mathrm{d} < r^3 >}{\mathrm{d}t} = k_{\mathrm{OR}} = \frac{8\gamma DC_{\mathrm{sat}}V_m^2}{9R_gT}$$
$$k_{\mathrm{OR}} = 28.0\,\mathrm{\mu m^3\,h^{-1}}(\mathrm{K_{72}})$$
$$\mathrm{or}\,k_{\mathrm{OR}} = 1.8\,\mathrm{\mu m^3\,h^{-1}}(\mathrm{ATP})$$
$$\Delta R\,(60\,\mathrm{min}) = 3.0 - 7.4\,\mathrm{\mu m}$$

(5.1)

We estimated the rate of change in average droplet volume by Ostwald ripening with Equation 5.1. [17] Complex coacervates are a mesh of near neutral complexes of ATP and K_{72}: [17 ATP:1 $K_{72}]^0$, and therefore we base our calculations on the least soluble droplet component, with the higher molecular volume to predict a lower limit for the expected ripening rate. K_{72} has a saturation concentration of about 5 μM and a molecular volume of ca. 65 nm^3, [18] yielding an increase in mean radius of 3-7 μm per hour due to ripening. [17] However, the droplets tracked have a radius of 0.4 to 3 μm, and analysis of their size over time, local growth rates, size-rate correlation and droplet count, which we discuss in detail in Chapter 6, do not agree with a ripening profile.

Those observations are supported by a quantitative video analysis shown in Figure 5.4: we tracked individual droplet radius traces, under two different ATP concentrations (to vary droplet density on the glass slide), and also the droplet count in each experiment. The analysis matches our qualitative observation of the absence of typical Ostwald ripening characteristics.

We then verified whether the lack of ripening was an artifact coming from our experimental setup by performing positive controls with oil droplets of 1-bromo-dodecane and 1-bromo-propane (Figure 5.5). We chose oils with higher density than water and of different solubilities expecting to obtain different ripening rates, both stabilized by sodium
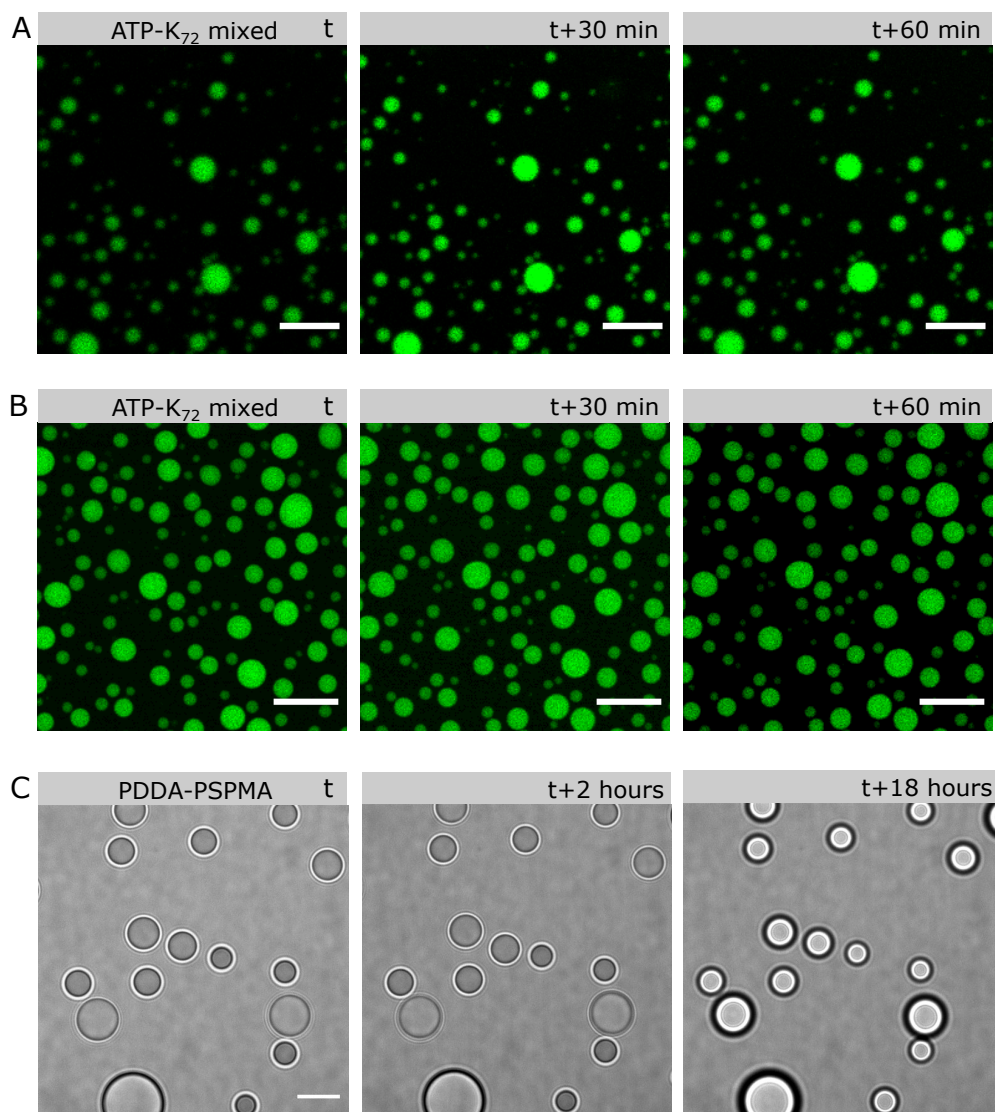
Figure 5.3: Complex coacervates under the microscope for extended periods. We observed this surprising feature in experiments with confocal fluorescence microscopy for Chapter 6, with (A) 1 mM ATP and 20 µM K_{72} and (B) 3 mM ATP and 20 µM K_{72}. (C) A different type of complex coacervates, studied by my colleague Tiemei Lu with bright field microscopy, also forms stable droplets for up to 18 hours. Scale bar: 20 µm for A and B; 10 µm for C.

dodecylsulfate (SDS) as a surfactant. For bromo-dodecane, the increase in average radius is subtle, but present; for bromo-propane, the shrinkage of droplets in the field of view is clear, and the decreasing droplet count is further evidence of Ostwald ripening. Those
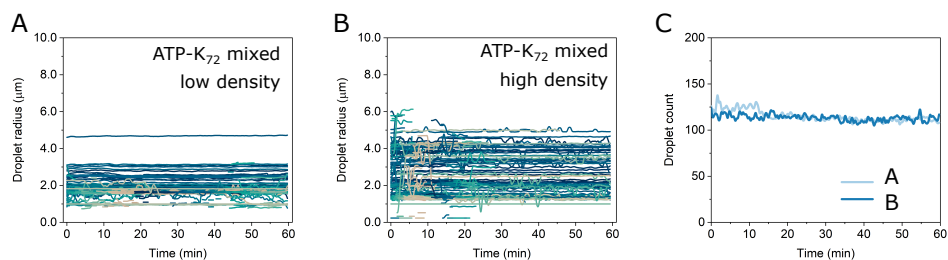
Figure 5.4: Radii traces and droplet count analysis of passive ATP-K$_{72}$ coacervates. (A) at 1 mM ATP, we observe a lower droplet density and stable sizes; (B) even at a higher density, at 3 mM ATP, radius is surprisingly stable. (C) Droplet count is stable in both cases, unlike in typical Ostwald ripening systems where a decay is observed together with average size changes.

behaviors are quite different than the ones depicted in Figure 5.3.
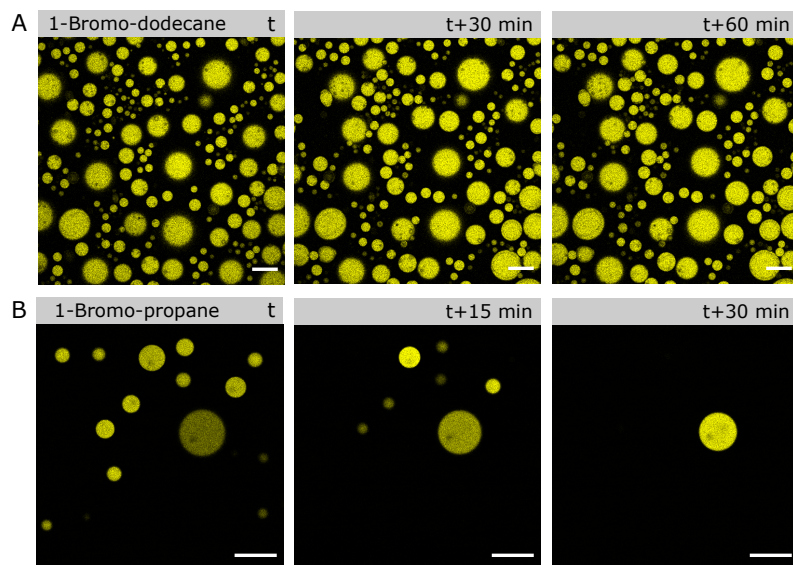
Figure 5.5: Oil droplets with surfactant SDS and stained with Nile red, in our usual experimental setup. (A) 1-Bromo-dodecane (2% v/v) droplets ripen slowly, and the growth of large droplets at the cost of shrinkage or disappearance of smaller droplets can only be seen upon quantification of the sizes of all droplets over time using our analysis protocol. (B) Droplets of a more soluble oil, 1-Bromo-propane (2% v/v) undergo fast Ostwald ripening, as captured by the gradual disappearance of droplets in the field of view; the increase of large droplets or a macrophase cannot be captured simultaneously. Scale bars are 100 μm in A and 200 μm in B.

An alternative measurement of the distinction between ripening and non-ripening droplets is shown in Figure 5.6. We define local rates as the first derivative of the radius

traces over time (as seen in Figure 5.4A and B), which we calculate with a MatLab script by segmenting the radius trace in small intervals (thus the 'local'). This property will be relevant for Chapter 6, where we distinguish growing from non-growing droplets.

Active coacervates composed of ADP, K_{72} and pyruvate kinase (Chapter 6), when fueled with phosphoenolpyruvate show a distribution of rates with a positive median, that is, on average, active droplets grow. Over time, the distribution spreads and the median approaches zero, because the droplets become passive after fuel depletion. Passive coacervates formed by mixing ATP and K_{72} show a similar distribution with a nearly null median, at higher or lower droplet density. In turn, by the same method of analysis, a significant fraction of oil droplets exhibits negative growth rates, which is a consequence of the shrinkage of droplets due to Ostwald ripening. This is less evident for the less-soluble bromo-dodecane, but clear for bromo-propane.
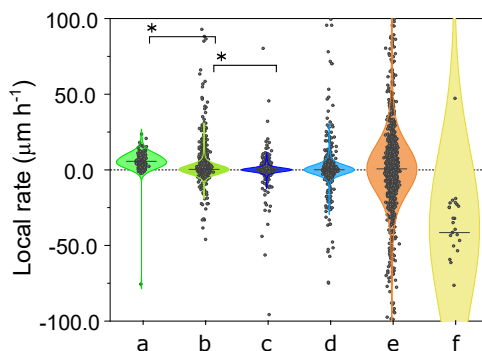
Figure 5.6: Growth rates of active coacervates, passive coacervates and passive oils compared. (a) Active coacervates composed of ADP, K_{72} and pyruvate kinase, fueled with phosphoenolpyruvate; (b) the same sample after fuel is depleted. (c, d) Passive coacervates formed by mixing ATP and K_{72}, at higher (c) or lower (d) droplet density. (e, f) Oil droplets stabilized with SDS and labeled with Nile red dye: bromo-dodecane (e) and bromo-propane (f).

Based on these findings, we propose that complex coacervates are special liquids that exhibit suppressed Ostwald ripening, and we propose that this is a result of their associative phase separation nature.

5.3   Ostwald ripening in complex coacervates

Typical ripening is driven by the increased Laplace pressure inside small droplets, but does not take into account the energy associated with either the disruption of attractive interactions when charged molecules are removed from the droplet, or the entropy and interfacial energy involved in removing an electroneutral complex of one or more K_{72} molecules bound to ATP from the droplet (Figure 5.7A). While it is hard to determine

which of these mechanisms is at play when we observe no ripening, we show that in both cases, the associated energy or energy barrier can be large enough to prevent ripening.
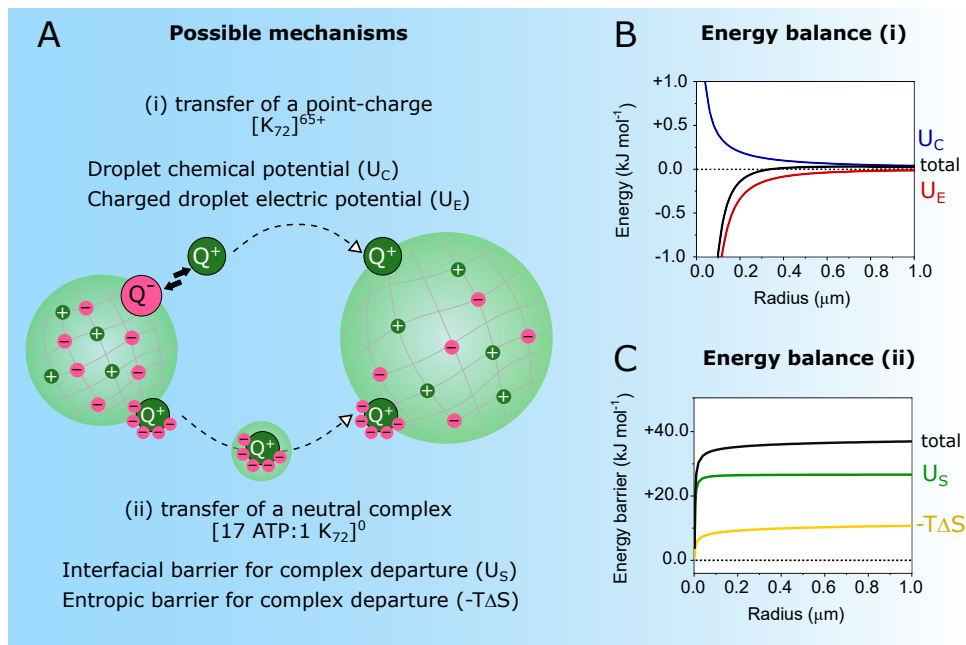
Figure 5.7: Rationalization of suppressed Ostwald ripening in complex coacervates. (A) Two mechanisms are possible: in (i), free poly-electrolytes, in this case K_{72}, are transferred, leaving an oppositely charged droplet. In (ii), coarsening happens through the transfer of electroneutral complexes from small to larger droplets. This complex has an interfacial area, represented by the green droplet encasing it. (B) Mechanism (i) is moderately endergonic, therefore being a poor driving force. (C) Mechanism (ii) is kinetically hampered.

5.3.1   Charged mechanism

We consider the transfer of poly-ions between droplets as a possible mechanism for Ostwald ripening. Despite complex coacervates organizing as assemblies of neutral complexes, the isolated poly-ions are extremely soluble in the dilute phase. Moreover, the electric interactions are a common feature of the complex coacervates for which we observed suppressed ripening, suggesting that it might play a important role.

For complex coacervates such as ATP-K_{72}, which contain small molecules and proteins with relatively low charge densities, and which include additional salt, the droplet components are likely unpaired in the dilute phase.[19] We therefore consider the removal and transfer of the least soluble component, K_{72}, as a separate species as a key step in coarsening. The separation of a positively charged K_{72} ($Q = +65e$) from a coacervate

droplet of radius r will leave a residual negative surface charge density of $\frac{-Q}{4\pi r^2}$, which comes with an electrostatic penalty that is larger for smaller droplets (U_E in Figure 5.7 A and B). Weighing that penalty against the Laplace pressure difference that drives Ostwald ripening (yielding the chemical potential component U_C), we find that the exchange of material between complex coacervate droplets may not necessarily occur in the direction from small to large droplets.

$$U_C = \frac{2\gamma V_m}{r}$$
$$U_E = -\frac{z^2 e^2}{4\pi\epsilon\kappa r^2}$$

(5.2)

With typical estimates of the surface tension, molecular volume and Debye length in our ATP-K$_{72}$ coacervate droplets (see Table 5.1), the transfer of charged material from one droplet to another is slightly endergonic regardless of the relative radii (total energy in Figure 5.7B). Moreover, with many protein condensates carrying a small net surface charge,[20] the transfer becomes even more restricted, either because of electrostatic attraction at the source droplet, or repulsion at the target droplet.

5.3.2 Electroneutral mechanism

In the alternative pathway, the electroneutral complex that makes the mesh of the droplets behaves like fatty acid or hydrocarbon molecules in Ostwald ripening: diffusing out of small droplets along a concentration gradient towards larger droplets. However, unlike fatty acids, these complexes, being an assembly of multiple macromolecules, are large and bring two additional energy barriers for departure: the creation of a new interface (the complex seen as a mini-droplet) and the restriction in polymer chain translation freedom (U_S and $-T\Delta S$ in Figure 5.7A and C).

The removal of an electroneutral complex of a positively charged K$_{72}$ with roughly 17 ATP molecules from the droplet is associated with an entropy loss proportional to the volume ratio between droplet and complex:

$$\begin{aligned}
-T\Delta S &= -TS_{\text{complex}} + TS_{\text{droplet}} \\
&= -\frac{1}{2}\,k_B T \ln\frac{V_{\text{complex}}}{\ell^3} + \frac{1}{2}\,k_B T \ln\frac{V_{\text{droplet}}}{\ell^3} \\
&= \frac{1}{2}\,k_B T \ln\frac{V_{\text{droplet}}}{V_{\text{complex}}} \\
&= k_B T \ln\left(\frac{4\pi r_1^3}{V_{m,K72} + 17V_{m,ATP}}\right)^{\frac{1}{2}}
\end{aligned}$$

(5.3)

This expression makes the assumption that K_{72} and ATP were able to move freely throughout the liquid coacervate droplet before they were removed, which is supported by complete FRAP recovery.
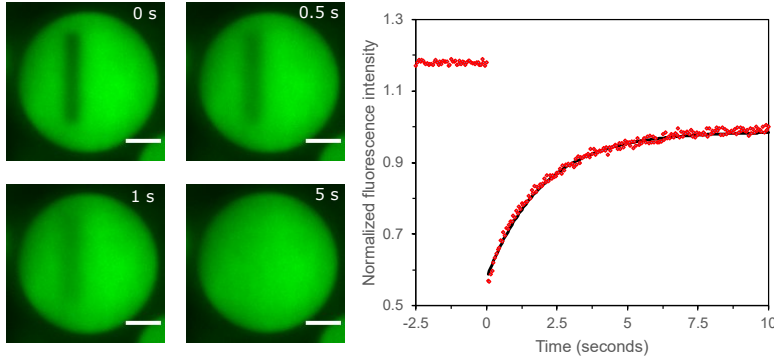
Figure 5.8: Fluorescence recovery after photobleaching (FRAP) of ATP-K_{72} droplets (typical passive coacervate composition, 3 mM ATP and 20 μM K_{72}). Scale bar: 5 μm.

In addition, the electroneutral complex can be regarded as a small droplet with an interfacial area A_{complex} and an interfacial energy U_S. We assume that the decrease in surface area of the droplet from which the electroneutral complex is removed is negligible, which is reasonable for droplets larger than several tens of nm.

$$
\begin{aligned}
U_S &= \gamma A_{\mathrm{complex}} = \gamma V_{\mathrm{complex}}^{2/3} \\
&= \gamma (36\pi)^{1/3} (V_{\mathrm{m,K72}} + 17 V_{\mathrm{m,ATP}})^{2/3}
\end{aligned}
\tag{5.4}
$$

With typical values of the surface tension (see Table 5.1), and molecular volumes, we find that both of these contributions impose a prohibitively large energy barrier on the Laplace pressure-driven ripening, ca. 20 times higher than the thermal energy. The total energy barrier is the sum of these two contributions ($U_S - T\Delta S$), which is $> 10 k_B T$ for all droplets larger than 10 nm using the parameter estimates in Table 5.1. Both terms are of the same order of magnitude for these parameter values, and will thus hamper Ostwald ripening.

5.3.3 Exchange of material between droplets

In either the charged or electroneutral mechanism, we cannot explain why large droplets would be favored over small droplets. If we explicitly calculate the energy associated with the transfer of poly-ions from droplet (1) to droplet (2) (ΔU), we find that the direction of small radius to large radius ($r_2 > r_1$) is not favoured for droplets beyond a critical

Table 5.1: Estimated typical properties of the coacervate droplets used.

Parameter	Description	Value	Source
θ	Volume fraction of coacervate phase	1–5%	centrifugation of coacervates, confocal slice extrapolation
η	Viscosity of the medium	10^{-3} Pa s	water
γ	Coacervate surface tension	5.0×10^{-4} N m^{-1}	ref. 21
D	Diffusivity in dilute phase	$\dfrac{k_B T}{6\pi\eta\ell}$	Stokes-Einstein (using molecular length scale ℓ as effective radius)
C_{sat}	Saturation concentration	5 μM (K$_{72}$) 1 mM (ATP)	minimal concentrations tested that led to coacervation
ℓ	Molecular length scale	2.5 nm (K$_{72}$) 0.77 nm (ATP)	ref. 18 ref. 22
V_m	Molecular volume	6.5×10^{-26} m^3 (K$_{72}$) 5.3×10^{-28} m^3 (ATP)	$\dfrac{4\pi\ell^3}{3}$
z	Net charge of K$_{72}$ with GFP tag	+65	at pH 7.4
κ	Inverse Debye length	7.1×10^8 m^{-1}	$\kappa \cong \sqrt{10I}$, for I = 50 mM salt
α_E	Electrostatic penalty constant	1.7×10^{-35} m^2	$\alpha_E = \dfrac{z^2 e^2}{4\pi\epsilon\kappa}$
α_{OR}	Ostwald ripening constant	6.5×10^{-29} m	$\alpha_{OR} = 2\gamma V_m$

radius of $r_1 = 0.34\,\mu$m, contrary to the situation in oils, where Ostwald ripening always favours large droplets over small ones.

The removal and transport of a point charge K$_{72}$ (charge Q = +65e) from just outside droplet 1 (radius r_1, surface charge $\frac{-Q}{4\pi r_1^2}$) to just outside droplet 2 (radius r_2, without net surface charge) has the following energy difference:

$$\Delta U = (U_{\mathrm{E},2} + U_{\mathrm{C},2}) - (U_{\mathrm{E},1} + U_{\mathrm{C},1})$$

$$= 0 + \frac{2\gamma V_m}{r_2} + \frac{z^2 e^2}{4\pi\epsilon\kappa r_1^2} - \frac{2\gamma V_m}{r_1}$$

$$\Delta U = \frac{z^2 e^2}{4\pi\epsilon\kappa r_1^2} + 2\gamma V_m \left(\frac{1}{r_2} - \frac{1}{r_1} \right) \qquad (5.5)$$

$$= \alpha_E \frac{1}{r_1^2} + \alpha_{OR} \left(\frac{1}{r_2} - \frac{1}{r_1} \right)$$

The free energy of the transfer is therefore positive for:

$$r_2 > \frac{r_1^2}{r_1 - \frac{\alpha_E}{\alpha_{OR}}}$$

.

For typical values of α_E and α_{OR} for our system (estimated using the parameters in Table 5.1), we find a negative value for the critical r_2, *i.e.* the transfer is always endergonic regardless of the relative radii. The magnitude of ΔU is smaller the larger droplet 1 is, but it is never negative. The radius-dependency that usually drives Ostwald ripening is removed because to energy U_C (droplet potential due to increased Laplace pressure across the interface) it must be added an energy U_E (the potential created by charge separation), with opposite sign and stronger radius dependency. If the ratio α_E/α_{OR} is orders of magnitude smaller than droplet size in the system ($\alpha_E <<< \alpha_{OR}$), which may be the case for complex coacervates based on low-charged components, a positive critical radius could occur and ripening by this mechanism can be expected.
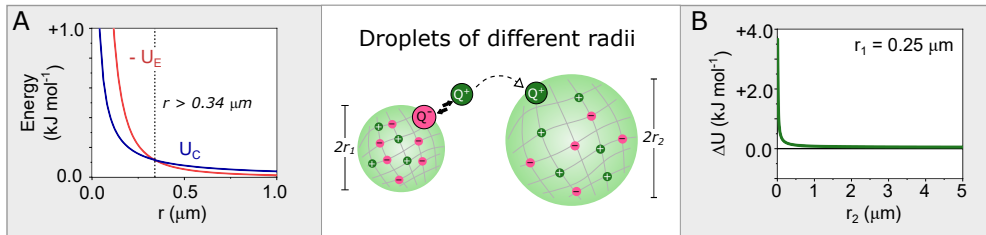
Figure 5.9: Larger droplets are not favored in complex coacervates. (A) Beyond a droplet radius of 0.34 μm, the electric component, U_E, overcomes the Laplace pressure-driven component, U_C. The consequence of this proximity is (B) the transfer of a charged molecule from a droplet of radius r_1 to a droplet of radius r_2 is not exergonic, and essentially the same for any given r_2.

The electroneutral mechanism is kinetically hampered for all droplets with a radius larger than 5–10 nm, which is close to the size of a single electroneutral complex of a single K_{72} and 17 ATP molecules and therefore the transfer from small to large droplets cannot be predicted at all. The dependency of the critical radius on the molecular volume of the electroneutral complex suggests that the formation of the complex is the barrier for

droplet nucleation: assemblies smaller than the complex are taken up by other droplets, while assemblies that satisfy the stoichiometry of the complex are stable and can nucleate and grow. For smaller molecular volumes (of individual components and the electroneutral complex form) or neutral complexes with fewer components — closer to the case of oil droplets —, the energy barrier decreases, but it remains a few times above thermal energy.

5.4   Conclusion

Unlike commonly studied emulsions, complex coacervate droplets are held together by electrostatic attraction. We show that the magnitude of the electric attraction between a droplet and a departing soluble component like K_{72} may compensate the driving force of Laplace pressure from small to larger droplets. Both a ripening mechanism based on transport of charged components and a mechanism based on transport of electroneutral complexes are hampered, one because the process is endergonic, the other because of a prohibitively large energy barrier. Overnight observations of passive complex coacervate droplets, in which we observe no change in size of any of the droplets, are in agreement with this analysis.

Ostwald ripening can be effectively suppressed by the nature of the interactions underlying droplet formation, and we expect other complex coacervates emulsions to also be stable for extensive times, provided that the charge of the building blocks is large enough. From a protocell perspective this means that if we introduce an active process in these slow- or non-ripening and slow-fusing droplets, the resulting active droplets could mimic cellular growth without interference from passive coarsening processes, and the growth can be controlled by the same parameters that control a chemical reaction. More than a technical advantage that allows us to measure growth rates without the competition of ripening, this is a requirement for a growing protocell: a surviving one.

5.5   Experimental details

5.5.1   Passive coacervates and Ostwald ripening controls

Passive ATP-K_{72} coacervates were used as negative controls for growth, and contained (in order of addition): 50 mM HEPES pH 7.4, 1–3 mM ATP, 20 μM K_{72} and 0.5 mM MgCl$_2$ The mixtures were prepared directly in the passivated microscopy chamber, and covered with a glass slide before recording 1-hour long videos. Oil droplets were used as positive controls for Ostwald ripening, and prepared at 2% v/v fractions, in the presence of 2% v/v SDS and Nile Red as fluorescent dye. We chose 1-bromo-dodecane and 1-bromo-propane based on their densities and solubilities.

Table 5.2: Short name/experimental conditions used in the passive droplets controls.

Series	Short name	Composition	Local rate median (μm h^{-1})
ATP-K$_{72}$	Video 23	20.0 μm K$_{72}$ and 3.0 mM ATP	0.0096
ATP-K$_{72}$	Video 24	20.0 μm K$_{72}$ and 1.0 mM ATP	0.0004
Oils	Video 25	1-bromo-dodecane (2% v/v) and SDS (2% v/v)	0.63
Oils	Video 26	1-bromo-propane (2% v/v) and SDS (2% v/v)	-42.17
Complex coacervates	Video 29	0.30 M PDDA and PSPMA	not measured

5.5.2 Fluorescence recovery after photo-bleaching

The fluorescence recovery after photobleaching profile was recorded at room temperature on a CSU X-1 Yokogawa spinning disk confocal unit connected to an Olympus IX81 inverted microscope, using a 100x piezo-driven oil immersion objective (NA 1.3) and a 488 nm laser beam. For bleaching, laser power of 100% for 3 cycles and exposure time of 1 s was used. Emission was measured at 500–550 nm at 30 fps, using an Andor iXon3 EM-CCD camera.

Acknowledgements

References

[1] E. Szathmáry and J. M. Smith, "From replicators to reproducers: The first major transitions leading to life," *Journal of Theoretical Biology*, vol. 187, no. 4, pp. 555–571, 1997.

[2] F. Bouchard, "Darwinism without populations: a more inclusive understanding of the "survival of the fittest"," *Studies in History and Philosophy of Science Part C: Studies in History and Philosophy of Biological and Biomedical Sciences*, vol. 42, no. 1, pp. 106–114, 2011.

[3] A. F. Mason, B. C. Buddingh, D. S. Williams, and J. C. Van Hest, "Hierarchical Self-Assembly of

a Copolymer-Stabilized Coacervate Protocell," *Journal of the American Chemical Society*, vol. 139, no. 48, pp. 17309–17312, 2017.

[4] N. N. Deng, "Complex coacervates as artificial membraneless organelles and protocells," *Biomicrofluidics*, vol. 14, no. 5, 2020.

[5] J. Li, X. Liu, L. K. Abdelmohsen, D. S. Williams, and X. Huang, "Spatial organization in proteinaceous membrane-stabilized coacervate protocells," *Small*, vol. 15, no. 36, p. 1902893, 2019.

[6] K. D. Seo, S. Shin, H. Y. Yoo, J. Cao, S. Lee, J.-W. Yoo, D. S. Kim, and D. S. Hwang, "Stabilizing coacervate by microfluidic engulfment induced by controlled interfacial energy," *Biomacromolecules*, vol. 21, no. 2, pp. 930–938, 2019.

[7] Y. Zhang, Y. Chen, X. Yang, X. He, M. Li, S. Liu, K. Wang, J. Liu, and S. Mann, "Giant coacervate vesicles as an integrated approach to cytomimetic modeling," *Journal of the American Chemical Society*, vol. 143, no. 7, pp. 2866–2874, 2021.

[8] F. P. Cakmak, A. M. Marianelli, and C. D. Keating, "Phospholipid membrane formation templated by coacervate droplets," *bioRxiv*, 2021.

[9] M. Tena-Solsona, J. Janssen, C. Wanzke, F. Schnitter, H. Park, B. Rieß, J. M. Gibbs, C. A. Weber, and J. Boekhoven, "Accelerated Ripening in Chemically Fueled Emulsions," *ChemSystemsChem*, vol. 2, no. e2000034, pp. 1–11, 2020.

[10] D. Zwicker, A. A. Hyman, and F. Julicher, "Suppression of Ostwald ripening in active emulsions," *Physical Review E - Statistical, Nonlinear, and Soft Matter Physics*, vol. 92, no. 1, pp. 1–13, 2015.

[11] C. A. Weber, D. Zwicker, F. Jülicher, and C. F. Lee, "Physics of active emulsions," *Reports on Progress in Physics*, vol. 82, no. 6, p. 064601, 2019.

[12] D. Zwicker, M. Decker, S. Jaensch, A. A. Hyman, and F. Jülicher, "Centrosomes are autocatalytic droplets of pericentriolar material organized by centrioles," *Proceedings of the National Academy of Sciences*, vol. 111, no. 26, pp. E2636–E2645, 2014.

[13] D. Pesce, Y. Wu, A. Kolbe, T. Weil, and A. Herrmann, "Enhancing cellular uptake of GFP via unfolded supercharged protein tags," *Biomaterials*, vol. 34, no. 17, pp. 4360–4367, 2013.

[14] H. Yang, C. Ma, K. Li, K. Liu, M. Loznik, R. Teeuwen, J. C. M. V. Hest, X. Zhou, A. Herrmann, and J. Wang, "Tuning Ice Nucleation with Supercharged Polypeptides," *Advanced Materials*, vol. 28, pp. 5008–5012, 2016.

[15] E. Te Brinke, J. Groen, A. Herrmann, H. A. Heus, G. Rivas, E. Spruijt, and W. T. S. Huck, "Dissipative adaptation in driven self-assembly leading to self-dividing fibrils," *Nature Nanotechnology*, vol. 13, no. September, pp. 849–856, 2018.

[16] E. Dine, A. A. Gil, G. Uribe, C. P. Brangwynne, and J. E. Toettcher, "Protein Phase Separation Provides Long-Term Memory of Transient Spatial Stimuli," *Cell Systems*, vol. 6, no. June 27, pp. 655–663, 2018.

[17] J. Berry, S. C. Weber, N. Vaidya, M. Haataja, and C. P. Brangwynne, "RNA transcription modulates phase transition-driven nuclear body assembly.," *Proceedings of the National Academy of Sciences of the United States of America*, vol. 112, no. 38, pp. E5237–45, 2015.

[18] H. P. Erickson, "Size and shape of protein molecules at the nanometer level determined by sedimentation, gel filtration, and electron microscopy," *Biological Procedures Online*, vol. 11, no. 1, 2009.

[19] K. T. Delaney and G. H. Fredrickson, "Theory of polyelectrolyte complexation—complex coacervates are self-coacervates," *The Journal of chemical physics*, vol. 146, no. 22, p. 224902, 2017.

[20] T. J. Welsh, G. Krainer, J. R. Espinosa, J. A. Joseph, A. Sridhar, M. Jahnel, W. E. Arter, K. L. Saar, S. Alberti, R. Collepardo-Guevara, *et al.*, "Single particle zeta-potential measurements reveal the role of electrostatics in protein condensate stability," *bioRxiv*, 2020.

[21] E. Spruijt, A. H. Westphal, J. W. Borst, M. A. Cohen Stuart, and J. Van Der Gucht, "Binodal compositions of polyelectrolyte complexes," *Macromolecules*, vol. 43, no. 15, pp. 6476–6484, 2010.

[22] T. K. Rostovtseva and S. M. Bezrukov, "Atp transport through a single mitochondrial channel, vdac, studied by current fluctuation analysis," *Biophysical journal*, vol. 74, no. 5, pp. 2365–2373, 1998.

Chapter 6

Growth of coacervate based protocells
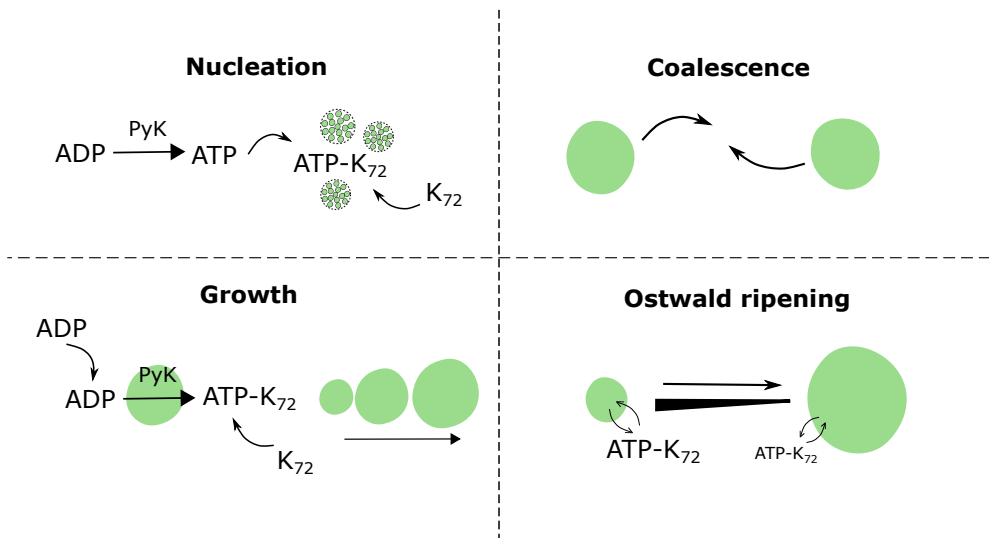
This chapter has been adapted from:

KK Nakashima, MHI van Haren, AAM André, I Robu & E Spruijt. Active coacervate droplets are protocells that grow and resist Ostwald ripening. *Nat Commun* 12, **2021**.

6.1 Growth in protocell models

Growth and division are essential processes in life, without which we cannot explain survival and reproduction. Modern cells rely on tightly coordinated mechanisms involving complex machinery, but the sustenance of life-like systems, from their origins to the emergence of a common ancestor, implies that primitive cells lacking similar specialized enzymes could already survive and perhaps even proliferate. This suggests that the behaviour can be reproduced (and explained) using solely chemical principles. [1,2] Such principles may shed light on the emergence of the first cells and help broadening the scope of chemical models used to mimic and decipher biological behaviour. [3] One of the simplest systems predicted to exhibit growth and division is a droplet coupled to a constant supply of droplet material or a chemical reaction: by keeping the reaction out of equilibrium (e.g., by continuously supplying droplet material or a fuel for the chemical reaction), the droplet can sustain an active behaviour like growth (*i.e.* an active droplet). [4–9] To ensure that the reaction can directly influence behaviour, the droplet must be an open compartment able to exchange material with its surroundings, and compatible with volume change. Coacervates are a promising system to fulfil these requirements. [10,11]

Coacervate droplets form spontaneously by phase separation in a saturated solution of macromolecules; when the phase separation is driven by attractive electrostatic interactions, they are called complex coacervates. Coacervates lack a membrane and thus have no physical barrier that limits their growth. The droplets are permeable to molecules from the surroundings with some selectivity, and concentrate the solutes through dynamic interactions, opening the way for its building blocks to be synthesized *in situ*. As coacervate droplets are governed by liquid-liquid phase separation (LLPS), they are closely linked to equilibrium concentrations of the building blocks, and when more material is supplied, the volume of the coacervate phase can grow while the overall internal concentration remains approximately constant. This perfectly aligns with the active droplet requirements and is crucial given that most protocell models so far have increased in size via passive mechanisms: vesicle fusion, [12] droplet coalescence and ripening, [13,14] or uptake of externally added building blocks. [15]

Coacervates can achieve growth more easily than vesicles, but are still subject to passive processes. Brownian-motion-induced coalescence and Ostwald ripening can compete with, or mask, reaction-diffusion limited growth, [16] and although these processes also lead to an increase in average droplet volume, growth comes at the expense of a decreased droplet number – completely disconnected from biological growth. Therefore, for coacervates to hold any potential as dynamic biomimetic models, it is crucial to develop a stable, active system. In addition, growing coacervates must be studied quantitatively and at a single-droplet level in order to undoubtedly distinguish active growth (which we refer to hereafter simply as growth) from passive coarsening. We thus set out to develop an active coacervate model, *i.e.* one that grows like cells do in two senses: via an increase
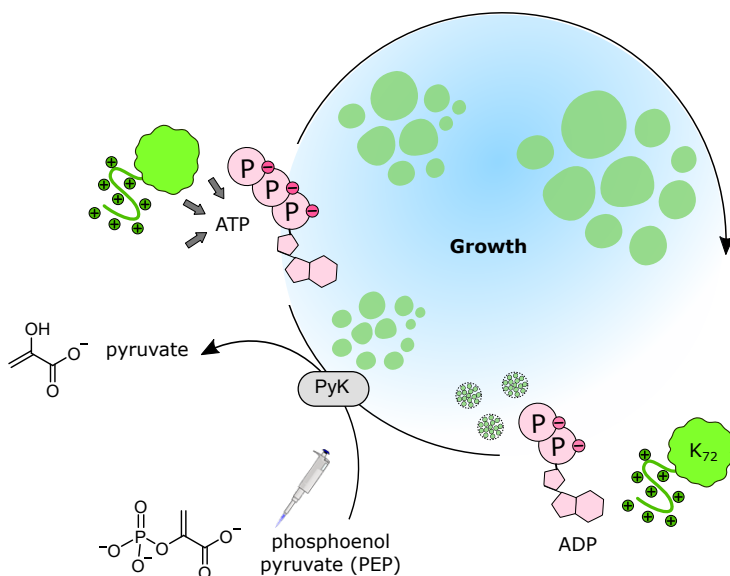
Figure 6.1: Active droplets scheme. The pyruvate kinase-catalyzed (PyK) conversion of ADP to ATP, combined with the liquid-liquid phase separation of ATP-K_{72} complexes, is a minimal translation of an active droplet. In this system, ADP is the substrate, and ATP (together with the lysine-rich protein K_{72}) is the droplet material. We fuel the droplets by a manual addition of the second substrate, PEP. The waste, pyruvate, is not re-used in our setup. The local increase in the amount of ATP inside the droplets causes recruitment of more protein, leading to droplet growth. Growth may compete with other active (nucleation) and passive (coalescence, Ostwald ripening) processes that need to be distinguished experimentally.

in droplet volume while keeping droplet count constant (growth), or via an increase in droplet count (nucleation). [17]

In Chapter 2 we claimed that a chemical reaction can cause dynamic behavior in coacervate droplets that would otherwise be in thermodynamic equilibrium. Now we will show that fine-tuning of the active ATP droplets can indeed lead to a life-like behavior: growth. And, most importantly, that we can accurately quantify this behavior in our membrane-less protocells.

6.2   Characterization of ATP based coacervates

ATP-based coacervates have previously been studied as dynamic membrane-less protocells compatible with growth, enzymatic reactions and RNA partitioning. [18,19] Inspired by the phosphorylation-mediated LLPS of peptide-RNA developed by the group of Keating, [20], in Chapter 2 we achieved reversible ATP-poly-*L*-lysine coacervates with the introduction of pyruvate kinase (PyK) to generate ATP *in situ* from ADP and phosphoenolpyruvate

(PEP). With the high efficiency of the PyK reaction and lack of side reactions that can overcomplicate non-enzymatic systems, we hypothesized we could achieve enough control of coacervation to obtain a coordinated behaviour like growth. In comparison to Chapter 2, we replaced poly-*L*-lysine by K_{72} protein as the positively charged component, which has already been used to form droplets with RNA.[21] K_{72} contains 72 repeats of the pentapeptide VPGKG (an elastin-like sequence)[22,23] and is labelled with green fluorescent protein (GFP). It can form condensates at low concentrations with ATP, which can be easily monitored by fluorescence microscopy. In Chapter 5 we found that these droplets do not undergo significant Ostwald ripening, making them perfect candidates to bring about growth.
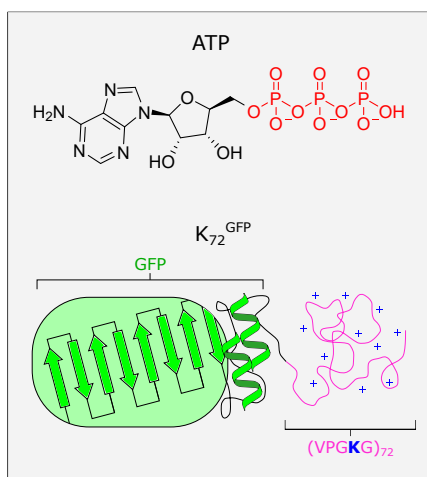
Figure 6.2: Building blocks of the coacervates used in this chapter.

The first step in the design of our system was to determine the conditions under which ATP, but not ADP, forms droplets with the K_{72} protein, just like in Chapter 2. The coacervation window under the binodal is the range of conditions where ATP-K_{72} droplets can nucleate and grow as a result of conversion of ADP into ATP, therefore even more crucial for this chapter. In addition to the phase diagram, we need partitioning coefficients of each component to create a kinetic map of the system and elucidate how these droplets grow. It is worth pointing out the advantages of this model system again: the efficiency of the enzymatic reaction allows us to avoid side reactions (keeping the system simple) and control the reaction rate, for example by changing the catalyst concentration. We can thus ensure that the reaction is fast enough to overcome passive coarsening, and slow enough to avoid spinodal decomposition.[24] Additionally, partitioning of the kinase offers an insight into the location of the reaction. With the fluorescent label in K_{72}, we analyze the growth at a single-droplet level, making it possible to investigate the dynamics of individual membrane-less protocells.

In order to determine the phase diagrams of K_{72} with ADP and ATP, we fixed K_{72} concentration and varied nucleotide concentration to perform salt titrations. By measuring the phase diagram in terms of salt concentration (Figure 6.4B), we estimate the stability of coacervate droplets to a chemical reaction that produces charged by-products – in this case, the pyruvate kinase-catalyzed formation of ATP also generates pyruvate. The typical phase diagram of ADP/ATP-K_{72} complex coacervates shows that at 3 mM of nucleotide and no added salt, the difference between ADP and ATP in affinity for K_{72} is maximal, which is ideal to translate progress of the chemical reaction into a volume change.

We note that, when a reaction is introduced, the dispersion will contain a mixture of ADP and ATP, as well as fuel and other reaction products. The equilibrium composition of both phases in such a multicomponent mixture will deviate from the binodal lines of pure ADP- K_{72} or pure ATP- K_{72}, most likely passing by intermediate binodal lines which we have not characterized but assume are in between the ones in Figure 6.4B. Nevertheless, our aim is to measure how droplets nucleate once a threshold ATP concentration is reached and grow via formation of additional ATP, for which the selected starting concentrations in Figure 6.4B are suitable. From the result in Figure 6.3C, we know that even above the critical salt concentration of ADP-K_{72}, ADP can be incorporated as a client if ATP is present.

The partitioning coefficients of K_{72} and PyK were determined using fluorescence microscopy, while that of ADP and ATP were determined by HPLC and UV detection. K_{72} is always labeled with a GFP tag, so the measured K_p is an accurate representation of the protein. Pyruvate kinase, in turn, is always used unlabeled to preserve its activity. Therefore we specifically labeled it with a fluorescence probe for K_p determination. In all other experiments, the unmodified enzyme was used. We tested labeling exposed lysine or cyteines residues in the enzyme with Alexa 647, a hydrophilic label; to assess whether the labelled enzyme was a good indication of the native enzyme's properties, we also measured the K_p of the free dye. From micrographs like the ones in Figure 6.3A, the K_p of K_{72} was determined to be 28.5 $\pm$ 2.2, based on three different samples, using five droplets near the center of the frame, and discounting the blank intensity at 488 nm excitation.

To determine enzyme K_p, we labelled it with Alexa Fluor-647 maleimide, targeting exposed cysteines. We chose a cysteine-reactive label to avoid modification of charged residues (lysines), which can affect the partitioning, as can be seen in Figure 6.3A. Indeed, while the free dye has $K_p = 19.9 \pm 3.6$, PyK labelled on lysine residues (PyK-(Lys)Alexa-647) has $K_p = 2.9 \pm 0.3$. PyK-(Lys)Alexa-647 partitions relatively poorly as more than one lysine residue is labelled, decreasing the net surface charge of the protein. The abundance of charged patches suggests the protein can partition inside charge-based coacervates, and that lysine residues are relevant to its partitioning behaviour (Figure 6.3B). PyK-(Cys)Alexa-647 is more representative of the unmodified enzyme, with a higher K_p than that of the free dye (26.4 $\pm$ 2.4).

We decided not to label the nucleotides, as any label would significantly affect their partitioning property. Instead, we prepared ATP-K_{72} droplets as hosts and added ADP as a client molecule, at 3 mM, i.e. below the ADP-K_{72} binodal. After separating the dilute from the dense phase we quantified the nucleotides in both phases with HPLC/UV-Vis (Figure 6.3C). The results were used in calculating K_p of ADP (1.1) and ATP (2.8) in ATP-K_{72} droplets, that showed us just like with poly-lysine, ATP has a greater tendency to form coacervates.

Based on the measured partitioning coefficients (Figure 6.4C), and the fast fluores-
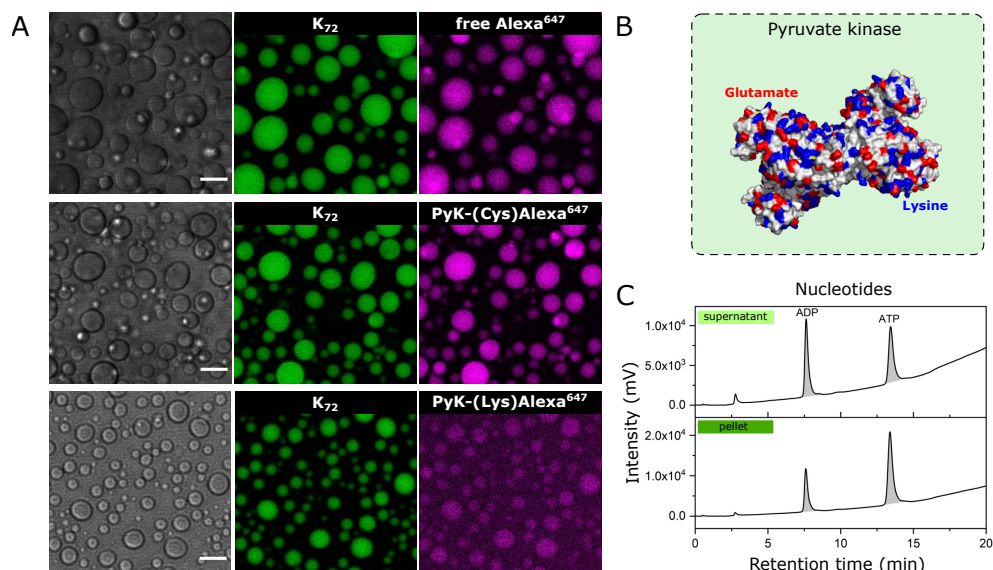
Figure 6.3: (A) Micrographs used to determine partitioning coefficients (K_p). All mixtures contain 20 μM K$_{72}$, 3 mM ATP, 50 mM HEPES pH 7,4 and 0.5 mM MgCl$_2$, plus the labelled component indicated in the figure. Transmission is shown in gray LUT, emission at 488 nm excitation is shown in green and at 640 nm excitation, in magenta. Alexa-647 is the free dye in the flow-through obtained after the labelling reaction of pyruvate kinase and purification (see Methods). Scale bar: 10 μm. (B) Exposed lysine (blue), glutamate (red) and cysteine (yellow) residues in a tetramer of recombinant rabbit muscle pyruvate kinase (PDB-1f3w). (C) Analysis of ATP-K$_{72}$ coacervates to which ADP was added as a client molecule. The sample is composed of 10 μM K$_{72}$, 3 mM ADP, 3 mM ATP, 50 mM HEPES pH 7.4 and 0.5 mM MgCl$_2$. At these buffer and salt conditions, ADP alone does not form droplets with K$_{72}$ as it is above the critical salt concentration found in the phase diagram. In the presence of ATP however, we can detect ADP in both phases. Chromatograms were measured at 254 nm after centrifugation of a coacervate sample. Both phases were diluted 50X from the original and the emulsion.

cence recovery (Methods), we can make the following assumptions: i) ADP can enter the droplets if they become depleted of it; ii) ATP, PyK and K$_{72}$ accumulate inside the droplets and can exchange with the surroundings; and iii) the reaction can occur inside the droplets, where the enzyme is concentrated. These are key requirements to keep the system out of equilibrium with a supply of substrate and attain reaction-driven growth.

6.3   Single droplet growth rate analysis

After mapping out the conditions under which active droplets could exist, we investigated if a fuel-driven reaction could bring about active growth as a step towards evolvable pro-
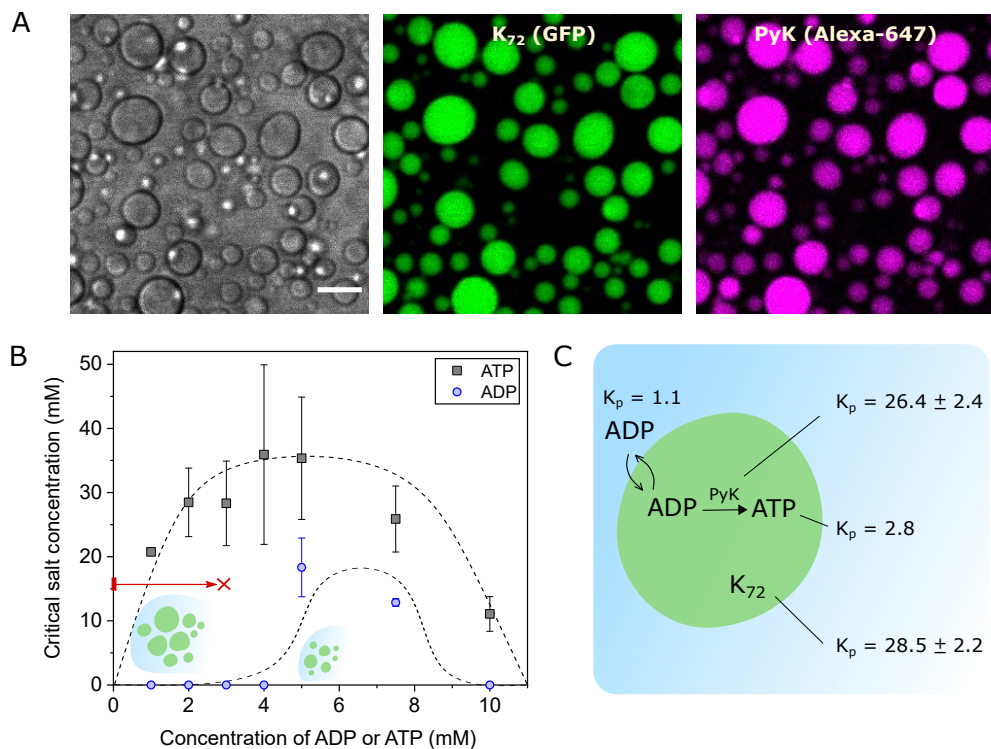
Figure 6.4: Main properties of ATP-K_{72} coacervate droplets. (A) ATP-K_{72} droplets containing Alexa Fluor-647 labelled pyruvate kinase. Channels are shown separately: gray (left) — transmission, green (middle) — GFP (attached to K_{72}), magenta (right) — Alexa Fluor-647. K_{72} always contains the GFP tag; PyK was labelled with Alexa-647 only for this experiment. Scale bar: 10 μm. (B) The phase diagrams of ADP-K_{72} and ATP-K_{72} mixtures confirm that the conversion of ADP to ATP can induce coacervation under certain conditions and lead to growth (e.g. along the red line). The dashed lines representing the approximate phase boundaries are meant as a guide to the eye. (C) The partitioning coefficients of the main components (measured via HPLC or fluorescence) are in accordance with Figure 6.1

tocells. Taking advantage of the fluorescence from the K_{72} proteins condensed inside the coacervates, we can monitor the evolution of individual coacervates nucleating, growing and resting on a plane above the glass surface for at least an hour with confocal laser scanning microscopy. To gain a fitness advantage, actively growing protocells must be able to overcome passive coarsening, occurring through coalescence or Ostwald ripening.

We first compared passive pre-formed ATP-K_{72} droplets at high and low volume fraction, in which we expected coalescence and Ostwald ripening at varying intensity, with active droplets growing by conversion of ADP into ATP. In our setup, by directly tracking droplet size, fusion events are not mistaken for growth, but it remains important to
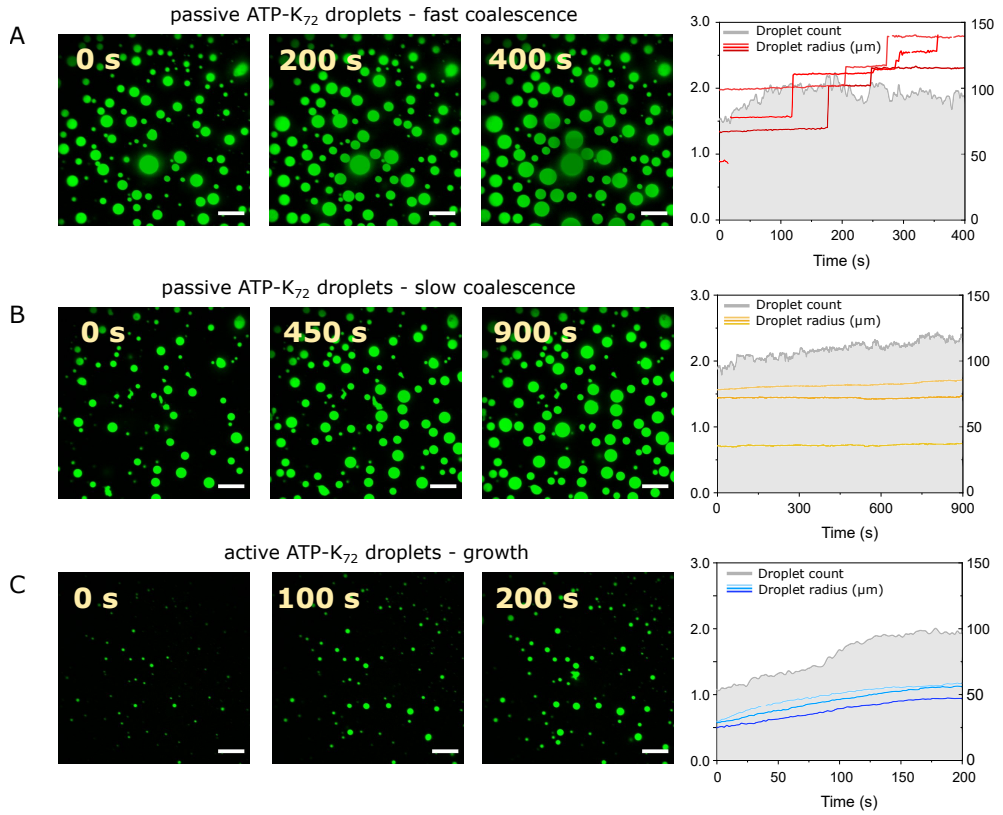
Figure 6.5: Passive and active droplets in radius profiles. (A) Passive coacervate droplets exhibit discrete increases in radius or (B) at lower volume fraction can remain stable for minutes. (C) The gradual increase in droplet radius over time is characteristic of active droplets, for which also the droplet count increases. All: left axes indicate droplet radius (in μm) and right axes indicate droplet count. Scale bars are 10 μm. For visual clarity, only three exemplary traces were chosen out of each experiment.

establish the conditions under which active growth can outcompete passive coarsening. We detect the droplets by their boundaries and extract properties such as area, centroid position, circularity and total fluorescence intensity. We label droplets by their centroid and then build a profile of radius over time, where each droplet has its own curve.

A high-volume-fraction passive system can be achieved at a high poly-electrolyte concentration. At 3 mM ATP, 20 μM K_{72}, we estimated the volume fraction based on centrifugation to be ca. 1%, a value in the same order of magnitude as if calculated from the microscopy images. At this volume fraction, most droplets exhibit steps in the radius profile (Figure 6.5A). At this volume fraction, frequent coalescence events lead to (discrete) increases in droplet volume of tens of fL (μm^3) every hour,[16] although the

droplet count does not decrease due to simultaneous gravitational settling from the top of the solution to the glass plane. The volume fraction, and hence coalescence, can be controlled by adjusting the concentration of the components.

> Rate of change in average droplet volume (proportional to r^3) by Brownian motion-induced coalescence (BMC):[16]
>
> $$\frac{\mathrm{d} <r^3>}{\mathrm{d}t} = k_{\mathrm{BMC}} = \frac{2\theta k_B T}{\pi \eta}$$
>
> $$k_{\mathrm{BMC}} = 93 \, \mu\mathrm{m}^3 \, \mathrm{h}^{-1}$$
>
> $$\Delta R \, (60 \, \mathrm{min}) = 11 \, \mu\mathrm{m}$$
>
> (6.1)

At a lower concentration, and therefore lower droplet density (1 mM ATP, 20 µM K$_{72}$), most passive droplets show a stable size (Figure 6.5B) that can persist for an hour. We observed significantly fewer coalescence events, as expected, and no measurable Ostwald ripening in the form of gradual expansion of large droplets and shrinkage of small droplets. The absence of Ostwald ripening, which we explain in more detail in Chapter 5, is a remarkable behaviour and of great importance for our goal to achieve active growth in very small coacervate droplets.

Based on our findings with passive droplets, we were hopeful to observe distinctly different kinetic traces for active droplets at low volume fractions. For ATP-K$_{72}$ droplets forming by chemical conversion from ADP, the initial volume fraction is even smaller than that in Figure 6.5B. Coalescence will therefore be even less frequent and is not expected to mask the onset of active growth. Indeed, the profiles of active growth (Figure 6.5C) are clearly distinct from the two sets of passive profiles (Figure 6.5A and B). When the ADP-K$_{72}$ mixture is placed under the confocal microscope and fuelled with PEP, droplets of 0.5 µm radius started forming within a minute. Especially at the initial times, the vast majority exhibited a continuous growth curve (Figure 6.6). The plateau coincides with the depletion of fuel, as predicted based on HPLC measurements of nucleotide concentration. Importantly, in contrast to passive droplets coarsening, growth does not compromise persistence and the droplet count in this case can increase (as shown in Figure 6.5C).

6.4 Proposed growth mechanism

Having established that ATP-K$_{72}$ complex coacervate droplets show negligible Ostwald ripening on the timescale of our interest, we return to the active droplets of Figure 6.5C to obtain a better understanding of the active growth. We find that the droplets start growing only after the addition of the pyruvate kinase's second substrate or fuel, phosphoenol pyruvate (PEP), and that they grow significantly over the course of an experiment. A typical growth curve has two regions: initial fast growth, seemingly of a linear increase of
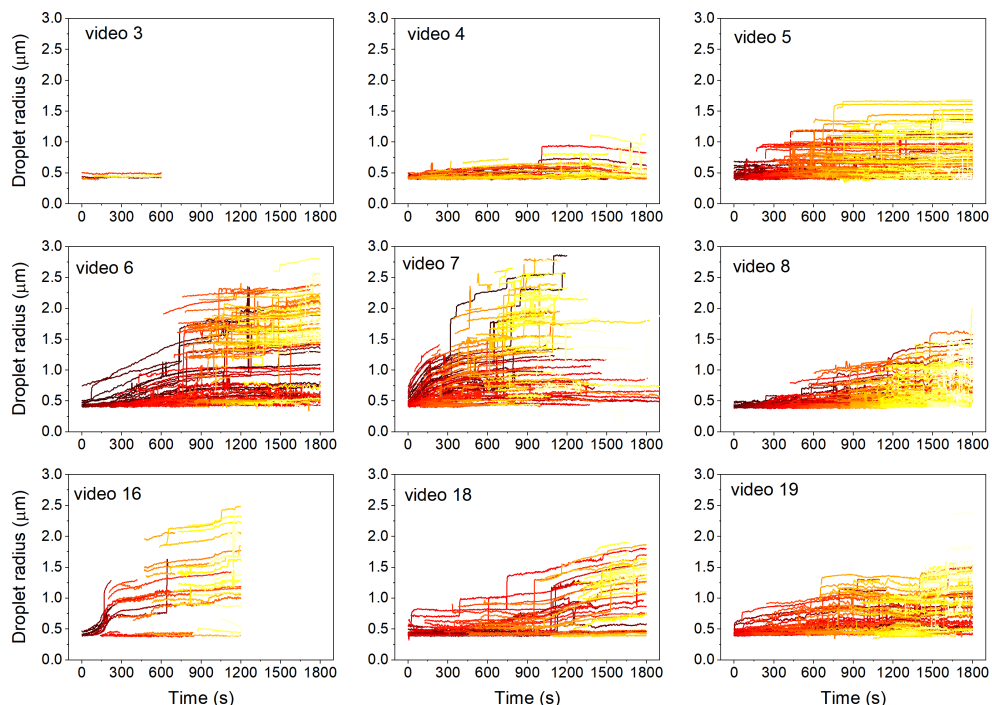
Figure 6.6: Radius traces during active droplet experiments. See Table 6.1 in Methods for the correspondence between short names ('video i') and sample conditions.
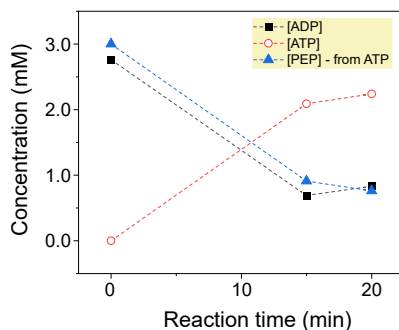
Figure 6.7: Formation of ATP in the presence of protein K_{72} (i.e. during coacervate formation). The total nucleotide concentration was measured with HPLC. Three different mixtures were prepared, and quenched with acetic acid at each time point. The emulsions contained: 20 µM K_{72}, 3 mM ADP, 3 mM PEP, 0.5 mM $MgCl_2$ and 0.42 µM PyK (same conditions as Video 6).

radius with time; after around 5 minutes growth slows down, and after 10 minutes most droplets have reached a plateau of stable size, as can be seen in Figure 6.6 and more closely, in Figure 6.8A) for a selected experiment. As predicted from the conclusions in

the previous section, if fuel is re-supplied, the droplets can regain growth (Figure 6.8B). At the third consecutive addition of fuel we did not observe significant growth, presumably because the system approaches, at least locally, the concentrated branch of the phase diagram, due to the accumulation of reaction products.
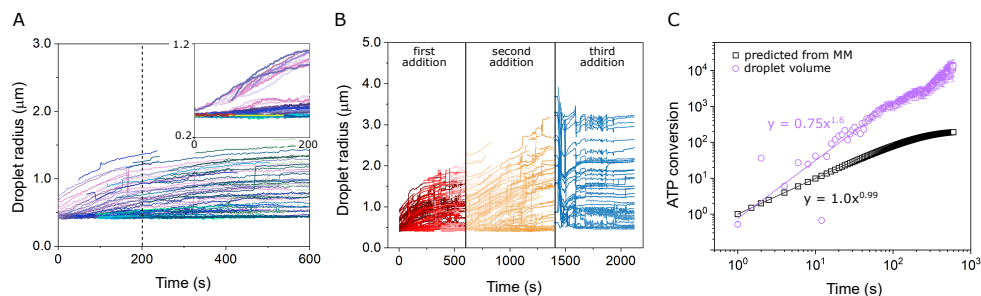
Figure 6.8: Growth of active droplets. (A) Radius traces of all droplets in a selected active droplet experiment (original: video 6). In the inset, the curves were shifted horizontally for better visualization of common behavior. (B) Stepwise addition of fuel (PEP) to active droplets. In each step, 1 mM of PEP was added, after the growth curve plateau was reached. Original videos: 9, 10 and 11 respectively. (C) Profile of the ATP conversion based on average droplet volume evolution (calculated from dataset in A), compared to the profile estimated based on Michaelis-Menten kinetics in solution, using k_2 of 0.3 min^{-1} and ADP starting concentration of 3 mM. The solid lines are power-law fits to the initial 50 seconds of growth (R^2 0.9, outliers not included). The calculated conversions have been normalized such that the initial slopes cross at (1,1). Note that the ATP conversion in growing droplets and solution cannot be compared directly, since the exact droplet volume fraction is not known. See Table 6.1 in Methods for the correspondence between short names ('video i') and sample conditions.

At a first glance, each droplet seems to have a unique trace, but that is mainly caused by the polydispersity in droplet size. All curves have the same overall shape and if horizontally shifted, two profiles become evident: non-growing droplets and droplets growing with a common profile (inset in Figure 6.8A), which is an indication that a common chemical mechanism underlies the growth. Droplets of small starting radii (R < 0.5 μm) show a separate group of traces and are always delayed (*i.e.* they start to grow when their size exceeds the 0.5 μm threshold radius). This delay becomes more evident at lower enzyme concentrations, suggesting that these small droplets might lack any enzyme at all and rely solely on the incorporation of ATP produced in the dilute solution. Indeed, if we estimate the inner enzyme concentration based on a total of 0.42 μM, a K_p of ca. 20 and a 1% volume fraction of droplets, the average number of enzymes in a 0.5 μm radius droplet is 2. Once these droplets surpass a threshold size at which they contain a higher enzyme count, they could start to grow more rapidly and their radius increases close to linearly in time.

To explain the observed growth profile, we consider the kinetics involved in droplet

nucleation and growth. Once the first droplets are formed by nucleation (or if we add a small amount of pre-existing ATP-K_{72} droplets), the reaction can happen in two phases: droplet and surroundings. We assume that the rate of ATP production in the droplet is higher than in the surrounding solution, based on the measured ADP and PyK partitioning (Figure 6.4C) and HPLC measurements of PyK kinetics in the presence of coacervates (Chapter 3), which show that the effective k_{cat} of PyK in a coacervate dispersion is the same as in solution.

For droplets that nucleate at a threshold size beyond 0.5 µm, the reaction taking place inside the droplets is dominant. Although we are not able to measure the effective in-droplet k_{cat} of PyK, we reason it is at least the same as for free enzyme, based on the conclusions of Chapters 3 and 4, in which case the high inner ADP and PyK concentrations would be sufficient for a faster reaction in the droplets. This behaviour is still fundamentally different from the classic enzyme kinetics of PyK in solution: in those cases, the amount of ATP produced is initially linear and decreases as substrates are being depleted and ATP reversibly inhibits the enzyme. [25] Inside complex coacervate droplets, inhibition by ATP has a much smaller effect on enzyme activity, possibly because it remains bound to the positively charged K_{72}.

The conversion of ADP into ATP inside the droplets results in a continuous replenishment of ADP and uptake of additional K_{72} and PyK to maintain partitioning equilibrium. If transport of those compounds would be fast compared to the reaction, we expect the amount of new ATP produced to be directly proportional to the actual volume of the coacervate droplet, leading to an exponential increase in droplet volume (and radius) in time, analogous to the kinetics of a pure autocatalytic reaction. [26] However, in our case the droplet size does not increase exponentially in time, suggesting that transport of building blocks from the surroundings into the droplet is limiting the growth.

Of all building blocks, K_{72} and PyK are the largest compounds, present at relatively low concentrations compared to ADP, and the slowest to diffuse. As K_{72} is required as droplet material to compensate the excess charges of ATP produced inside the droplets, we reason that transport of K_{72} limits the growth of droplets. The flux of molecules across the interface is proportional to the surface area $(4\pi R^2)$ and the concentration gradient at the interface $(d[K_{72}]/dR)$. This situation is analogous to the growth of condensed cloud droplets in a saturated vapour phase, and the radial growth is predicted to follow: $R(t) = (R_0 + 2\epsilon t)^{1/2}$ after nucleation, where ϵ is a function of the supersaturation of the environment, which is set in our case by the concentration of K_{72} in solution and the reaction rate. For simplicity, we assume that ϵ is constant in a short interval of time, and we find that the droplet volume will increase as $V(t) = (4\pi/3)(R_0 + 2\epsilon t)^{3/2}$, in perfect agreement with our results in Figure 6.8C, where we obtained an exponent of 1.61 $\pm$ 0.06.

In short, the active droplets in our experiments grow as a result of an autocatalytic conversion of ADP into ATP, but the overall growth is limited by the diffusion of K_{72}

from the surrounding solution to the droplet interface, where it can be taken up. We note that transport of other compounds, including PyK and PEP, could also limit the growth when their concentrations are altered. However, this would only change the growth rate constant ϵ and not change the scaling of droplet size in time, as these compounds must also be transported by diffusion to the droplet interface. [5,27]

6.5 Growth at a population level

In order to corroborate our model and analyze the effects of varying the concentrations of fuel, catalyst and building blocks, we need to quantify the typical growth rate (the "fitness") of an entire population of droplets. Since the droplets vary in size but show a universal growth profile (Figure 6.8A), we chose to average their local growth rates, defined as the first derivative of the radius versus time curve in a defined interval, and given in units of $\mu m \, h^{-1}$. The derivative is calculated using a linear approximation over small intervals of 20 s, during the first 2 minutes of the reaction. We analyzed hundreds of droplets together in every experiment and found that also at the population level active droplets have a distinct behaviour from passive droplets. The distance to neighbouring droplets, position in the well and droplet size (past a threshold) do not affect the droplet growth rate.

We varied reaction and diffusion conditions as shown in Figure 6.9A. Active droplets formed from 2 mM substrate (ADP) grow 20x faster than passive droplets (1.24 versus 0.06 $\mu m \, h^{-1}$, see Methods); droplets can grow 100x faster than passive droplets when ADP is increased to 3 mM. Higher K_{72} concentration indeed accelerate growth, but at 40 μM there is a reversal in the effect, which we attribute to a rising droplet count (Figure 6.9B). The increase in droplet count, although also a feature of an active system, competes with growth. Similarly, when protein concentration is low (10 μM K_{72}), we observe maximal growth rate at the lowest enzyme concentration tested. The increase in enzyme concentration from 0.10 to 0.42 μM is also accompanied by an increase in the initial number of droplets, that we cannot control in our setup. The solution reaches supersaturation more rapidly, which facilitates widespread nucleation of multiple nuclei that then grow limited by diffusion, rather than growth or localized nucleation around some seeding droplets, and the measure growth rate is lower. [28] When enzyme concentration is varied and the protein concentration is higher (20 μM K_{72}), the optimal enzyme concentration for growth also shifts to a higher value (0.42 μM). The complex balance between the two phases, and the two processes (reaction and diffusion), may result in two distinct active droplet regimes – nucleation-dominated or growth-dominated – but both are relevant as protocell models (Figure 6.9C).

Our claim is further supported by our findings in Chapter 5, of suppressed and delayed ripening of complex coacervate droplets. Moreover, we investigated whether growth could be explained by a factor other than the chemical reaction by determining the correlation
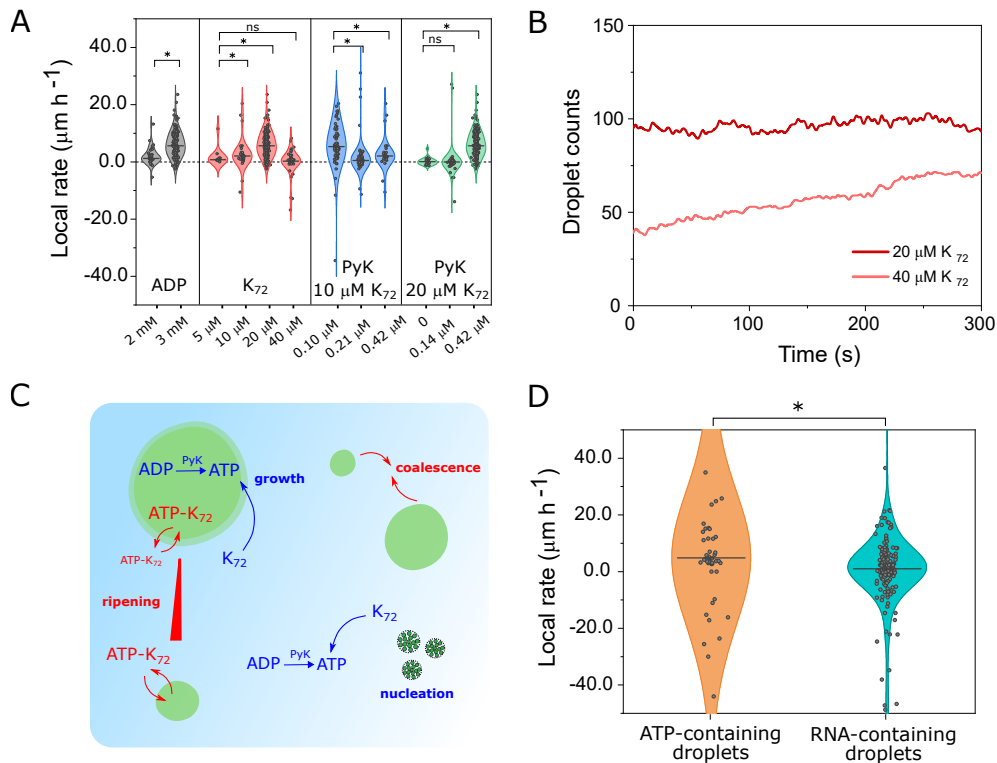
Figure 6.9: Growth rate of active droplets. (A) Growth rate dependence on different reaction-diffusion conditions. The local rate was measured for all droplets in a frame within 200 s of experiment. In different experiments, the concentration of ADP, K_{72} and PyK was varied. Median growth rate differences were evaluated as significant (*) or non-significant (ns) in a Mood's median test ($p < 0.05$). A complete overview of conditions and sample size can be found in Table 6.1. (B) Droplet count during the growth phase of two of the experiments depicted in (A). (C) Active droplets undergo the processes in blue: they grow around seeding droplets or also nucleate in a supersaturated solution of K_{72}. The passive processes in red – ripening and coalescence – are suppressed or minimized in our system. (D) Active droplets of different compositions grow at significantly different rates.

coefficient between growth rate a factors such as: position of the droplet to other droplets, droplet size and (x,y) coordinates of the droplets. The following figures show none or weak correlation, evidencing that what we observe is reaction-driven growth. Heterogeneities in fuel concentration due to our method of supplying phosphoenol-pyruvate and diffusion between droplets do not play a role in the behavior observed.

The fact that we obtain significantly different growth rates by varying substrate, catalyst or building block concentration means that our protocell model can have different fitness depending on its composition and the environmental conditions. This is crucial for

A. Droplets with PyK-Alexa^{647}

| K_p (K$_{72}$) = 57.7 ± 3.8 | K_p (PyK) = 49.4 ± 6.3 |

B. Droplets with RNA-Cy5

| K_p (K$_{72}$) = 39.7 ± 3.7 | K_p (RNA) = 18.7 ± 1.8 |
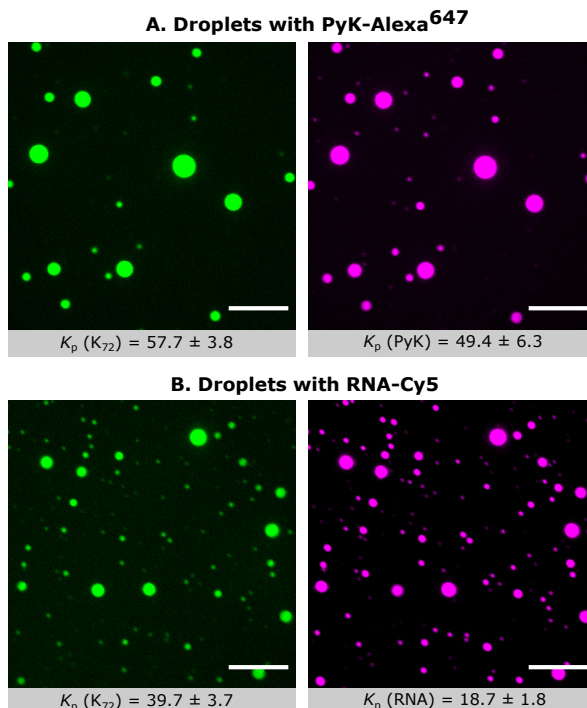
Figure 6.10: (A) ATP-RNA-K$_{72}$ droplets containing the Alexa-647 labelled PyK. Green (488 nm, GFP) and magenta (640 nm, Alexa-647) excitation channels. (B) ATP-RNA-K$_{72}$ droplets containing RNA-Cy5 (1 μM). Green (488 nm, GFP) and magenta (640 nm, Cy5) excitation channels. RNA stands for ss-(ACGU)$_6$. Scale bars: 10 μm.

research aiming to achieve Darwinian evolution with populations of artificial cells. [29,30] We tested this feature by subjecting two different populations to the same environmental conditions: one composed of K$_{72}$, ADP and a seeding concentration of ATP, enough to have droplets from the start; and another mixture where the seeding ATP was replaced by RNA oligomer ((ACGU)$_6$), which also phase separates with K$_{72}$. As in the case of ATP-K$_{72}$ droplets, the enzyme PyK has a high partitioning coefficient in the RNA-containing droplets (K$_p$ = 18), but RNA, with a K_p of 18, displaces ADP in the droplets, [31] so we expected lower growth rates. Indeed, although the RNA-droplets start larger, they grow at 5x smaller rates than the ATP-only droplets. RNA-containing droplets could be designed to grow faster by using an enzyme with a higher preference for RNA droplets, or by making use of RNA's catalytic capacity. [8,32]
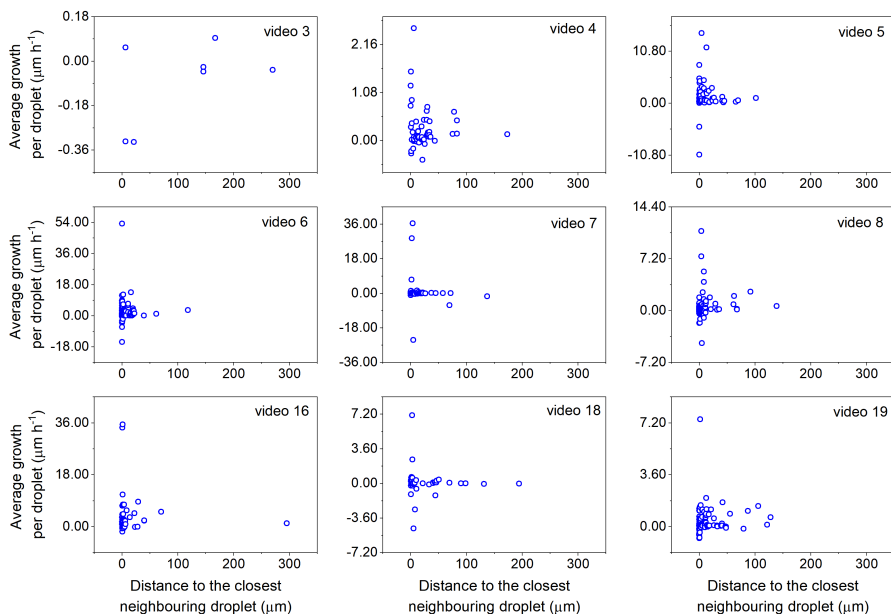
Figure 6.11: Relation between growth rate (averaged from the list of local growth rates) of a droplet and its position relative to other droplets. In other words, the relation between the growth rate of a droplet during an experiment and the presence of a nearby droplet.

6.6   Conclusion

We developed a protocell model that mimics two key features of cellular growth: the volume expansion with a constant protocell count and the intrinsic relation between content and size. The ATP-K_{72} coacervates grow as result of a reaction that converts ADP into droplet-forming ATP, catalyzed by pyruvate kinase. The catalyst is an important component, that due to its efficiency and lack of side reactions, allows for a fine control of ATP formation. Although the use of an enzyme may seem to decrease the prebiotic relevance of our model, we argue that the active coacervate droplets do not rely on any specific interaction and the principles found here can be applied to any complex coacervate.

An advantage of our approach is that we are able to follow individual droplets. This allows to separate the contribution of (rare) fusion events from steady, active growth; and additionally, to obtain a precise profile of droplet sizes and to evaluate the influence of reaction rates and environmental factors on the growth rate of droplets. Most active droplet studies so far have focused on droplet count and average size, which are more susceptible to the interference of droplet motion.[14,33] Based on individual droplet traces,
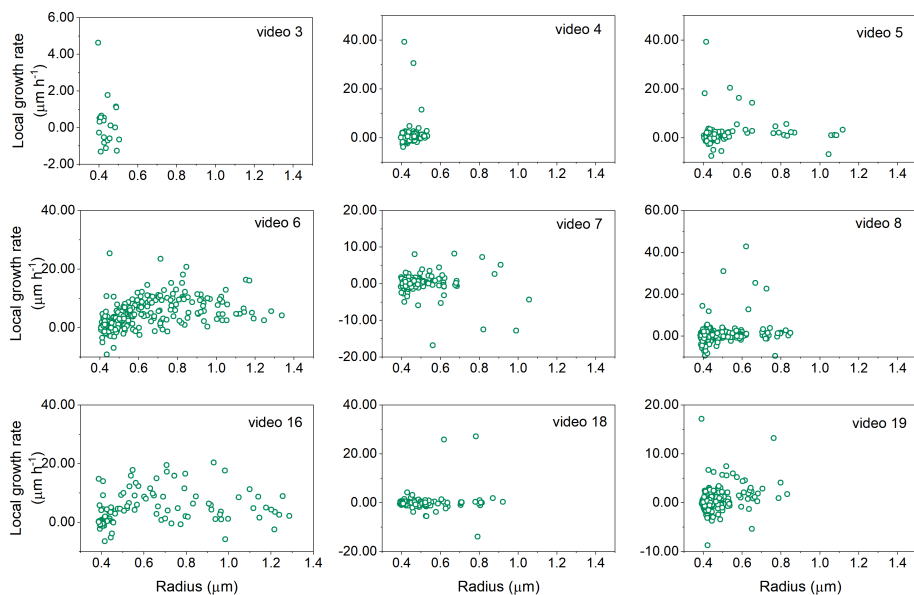
Figure 6.12: Relation between growth rate (taken from the list of all derivatives) and average droplet size at which the derivative was calculated.

we found that our fuel-driven active droplet grow by diffusion, in a classical nucleation-growth fashion, but that the rate is determined by the ATP-forming reaction. As a result, droplet radius has a $t^{1/2}$ dependency, and the speed can be controlled by substrate, catalyst and protein concentrations. Moreover, the growth profile shows that LLPS alters the overall kinetics of the kinase reaction, by introducing a positive feedback where larger droplets have an increased enzyme and ADP copy number, similar to the effect of physical autocatalysis.[34]

Growth and survival are, ultimately, properties of a population, and we show that we can use our model system to create populations with distinct growth rates, which can lead to distinct fitness. From microscopy experiments where the droplets do not need to be immobilized or stabilized, we extract growth rates of all droplets in both populations and found that RNA-containing droplets grow 5x more slowly than the original ATP-K$_{72}$ droplets, which can be rationalized in terms of the partitioning of ADP and therefore, the strength of the positive feedback in the kinase reaction. We point out that the eventual slowing down of growth is not an intrinsic property of active coacervates, but a consequence of the limited amount of K$_{72}$ and PyK. We envision that by designing systems with a higher catalytic efficiency in the presence of RNA, and by introducing a
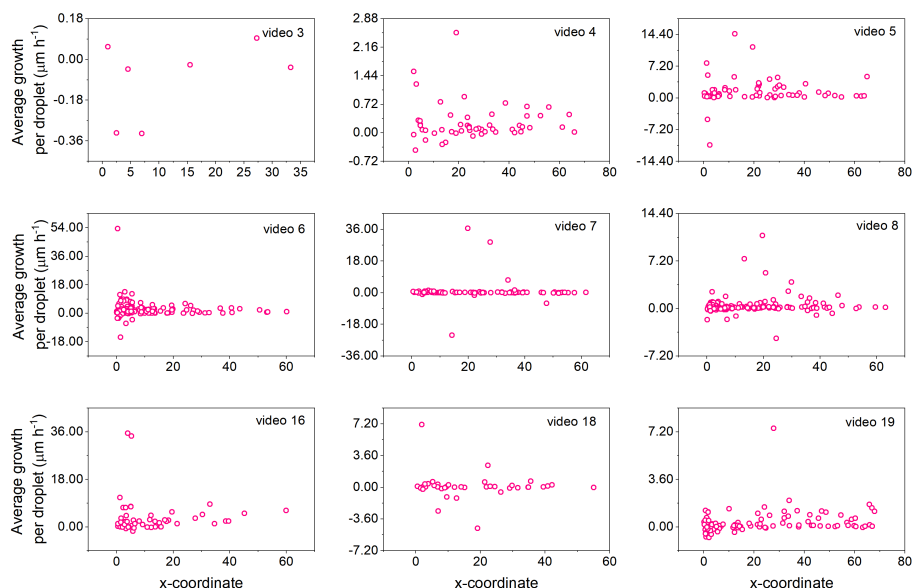
Figure 6.13: Relation between growth rate (averaged over the list of local growth rates) of a given droplet and its x-axis position in the well.

common substrate supply, this is a first step towards competition and evolution of active coacervate protocells.

6.7 Experimental details

6.7.1 Materials and solution compositions

For the coacervates preparation, magnesium chloride anhydrous, sodium chloride, ATP disodium salt, ADP disodium salt and pyruvate kinase type VII from rabbit muscle (EC 2.7.1.40, 2.8 mg mL^{-1}, ca. 1400 units mL^{-1}, molecular weight used: 223 kDa — tetramer) were purchased from Sigma-Aldrich; HEPES free acid and phosphoenolpyruvate monopotassium salt were purchased from FluoroChem. For the microscopy chambers: methoxy PEG silane (MW 5000) was purchased from JenKem Technology USA and 8 or 18 wells chambered μ-slides with glass bottom (No. 1.5 polymer coverslip) were acquired from Ibidi. For enzyme labeling, Alexa Fluor 647 C2 maleimide was purchased from Fischer Scientific. For HPLC experiments, potassium phosphate mono and dibasic salts were purchased from Sigma-Aldrich.
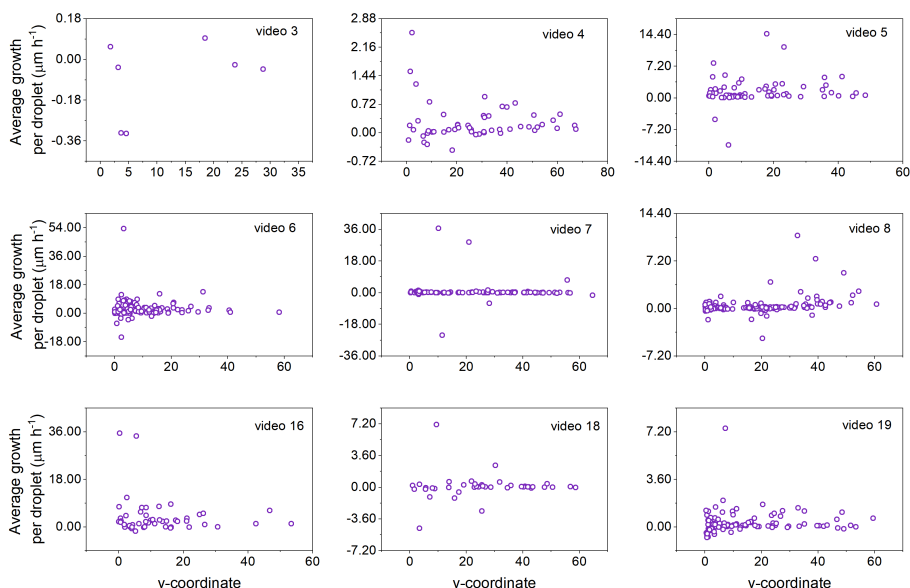
Figure 6.14: Relation between growth rate (averaged over the list of local growth rates) of a given droplet and its y-axis position in the well.

The following stock solutions were prepared by dissolving or diluting in MilliQ: 500 mM and 100 mM HEPES pH 7.4 (adjusted with NaOH 6 M), 10 mM $MgCl_2$, 1 M NaCl, 100 mM ADP, 100 mM ATP, pyruvate kinase 1 mg mL^{-1}. A 100 mM PEP solution was prepared in the 500 mM HEPES. All of the latter were stored at -20 °C for no longer than a month. mPEG silane was dissolved and sonicated in dry DMSO to a 30 mg mL^{-1} concentration, and the stock kept for no longer than a week at room temperature. Alexa Fluor 647 NHS ester was dissolved in dry DMF to a concentration of 10 mg mL^{-1} and kept at -20 °C.

6.7.2 Pyruvate kinase labeling

We followed Thermo-Fischer instructions: 100 µL of enzyme stock, directly as purchased (PyK 2.8 mg mL^{-1} or ca. 12 µM), were mixed with 100 µL of HEPES 0.1 M to reach pH 7 and a concentration of ca. 6 µM. Disulfide bonds were reduced by adding a large excess of DTT (2 µL of a 0.1 M stock); the excess was removed after 30 minutes by centrifugal filtering (MWCO 3 kDa, 2 mL, Centricon, Merck) with degassed HEPES buffer, until the volume reached ca. 200 µL again. Alexa Fluor-647 C2 maleimide was freshly dissolved in DMF (10 mg mL^{-1} or 7.7 mM stock) and 1.5 µL were added to the mixture (final

60 μM of dye, or 10 equiv. in regards to PyK tetramer). The mixture was placed on a thermoshaker for 2 hours, at 600 rpm and room temperature (ca. 21 °C). For removal of unreacted dye, the reaction mixture was diluted to 2 mL with phosphate buffer (20 mM, pH 7) and transferred to a previously wetted centrifugal filter (MWCO 3 kDa, 2 mL, Centricon, Merck). Following fabricator instructions, the mixture was centrifuged at 500 xg for 30 minutes at 4 °C. Until the filtrate was colorless and 50 μL in volume, the following steps were repeated: re-suspend with a pipette, dilute to 2 mL with phosphate buffer, and centrifuge. The flow-through was kept for control experiments, and the enzyme solution was further purified by dialysis against 14 mL of MilliQ overnight (Thermo Scientific Slide-A-Lyzer MINI Dialysis Device, 3.5K MWCO, 2 mL).

6.7.3   Phase diagram

Coacervation of K_{72} and nucleotides ADP or ATP was always assessed with a commonly used turbidity assay, combined with microscopy. The absorbance at 600 nm was measured using a plate reader Spark M10 (Tecan), for samples containing: 25 mM HEPES pH 7.4, 20 μM K_{72}, 1 mM $MgCl_2$ and a varying concentration of ADP or ATP ranging from 1–10 mM. The samples were prepared in a 30 μL scale and placed in a 384-well plate (Nunc, flat bottom). Absorbance (Abs) was measured before and after 2 μL additions of NaCl 0.5 M, until it reached the value of the control lacking any nucleotide. Turbidity(%) was calculated as $100(1 - 10^{-Abs})$. Critical salt concentration was calculated using the last three values of absorbance measured to extrapolate the concentration needed for Abs = 0 (relative to the control).

6.7.4   Partitioning coefficients

Partitioning of K_{72}, which always contains the GFP label, and of pyruvate kinase was calculated via confocal microscopy. The active coacervates were prepared in the default composition, and 1% volume of Alexa 647-labeled pyruvate kinase (as obtained after purification) was added to the mixture. The averaged intensity of GFP and Alexa 647 emission was calculated for multiple droplets. A blank for both channels was obtained with a sample containing only buffer, and the averaged intensity taken as background intensity. The partitioning coefficient of the protein or the enzyme was then calculated as $K_p = \frac{I_{\text{coacervate}} - I_{\text{background}}}{I_{\text{dilute phase}} - I_{\text{background}}}$. K_p of labeled pyruvate kinase was considered to represent the K_p of un-labeled enzyme.

Partitioning of ADP, ATP and PEP was measured using centrifugation and anion-exchange HPLC. Passive coacervates in their default composition were prepared, but now PEP and ADP were added as well (3 mM each), in a total volume of 100 μL. The sample was centrifuged for 30 min, after which the coacervate phase (cc) can be seen as a pellet at the bottom of the Eppendorf. The dilute phase (dp) was removed, avoiding as much as possible to collect coacervate phase (cp) as well. The pellet was dissolved with 30 μL of

NaCl 1 M, and then pipetted back to measure its volume. Both phases were then analyzed using a Shim-pack WAX-1 column (particle size 5 μM, 4.6 x 50 mm, Shimadzu), at 1 mL min^{-1} flow and 45 °C, using a gradient 0–100% B in 15 minutes (A: potassium phosphate buffer pH 7, 20 mM; B: potassium phosphate buffer pH 7, 480 mM). The peaks in the 254 nm-chromatogram with retention times of 10.0 and 12.4 min were identified as ADP and ATP, respectively. The peak in the 215 nm-chromatogram with retention time 9.5 min corresponds to PEP. The partitioning coefficient was then calculated from peak areas as $K_p = \frac{\text{area}_{\text{cp}} \times \text{dilution}_{\text{cp}}}{\text{area}_{\text{dp}} \times \text{dilution}_{\text{dp}}}$.

6.7.5 Microscopy chambers preparation

The Ibidi μ-slides were functionalized with methoxy-PEG to minimize splashing of the coacervate droplets and allow a more accurate measurement of radius over time. The protocol was adapted from Gidi, ACS App Mat 2018. Methoxy-PEG silane (MW 5000) was added to dry DMSO (30 mg mL^{-1}, ca. 20 μL per well to be functionalized) and placed in a thermoshaker at 60 °C. While it dissolved completely, the μ-slides were cleaned thoroughly: washed with dilute detergent, distilled water and ethanol, and dried with pressurized air; then placed in a plasma cleaner (in a usual cleaning cycle according to fabricator instructions) or an ozone cleaner. This removes adsorbed particles, making all hydroxyl groups available for bonding with the PEG silane. The slide was then placed in the oven at 60 °C to prevent precipitation when the PEG silane solution comes into contact with the glass. Finally, the solution was added to each well, the slide was placed in a covered glass Petri dish, and the Petri dish inside an oven at 60 °C. After 2 hours, the slide was washed thoroughly with ethanol, MilliQ water (with sonication for 5 min) and ethanol, then dried with pressurized air and placed in an oven to dry completely. The slides were used the day after, for a maximum of 2 weeks or surface defects start to be observed.

6.7.6 Image and video acquisition

Images and time lapses were recorded at room temperature on a CSU X-1 Yokogawa spinning disk confocal unit connected to an Olympus IX81 inverted microscope, using a 100x piezo-driven oil immersion objective (NA 1.3) and a 488 nm laser beam at 10% power. Emission was measured at 500–550 nm, with 100 ms of exposure time, at a rate of 30 frames per minute, using an Andor iXon3 EM-CCD camera. The acquired images have a pixel size of 141 nm.

Indicated samples were recorded on a Liachroic SP8 confocal inverted microscope (Leica Microsystems, Germany) equipped with a DMi8 CS motorized stage, using the LAS X v.3.5 acquisition software and a 20x air (0.75NA) or a 10x air (0.45NA) objective, depending on the nature of the droplets. For the GFP channel, 0.6% of the nominal power of a cyan laser @488 nm and a normal PMT detector were used, measuring at 493–620
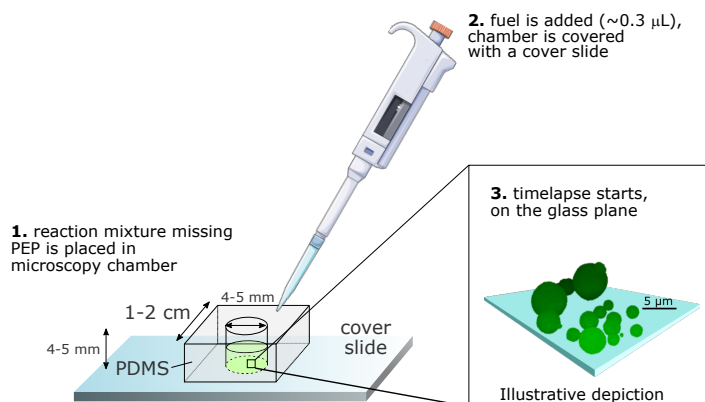
Figure 6.15: Scheme of the microscopy chambers used in active droplets experiments. The cover slide (nr. 1.5) is passivated with the PEGylation protocol described.

nm, with a gain of 600V and an offset of -0.1%. For the Alexa-647 channel, 1.5% of the total power of a red laser @638 nm and HyD SP GaAsP detector in Standard mode acquiring at 658–779 nm were used. Images were acquired at a rate of 12–30 frames per minute and have a pixel size of 377 nm or 1.88 μm depending on the objective.

6.7.7 Active coacervates experiments

All samples were prepared just before an experiment, usually in a 20 μL size; the components were kept in ice during preparation, but not the mixture. Active coacervates had the default composition of (in order of addition): 50 mM HEPES pH 7.4, 0.5 mM $MgCl_2$, 3 mM ADP, 20 μM K_{72}, 0.42 μM pyruvate kinase and 3 mM PEP. For investigating the effect of kinase activity, substrate concentration and protein diffusion on growth rate, the default concentrations were used, but the following were changed, respectively: the enzyme concentration was varied ranging from 0.1–0.42 μM, PEP was varied from 1–3 mM, or K_{72} was varied from 5–40 μM. A negative control without enzyme was performed. See below for the full list of conditions.

6.7.8 Competition experiment

The two droplet populations were analyzed separately, but prepared with common enzyme and protein stocks. The reference population was based on our default system: 50 mM HEPES pH 7.4, 3 mM ADP, 20 μM K_{72} and 0.5 mM $MgCl_2$, with the important difference of 1 mM ATP being added to pre-nucleate droplets. The second population had the same composition, with the addition of 10 μM Cy5-$(ACGU)_6$ RNA oligomer. Under these conditions, there are droplets before any ADP conversion.

Table 6.1: Short-name/experimental conditions correspondence for all videos analyzed. Final concentrations in the microscopy chambers.

Series	Short name	$[K_{72}]$ (µM)	[ADP] (mM)	[PEP] (mM)	[PyK] (µM)	$[ATP]_0$ (mM)	Local rate median (µm h^{-1})	Average droplets detected
PyK	Video 3	20.0	3.0	3.0	-	-	0.06	6
K$_{72}$	Video 4	5.0	3.0	3.0	0.42	-	0.74	42
	Video 5	10.0	3.0	3.0	0.42	-	2.09	28
	Video 6-I	20.0	3.0	3.0	0.42	-	5.63	58
	Video 6-II	20.0	3.0	3.0	0.42	-	0.27	80
	Video 7	40.0	3.0	3.0	0.42	-	0.23	3
PyK	Video 8	10.0	3.0	3.0	0.21	-	0.50	44
Steps	Video 9	20.0	3.0	1.0	0.42	-	3.63	78
	Video 10	20.0	2.0	1.0	0.42	-	4.98	84
	Video 11	20.0	1.0	1.0	0.42	-	0.52	40
PyK	Video 16	10.0	3.0	3.0	0.10	-	5.36	15
PyK	Video 18	20.0	3.0	3.0	0.14	-	0.04	21
ADP	Video 19	20.0	2.0	3.0	0.42	-	1.24	53

Table 6.2: Short name/experimental conditions used in the competition experiment.

Short name	$[K_{72}]$ (µM)	[ADP] (mM)	[PEP] (mM)	[PyK] (µM)	$[ATP]_0$ (mM)	Local rate median (µm h^{-1})	Average droplets detected
Video 27	20.0	3.0	3.0	0.42	1.0	4.96	100

Short name	$[K_{72}]$ (µM)	[ADP] (mM)	[PEP] (mM)	[PyK] (µM)	$[RNA]_0$ (µM)	Local rate median (µm h^{-1})	
Video 28	20.0	3.0	3.0	0.42	10	0.99	19

6.7.9 Pyruvate kinase activity

Enzyme activity in the presence of coacervates was determined by measuring ATP concentration in the emulsion as whole, at different reaction times. Ten copies of the active coacervates (default composition) were prepared, and for each copy the reaction was quenched at a different time, using acetic acid (to pH 2, or 1% v/v). Conveniently, the low pH also dissolves the coacervates. The analysis was done by HPLC, using the same column and run as described in Partitioning coefficients. The control experiment was a sample of equal composition, with the addition of 100 mM NaCl to dissolve existing ADP-K_{72} coacervates, and prevent formation of ATP-K_{72} coacervates.
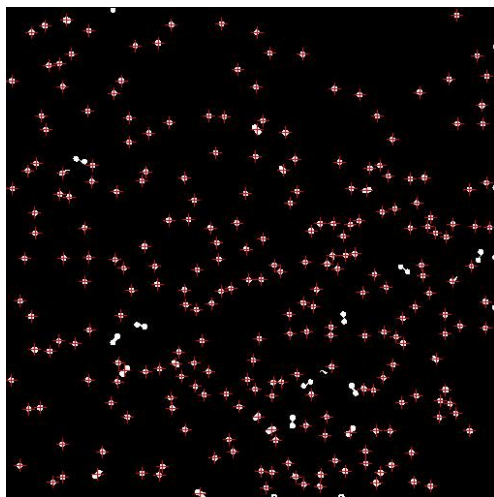
Figure 6.16: Example of edge-detected droplets, filled and labelled by their centroids. The video analysis used a MatLab based script available at the end of Methods.

6.7.10 Quantitative video analysis

Raw fluorescence confocal microscopy videos were processed and analyzed with MatLab 2019 Image Processing Toolbox. In brief, the script: uses customized blurring and smoothing kernels to correct for background emission and prepare the video for edge detection; performs edge detection of objects on each frame with a canny operator, with thresholds customized per video; labels the objects based on their centroid and extracts area, circularity and pixel intensity. Across frames, the script compares centroids to distinguish between fusion, settling and growing events. We select relevant droplets based on an aspect ratio ¡ 2.5 and on a minimum number of 30 frames accurately tracked.

   The properties are then analyzed in a second pipeline that lists properties such as area, radius, volume and pixel intensity, per droplet, and per frame. It also determines the slope of the radius versus time curve in intervals of 10 frames (or 20 s in most cases), after outliers are removed with a moving average interpolation. Within that interval, a linear approximation is valid and the linear slope is taken as the local rate. This means that each droplet may have up to ten different local rates determined, but this parameter and method are a convenient and sufficient way to group droplets in the same experiment.

6.7.11 Statistical analysis

The local rate plots contain all slopes that could be determined from the linear approximation, at the time interval indicated in Table 6.1; the actual number of droplets analyzed in each experiment can be found in the same table. Violin plots were built in OriginLab

2020, using a kernel-smooth distribution and scaled by width; data points are jittered for visualization and the median line are included (actual values in Table 6.1 and Table 6.2). The difference between the results is significantly different if $p < 0.05$ in a Mood's median test.

6.7.12 K_{72} expression and purification

We adapted the procedure previously described by Pesce et al and Te Brinke et al.[21,22] BL21(DE3) cells were transformed with the pET25-sfil-K_{72} plasmid. Expression was performed in Terrific Broth medium (TB; 12 g L^{-1} tryptone and 24 g L^{-1} yeast autolysate) enriched with phosphate buffer (2.31 g L^{-1} potassium phosphate monobasic and 12.54 g L^{-1} potassium phosphate dibasic), glycerol (4 mL per 1 L TB), glucose (0.1 wt%) and 100 µg mL^{-1} ampicillin. Because of the proline- and lysine-rich nature of K_{72}, the TB was supplemented with 0.10 g of amino acids per 1 L of TB. The bacterial cultures were grown at 37 °C till an optical density OD600 reached saturation (1.5–1.8), subsequently cells were cooled to 18 °C to allow expression overnight. Cells were pelleted at 5000 g and resuspended in lysis buffer consisting of 10 mM Tris, 300 mM NaCl, 20 mM imidazole, pH 8, supplemented with 1x complete protease inhibitor cocktail (Roche). Cells were disrupted through sonication on ice and cleared by centrifugation at 20000 g at 4 °C.

His-tag labelled K_{72} was purified from the soluble fraction with a HisTrap column (GE Healthcare, elution buffer: 10 mM Tris pH 8, 300 mM NaCl, 500 mM imidazole). After dialysis against size exclusion (SEC) buffer (10 mM Tris pH 8, 300 mM NaCl), the protein was concentrated to 2–4 mL using a Vivaspin 15 concentrator (MWCO of 30 kDa). Then the protein was passed through a S200 SEC column (GE-Healthcare). Protein purity was analyzed by SDS-PAGE using a 4–20% mini-Protean gel (Bio-Rad) stained with instant blue, pure K_{72} fractions with corresponding size were combined and dialyzed against MilliQ. K_{72} stock solution was obtained by concentrating the protein using a Vivaspin 15 concentrator (MWCO 30 kDa) till the protein reached a concentration of 80 µM. Aliquots of the stock solution were snap frozen and stored at -80 °C.

Acknowledgements

References

[1] E. Szathmáry and J. M. Smith, "The major evolutionary transitions," *Nature*, vol. 374, no. 6519, pp. 227–232, 1995.

[2] I. A. Chen, "The emergence of cells during the origin of life," *Science*, vol. 314, no. 5805, pp. 1558–1559, 2006.

[3] Y. Qiao, M. Li, R. Booth, and S. Mann, "Predatory behaviour in synthetic protocell communities," *Nature Chemistry*, vol. 9, no. 2, pp. 110–119, 2017.

[4] D. Zwicker, R. Seyboldt, C. A. Weber, A. A. Hyman, and F. Jülicher, "Growth and division of active droplets provides a model for protocells," *Nature Physics*, vol. 13, pp. 408–413, 2017.

[5] J. D. Wurtz and C. F. Lee, "Chemical-Reaction-Controlled Phase Separated Drops: Formation, Size Selection, and Coarsening," *Physical Review Letters*, vol. 120, no. 7, pp. 1–25, 2018.

[6] C. A. Weber, D. Zwicker, F. Jülicher, and C. F. Lee, "Physics of active emulsions," *Reports on Progress in Physics*, vol. 82, no. 6, 2019.

[7] T. Beneyton, D. Krafft, C. Bednarz, C. Kleineberg, C. Woelfer, I. Ivanov, T. Vidaković-Koch, K. Sundmacher, and J. C. Baret, "Out-of-equilibrium microcompartments for the bottom-up integration of metabolic functions," *Nature Communications*, vol. 9, no. 1, pp. 1–10, 2018.

[8] B. Drobot, J. M. Iglesias-Artola, K. Le Vay, V. Mayr, M. Kar, M. Kreysing, H. Mutschler, and T. Y. Tang, "Compartmentalised RNA catalysis in membrane-free coacervate protocells," *Nature Communications*, vol. 9, no. 3643, 2018.

[9] M. Tena-Solsona, J. Janssen, C. Wanzke, F. Schnitter, H. Park, B. Rieß, J. M. Gibbs, C. A. Weber, and J. Boekhoven, "Accelerated Ripening in Chemically Fueled Emulsions," *ChemSystemsChem*, vol. 2, no. e2000034, pp. 1–11, 2020.

[10] E. Astoricchio, C. Alfano, L. Rajendran, P. A. Temussi, and A. Pastore, "The Wide World of Coacervates: From the Sea to Neurodegeneration," *Trends in Biochemical Sciences*, vol. 45, no. 8, 2020.

[11] B. Ghosh, R. Bose, and T.-Y. D. Tang, "Can coacervation unify disparate hypotheses in the origin of cellular life," *Current Opinion in Colloid & Interface Science*, no. 101415, 2020.

[12] T. F. Zhu and J. W. Szostak, "Coupled growth and division of model protocell membranes," *Journal of the American Chemical Society*, vol. 131, no. 15, pp. 5705–5713, 2009.

[13] I. Ivanov, R. B. Lira, T. D. Tang, T. Franzmann, A. Klosin, L. Caire, A. Hyman, K. Landfester, R. Lipowsky, K. Sundmacher, and R. Dimova, "Directed Growth of Biomimetic Microcompartments," *Advanced Biosystems*, vol. 3, no. 1800314, pp. 1–9, 2019.

[14] S. Deshpande, F. Brandenburg, A. Lau, M. G. Last, W. K. Spoelstra, L. Reese, S. Wunnava, M. Dogterom, and C. Dekker, "Spatiotemporal control of coacervate formation within liposomes," *Nature Communications*, vol. 10, no. 1800, pp. 1–11, 2019.

[15] K. Takakura, T. Toyota, and T. Sugawara, "A novel system of self-reproducing giant vesicles," *Journal of the American Chemical Society*, vol. 125, pp. 8134–8140, 2003.

[16] J. Berry, S. C. Weber, N. Vaidya, M. Haataja, and C. P. Brangwynne, "RNA transcription modulates phase transition-driven nuclear body assembly.," *Proceedings of the National Academy of Sciences of the United States of America*, vol. 112, no. 38, pp. E5237–45, 2015.

[17] A. Campbell, "Synchronization of cell division," *Bacteriology Reviews*, vol. 21, no. 4, pp. 263–272, 1957.

[18] S. Koga, D. S. Williams, A. W. Perriman, and S. Mann, "Peptide-nucleotide microdroplets as a step towards a membrane-free protocell model.," *Nature chemistry*, vol. 3, no. 9, pp. 720–4, 2011.

[19] E. A. Frankel, P. C. Bevilacqua, and C. D. Keating, "Polyamine/Nucleotide Coacervates Provide Strong Compartmentalization of Mg2+, Nucleotides, and RNA," *Langmuir*, vol. 32, no. 8, pp. 2041–2049, 2016.

[20] W. M. Aumiller Jr and C. D. Keating, "Phosphorylation-mediated RNA/peptide complex coacervation as a model for intracellular liquid organelles," *Nature Chemistry*, vol. 8, no. 2, pp. 129–137,

2015.

[21] E. Te Brinke, J. Groen, A. Herrmann, H. A. Heus, G. Rivas, E. Spruijt, and W. T. S. Huck, "Dissipative adaptation in driven self-assembly leading to self-dividing fibrils," *Nature Nanotechnology*, vol. 13, no. September, pp. 849–856, 2018.

[22] D. Pesce, Y. Wu, A. Kolbe, T. Weil, and A. Herrmann, "Enhancing cellular uptake of GFP via unfolded supercharged protein tags," *Biomaterials*, vol. 34, no. 17, pp. 4360–4367, 2013.

[23] H. Yang, C. Ma, K. Li, K. Liu, M. Loznik, R. Teeuwen, J. C. M. V. Hest, X. Zhou, A. Herrmann, and J. Wang, "Tuning Ice Nucleation with Supercharged Polypeptides," *Advanced Materials*, vol. 28, pp. 5008–5012, 2016.

[24] D. Bracha, M. T. Walls, M. T. Wei, L. Zhu, M. Kurian, J. L. Avalos, J. E. Toettcher, and C. P. Brangwynne, "Mapping Local and Global Liquid Phase Behavior in Living Cells Using Photo-Oligomerizable Seeds," *Cell*, vol. 175, no. 6, pp. 1467–1480.e13, 2018.

[25] J. Oria-Hernández, N. Cabrera, R. Pérez-Montfort, and L. Ramírez-Silva, "Pyruvate kinase revisited: The activating effect of K+," *Journal of Biological Chemistry*, vol. 280, no. 45, pp. 37924–37929, 2005.

[26] P. Adamski, M. Eleveld, A. Sood, Á. Kun, A. Szilágyi, T. Czárán, E. Szathmáry, and S. Otto, "From self-replication to replicator systems en route to de novo life," *Nature Reviews Chemistry*, vol. 4, 2020.

[27] D. Zwicker, A. A. Hyman, and F. Julicher, "Suppression of Ostwald ripening in active emulsions," *Physical Review E - Statistical, Nonlinear, and Soft Matter Physics*, vol. 92, no. 1, pp. 1–13, 2015.

[28] Y. Shin, Y. C. Chang, D. S. Lee, J. Berry, D. W. Sanders, P. Ronceray, N. S. Wingreen, M. Haataja, and C. P. Brangwynne, "Liquid Nuclear Condensates Mechanically Sense and Restructure the Genome," *Cell*, vol. 175, no. 6, pp. 1481–1491.e13, 2018.

[29] K. Adamala and J. W. Szostak, "Competition between model protocells driven by an encapsulated catalyst," *Nature Chemistry*, vol. 5, no. 6, pp. 495–501, 2013.

[30] I. A. Chen, R. W. Roberts, and J. W. Szostak, "The emergence of competition between model protocells," *Science*, vol. 305, no. 5689, pp. 1474–1476, 2004.

[31] F. P. Cakmak, S. Choi, M. C. Meyer, P. C. Bevilacqua, and C. D. Keating, "Prebiotically-relevant low polyion multivalency can improve functionality of membraneless compartments," *Nature Communications*, vol. 11, no. 5949, pp. 1–11, 2020.

[32] R. R. Poudyal, R. M. Guth-Metzler, A. J. Veenis, E. A. Frankel, C. D. Keating, and P. C. Bevilacqua, "Template-directed RNA polymerization and enhanced ribozyme catalysis inside membraneless compartments formed by coacervates," *Nature Communications*, vol. 10, no. 1, pp. 1–13, 2019.

[33] C. Donau, F. Späth, M. Sosson, B. A. Kriebisch, F. Schnitter, M. Tena-Solsona, H. S. Kang, E. Salibi, M. Sattler, H. Mutschler, and J. Boekhoven, "Active coacervate droplets as a model for membraneless organelles and protocells," *Nature Communications*, vol. 11, no. 1, pp. 1–10, 2020.

[34] A. J. Bissette, B. Odell, and S. P. Fletcher, "Physical autocatalysis driven by a bond-forming thiol–ene reaction," *Nature Communications*, vol. 5, pp. 1–8, 2014.

MatLab code I: video analysis

Obs: this script uses the cntrd function, developed by Prof. Dr. Eric Dufresne's group.

```matlab
1  %% Analyzes a video of coacervate droplets
2  % Used in the manuscript "Active coacervate droplets are protocells that
3  % grow and resist Ostwald ripening" (KK Nakashima, MHI van Haren, AAM Andre, I
      Robu, E Spruijt)
4  % Irina Robu, Evan Spruijt, Karina Nakashima — updated 30/01/2021
5  % Example call: % analyzeDroplets('video1.tif', 10.1, 'props-video1.csv', false)
6
7  function analyzeDroplets(szFilename, nScale, szOutput, isVideoOutput)
8      % These are default values for edge detection
9      edgeThreshold  = [0.1 0.5];
10     nDiskRadius    = 2;
11
12     % Input for cntrd function (from Dufresne group, must be an odd integer)
13     nCntrdDiameter  = 3;
14
15    % These are the default values that work for us in the normalisation routine
16     nSmoothSize    = 4;
17     nCropBorder    = 2;
18     nBlurSize      = 10;
19
20    % Get the amount of frames of the video file szFilename
21     nFrames = length(imfinfo(szFilename));
22
23    % Excel maximum columns is 0x4000; so we use this as maximum array size;
24     maxArraySize = 0x4000;
25
26    % Initialize the arrays or 'lists' with null
27     lstDropArea          = zeros(nFrames, maxArraySize);
28     lstDropPerimeter     = zeros(nFrames, maxArraySize);
29     lstDropMajorAxes     = zeros(nFrames, maxArraySize);
30     lstDropMinorAxes     = zeros(nFrames, maxArraySize);
31     lstDropIntensity     = zeros(nFrames, maxArraySize);
32     lstDropmaxMaskIntensityensity  = zeros(nFrames, maxArraySize);
33     lstCentroids         = zeros(nFrames, maxArraySize);
34     lstPreviousCentroids = zeros(1, maxArraySize);
35
36    % Initialize our droplets per frame counter
37     nMaxDroplets = 0x0;
38
39    % Create a disk shaped structural element
40     seDisk = strel('disk', nDiskRadius);
41
42    % A array to store the maximum amount droplets per frame
43     lstMaxDroplets = zeros(nFrames, 1);
44
45    % If video output is wanted, open video stream here
46     if isVideoOutput
47       % Create and open the video object
48       videoOutput = VideoWriter('analyzeDroplets.avi');
49       open(videoOutput);
50     end
51
52    % Loop through all the frames from 1 to nFrames
53       for i = 1:nFrames
54           % Read frame i from szFileName
```

```
55          iFrame = double(imread(szFilename, i));
56
57            % Evens out the background intensity by blurring
58            normFrame = double(iFrame)./(conv2(iFrame,1/nBlurSize^2*ones(nBlurSize), '
                 same'));
59
60         % Remove the nCropBorder amount of pixels from the border (if needed)
61         normFrame = normFrame(1+nCropBorder:end-nCropBorder, 1+nCropBorder:end-
               nCropBorder);
62
63         % Smoothen out the pixels in the matrix
64            normFrame = conv2(normFrame, 1/nSmoothSize^2*ones(nSmoothSize), 'same');
65
66         % Detect all edges in the normalised frame and discard ones smaller than 10
               pixels
67            bwEdges = bwareaopen(imclose(edge(normFrame,'canny', edgeThreshold),
                 seDisk), 10);
68
69         % Remove all objects close to the border of the frame
70            bwEdges(1:5, 1:5) = 1;
71            bwEdges(1:5, end-4:end) = 1;
72            bwEdges(end-4:end, 1:5) = 1;
73            bwEdges(end-4:end, end-4:end) = 1;
74            bwEdges = imclearborder(bwEdges, 4);
75
76         % Turn the circles (edges) into opaque disks and label them
77         % Returning the labeled matrix bwLabelMatrix containing the droplets 1 to
               lstMaxDroplets(i)
78            [bwLabelMatrix, lstMaxDroplets(i)] = bwlabel(imfill(bwEdges, 'holes'));
79
80            % Properties of all the droplets in this frame
81            props = regionprops(bwLabelMatrix, 'Area', 'Perimeter', 'MajorAxisLength',
                 'MinorAxisLength', 'Centroid');
82
83         % Grab the properties we need
84            propArea      = [props.Area];
85            propPerims     = [props.Perimeter];
86            propCentroids   = [props.Centroid];
87            propMajorAxis   = [props.MajorAxisLength];
88            propMinorAxis   = [props.MinorAxisLength];
89
90         % Find all circles < 2.5 circularity
91            lstCircles = find((propMajorAxis./propMinorAxis) < 2.5);
92
93         % Keep the properties of the qualified objects
94            propArea      = propArea(lstCircles);
95            propPerims     = propPerims(lstCircles);
96            propMajorAxis   = propMajorAxis(lstCircles);
97            propMinorAxis  = propMinorAxis(lstCircles);
98
99         % Save all centroids in a temporary array
100        propTempCentroids = propCentroids;
101
102        % Clear out the centroid properties in the origional list
103        propCentroids(:,:) = 0;
104
105        % Save the centroids of the circles back in the origional list
106        for j = 1:length(lstCircles)
107          propCentroids(j * 2 - 1) = propTempCentroids(lstCircles(j) * 2 - 1);
108          propCentroids(j * 2) = propTempCentroids(lstCircles(j) * 2);
```

```
109        end
110
111            % Initialize temp variables
112        maxMaskIntensity = 0;
113            sumIntensity=0;
114
115        % Loop through all droplets of this frame (or max array size if smaller)
116        for j = 1:min(lstMaxDroplets(i), maxArraySize)
117          % Makes a mask to calculate fluorescence intensities in the normalised image
118          tempMask = [bwLabelMatrix==j];
119
120          % Save maximum intensity and the sum
121          maxMaskIntensity(j) = max(max(tempMask.*normFrame));
122          sumIntensity(j)     = sum(sum(tempMask.*normFrame));
123        end
124
125            % Initialize new coordinates array
126            repoCentroids = zeros(length(propCentroids) / 2, 2);
127
128        % Re-position the (X,Y) coordinates
129        for j = 1:((length(propCentroids))/2)
130          repoCentroids(j, 1) = propCentroids(1, j * 2 - 1);
131          repoCentroids(j, 2) = propCentroids(1, j * 2);
132        end
133
134            % The centroids from 'regionprops' is not accurate for our purpose
135        % So we re-evaluate the positions using 'cntrd' from Dufresne group
136        tempCentroids       = cntrd(normFrame,(round(repoCentroids)), nCntrdDiameter);
137            accurateCentroids   = tempCentroids(:,1:end-2);
138            accurateCentroids   = accurateCentroids';
139            accurateCentroids   = accurateCentroids(:)';
140
141            % Initialize new array
142            lstMatches = zeros(1, length(accurateCentroids)/2);
143
144        % Loop though the new centroids list, divided by two because of (X,Y)
145        for j = 1:length(accurateCentroids)/2
146          % Empty the distance array
147          centroidDistance = [];
148
149          % Loop through original ones
150          for k = 1:length(propCentroids)/2
151            % Save the distance of centroids in the two lists of the same droplet
152            centroidDistance(k) = (accurateCentroids(2 * j - 1) - propCentroids(2 * k
                  - 1))^2 + (accurateCentroids(2 * j) - propCentroids(2 * k))^2;
153          end
154
155          % Return the index of the minimum value
156          [~, lstMatches(j)] = min(centroidDistance); %minimal distance difference
                  between all objects from frame to frame
157        end
158
159        % Keep the properties of the qualified objects
160            propArea        = propArea(lstMatches);
161            propPerims      = propPerims(lstMatches);
162            propMajorAxis    = propMajorAxis(lstMatches);
163            propMinorAxis    = propMinorAxis(lstMatches);
164            sumIntensity    = sumIntensity(lstMatches);
165            maxMaskIntensity = maxMaskIntensity(lstMatches);
166
```

```
167         % Clear (or initialize) temporary lists
168             tempPropArea     = zeros(1, maxArraySize);
169             tempPropPerims    = zeros(1, maxArraySize);
170             tempPropCentroids  = zeros(1, maxArraySize);
171             tempPropMajorAxis  = zeros(1, maxArraySize);
172             tempPropMinorAxis  = zeros(1, maxArraySize);
173             tempMaxIntensity   = zeros(1, maxArraySize);
174             tempSumIntensity   = zeros(1, maxArraySize);
175
176             %% Look through all the droplets in the current frame
177         for j = 1:(length(accurateCentroids)/2)
178           % Empty the distance array
179           centroidDistance = [];
180
181           % Loop through droplets of previous frame and calculate distance
182           for k = 1:(length(lstPreviousCentroids)/2)
183             % Save the distance from the droplet in this frame with respect to the
                   previous frame
184             centroidDistance(k) = (accurateCentroids(2 * j - 1) - lstPreviousCentroids
                   (2 * k - 1))^2 + (accurateCentroids(2 * j) - lstPreviousCentroids(2 *
                   k))^2;
185           end
186
187           % Save the minimal distance and the indexes of the matches
188           [minDistance, matchDroplet] = min(centroidDistance);
189
190           % Checks if the droplet matches the any of the ones in the previous frame
191           if minDistance < 30
192             % Save the values if the droplets are matched
193             tempPropArea(matchDroplet)    = propArea(j);
194             tempPropPerims(matchDroplet)  = propPerims(j);
195             tempPropCentroids(2 * matchDroplet - 1:2 * matchDroplet) =
                   accurateCentroids(2 * j - 1:2 * j);
196             tempPropMajorAxis(matchDroplet) = propMajorAxis(j);
197             tempPropMinorAxis(matchDroplet) = propMinorAxis(j);
198             tempSumIntensity(matchDroplet)  = sumIntensity(j);
199             tempMaxIntensity(matchDroplet)  = maxMaskIntensity(j);
200           else
201             % Here we move on to the second previous frame
202             lstPreviousCentroids = lstCentroids(max(i-2,1),1:2*nMaxDroplets);
203
204             % Empty the distance array
205             centroidDistance = [];
206
207             % Loop through droplets of second previous frame and calculate distance
208             for k = 1:(length(lstPreviousCentroids)/2)
209               % Save the distance from the droplet in this frame with respect to the
                     second previous frame
210               centroidDistance(k)=(accurateCentroids(2 * j - 1) - lstPreviousCentroids
                     (2 * k - 1))^2 + (accurateCentroids(2 * j) - lstPreviousCentroids(2
                     * k))^2;
211             end
212
213             % Save the minimal distance and the indexes of the matches
214             [minDistance, matchDroplet] = min(centroidDistance);
215
216             % Checks if the droplet matches the any of the ones in the second previous
                   frame
217             if minDistance < 30
218               % Save the values if the droplets are matched
```

```
219              tempPropArea ( matchDroplet )     = propArea ( j ) ;
220              tempPropPerims ( matchDroplet )  = propPerims ( j ) ;
221              tempPropCentroids (2 * matchDroplet − 1:2 * matchDroplet ) =
                      accurateCentroids (2 * j − 1:2 * j ) ;
222              tempPropMajorAxis ( matchDroplet ) = propMajorAxis ( j ) ;
223              tempPropMinorAxis ( matchDroplet ) = propMinorAxis ( j ) ;
224              tempSumIntensity ( matchDroplet )  = sumIntensity ( j ) ;
225              tempMaxIntensity ( matchDroplet )  = maxMaskIntensity ( j ) ;
226          else
227            % Here we move on to the third previous frame
228            lstPreviousCentroids = lstCentroids ( max ( i −3,1) ,1:2∗nMaxDroplets ) ;
229
230            % Empty the distance array
231            centroidDistance = [ ] ;
232
233            % Loop through droplets of third previous frame and calculate distance
234            for k = 1:( length ( lstPreviousCentroids ) /2)
235              % Save the distance from the droplet in this frame with respect to the
                      third previous frame
236              centroidDistance ( k )=( accurateCentroids (2 * j − 1) −
                      lstPreviousCentroids (2 * k − 1))^2 + ( accurateCentroids (2 * j ) −
                      lstPreviousCentroids (2 * k ))^2;
237            end
238
239            % Save the minimal distance and the indexes of the matches
240            [ minDistance , matchDroplet ] = min ( centroidDistance ) ;
241
242            % Checks if the droplet matches the any of the ones in the third
                      previous frame
243            if minDistance < 30
244              % Save the values if the droplets are matched
245              tempPropArea ( matchDroplet )     = propArea ( j ) ;
246              tempPropPerims ( matchDroplet )  = propPerims ( j ) ;
247              tempPropCentroids (2 * matchDroplet − 1:2 * matchDroplet ) =
                      accurateCentroids (2 * j − 1:2 * j ) ;
248              tempPropMajorAxis ( matchDroplet ) = propMajorAxis ( j ) ;
249              tempPropMinorAxis ( matchDroplet ) = propMinorAxis ( j ) ;
250              tempSumIntensity ( matchDroplet )  = sumIntensity ( j ) ;
251              tempMaxIntensity ( matchDroplet )  = maxMaskIntensity ( j ) ;
252            else
253              % Here we move on to the fourth previous frame
254              lstPreviousCentroids = lstCentroids ( max ( i −4,1) ,1:2∗nMaxDroplets ) ;
255
256              % Empty the distance array
257              centroidDistance = [ ] ;
258
259              % Loop through droplets of third previous frame and calculate distance
260              for k = 1:( length ( lstPreviousCentroids ) /2)
261                % Save the distance from the droplet in this frame with respect to
                        the third previous frame
262                centroidDistance ( k )=( accurateCentroids (2 * j − 1) −
                        lstPreviousCentroids (2 * k − 1))^2 + ( accurateCentroids (2 * j ) −
                        lstPreviousCentroids (2 * k ))^2;
263              end
264
265              % Save the minimal distance and the indexes of the matches
266              [ minDistance , matchDroplet ] = min ( centroidDistance ) ;
267
268              % Checks if the droplet matches the any of the ones in the fourth
                        previous frame
```

```
269                  if  minDistance  <  30
270                    %  Save  the  values  if  the  droplets  are  matched
271                    tempPropArea ( matchDroplet )    =  propArea ( j );
272                    tempPropPerims ( matchDroplet )  =  propPerims ( j );
273                    tempPropCentroids (2  *  matchDroplet  −  1:2  *  matchDroplet )  =
                            accurateCentroids (2  *  j  −  1:2  *  j );
274                    tempPropMajorAxis ( matchDroplet )  =  propMajorAxis ( j );
275                    tempPropMinorAxis ( matchDroplet )  =  propMinorAxis ( j );
276                    tempSumIntensity ( matchDroplet )   =  sumIntensity ( j );
277                    tempMaxIntensity ( matchDroplet )   =  maxMaskIntensity ( j );
278                  else
279                    %  Here  we  move  on  to  the  fifth  previous  frame
280                    lstPreviousCentroids  =  lstCentroids ( max ( i −5,1) ,1:2*nMaxDroplets );
281
282                    %  Empty  the  distance  array
283                    centroidDistance  =  [ ] ;
284
285                    %  Loop  through  droplets  of  third  previous  frame  and  calculate
                            distance
286                    for  k  =  1 : ( length ( lstPreviousCentroids ) /2)
287                      %  Save  the  distance  from  the  droplet  in  this  frame  with  respect  to
                              the  third  previous  frame
288                      centroidDistance ( k )=( accurateCentroids (2  *  j  −  1)  −
                              lstPreviousCentroids (2  *  k  −  1))^2  +  ( accurateCentroids (2  *  j )
                              −  lstPreviousCentroids (2  *  k ))^2;
289                    end
290
291                    %  Save  the  minimal  distance  and  the  indexes  of  the  matches
292                    [ minDistance ,  matchDroplet ]  =  min ( centroidDistance );
293
294                    %  Checks  if  the  droplet  matches  the  any  of  the  ones  in  the  fifth
                            previous  frame
295                    if  minDistance  <  30
296                      %  Save  the  values  if  the  droplets  are  matched
297                      tempPropArea ( matchDroplet )    =  propArea ( j );
298                      tempPropPerims ( matchDroplet )  =  propPerims ( j );
299                      tempPropCentroids (2  *  matchDroplet  −  1:2  *  matchDroplet )  =
                              accurateCentroids (2  *  j  −  1:2  *  j );
300                      tempPropMajorAxis ( matchDroplet )  =  propMajorAxis ( j );
301                      tempPropMinorAxis ( matchDroplet )  =  propMinorAxis ( j );
302                      tempSumIntensity ( matchDroplet )   =  sumIntensity ( j );
303                      tempMaxIntensity ( matchDroplet )   =  maxMaskIntensity ( j );
304                    else
305                      %%  In  case  no  match  was  found  with  the  previous  five  frames ,  the
                              droplet  is  added  to  a  new  column
306                      lstPreviousCentroids  =  lstCentroids ( max ( i −1,1) ,1: length (
                              accurateCentroids ));
307                      nMaxDroplets=nMaxDroplets+1;
308
309                      %  Make  sure  array  is  not  out  of  bounds
310                      if  nMaxDroplets  <=  maxArraySize
311                        tempPropArea ( nMaxDroplets )  =  propArea ( j );
312                        tempPropPerims ( nMaxDroplets )  =  propPerims ( j );
313                        tempPropCentroids (2*nMaxDroplets−1:2*nMaxDroplets )  =
                                accurateCentroids (2*j−1:2*j );
314                        tempPropMajorAxis ( nMaxDroplets )  =  propMajorAxis ( j );
315                        tempPropMinorAxis ( nMaxDroplets )  =  propMinorAxis ( j );
316                        tempSumIntensity ( nMaxDroplets )  =  sumIntensity ( j );
317                        tempMaxIntensity ( nMaxDroplets )  =  maxMaskIntensity ( j );
```

```
318                    else
319                      % Array is out of bounds, throw an error
320                      break
321                    end
322                  end
323                end
324              end
325            end
326          end
327        end
328
329        % Add the properties of the droplets of this frame to the list
330            lstDropArea(i,:)      = tempPropArea;
331            lstDropPerimeter(i,:)   = tempPropPerims;
332            lstCentroids(i,:)       = tempPropCentroids;
333            lstDropMajorAxes(i,:)   = tempPropMajorAxis;
334            lstDropMinorAxes(i,:)   = tempPropMinorAxis;
335            lstDropmaxMaskIntensityensity(i,:) = tempMaxIntensity;
336            lstDropIntensity(i,:)   = tempSumIntensity;
337            lstPreviousCentroids   = lstCentroids(i, 1:2 * nMaxDroplets);
338
339
340        % Write frame to video if wanted
341        if isVideoOutput
342          % disp(sprintf('frame %d',i));
343          for j=1:(length(lstCentroids)/2)
344            % Plot centroid j
345            plot(lstCentroids(1,j*2−1),lstCentroids(1,j*2),'+r');
346          end
347
348          % Write frame to file videoOutput
349          writeVideo(videoOutput, getframe); %write the image to file
350
351          % Uncomment this if you want to watch frame−by−frame
352          % imshow(bwLabelMatrix);
353          % hold on
354        end
355        end
356
357    % If video output is wanted
358    if isVideoOutput
359      % Close video file videoOutput
360      close(videoOutput);
361
362      % Play the video
363      implay('analyzeDroplets.avi');
364    end
365
366    % Here we convert from pixels to the nScale defined as input
367    lstDropArea       = lstDropArea.*((1./nScale).^2);
368    lstDropPerimeter  = lstDropPerimeter./nScale;
369    lstRadius         = (lstDropArea ./ pi) .^ 0.5;
370    lstCentroids      = lstCentroids./nScale;
371    lstDropMajorAxes  = lstDropMajorAxes./nScale;
372    lstDropMinorAxes  = lstDropMinorAxes./nScale;
373
374    % Concatinate the data to one matrix
375    dataOutput = [lstDropArea(:,1:nMaxDroplets) lstDropPerimeter(:,1:nMaxDroplets)
376            lstRadius(:,1:nMaxDroplets) lstCentroids(:,1:2*nMaxDroplets)
377            lstDropMajorAxes(:,1:nMaxDroplets) lstDropMinorAxes(:,1:nMaxDroplets)
```

```
            lstDropmaxMaskIntensityensity (: ,1:nMaxDroplets)  lstDropIntensity (: ,1:
            nMaxDroplets ) ];
376
377    % Initialize a new array for the filtered data
378    dataOutputFiltered = zeros ( nFrames , length ( dataOutput ) );
379
380    % Loop though output data
381    for i = 1:( length ( dataOutput ) )
382      % Taking only the droplets present in 30+ frames
383      if ( length ( find ( dataOutput (: , i ) ) ) > 30 )
384        % Save the data of this droplet to the filtered variable
385        dataOutputFiltered (: , i ) = dataOutput (: , i );
386      end
387      end
388
389    % Re−arrange data in dataOutputFiltered
390    dataOutputFiltered (: , ~any ( dataOutputFiltered , 1 ) ) = [];
391
392    % Write dataOutputFiltered to szOutput
393    writematrix ([ dataOutputFiltered lstMaxDroplets ], szOutput );
394  end
```

MatLab code II: extraction of growth rates

```matlab
1  %% Calculates and plots properties of analyzed droplets
2  % Used in the manuscript "Active coacervate droplets are protocells that
3  % grow and resist Ostwald ripening" (KK Nakashima, MHI van Haren, AAM Andre, I
       Robu, E Spruijt)
4  % Irina Robu, Evan Spruijt, Karina Nakashima — updated 30/01/2021
5  % Example call: % plotDropletProps('props-video1.csv', 1, 600, 20, 50, 250, 0.5, '
       output-video1.xlsx')
6  %
7  % Summary:
8  % 1) Radius (um) Vs time (s)
9  % 2) Overall growth rate (um/s) per droplet [the slope of radius trace]
10 % 3) Local rate (um/s) Vs time (s) [for all droplets, all frames]
11 % 4) Local rate (um/s) Vs size (um) [for all droplets, all frames]
12 % 5) Local rate (um/s) Vs size (um) [for all droplets, 1:linearFirstFrame frames]
13 % 6) Growth rate (um/s) Vs mindist (um) [overall growth rate]
14 % 7) linearIntervalensity (a.u.) Vs time (s) [total linearIntervalensity inside
       each droplet, over all frames]
15 % 8) Density (a.u./um^2) Vs time (s) [total linearIntervalensity/area for each
       droplet, over all frames]
16 % 9) Growth rate (um/s) Vs coordx and coordy (px) [overall growth rate versus
       position for each droplet, each frame]
17 % 10) Maximum growth rate (um/s) Vs size (um) [the max local rate for a droplet,
       and the radius at that polinearInterval]
18
19 function plotDropletProps(sInput, FirstFrame, LastFrame, linearInterval,
       linearFirstFrame, linearLastFrame, framerate, sOutput)
20
21 % Read input into data matrix
22 data = readmatrix(sInput);
23
24 %% Choose which property from data file to follow overtime
25 % For radius column
26 prop = 3;
27
28 %% 1) Radius Vs time
29 % Taking the right property (column) and time interval
30 ndrops = (length(data(1,:)))/9;
31 % The number of the first column containing that property in data matrix
32 firstcolumnprop = (ndrops*prop) + 1 - ndrops;
33 % The number of the last column containing that property in data matrix
34 lastcolumnprop = (ndrops*prop);
35
36 %lindata is a matrix of only the property previously selected, where lines
37 %are different frames and columns are different droplets. Here we take all
38 %timeframes that came from video analysis.
39 lindata = data(FirstFrame:LastFrame,firstcolumnprop:lastcolumnprop);
40
41 % Taking out the outliers (high peaks in intensity)
42 for i = 1:length(lindata(1,:))
43     thiscoldata = lindata(:,i);
44     tf = ~isoutlier(thiscoldata,'movmean',20);
45     thiscoldata = tf.*thiscoldata;
46     thiscoldata(thiscoldata==0) = NaN;
47     lindata(:,i) = thiscoldata;
48 end
49
```

```matlab
50    % Creating the time column−vector and the corrected data matrix.
51    time = [(1/framerate):(1/framerate):(length(lindata(:,1))./framerate)]';
52
53    writematrix([time lindata],sOutput,'Sheet',1);
54    plot1 = figure;
55    plot(time, lindata);
56    xlabel('Time (s)');
57    ylabel('Radius (um)');
58
59    %% 2) Growth rate Vs droplet
60    p = [];
61    % Removing the NaN values from the plot to calculate the slope.
62    for i = 1:ndrops
63        % Overall growth rate
64        thisCol = lindata(:, i);
65        x = time;
66        nanIndexes = isnan(thisCol);
67        thisCol(nanIndexes) = [];
68        x2 = x(~nanIndexes);
69        % Fit a polynom of degree 1 − this is done per droplet
70        p(2 * i − 1:2 * i) = polyfit(x2,thisCol,1);
71        px = polyfit(x2,thisCol,1);
72        yfit = polyval(px,x2);
73        yresid = thisCol − yfit;
74        SSresid = sum(yresid.^2);
75        SStotal = (length(thisCol)−1) * var(thisCol);
76        rsq(j) = 1 − SSresid/SStotal;
77    end
78
79    % Taking columns 1 to end (every two). Those are the p1 coefficients from
80    % polyfit (slope) for different droplets
81    growthrate = p(:,1:2:end);
82    growthrate(growthrate==0) = NaN;
83
84    writematrix([[1:ndrops]' growthrate'],sOutput,'Sheet',2);
85    plot2 = figure;
86    plot([1:ndrops]', growthrate');
87    xlabel('Radius (um)');
88    ylabel('Local rate (um/s)');
89
90    %% 3) Local rate Vs time
91    localrate = [];
92    p2       = [];
93    rsq2     = [];
94    px       = [];
95    yfit     = [];
96    yresid   = [];
97    SSresid  = [];
98    SStotal  = [];
99    p        = [];
100
101   %Removing the NaN values from the plot to find the right slope
102   for i = 1:length(time)/linearInterval
103       for j = 1:ndrops
104           thisCol = lindata( (i − 1) * linearInterval + 1:(i − 1) * linearInterval +
                      linearInterval , j);
105           x = time( (i − 1) * linearInterval + 1:(i − 1) * int + linearInterval);
106           nanIndexes = isnan(thisCol);
107           thisCol(nanIndexes) = [];
108           x2 = x(~nanIndexes);
```

```
109            p(i,2*j-1:2*j) = polyfit(x2,thisCol,1);
110            px = polyfit(x2,thisCol,1);
111            yfit = polyval(px,x2);
112            yresid = thisCol - yfit;
113            SSresid = sum(yresid.^2);
114            SStotal = (length(thisCol)-1) * var(thisCol);
115            rsq(j) = 1 - SSresid/SStotal;
116        end
117    end
118
119    localrate = p(:,1:2:end);
120
121    % Turn the 0 values (when no slope is possible) to NaN as to preserve
122    % median and mean calculations.
123    localrate(localrate==0) = NaN;
124
125    % Change time for the interval where rates were taken.
126    time2 = [(1/framerate):(1/framerate):((length(lindata(:,1))./linearInterval)./
               framerate)]';
127    time2 = time(1:(length(time)/linearInterval),:);
128
129    writematrix([time2 localrate],sOutput,'Sheet',3);
130    plot3 = figure;
131    plot(time2, localrate);
132    xlabel('Time (s)');
133    ylabel('Local growth rate (um/s)');
134
135    %% 4) Local rate Vs size
136    %Create a matrix where lines are timepoints (as many as nr of frames/int) and
               columns
137    %are different droplets
138    localsize=[];
139        for i = 1:(length(lindata(:,1))/linearInterval)
140            for j = 1:ndrops
141                localsize(i,j) = nanmean(lindata( (i - 1) * linearInterval + 1:(i - 1)
                        * linearInterval + linearInterval ,j));
142            end
143        end
144
145    %Linearize that matrix, so data from different droplets are stacked on top
146    %of eachother
147    localsizelinear = localsize(:);
148    localratelinear = localrate(:);
149
150    writematrix([localsizelinear localratelinear],sOutput,'Sheet',4);
151    plot4 = figure;
152    plot(localsizelinear, localratelinear, '+');
153    xlabel('Radius (um)');
154    ylabel('Local rate (um/s)');
155
156    %% 5) Local rate Vs size with time range
157    % Cut the localrate Vs size matrix before stacking droplet on top of
158    % droplet, to restrict data to a certain time range: from FirstFrameframe to
159    % cutlinear.
160
161    % Defining the positions of the cut
162    firstrow = linearFirstFrame/linearInterval;
163        if firstrow < 1
164            firstrow = 1;
165        end
```

```matlab
166    lastrow = linearLastFrame/linearInterval;
167
168    % Cutting the matrix
169    localsizecut = localsize(firstrow:lastrow,:);
170    localratecut = localrate(firstrow:lastrow,:);
171
172    % Linearizing the matrix it for plotting
173    localsizecutlinear = localsizecut(:);
174    localratecutlinear = localratecut(:);
175
176    writematrix([localsizecutlinear localratecutlinear],sOutput,'Sheet',5);
177    plot5 = figure;
178    plot(localsizecutlinear, localratecutlinear, '+');
179    xlabel('Radius (um)');
180    ylabel('Local growth rate (um/s)');
181
182    %% 6) Growth rate Vs Mindist
183    centroids = data(:,((ndrops*4)+1-ndrops):(ndrops*5));
184    for i = 1:(length(centroids(1,:))/2)
185        dist2 = [];
186            for j = 1:(length(centroids(1,:))/2)
187                dist2(k)=(nanmean(centroids(:,2 * i - 1)) - nanmean(centroids(:,2 * j
                    - 1)))^2 + (nanmean(centroids(:,2 * i)) - nanmean(centroids(:,2 *
                    j)))^2;
188            end
189        dist3(:,i) = dist2;
190        mindist(i) = nanmin(dist2(dist2 > 0));%takes the smallest value not equal to 0
191    end
192
193    % Sorting out in an ascending order
194    [sortedmindist, sortIndex1] = sort(mindist);
195    sortedgr = growthrate(sortIndex1);
196
197    writematrix([sortedmindist' sortedgr'],sOutput,'Sheet',6);
198    plot6 = figure;
199    plot((sortedmindist)', (sortedgr)','+');
200    xlabel('Minimum distance to another droplet (um)'); %Assumes 1 fps
201    ylabel('Growth rate (um/s)');
202
203    %% 7) Totint vs Time
204    lintotint = data(FirstFrame:LastFrame,((ndrops*9)+1-ndrops):(ndrops*9));
205    for i=1:ndrops
206        for j=1:length(time)
207            if lintotint(j,i)<0.5*nanmax(lintotint(:,i))
208                lintotint(j,i)=NaN;
209            end
210        end
211    end
212
213    writematrix([time lintotint],sOutput,'Sheet',7);
214    plot7 = figure;
215    plot(time, lintotint,'+');
216    xlabel('Time (s)');
217    ylabel('Intensity (a.u.)');
218
219    %% 8) Density Vs Time
220    area = data(FirstFrame:LastFrame,((ndrops*1)+1-ndrops):(ndrops*1));
221    density = lintotint./area;
222    writematrix([time density],sOutput,'Sheet',8);
223    plot8=figure;
```

```matlab
224    plot(time, lintotint./area, '+');
225    xlabel('Time (s)');
226    ylabel('Density (a.u.)');
227
228    %% 9) Growth rate Vs coordinates
229    coordx = [];
230    coordy = [];
231    for i = 1:(length(centroids(1,:))/2)
232        coordx(1,i) = nanmean(centroids(:,2 * i - 1));
233        coordy(1,i) = nanmean(centroids(:,2 * i));
234    end
235
236    % Growth rate is taken out of calculation step 2, so an average over all
237    % frames. Change it to localratecut to perform it over a time range, and
238    % localrate to perform it over all local rates.
239    writematrix([coordx' growthrate' coordy' growthrate'], sOutput, 'Sheet',9);
240
241    plot9a = figure;
242    plot(coordx, growthrate, '+');
243    xlabel('x-coordinate');
244    ylabel('Growth rate (a.u.)');
245    plot9b=figure;
246    plot(coordy, growthrate, '+');
247    xlabel('y-coordinate');
248    ylabel('Growth rate (a.u.)');
249
250    %% 10) Max growth rate Vs Radius (at that timepoint)
251    maxgr   = [];
252    maxsize = [];
253
254    % Maximum rate is taken out of localratecut matrix for large droplets
255    for i = 1:ndrops
256        if localsizecut(end,i) < 0.5
257            localratecut(:,i) = NaN;
258        end
259    end
260
261    for i = 1:ndrops
262        [maxgr(1,i),id] = nanmax(localratecut(:,i));
263        maxsize(1,i) = localsizecut(id,i);
264    end
265
266    writematrix([maxsize' maxgr'], sOutput, 'Sheet',10);
267    plot10 = figure;
268    plot(maxsize, maxgr, '+');
269    rmg = corrcoef(maxsize, maxgr, 'Rows','complete')
270
271    end
```

Part IV

Finale

Chapter 7

General discussion
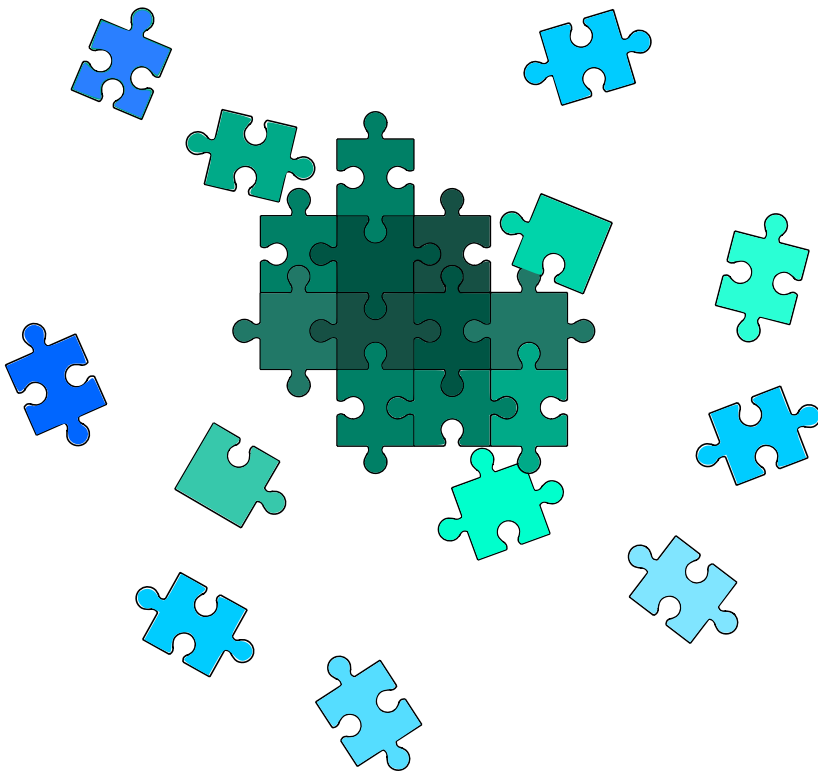
E pluribus unum
Out of many, one

This thesis lies at the intersection of three fields: coacervates in the physical-organic chemistry sense of the term, as started by Bungenberg de Jong; coacervates in the conception of Oparin-Haldane for the origin of life; and liquid condensates in the cellular context, as triggered by membraneless organelles research. In the introduction, we claimed that connecting them has a synergistic effect on the the discussion, and we hope to have done just that throughout this thesis.

Looking back at our overview of protocellular models in Figure 1.6, we can now say that coacervates offer the best of two worlds: consistency and functionality. Consistency is the prebiotic plausibility of the model, whether it relates to what we know about early Earth's composition and conditions. In other words, the model's potential as a protocell. By functionality, we mean the model's potential as a biomimic, whether it displays behavior that we see now in living systems, or aim for in artificial cells. The range of chemical compositions, and the spontaneous assembly of coacervate droplets makes them plausible from a prebiotic chemistry perspective, while the range of behaviors they can display makes them functional biomimics (Figure 7.1).
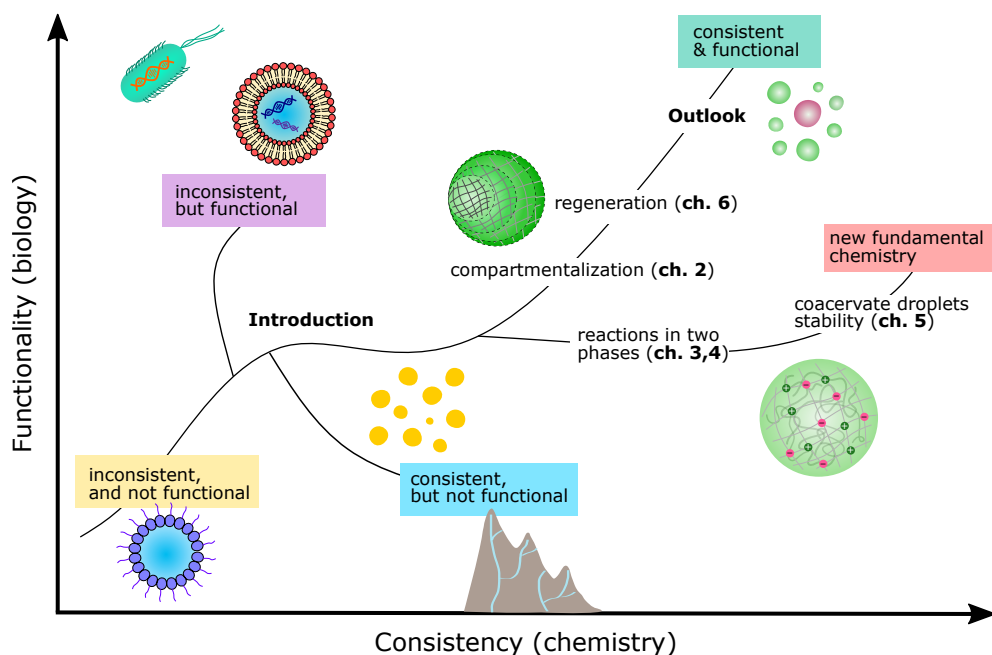

Figure 7.1: Output of this thesis in a functionality-consistency diagram.

We tackled the challenge of improving coacervates as biomimics by achieving reaction-driven growth in Chapters 2 and 6, which we now discuss together in Section 7.1. Motivated by early findings in our main branch, we tackled a second challenge: to unveil fundamental chemistry aspects of coacervates, the general goal of Chapters 3, 4 and 5.

While in the first two chapters we exalted coacervates as open micro-reactors, in the latter we found them to be extremely stable compartments towards ripening, a paradox we address in Section 7.2.

7.1 Reactions to control coacervates

Coacervation is a spontaneous process, that is, if we mix two macro-ions **A** and **B** under metastable conditions — of pH, ionic strength, concentration, temperature —, the system goes downhill in free-energy, towards a two-phase equilibrium state. Most studies of coacervation are performed under thermodynamic equilibrium, but for the purpose of using coacervates as protocells or model organelles, control over the final structure is needed, which requires a better knowledge of the kinetics of the phase-ordering process.[1] Accordingly, for our ambition to develop growing droplets, mixing **A** and **B** is not very useful; we aimed at a system that could, as independently as possible, reach a saturation point and phase separate via a *nucleation-growth* mechanism.

Nucleation-growth (NG) is characterized by local, high concentration fluctuations, and leads to spherical droplets dispersed in a continuous, dilute phase.[2] NG is not the only mechanism available; *spinodal decomposition* (SD) is a pathway without any energy barrier characterized by widespread concentration fluctuations that lead to bicontinuous networks of dilute and dense phases (Figure 7.2A).[2] Kinetics does not receive nearly as much attention as thermodynamics in the field of protocells and membraneless organelles, but in many cases coacervation is thought to take place via NG mechanism: reasonably, protocell research works with dilute solutions and gradually changes parameters, which favors NG over SD.[3] Although both Chapter 2 and Chapter 6 used the same form of control — gradually increasing ATP concentration via a reaction —, in Chapter 6 we obtained a direct observation of nucleation-growth (Figure 7.2B and C).

The phase diagrams we built are measurements of the binodal boundaries, and we can only speculate about the spinodal curves of each system. A narrower binodal region for ATP-PLL (Chapter 2) than for ATP-K_{72} (Chapter 6) mixtures could explain the difference in the final state, and tends to occur at low polymer fractions.[4] The phase diagram of ATP-PLL is much wider than ATP-K_{72}, with the partitioning coefficient of ATP being respectively ca. 52 and 3; both the binodal and spinodal curves are shifted to lower concentrations of ATP, leaving not much room for shallow quenches into the two-phase region. Kinase activity in the presence of PLL and K_{72} is similar, given that in both mixtures the substrates ADP and PEP are depleted within 20 minutes (Figures 3.5 and 6.7), which suggests both mixtures reach supersaturation at comparable rates, but only for ATP-PLL the spinodal curve is reached directly. Combined with the ideal composition of ATP-K_{72} coacervates, our single droplet imaging protocol is a promising method to study the nucleation-growth mechanism out of the protocell context, as a more accessible alternative to time-resolved methods such as light scattering and optocontrol of droplet
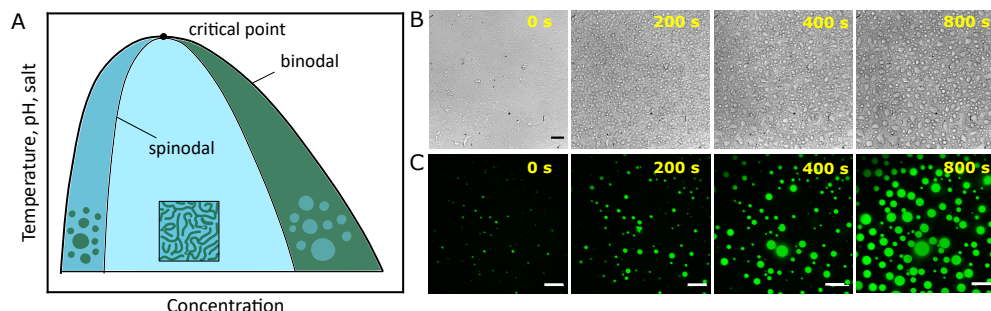
Figure 7.2: (A) Spinodal and binodal curves in a typical phase diagram. Between the binodal and spinodal, phase separation happens via nucleation followed by diffusion-limited growth; under the spinodal, spinodal decomposition takes place. Figure based on ref. 7. To the right, qualitative comparison of phase-separation kinetics in Chapters 2 and 6: (B) ATP-PLL phase separation resembles spinodal decomposition, resulting in an interconnected networks (scale bar: 20 μm); (C) ATP-K_{72} coacervation proceeds via nucleation-growth, yielding spherical (fluorescent) droplets dispersed in a continuous dilute phase (scale bar: 10 μm).

condensation. [5,6]

Integrated, the two chapters add a new meaning to "reaction controlled coacervation": to the thermodynamic control depicted in Figure 2.2, Chapter 6 adds a kinetic control, to the level of droplet growth rate. We believe this distinguishes our work from others in the literature that have attempted to control coacervation and coacervates with a chemical reaction. The attained control over droplet formation is promising for achieving more out-of-equilibrium behaviors coupled to growth, such as division and motility.

7.2 Coacervates to control reactions

We first focused on the effect a reaction can play in the thermodynamics and kinetics of phase separation. During the making of Chapter 2, it became clear though that a one-directional influence only holds for the initial stages of the reaction, and when the coacervate phase starts to grow, an interplay between reaction and coacervation must be considered as molecules constantly re-distribute over the two phases. In Chapter 3 we developed the methods that we used in Chapter 6 to infer that the droplets grow from within, and in Chapter 4, we de-coupled, for simplicity, reaction components from coacervate components and showed that partitioning can be extremely relevant for reactions with two substrates or product inhibition, for example.

These results highlighted the permeability of coacervate droplets compartments, which contrasts to our finding in Chapter 5 that Ostwald ripening is suppressed in charge-based complex coacervates. *If reactants and products are constantly reshuffling between the dilute phase and the dense phase, how can Ostwald ripening be suppressed by the energy*

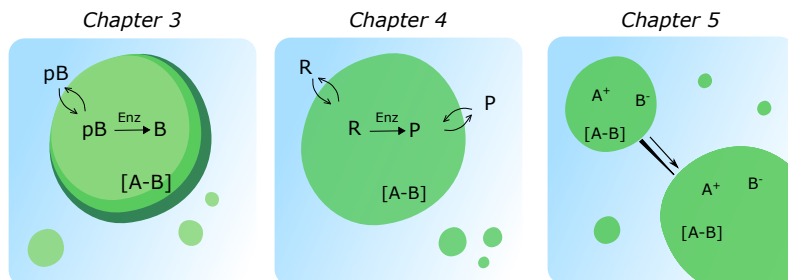*cost of transferring a macro-ion or a neutral complex from droplet to droplet?*

Figure 7.3: Coacervate droplet permeability as assumed in different chapters: in Chapter 3 we looked at the ATP-PLL droplets that form by taking up ATP; in Chapter 4 we looked at reactions between client molecules that can enter and leave the droplet without affecting its integrity; and in Chapter 5 we looked at the droplets themselves, and how they exchange building blocks with each other.

The difference could be explained by reasoning that Ostwald ripening suppression does not imply impermeability; complex coacervate droplets exchange macro-ions or electroneutral complexes with the dilute solution, as indicated by our FRAP experiment in Chapter 5, but there is simply no preference for components to accumulate in larger droplets. In most liquids, with no forces involved other than the interfacial pressure, over time there is diffusion of building blocks towards larger droplets driven by energy minimization. In complex coacervates, even with the energy barriers of removing charged molecules or large complexes, that is likely to be in equilibrium with the reverse process, and no net ripening is observed. Still, the structure of complex coacervates remains widely misunderstood (as to whether macro-ions or electroneutral complexes dissociate from it)[8] and here we show how this physical-chemical mystery may have direct implications for protocell research.

References

[1] C. Sanchez, G. Mekhloufi, and D. Renard, "Complex coacervation between β-lactoglobulin and acacia gum: A nucleation and growth mechanism," *Journal of Colloid and Interface Science*, vol. 299, no. 2, pp. 867–873, 2006.

[2] S. Turgeon, M. Beaulieu, C. Schmitt, and C. Sanchez, "Protein–polysaccharide interactions: phase-ordering kinetics, thermodynamic and structural aspects," *Current opinion in colloid & interface science*, vol. 8, no. 4-5, pp. 401–414, 2003.

[3] M. Abbas, W. P. Lipiński, J. Wang, and E. Spruijt, "Peptide-based coacervates as biomimetic protocells," *Chemical Society Reviews*, 2021.

[4] J. Heckel, F. Batti, R. T. Mathers, and A. Walther, "Spinodal decomposition of chemically fueled polymer solutions," *Soft Matter*, 2021.

[5] E. Dine, A. A. Gil, G. Uribe, C. P. Brangwynne, and J. E. Toettcher, "Protein Phase Separation Provides Long-Term Memory of Transient Spatial Stimuli," *Cell Systems*, vol. 6, no. June 27, pp. 655–663, 2018.

[6] Y. Shin, J. Berry, N. Pannucci, M. P. Haataja, J. E. Toettcher, and C. P. Brangwynne, "Spatiotemporal control of intracellular phase transitions using light-activated optodroplets," *Cell*, vol. 168, no. 1-2, pp. 159–171, 2017.

[7] S. Alberti, A. Gladfelter, and T. Mittag, "Considerations and challenges in studying liquid-liquid phase separation and biomolecular condensates," *Cell*, vol. 176, no. 3, pp. 419–434, 2019.

[8] K. T. Delaney and G. H. Fredrickson, "Theory of polyelectrolyte complexation—complex coacervates are self-coacervates," *The Journal of chemical physics*, vol. 146, no. 22, p. 224902, 2017.

Chapter 8

Thesis outlook
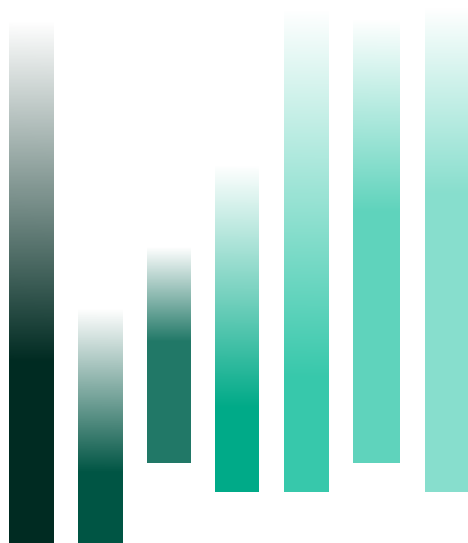
Finis coronat opus
The end crowns the work

We believe with this thesis we achieved the first growing protocell whose behavior could be completely explained at the molecular level; and made progress on creating a solid understanding of chemistry in coacervates, a crucial step towards unravelling the function of membraneless organelles. We anticipate that the findings in Chapter 6 will encourage a new approach in protocell research and instigate physical chemistry research on the structure of complex coacervates.

8.1   Divide and conquer

In this thesis we achieve cellular-like growth, but in nature, growth is always coupled with division. Division would be a natural continuation of our work, following ref. 1. Taylor *et al* observed droplet fission with active oil droplets,[2] and Donau *et al* observed fragmentation of active coacervate droplets (Figure 8.1A and B).[3] However the best biomimetic division model so far was obtained not with active coacervates, but with coacervate droplets (incidentally, of RNA-K_{72}) doped with the bacterial division protein FtsZ (Figure 8.1C).[4] In this case there is a chemical reaction driving the behavior — GTP-dependent FtsZ elongation —, but not linked to coacervation itself, and therefore division is not linked to growth. This example employs a rather specialized division protein, but we propose that applying a similar logic to our ATP-based coacervates could lead to reaction driven growth-and-division.

Similar to FtsZ, actin is a globular protein that polymerizes into filaments in the presence of ATP. We performed some preliminary tests with ATP-PLL coacervates and actin; unlike FtsZ in RNA-K_{72}, actin accumulates at the interface of the droplets (Figure 8.2A). This could be a promising ATP-based system for reaction driven growth and division. The pseudo-membrane formed by actin might introduce instabilities that lead to the break up of droplets that grow past a critical size, as polymerized actin is known to generate mechanical forces against the lipid bilayer. An instability could also arise from the charging of the actin-coated droplet surface (actin filaments are negatively charged, with a charge density of -e/0.25 nm),[5] which causes a pressure imbalance across the interface (Rayleigh instability). As the overall surface charge is size-dependent, the instability would select for droplets larger than a certain size to break up in two (Figure 8.2B).[6] It would be also interesting to explore if the pseudo-membrane behaves as a lipid membrane when it comes to budding and fission behavior.

The pseudo-membrane and charge are not a requirement for division, as Zwicker *et al* predicted that the concentrations fluxes generated by the chemical reactions in neutral active droplets are sufficient for a shape instability that leads to division (Figure 8.2C).[1] In this case actin polymerization would drive the efflux of ATP, while the pyruvate kinase reaction would create the influx across the interface. Importantly, although the internally maintained ATP-K_{72} droplets (ATP is produced from ADP concentrated within the droplets) served us well for the purpose of growth, they might not be suitable for the
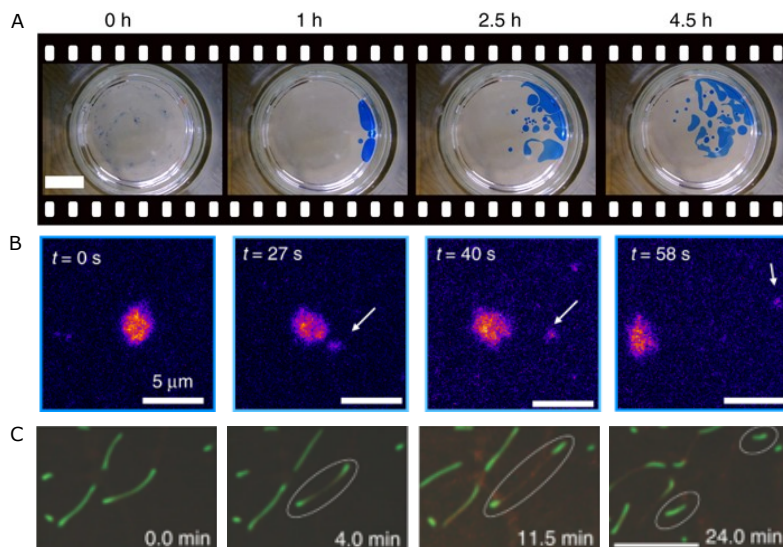
Figure 8.1: Overview of self-dividing protocells in the literature. (A) Active oil droplets (blue) fueled by a replicating imine reaction undergo fission. Figure from ref. 2. (B) Active coacervates of RNA and a cationic anhydride form, grow and release fragments as anhydride formation and hydrolysis takes place. Figure from ref. 3. (C) RNA-K_{72} coacervate droplets containing FtsZ filaments (green) elongate and divide in response to fuel (GTP) availability. Figure from ref. 4.

goal of division. Weber and Zwicker later distinguished between internally and externally maintained droplets, only being able to predict spontaneous division for the latter.[7] Here it is worth noticing that the enzyme pyruvate kinase locates in the interior of ATP-K_{72} droplets, but at the interface of ATP-PLL coacervates, which results in different fluxes. Work in this direction could provide a mechanism for coupled growth and division when the onset of instability is reached.

8.2 More is different

In continuation to growth and division, comes proliferation, and we propose to study the collective behavior of coacervate droplets would as an interesting continuation from Chapter 6. Harold Morowitz wrote in his 1992 book *The beginnings of cellular life*: "Sustained life is a property of an ecological system rather than a single organism or species. Traditional biology has tended to concentrate attention on individual organisms rather than on the biological continuum". The idea that a single protocell cannot explain the emergence of life might be obvious — especially for systems chemists —, but it pushes research in a direction not too explored so far. A prebiotic ecosystem needs more than one population, and performing experiments with interacting protocell populations can
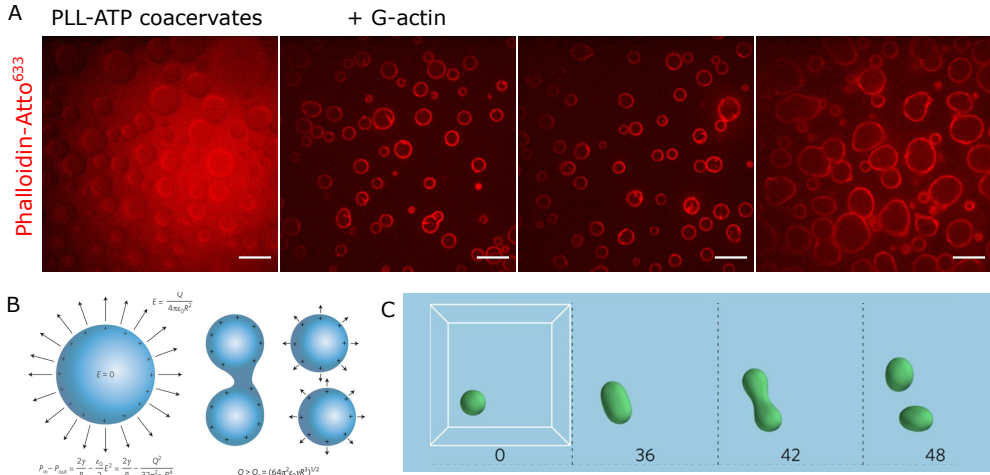
Figure 8.2: (A) Actin on the interface of ATP-PLL coacervate droplets. Phalloidin-Atto 633 fluorescence (red) distributes evenly in ATP-PLL droplets, but it has high affinity for F-actin. Monomeric actin (1 µM) was added to three samples of droplets (10 mM total in ATP-Mg and PLL), revealing polymerized actin assembled as pseudo-membrane around the droplets. Scale bar: 10 µm. (B) Charge-induced shape instability and (C) prediction of chemically induced division. Figures from ref. 6 and 1.

be challenging, as it requires protocells to maintain their identity. This has been achieved between coacervate droplets and proteinosomes leading to primitive predation, [8] between stabilized coacervate droplets, bringing about signalling in an enzymatic cascade, [9] and between lipid vesicles resulting in competition. [10]

In Chapter 6 we showed that different populations of coacervates can have, on average, different growth rates, but we were not able to combine the two populations in a single sample, with a common source of fuel, because uncoated coacervate droplets exchange material when in contact and can undergo fusion. A promising way to achieve competition between coacervate protocells would be to spatially segregate them in microfluidic chip. Joesaar *et al* controlled the communication between three semi-permeable proteinosome populations using microfluidic trapping devices (Figure 8.3A). [11] Combined with our findings from Chapter 6, we would expect to observe the emergence of competition, with the fastest growing population causing the shrinkage of the slow ones (Figure 8.3B). Even more interestingly, different types of fitness could be combined, allowing the different populations to co-exist. [12] Here, again, is will be worth exploring further the mechanisms of suppression of Ostwald ripening, as they might provide strategies to prevent the mixing of coacervate droplets, at least of its integral components.
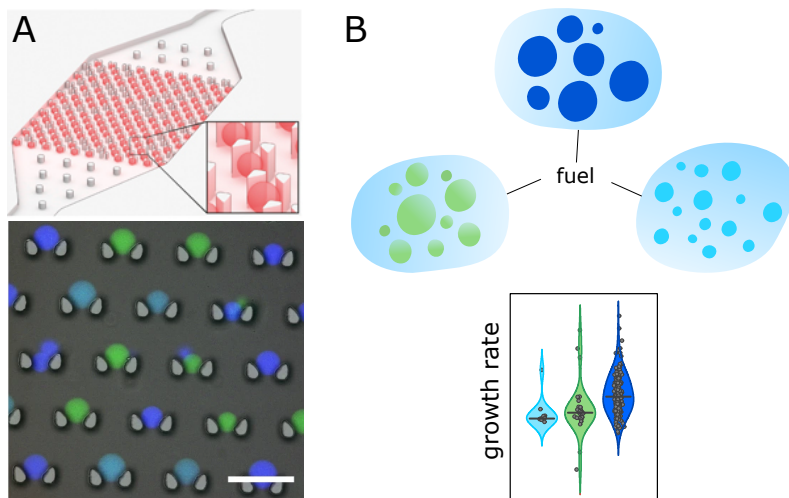
Figure 8.3: (A) A microfluidic trap for proteinosome droplets of three different populations for communication experiments. Figure taken from ref. 11. (B) Illustrative depiction of how coacervate droplets, spatially segregated and desgined with different fitness (growth rate), could compete for fuel.

8.3 Societal impact

In this thesis we investigated which components and principles are needed to imitate, with Chemistry, several aspects of life, from the origin of primitive cells, to the functioning of modern cells that contain membraneless organelles. Our goals were to develop a prototype of a cell that could grow using coacervates, a type of molecular assembly; and to contribute to our general understanding of chemical reactions in coacervates. But these were our intentions, and in this section we reflect on intentional and unintentional implications of this research and others in the protocell field.

The absence of an explanation to the origin of life leads us to a series of questions — why can't we know or prove any hypothesis, which science is responsible for providing an answer and ultimately, what is life. We only addressed the debate at the level of the hard sciences: whether metabolism, replication or compartmentalization are the essence of life. But the question about life and its origins comes in different shapes throughout different segments of society. In fact, it started in a now unrecognizable form, with the Aristotelian view that things that are alive have some sort of soul (*anima*) and the alchemists' quest to achieve a humanoid. For scientific teams developing artificial life, be it protocells, organoids or artificial intelligence, the question *what is life* morphs into whether a system can exist self-sufficiently outside of the lab. For some religious groups, alive/not alive is a distinction made not at the level of molecules and cells, but at the level of an embryo. This is all to say protocell research is not the only field wondering about the definition of

life, and we need to be aware that the answers we provide can be taken up without our knowledge, out of context.

Origin of life is an exemplary case of the ways by which we build knowledge. In the span of a hundred years: Needham proved spontaneous generation of life, Spallanzani disproved it, Voltaire refuted it and Pasteur undoubtely disproved it, only for abiogenesis to come back reformulated as origin of life theories. At the time, the investigation of the origin of life and developmental theories influenced each other, as they were both linked to the idea of creation. It is not far fetched to think that protocell research can still be influenced by other fields and scientists' personal beliefs, and it might be humbling to realize we too are a part of public opinion. A complete demonstration that the transition from non-life to life is possible would imply that we can understand biology in terms of chemistry, which might ignite a reductionist approach in other fields — one that comes to mind that also tries to explain the physical basis of a complex biological phenomenon is neuroscience, tackling common knowledge concepts such a mind and consciousness.

Aside from the multiple meanings of the questions we pose and answer, we can think about the ethics of working with what is, in essence, an artificial form of life. That concern is stronger for research that uses genetic material or genetically modified organisms — which also receives more positive attention than principle-focused research like the one in this thesis —, but the sole idea of a replicating chemical system that can overcome biological systems generates concern and backlash to this type of research. Regulation and the simple acknowledgement of this possibility in the long run can help in diffusing protocell research and improving society's assimilation without distortions.[13] With membraneless organelles revolutionizing our understanding of cellular biochemistry, we expect the concept of coacervate, which has always been tied to protocells, to achieve a status of common knowledge in the next 10 years, in which case we might already be late in contributing to educational resources on the topic.

Chemists interested in the emergence of complex behavior are just one of the players trying to contribute to knowledge of life, in parallel with chemists of different backgrounds, scientists from other fields, and the wide audience of course. Questions of who ultimately gets to decide what is life and the consensual model for its emergence on Earth do not have an obvious answer — let alone an impartial one —, but the exploration has so far been very enriching for the discovery of natural principles. We believe those are reflections that contribute to the way we plan, understand and communicate our projects, and that should also be taken into account when writing and reading this thesis.

References

[1] D. Zwicker, R. Seyboldt, C. A. Weber, A. A. Hyman, and F. Jülicher, "Growth and division of active droplets provides a model for protocells," *Nature Physics*, vol. 13, pp. 408–413, 2017.

[2] J. Taylor, S. Eghtesadi, L. Points, T. Liu, and L. Cronin, "Autonomous model protocell division driven by molecular replication," *Nature communications*, vol. 8, no. 1, pp. 1–6, 2017.

[3] C. Donau, F. Späth, M. Sosson, B. A. Kriebisch, F. Schnitter, M. Tena-Solsona, H. S. Kang, E. Salibi, M. Sattler, H. Mutschler, and J. Boekhoven, "Active coacervate droplets as a model for membraneless organelles and protocells," *Nature Communications*, vol. 11, no. 1, pp. 1–10, 2020.

[4] E. Te Brinke, J. Groen, A. Herrmann, H. A. Heus, G. Rivas, E. Spruijt, and W. T. S. Huck, "Dissipative adaptation in driven self-assembly leading to self-dividing fibrils," *Nature Nanotechnology*, vol. 13, no. September, pp. 849–856, 2018.

[5] L. K. Sanders, W. Xian, C. Guáqueta, M. J. Strohman, C. R. Vrasich, E. Luijten, and G. C. Wong, "Control of electrostatic interactions between f-actin and genetically modified lysozyme in aqueous media," *Proceedings of the National Academy of Sciences*, vol. 104, no. 41, pp. 15994–15999, 2007.

[6] R. Golestanian, "Division for multiplication," *Nature Physics*, vol. 13, no. 4, pp. 323–324, 2017.

[7] C. A. Weber, D. Zwicker, F. Jülicher, and C. F. Lee, "Physics of active emulsions," *Reports on Progress in Physics*, vol. 82, no. 6, p. 064601, 2019.

[8] Y. Qiao, M. Li, R. Booth, and S. Mann, "Predatory behaviour in synthetic protocell communities," *Nature chemistry*, vol. 9, no. 2, pp. 110–119, 2017.

[9] A. F. Mason, B. C. Buddingh', D. S. Williams, and J. C. van Hest, "Hierarchical self-assembly of a copolymer-stabilized coacervate protocell," *Journal of the American Chemical Society*, vol. 139, no. 48, pp. 17309–17312, 2017.

[10] K. Adamala and J. W. Szostak, "Competition between model protocells driven by an encapsulated catalyst," *Nature chemistry*, vol. 5, no. 6, p. 495, 2013.

[11] A. Joesaar, S. Yang, B. Bögels, A. van der Linden, P. Pieters, B. P. Kumar, N. Dalchau, A. Phillips, S. Mann, and T. F. de Greef, "Dna-based communication in populations of synthetic protocells," *Nature nanotechnology*, vol. 14, no. 4, pp. 369–378, 2019.

[12] S. Gude, E. Pinçe, K. M. Taute, A.-B. Seinen, T. S. Shimizu, and S. J. Tans, "Bacterial coexistence driven by motility and spatial competition," *Nature*, vol. 578, no. 7796, pp. 588–592, 2020.

[13] M. A. Bedau, E. C. Parke, U. Tangen, and B. Hantsche-Tangen, "Social and ethical checkpoints for bottom-up synthetic biology, or protocells," *Systems and synthetic biology*, vol. 3, no. 1, pp. 65–75, 2009.

Se procurar bem você acaba encontrando.
Não a explicação (duvidosa) da vida,
Mas a poesia (inexplicável) da vida.

Carlos Drummond de Andrade,
Lembrete

Research data management

This thesis research has been carried out in accordance with the research data management policy of the Institute for Molecules and Materials of Radboud University, the Netherlands.* The following datasets have been produced during this research:

- **Chapter 2:** Nakashima, KK, Baaij JF and Spruijt E. Reversible generation of coacervatedroplets in an enzymatic network. *Soft Matter* (2020). https://doi.org/10.1039/C7SM01897E. Data stored in: huckdfs-srv.science.ru.nl/huckdfs/Archive/Spruijt/Publications/001_2018_SoftMatter_Enzyme-controlled_coacervation, CNCZ, Radboud University.

- **Chapter 3:** Nakashima KK[†], André AAM[†] and Spruijt E. Enzymatic control over coacervation. *Methods in Enzymology* (2021). https://doi.org/10.1016/bs.mie.2020.06.007. Data stored in: huckdfs-srv.science.ru.nl/huckdfs/Archive/Spruijt/Publications/007_2020_Methods_in_Enzymology, CNCZ, Radboud University.

- **Chapter 4:** Nakashima KK. Data stored in: huckdfs-srv.science.ru.nl/huckdfs/Spruijt/Projects/Growing_Coacervates/2021_Model_of_reactions_in_coacervates and huckdfs-srv.science.ru.nl/huckdfs/Spruijt/Projects/Growing_Coacervates/2020_lipase coacervates, CNCZ, Radboud University.

- **Chapters 5 and 6:** Nakashima KK, van Haren MHI, André AAM, Robu I and Spruijt E. Active coacervate droplets are protocells that grow and resist Ostwald ripening. *Nature Communications* (2021). https://doi.org/10.1038/s41467-021-24111-x.

  Data stored in: //huckdfs-srv.science.ru.nl/huckdfs/Spruijt/Publications/014_2021_Growing_ATP_coacervates, CNCZ, Radboud University.

---

*https://www.ru.nl/rdm/vm/policy-documents/policy-imm/, last accessed 08 May 2021.
[†]equal contributions

Acknowledgements

Just like defining life, it is sometimes difficult to put acknowledgements into words. In the Introduction chapter, I mentioned the pillars of life, as a way to organize the discussion about life from a chemical perspective. It turns out the seven pillars perfectly apply to describe how different people were crucial to my work leading to this thesis, in addition to the specific remarks I made at the end of each chapter.

1) Program: I am extremely grateful to **Evan** for providing me with a meaningful PhD topic and project. He did not spare *any* time or patience in helping me stick to the plan, or deviate from it when needed. Beyond the details of the plan, Evan helped me understand the mechanisms of science and how to navigate it. It was an honor to witness the growth of his group and science, and it will stay as an example for me of success achieved through a fundamental question. I wish I would have been easier sometimes, but I do not regret our honest conversations, because they were a showcase of mutual respect.

2) Compartmentalization: I thank **Wilhelm** for providing the protective encasing to my PhD and being my official supervisor, while still giving Evan the space to follow his own direction. Also important in setting the scenery was the constant financial support by the **Dutch Research Council (NWO)**, and the disposition of **Désirée** in making arrangements from my arrival to my departure from Radboud. Here I also wish to thank the ones involved in my basic education, from Universidade de São Paulo all the way back to Colégio Albert Sabin, for providing me with the tools so that I could find my place in the narrow compartment of academia.

3) Seclusion: although well compartmentalized, PhD research does not thrive in isolation, and it is very reassuring to share the lab, techniques and knowledge with people with similar goals. I am grateful for their comradeship during moments of distress and silly joy. **Alain**'s arrival marked the beginning of our coacervate union, and greatly increased my appreciation for reproducibility, science gossip and Dutch news. **Tiemei**'s spontaneity and work ethics are contagious, and I can't thank her enough for all the food, support and concrete help in the lab. I also appreciate our friendship and her acceptance to be paranymph, despite the stress it brings. Completing our subgroup, I want to thank **Wojtek** for his kindness and genuine engagement in side projects.

Some collaborations came about a bit more by chance: the bond with **Britta** made me push through in moments where I doubted my own sanity, and our little lunch routine is a good memory of an ugly year. The friendship with **Mahesh** was almost immediate, and although I complained a lot, those first two years leave so much *saudade*. His PhD pathway and thesis were a major

inspiration, and I wrote parts of this thesis with him as a reader in mind.

4) Improvisation: while a plan and a big picture are crucial, being able to change plans and succeed also makes a PhD. I am grateful to the students I (co)supervised for helping me with that skill. **Jochem** started in the lab when I was still very green, but thanks to his curiosity, what started as a summer internship project turned out to produce the model system present in every chapter of this thesis. When **Merlijn**'s initial project simply would not work out, he adjusted to new goals, and that became the main publication of my PhD. **Haibin** suddenly needed a three-month internship, and had the courage and motivation to work on a raw project. Although brief, he left many contributions that we still resort to years after. Finally, **Irina** worked around the interruption of her internship in the wet lab due to the global pandemic, to end up solving my issues with video analysis in matlab.

5) Adaptability: similar to improvisation, but in a shorter timespan, the ability to respond to sudden or difficult life changes, and recover afterwards is crucial. **Anna** has been an interdecadal, intercontinental friend, that increases my courage in trying the unknown and is all support, no judgement. As a PhD, **Aninha** was an example to me and she continues to be one, while we explore european academia and culture. We experienced the bad side of academia together, and now I am glad we get to experience the good side of it together as well.

6) Regeneration: even if external conditions remain fairly constant, a PhD involves continuous growth and replenishment of resources to keep showing up during four years. Here I want to thank Anne and Isabel, as friends who set the example and made me want to get the best out of it. The mere fact I pursued a project on the origin of life shows how impactful the friendship with **Isabel** is, and I learned it from her to give my personal take on standardized things. I thank **Anne** for being paranymph, my partner in crime, for the sponsored coffebreaks, and for making my PhD meaningful in a bigger sense. Anne is a pillar of her own, but regeneration is a good start at a metaphor.

7) Energy: the driving force for this PhD is my family. This was my way to put into motion all the energy they put in my upbringing and in my day-to-day — stimulating me to study, to have principles and to try and change things for better. I thank **Scott** for helping me recharge, by making life easier and happier, and for fueling my perfectionism when it mattered the most. I want to thank my aunt **Rosângela** for her humor and affection, my uncle **Pulinho** for his curiosity and love for culture, and my dad **Jorge** and my mom **Benvinda** for the support, the example and the strength.

Supervisors
Evan Spruijt
Wilhelm Huck

Doctoral examination board
Christine Keating
Claudia Bonfio
Daniela Wilson
Jan van Hest
Job Boekhoven
Martien Cohen Stuart

Helpful people
Arne Noot
Bianca Leenders
Conny Mooren
Désirée van der Wey
Ioannis Alexopoulous
Jan Dommerholt
Marianne Driessen
Theo Peters

Lab mates
Alain André
Aleksandr Pogodaev
Amy Yewdall
Andrei Sakai
Anne-Déborah Nguindjel
Annemiek Slootbeek
Bob van Sluijs
Brent Visser
Britta Helwig
Elena Daines
Eleonora Bailoni
Erik van Buijtenen
Esra te Brinke
Francesca Rivello
Haibin Qian
Hiroaki Suzuki
Irina Robu
Iris Smokers
James Taylor
Jan Harm Westerdiep
Jean-Pierre Welters
Jing Xie

Jochem Baaij
Johan Pastoors
Kinga Matula
Lía Regueiro
Lifei Zheng
Ludo Schoenmakers
Maaruthy Yelleswarapu
Mahesh Vibhute
Manzar Abbas
Merlijn van Haren
Miglė Jakštaitė
Oliver Maguire
Peer van Duppen
Roel Maas
Sandra Schoenmakers
Sjoerd Postma
Tiemei Lu
Wojciech Lipiński (Wojtek)
Xinyu Hu
Yaxun Fan
Yorick van Aalst

Friends
Ana Clara Beltran (Aninha)
Anna Wiesenhofer
Carolina Hovaguimian
Caroline Matos
Débora Morf
Fabiana Takara
Felipe Teixeira
Isabel Bacellar
Luísa Madeira
Mariana Figueiredo
Nathalia Mikami
Olívia Pena

Family
Scott van Dinter (& Luninha)
Rosângela Vecchione
Carmela Vecchione
Nino Vecchione
Paulo de Oliveira Jr. (Pulinho)
Maria Benvinda Nakashima (Bebete)
Jorge Nakashima (*in memoriam*)

Curriculum vitae

Karina K. Nakashima

ORCID iD: 0000-0002-7402-8618 — Lattes iD: 4078931580397855

Currently: postdoctoral researcher, Katsonis group, University of Groningen

Publications

- Nakashima KK, van Haren MHI, André AAM, Robu I and Spruijt E. Active coacervate droplets are protocells that grow and resist Ostwald ripening. *Nat Commun* **12**, 3819 (2021). *link*

- Lu T, Nakashima KK and Spruijt E. Temperature-responsive peptide-nucleotide coacervates. *J Phys Chem B* **125**, 12 (2021). *link*

- Nakashima KK*, André AAM* and Spruijt E. Enzymatic control over coacervation. *Methods Enzymol* **646** (2021). *link*

- Abbas M*, Lipiński WP*, Nakashima KK, Huck WTS and Spruijt E. A short peptide synthon for liquid-liquid phase separation. *ChemRxiv* (2020). *link*

- van Haren MHI, Nakashima KK and Spruijt E. Coacervate-based protocells: integration of life-like properties in a droplet. *J Sys Chem* (2020). *link*

- Nakashima KK and Bastos EL. Rationale on the high radical scavenging capacity of betalains. *Antioxidants* **8**, 7 (2019). *link*

- Nakashima KK*, Vibhute MA* and Spruijt E. Biomolecular chemistry in liquid phase separated compartments. *Frontiers Biomol Sci* **6:21** (2019). *link*

- Nakashima KK, Baaij JF and Spruijt E. Reversible generation of coacervate droplets in an enzymatic network. *Soft Matter* **14** (2018). *link*

---

*equal contributions

Supervision during PhD

- *MSc students:* Merlijn van Haren, Haibin Qian (2019)
- *BSc students:* Irina Robu (2020), Yorick van Aalst, Jean-Pierre Welters, Saurabh Mathur (2018), Jochem F. Baaij (2017)

Conferences

- European Chemical Biology Symposium, virtual (2021). Active coacervates are protocells that grow and survive.[‡]
- Systems Chemistry, international virtual symposium (2020). Active coacervate droplets as protocells.[†]
- 2nd ICMSE, International Conference on Molecular Systems Engineering, Nijmegen, NL (2019). Artificial organelles fueled by ATP.[‡]
- CHAINS, The Dutch Chemistry Conference, Veldhoven, NL (2019). Active coacervate droplets as protocells.[†]
- sIMMposium, Symposium of the Institute for Molecules and Materials, Nijmegen, NL (2018). Chemistry inside active coacervate droplets.[‡]
- CHAINS, The Dutch Chemistry Conference, Veldhoven, NL (2017). Reversible generation of coacervate droplets with an enzymatic network.[†]

Public outreach

- Radboud University alumni lecture: Integrating Chemistry, Physics and Biology to understand life (2020). *link*
- Organizing committee of the annual workshop *A week of Chemistry* — edition Origin of Life, University of São Paulo (2010).

Education

- 2017-2021 PhD in Chemistry, Radboud University, Nijmegen, NL
- 2013-2015 MSc in Chemistry, Universidade de São Paulo, São Paulo, BR
- 2009-2012 BSc & Lic in Chemistry, Universidade de São Paulo, BR
- 1998-2008 Basic education at Colégio Albert Sabin, São Paulo, BR

[‡]oral presentation
[†]poster presentation